The mitotic checkpoint in cancer and aging

Darren James Baker

The studies in this thesis were performed in the Departments of Pediatric and Adolescent Medicine and Biochemistry and Molecular Biology, Mayo Clinic College of Medicine, Rochester, Minnesota, USA, and supported by National Institutes of Health (NIH) grants RO1 CA77262, RO1 CA96985, RO1 CA126828, the Ellison Medical Foundation and the Ted Nash Long Life Foundation.

Cover: The background shows an example of premature sister chromatid separation, a hallmark of unscheduled anaphase-promoting complex activity in early mitosis, which was visualized using spectral karyotype (SKY) anaylsis. The mouse to the left is a a 5-month-old BubR1 mutant mouse that shows early aging-associated phenotypes, while the mouse on the right is a 5-month-old wild-type mouse.

Printed by Gildeprint Drukkerijen BV, Enschede, The Netherlands

The mitotic checkpoint in cancer and aging

een wetenschappelijke proeve op het
gebied van de Medische Wetenschappen

Proefschrift

ter verkrijging van de graad van doctor
aan de Radboud Universiteit Nijmegen
op gezag van de rector magnificus prof. mr. S.C.J.J. Kortmann
volgens besluit van het College van Decanen
in het openbaar te verdedigen
op woensdag 4 juni 2008
om 10.30 uur precies

door

Darren James Baker

geboren op 24 februari 1979
te Willmar, Minnesota, USA

Promotores:

Prof. dr. B. Wieringa
Prof. dr. J. M. A. van Deursen

Manuscriptcommissie:

Prof. dr. A. Geurts van Kessel
Prof. dr. M. van Lohuizen (NKI- AVL)
Dr. G. Kops (UMC- Utrecht)

To Betsy, Andrew and Caleb

Contents **Page**

Chapter 1 Outline of this Thesis 9

Chapter 2 Introduction 15

2.1 The Cell Cycle 17
2.2 The Anaphase Promoting Complex (APC/C) 23
2.3 Controlling APC/C function during mitosis 29
2.4 Functional analyses of mitotic checkpoint proteins 34
2.5 Human cancer and the mitotic checkpoint 43
2.6 Aging and the spindle assembly checkpoint 49

Parts of the introduction were published in two separate reviews:
Mitotic regulation of the anaphase-promoting complex
Darren J. Baker, Meelad M. Dawlaty, Paul Galardy, and Jan M. van Deursen
Cellular and Molecular Life Sciences, **64**, 589-600 (2007)

The mitotic checkpoint in cancer and aging: what have mice taught us?
Darren J. Baker, Junjie Chen, and Jan M. van Deursen
Current Opinions in Cell Biology, **17**, 583-589 (2005)

Chapter 3 BubR1 insufficiency causes early onset of aging-associated phenotypes and infertility in mice 81
Darren J. Baker, Karthikbabu Jeganathan, J. Douglas Cameron, Michael Thompson, Subhash Jeneja, Alena Kopecka, Rajiv Kumar, Robert B. Jenkins, Piet C. de Groen, Patrick Roche, and Jan M. van Deursen
Nature Genetics, **36**, 744-749 (2004)

Chapter 4 Aging-associated vascular phenotype in mutant mice with low levels of BubR1 97
Takuya Matsumoto, Darren J. Baker, Livius V. d'Uscio, Mozammel Gazi, Zvonimir S. Katusic, and Jan M. van Deursen
Stroke, **38**, 1050-1056 (2007)

Chapter 5	Opposing roles for $p16^{Ink4a}$ and $p19^{Arf}$ in senescence and aging caused by BubR1 insufficiency Darren J. Baker, Carmen Perez-Terzic, Fang Jin, Kevin Pitel, Nicolas J. Niederlander, Karthik Jeganathan, Satsuki Yamada, Santiago Reyes, Lois Rowe, H. Jay Hiddinga, Norman L. Eberhardt, Andre Terzic and Jan M. van Deursen *Nature Cell Biology* (In press)	107
Chapter 6	Early aging-associated phenotypes in Bub3/Rae1 haplo-insufficient mice Darren J. Baker, Karthikbabu Jeganathan, Liviu Malureanu, Carmen Perez-Terzic, Andre Terzic, and Jan M. van Deursen *Journal of Cell Biology*, **172**, 529-540 (2006)	141
Chapter 7	Securin associates with APC^{Cdh1} in prometaphase but its destruction is delayed by Rae1 and Nup98 until the metaphase/anaphase transition Karthikbabu Jeganathan, Darren J. Baker, and Jan M. van Deursen *Cell Cycle*, **5**, 366-370 (2006)	159
Chapter 8	Bub1 mediates cell death in response to chromosome missegregation and acts to suppress spontaneous tumorigenesis Karthikbabu Jeganathan*, Liviu Malureanu*, Darren J. Baker*, Susan C. Abraham, and Jan M. van Deursen *Journal of Cell Biology* **179**, 255-67 (2007) ***Shared first authorship**.	167
Chapter 9	Summary, Discussion and Future Outlook	185
Acknowledgements		195
Publications		197
Curriculum Vitae		199

Chapter 1

Outline of this Thesis

The studies in this thesis began with the observation that the mitotic checkpoint protein BubR1 was mutated in two of 19 cell lines established from human patients with colon cancer [1]. We set out to determine the physiological role of BubR1 in normal and malignant cell growth. To this end, we used a gene targeting strategy to create a hypomorphic BubR1 allele in mouse embryonic stem (ES) cells. We found that mice that are homozygous for this hypomorphic allele express very low amounts of BubR1 protein and cells from these animals undergo frequent chromosome missegregation and develop severe aneuploidy. These mice are also more susceptible to carcinogen-induced tumorigenesis, although the incidence of spontaneous tumor formation remained very low. Surprisingly, we found that BubR1 hypomorphic mice exhibit a variety of progeroid features, including reduced lifespan, cachetic dwarfism, lordokyphosis (abnormal rearward curvature of the spine), muscle atrophy (sarcopenia), cataracts, craniofacial dysmorphisms, heart arrhythmias, arterial stiffening, loss of subcutaneous body fat, and impaired wound healing. These findings were strengthened by a recent discovery of biallelic BubR1 mutations in patients with mosaic variegated aneuploidy (MVA) syndrome, a recessive disorder characterized by aneuploidy, tumor susceptibility and progeroid features [2]. Thus, BubR1 appears to behave as both a suppressor of tumor formation and aging (Chapter 3).

BubR1 hypomorphic mice die at a very early age with a decline in overall health. To determine if these mutants exhibit physiological consequences of low amounts of BubR1 in the vasculature, we performed a series of experiments. We found that BubR1 mutant mice have reduced arterial wall thickness and low numbers of smooth muscle cells. These mice also had profound arterial fibrosis, and consistent with these findings, had a profound reduction in elasticity. Importantly, the expression of BubR1 in aortas of wild-type mice declines significantly with age, suggesting that BubR1 may play a natural role in the suppressing the aging process in the vasculature (Chapter 4).

We were interested in establishing the mechanism by which reduced BubR1 expression promotes cancer and aging. Various effectors of cellular senescence are induced when BubR1 levels decline, including p53, $p21^{Cip1}$, $p19^{Arf}$, and $p16^{Ink4a}$. We first sought to determine the contribution of the pRb-$p16^{Ink4a}$ pathway in the development of progeroid phenotypes in hypomorphic BubR1 mice. Recent work has shown that $p16^{Ink4a}$ null mice have delayed age-related changes in specific cell types, including pancreatic islet cells regenerative potential [3], forebrain progenitor cell depletion [4], and hematopoietic stem cell maintenance [5]. Several tissues of BubR1 hypomorphic mice have elevated levels of $p16^{Ink4A}$, including fat tissue, skeletal muscle, and the eye. By using $p16^{Ink4a}$ knockout mice, we show that loss of this tumor suppressor accelerates lung tumorigenesis and prevents the development of a subset of age-related disorders in BubR1 hypomorphic mice, including muscle atrophy, lordokyphosis, cataracts, and loss of adipose tissue. These findings suggest

that, in certain cell types, in tissues that display age-related pathologies that also have elevated levels of $p16^{Ink4A}$ benefit by the disruption of this gene. However, low amounts of BubR1 synergize with $p16^{Ink4A}$ deficiency to promote lung tumorigenesis specifically (Chapter 5). After discovering that the Rb-$p16^{Ink4a}$ pathway is required for the establishment of certain age-related characteristics in hypomorphic BubR1 mice, we then were interested to determine whether disruption of the p53-$p19^{Arf}$ pathway was able to modulate the development of progeroid features. It has been difficult to establish whether p53 or $p19^{Arf}$ contribute to the process of natural aging, as disruption leads to early tumorigenesis. By using our mouse model, we found that disruption of $p19^{Arf}$ leads to an earlier onset of aging in several tissues. This earlier onset of age-related diseases appears to result from an increased rate of cellular senescence when $p19^{Arf}$ is lacking in hypomorphic BubR1 mice. This suggests that $p19^{Arf}$ is upregulated in an attempt to combat the process of aging, whereas elevated levels of $p16^{Ink4A}$ act to promote aging processes (Chapter 5).

After discovering that BubR1 was implicated in aging, we then asked if aging was a general consequence of impaired spindle assembly checkpoint function by using mice with mutations in other mitotic checkpoint proteins. We used mice that were haploinsufficient for Bub3 or Rae1 and found that these mice, despite developing an increase in aneuploidy, both *in vitro* and *in vivo*, were not predisposed to spontaneous tumorigenesis, despite the fact that both models had a clear susceptibility to carcinogen induced tumor formation [6]. These mice also displayed no overt acceleration to the development of age-related features that are also detectable in wild-type mice of advanced age. However, mice that were compound haplo-insufficient for both Bub3 and Rae1 did have accelerated aging in certain tissues, although the onset was substantially delayed in comparison to hypomorphic BubR1 mice. We also found that cells from combined haplo-insufficient Bub3/Rae1 mice exhibit premature cellular senescence. Combined, the results from these experiments, along with the findings from the BubR1 hypomorphic model, suggest that early onset of aging-related phenotypes in mice with mitotic checkpoint defects is linked to cellular senescence and activation of the p53 and $p16^{Ink4a}$ pathways rather than to aneuploidy (Chapter 6).

Rae1 and Nup98, two proteins that play key roles in regulation of mRNA export from the nucleus during interphase, also are involved maintenance of genomic stability [6, 7]. Cells that have only one functional copy of Rae1 and Nup98 are highly aneuploid [7]. To determine the consequences of this aneuploidy *in vivo*, we monitored a cohort of double haplo-insufficient Nup98/Rae1 mice. We found that although these mice are susceptible to DMBA induced tumorigenesis, they do not have an increase in spontaneous tumor formation, which is similar to the results we obtained when looking at Bub3/Rae1 double haploinsufficient mice. These data demonstrate a common theme that although mice may

be predisposed to tumor formation when challenged with carcinogens, these cooperating events may not occur under normal situations in their lifespan (Chapter 7).

Bub1, a BubR1-related checkpoint gene which is mutated or expressed at lower levels in a variety of human tumors [1, 8-13], plays many roles during mitosis to ensure accurate chromosome segregation. To determine the physiological role of Bub1, we generated a series of mice in which the expression of Bub1 is reduced in graded fashion by the use of wild-type, hypomorphic, and knockout alleles. We find that Bub1 null mice are embryonically lethal, but that Bub1 hypomorphic mice with very low levels of wild-type Bub1 protein are viable. We show that Bub1 prevents aneuploidy and spontaneous tumor development in a dose dependent fashion, and we provide evidence for a novel role of Bub1 in eliminating cells that have undergone chromosome missegregation (Chapter 8).

References

1. Cahill, D.P., Lengauer, C., Yu, J., Riggins, G.J., Willson, J.K., Markowitz, S.D., Kinzler, K.W., and Vogelstein, B. (1998). Mutations of mitotic checkpoint genes in human cancers. Nature *392*, 300-303.
2. Hanks, S., Coleman, K., Reid, S., Plaja, A., Firth, H., Fitzpatrick, D., Kidd, A., Mehes, K., Nash, R., Robin, N., Shannon, N., Tolmie, J., Swansbury, J., Irrthum, A., Douglas, J., and Rahman, N. (2004). Constitutional aneuploidy and cancer predisposition caused by biallelic mutations in BUB1B. Nat Genet *36*, 1159-1161.
3. Krishnamurthy, J., Ramsey, M.R., Ligon, K.L., Torrice, C., Koh, A., Bonner-Weir, S., and Sharpless, N.E. (2006). p16INK4a induces an age-dependent decline in islet regenerative potential. Nature *443*, 453-457.
4. Molofsky, A.V., Slutsky, S.G., Joseph, N.M., He, S., Pardal, R., Krishnamurthy, J., Sharpless, N.E., and Morrison, S.J. (2006). Increasing p16INK4a expression decreases forebrain progenitors and neurogenesis during ageing. Nature *443*, 448-452.
5. Janzen, V., Forkert, R., Fleming, H.E., Saito, Y., Waring, M.T., Dombkowski, D.M., Cheng, T., DePinho, R.A., Sharpless, N.E., and Scadden, D.T. (2006). Stem-cell ageing modified by the cyclin-dependent kinase inhibitor p16INK4a. Nature *443*, 421-426.
6. Babu, J.R., Jeganathan, K.B., Baker, D.J., Wu, X., Kang-Decker, N., and van Deursen, J.M. (2003). Rae1 is an essential mitotic checkpoint regulator that cooperates with Bub3 to prevent chromosome missegregation. J Cell Biol *160*, 341-353.

7. Jeganathan, K.B., Malureanu, L., and van Deursen, J.M. (2005). The Rae1-Nup98 complex prevents aneuploidy by inhibiting securin degradation. Nature *438*, 1036-1039.
8. Shichiri, M., Yoshinaga, K., Hisatomi, H., Sugihara, K., and Hirata, Y. (2002). Genetic and epigenetic inactivation of mitotic checkpoint genes hBUB1 and hBUBR1 and their relationship to survival. Cancer Res *62*, 13-17.
9. Ohshima, K., Haraoka, S., Yoshioka, S., Hamasaki, M., Fujiki, T., Suzumiya, J., Kawasaki, C., Kanda, M., and Kikuchi, M. (2000). Mutation analysis of mitotic checkpoint genes (hBUB1 and hBUBR1) and microsatellite instability in adult T-cell leukemia/lymphoma. Cancer Lett *158*, 141-150.
10. Ru, H.Y., Chen, R.L., Lu, W.C., and Chen, J.H. (2002). hBUB1 defects in leukemia and lymphoma cells. Oncogene *21*, 4673-4679.
11. Doak, S.H., Jenkins, G.J., Parry, E.M., Griffiths, A.P., Baxter, J.N., and Parry, J.M. (2004). Differential expression of the MAD2, BUB1 and HSP27 genes in Barrett's oesophagus-their association with aneuploidy and neoplastic progression. Mutat Res *547*, 133-144.
12. Shigeishi, H., Oue, N., Kuniyasu, H., Wakikawa, A., Yokozaki, H., Ishikawa, T., and Yasui, W. (2001). Expression of Bub1 gene correlates with tumor proliferating activity in human gastric carcinomas. Pathobiology *69*, 24-29.
13. Shigeishi, H., Yoneda, S., Taki, M., Nobumori, T., Ohta, K., Higashikawa, K., Yasui, W., and Kamata, N. (2006). Correlation of human Bub1 expression with tumor-proliferating activity in salivary gland tumors. Oncol Rep *15*, 933-938.
14. Kalitsis, P., Fowler, K.J., Griffiths, B., Earle, E., Chow, C.W., Jamsen, K., and Choo, K.H. (2005). Increased chromosome instability but not cancer predisposition in haploinsufficient Bub3 mice. Genes Chromosomes Cancer.

Chapter 2

Introduction

2.1 THE CELL CYCLE

2.1.1 Introduction

A requisite for cellular reproduction is the duplication of all cellular components, including genetic material, followed by an equal division into two daughter cells. For unicellular organisms, this process results in the creation of an additional organism. In higher organisms, many rounds of cell division are required to both create and maintain an individual. Human adults have a variety of tissues containing cells that turn over with high frequency, and loss of division in these cells can cause death in a short period of time. The process of this cell-division cycle, simply called the cell cycle, is the fundamental means by which all living organisms are propagated and preserved.

2.1.2 Stages of the cell cycle

The process of cell division consists of four phases: G_1, S, G_2 and M (Fig. 1) [1]. First, the cell prepares for DNA duplication by growing throughout the interval of G_1, which is the first gap phase of the cell cycle that occurs between the end of mitosis and the beginning of S phase [1]. Next, replication of DNA occurs during S phase, which lasts for 10-12 hours in a typical mammalian cell and results in two complete sets of DNA. During G_2, the second gap phase, the cell assures that all necessary components for traversing into and through mitosis are present [1]. The three phases of G_1, S, and G_2 are commonly referred to as interphase [2]. The separation of duplicated sets of DNA into daughter cells occurs during M phase, which can take less than an hour to complete in mammals. After mitosis, cells may enter into a quiescent resting state referred to as G_0 where they have the capacity to remain uncommitted to resume the cell cycle [3, 4]. This delay may last for several years in some human cells, as is the case for neurons. Cells in G_0 have the potential to re-enter the cell cycle by the tightly regulated process of mitogenic stimulation [5].

2.1.3 Mitosis

The M phase of the cell cycle can be further divided into 6 major stages and must occur in sequential order (Fig. 1) [6]. These stages are prophase, prometaphase, metaphase, anaphase, telophase and cytokinesis [7]. In early prophase, duplicated centrosomes separate and move towards opposite poles of the cell and DNA begins to condense. At late prophase, the DNA is highly condensed, with the two chromatids from each chromosome held tightly together. Prometaphase begins when the nuclear envelope breaks down. This liberation of genetic material into the mitotic cytosol allows for DNA to attach to microtubules originating from the centrosomes/spindle poles. At metaphase, the sister chromatids align at the metaphase plate, which lies at the equator between the two poles. The sister chromatids are attached to opposite poles by spindle microtubules bound to the kinetochore, a highly specialized centromeric protein-rich area that will be expanded upon later. Anaphase occurs when the sister chromatids separate completely and move towards opposite poles of the cell. Microtubules disassemble during telophase and chromosomal movement is completed, followed by formation of a new nuclear envelope. This event marks the end of mitosis. Finally, the cytoplasm divides during cytokinesis, with each daughter cell receiving cytoplasmic contents from the progenitor cell [8]. The completion

of cytokinesis marks the end of M phase and the two daughter cells can now themselves enter new rounds of the cell cycle [7].

Aberrant maintenance in genetic integrity or missegregation of duplicated DNA may unfortunately result in tumor initiation. Point mutations, which are single DNA base-pair replacements, have the potential to begin the multi-step process of tumorigenesis by converting a normal functioning gene into potent oncogene. In a variety of human tumors for example, there are frequent single-nucleotide alterations in members of the Ras family, a group of proteins which promote proliferation when the proper mitogenic signals are received by receptor tyrosine-kinases [9]. These point mutations render Ras molecules that are unable to be switched off after the mitogenic signal is removed, resulting in an endless promotion of the proliferation signal [9]. Larger alterations in DNA integrity constitute the condition of aneuploidy. This is a general term that is utilized for describing several DNA abnormalities, which can cause confusion. In the literature, structural aberrations of DNA including inversions, duplications, translocations, and deletions are often collectively referred to as aneuploidy [10]. However, in this thesis, aneuploidy will refer specifically to cells that have a non-modal chromosome number. In normal human cells, the total number of chromosomes is 46 (23 pairs). Therefore, cells with more or less than 46 chromosomes are called aneuploid. Additionally, a cell may have 46 total chromosomes, but it may be lacking one copy of a particular chromosome with a gain of additional one. Based on our description, this cell would also be considered aneuploid, as it contains a non-modal number of chromosome pairs. The condition of numerical aneuploidy is seen in the vast majority of human cancers [10], but whether it is a

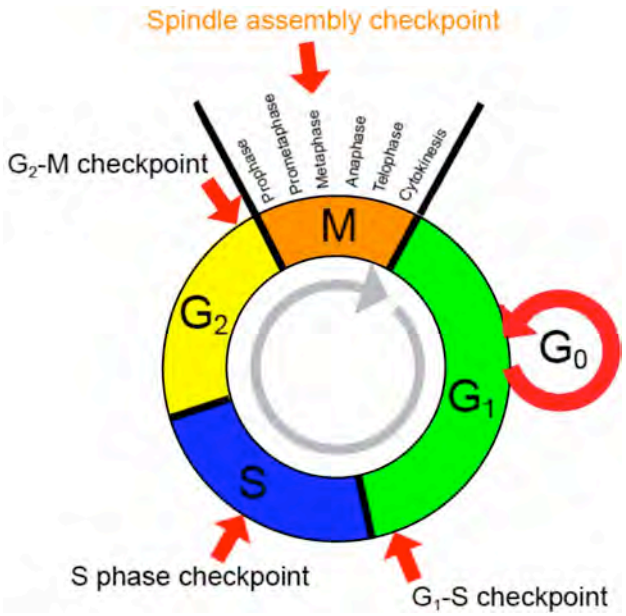

Fig. 1- Checkpoints during the cell cycle. The mammalian cycle of growth and division is divided into four phases, G_1, S, G_2, and M. A fifth state, G_0, is a resting, non-proliferating state where cells withdrawn from the active cell cycle. M phase is further divided into 6 distinct stages. They occur in the following order: 1) prophase, 2) prometaphase, 3) metaphase, 4) anaphase, 5) telophase, and 6) cytokinesis. Checkpoints impose quality control to ensure that a cell has completed all the requisite steps of one phase of the cell cycle before it is allowed to enter into the next phase. The four main cell cycle checkpoints are the G_1-S, S phase, G_2-M, and spindle assembly checkpoint.

cause or consequence of the tumor process remains a topic of intense debate. Cells that contain multiple sets of complete DNA material, or polyploidy, are a unique form of aneuploidy [11, 12]. Several cellular defense mechanisms, including those called checkpoints, exist to prevent genetic aberrations such as the development of aneuploidy.

2.1.4 Cell cycle checkpoints

The strict maintenance of genetic integrity is crucial for proper cellular function. In the process of DNA replication during S phase, endogenous damage can occur which produces a variety of errors, including mismatched bases, as well as single and double strand breaks [13]. Exogenous agents (external exposures) can also directly damage nucleotides or break the phosphodiester backbone [14]. Fortunately, the cell has devised multiple ways to deal with this constant barrage of attacks, which includes several elegant DNA-repair processes [15-19]. Unfortunately, these repair processes are not perfect, and damaged DNA can be propagated after stable incorporation into the genome. In order to allow sufficient time for complete correction of severe damage to DNA, a stoppage of the cell cycle may occur while the process of DNA repair occurs. Apoptosis, or programmed cell death, may occur if the damage is deemed irreparable. Checkpoints differ from DNA repair processes, in that they are "scheduled stops" during the cell cycle, where the maintenance of genetic stability is ensured by intricate surveillance machinery [14, 15]. Many of the key proteins that contribute to these checkpoints have been well characterized, which will be discussed in detail later. Checkpoints exist to ensure that once a particular step in the cell cycle has been completed, it will not be repeated until the following cell cycle. The four main cell cycle checkpoints are the G_1-S checkpoint, the S phase checkpoint, the G_2-M checkpoint, and the spindle assembly/mitotic checkpoint (Fig. 1) [15, 20, 21]. The G_1-S checkpoint ensures that cells that require genome repair do not enter into S phase from G_1. In the S phase checkpoint, DNA replication will be stalled or delayed in response to significant damage to DNA. The third checkpoint will not permit a cell to transition from G_2 into M until the complete replication of DNA has occurred during S phase. The spindle assembly checkpoint, which blocks the entry into anaphase until all chromosomes are properly attached to the mitotic spindle, is the main focus of this work and will be expanded upon later. In addition to the spindle assembly checkpoint during M, a decatenation checkpoint exists in late G_2 to prevent entry into mitosis until the replicated pair of DNA-helices has been untangled from each other [22]. These checkpoints ensure that a cell is ready to move into the next stage of the cell cycle. Progression through the cell cycle itself is accomplished by an intricate network of kinases, whose activity is regulated by a class of proteins referred to as cyclins.

2.1.5 Controlling the cell cycle

The cell cycle requires the coordinated activity of cyclin-dependent kinases, or Cdks, for cycle progression [1, 23]. Active Cdks are composed of at least two subunits, a Cdk and a regulatory cyclin, but often contain other proteins as well [23]. Cdks have catalytic activity for phosphorylating serine and threonine residues on target proteins [1]. At least 11 vertebrate Cdks have so far been identified, each with an activity that is restricted to a distinct portion of the cell cycle [24, 25]. The activity of Cdks is kept under tight control, for improper activation would lead to aberrant cell cycle progression [1, 24]. The critical

regulation of Cdk activity is performed largely by cyclins, but there are additional mechanisms to control Cdks. These include activation by phosphorylation and inhibition by binding of inhibitory proteins.

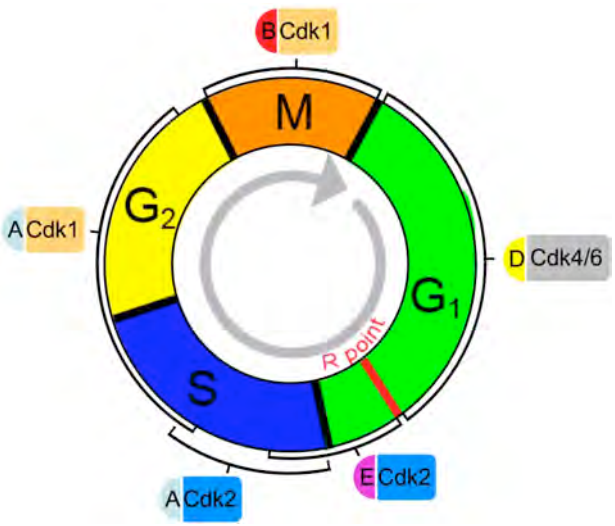

Fig. 2- Cell cycle pairing of cyclins (half circles) with cyclin-dependent kinases (rectangles). D type cyclins associate with Cdk4 or Cdk6, E type cyclins bind to Cdk2, A type cyclins bind to Cdk1 and Cdk2, and B type cyclins bind to Cdk1. Brackets indicate periods during the cell cycle where these various complexes are present and active.

The first cyclin was discovered in 1982 by a marine biologist who noted that the level of this protein increased and decreased during certain periods of the cell cycle [26]. The protein accumulated throughout interphase, but was abruptly degraded in mitosis [27, 28]. This fluctuation in protein level is cyclical during a standard cell cycle; therefore it has been given the general name cyclin [1, 26, 29]. All cyclins share a conserved stretch of 150 amino acids termed the "cyclin box". This domain is formed by five helical regions that allows for the interaction of these proteins with various proteins, including Cdks. Their binding to the properly phosphorylated Cdk is necessary for complete Cdk activation [1]. In a recent genetic screen of the human genome, 31 proteins were found to contain the "cyclin box" motif and have generically been termed cyclins of various families, although it is not known for several of these proteins if they are synthesized and destroyed cyclically [25]. Cdk4 and Cdk6 are two similarly acting Cdks that function during G_1 which bind to cyclins of the D and E family (Fig. 2). An important cellular decision occurs late in G_1 at the restriction or R point. Transitioning through the R point marks the switch to a mitogen-independent growth state and a commitment to replication of DNA and subsequent cellular division [30]. Cdk2 associates with E type cyclin late in G_1 until A type cyclins replace these E cyclins in S phase. In late S, Cdk1 replaces Cdk2 in cyclin A containing complexes. Finally, B-type cyclins replace cyclin A in Cdk1 complexes during M. The activity of the various Cdk-cyclin bimolecular complexes, which occur at distinct periods of the cell cycle, are responsible for sending out the signals that are required for traversing through the cell cycle. In order to prevent aberrant Cdk activity, the highly regulated process of cyclin degradation occurs, which cripples the catalytic activity of Cdk molecules [1, 26, 29].

Proteins known as CKIs (cyclin-dependent kinase inhibitors) negatively regulate Cdk activity by inhibiting the transfer of phosphorylation groups to target proteins [31, 32]. In higher eukaryotes, the two main families of CKIs are the Ink4 family and the CIP/KIP family [1, 32]. The members of the Ink4 family get their name because they mainly inhibit Cdk4, although they can also inhibit Cdk6 [32]. $p16^{Ink4a}$, $p15^{Ink4b}$, $p18^{Ink4c}$, and $p19^{Ink4d}$ are the four Ink proteins that exist in human cells [33-37]. The CIP/KIP family, which includes $p21^{Cip1}$, $p27^{Kip1}$, and $p57^{Kip2}$, negatively regulate Cdk1, Cdk2, Cdk4 and Cdk6 [32]. All members of the CIP/KIP family contain motifs within the amino-terminal region that permit binding to both cyclins as well as Cdks [38-50]. Both families of CKIs can effectively stall cell cycle progression by inhibiting Cdk phosphorylation at key transition periods during the cell cycle.

In cancer cells, the normal requisite for mitogenic stimulation for cell cycle reentry is ablated. Therefore, a large degree of focus in the area of tumor biology is on two key periods: 1) the transition out of G_0 and into G_1 and 2) the commitment to proceed through the R point in late G_1. Later, the molecular mechanism behind the G_0-G_1 transition will be discussed when cellular senescence is examined in greater detail. The key protein responsible for the transition through the R point in late G_1 is the tumor suppressor Rb, which blocks the entry into S phase [32, 51-53]. Cells that are in G_0 have Rb protein (pRb) that is essentially unphosphorylated (Fig. 3). A small number of serine and threonine residues on pRb become phosphorylated (hypophosphorylated) as cells enter into G_1, and many additional residues are phosphorylated (hyperphosphorylated) as cells transition through the R point [54]. Once this critical period has been passed, pRb is maintained

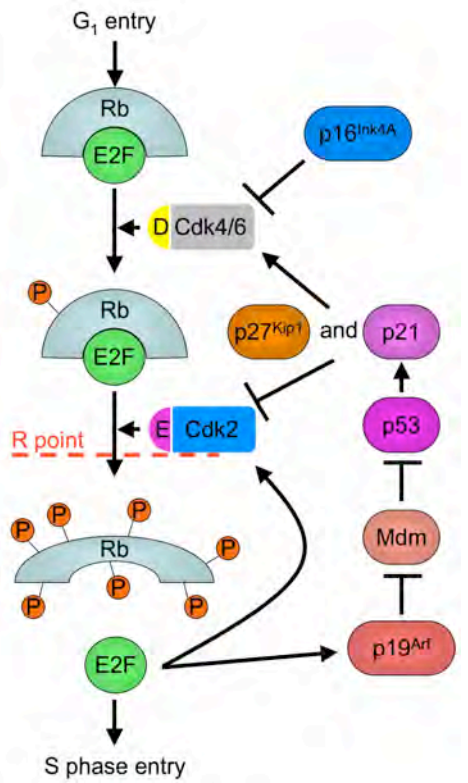

Fig. 3- Molecules governing progression through the R point. As cells exit mitosis, Rb is unphosphorylated. As cyclin-Cdk complexes phosphorylate Rb, the inhibition of E2F transcription factors is relaxed and S phase can begin. A variety of molecules participate in controlling the promotion or prevention of S phase entry. If the $p19^{Arf}$-p53-p21 and Rb-$p16^{Ink4a}$ pathways that restrain E2F release are hyperactivated, a cell may never enter into S phase and remain in a senescent state.

in a hyperphosphorylated state until the cell exits mitosis at the end of the cell cycle. The initiating pRb phosphorylation modifications are dependent on mitogenic stimuli that stabilize cyclin D [55]. Without these mitogens, cyclin D levels drastically reduce and all phosphate groups on pRb are quickly removed. Without these initial phosphorylation modifications of pRb, cyclin E/Cdk2 complexes cannot recognize pRb and pRb hyperphosphorylation is prevented. pRb binds to E2F transcription factor family members, thereby maintaining them in an inactive state [56]. The activity of these transcription factors is absolutely essential for entry into S phase and DNA synthesis [55]. Once pRb is hyperphosphorylated, E2F is released and subsequent gene transcription occurs. If cells retain pRb in a hyperphosphorylated state after mitosis, mitogens are not required for cell division and cell cycle control is ablated, demonstrating that this pathway is critical for preventing the formation of cancer. Therefore, it is critical that Cdk activity during this period be highly coordinated. Targeting cyclin D and E for destruction is one way to alter the activity of Cdk4/6 and Cdk2 in G_1. This destruction can proceed through the ubiquitin-proteasome system, which will be addressed shortly. As an alternative, CKI binding can influence the effects of cyclin/Cdk complexes. Early in G_1, $p16^{Ink4a}$ blocks the formation of cyclin D-Cdk4/6 complexes by reducing Cdk4/6 affinity for cyclin D and also prevents the activity of already formed complexes through distortion of the catalytically active Cdk4/6 site [54]. The induction of $p16^{Ink4a}$ expression proceeds by an as yet to be identified mechanism, but relies on Ets1/2 transcription factor activity that may result from several different types of stresses [57]. Also, how this inhibitory function of $p16^{Ink4a}$ is quenched to allow for cell cycle progression is currently unknown. Interestingly, the CKI's $p21^{Cip1}$ and $p27^{Kip1}$ stimulate the formation of cyclin D-Cdk4/6 complexes, while they prevent the formation and/or activity of other cyclin-Cdk complexes [58]. Therefore, $p21^{Cip1}$ and $p27^{Kip1}$ promote pRb hypophosphorylation. However, these proteins prevent the activity of cyclin E-Cdk2 complexes and further phosphorylation of pRb. Progression through the R point requires a change from cyclin D-Cdk4/6 complex activity to cyclin E-Cdk2 complexes. How then does a cell transit from active cyclin D-Cdk4/6 complexes into cyclin E-Cdk2 complexes? It appears that as cells progress towards the R point, additional active cyclin D-Cdk4/6 complexes continue to form, which act to sequester $p21^{Cip1}$ and $p27^{Kip1}$ away from cyclin E-Cdk2 complexes. This allows the liberation of active cyclin E-Cdk2 complexes, subsequent pRb hyperphosphorylation, and transition through the R point. After E2F is released from pRb, this signal is reinforced by additional transcription of cyclin E and Cdk2. Whereas SCF ubiquitin ligases control the amounts of $p27^{Kip1}$ by targeting it for destruction, the expression of $p21^{Cip1}$ is dependent upon p53, a transcription factor that functions throughout the cell cycle as a master guardian of several checkpoints as well as an executioner of the apoptotic program.

The transcriptional activity of p53 is able to induce a variety of downstream effects, including cell-cycle arrest, DNA repair, and apoptosis (Fig. 4) [59]. Under normal situations, a cell continuously synthesizes p53 molecules, but because p53 protein is degraded very quickly unless it receives post-translational stabilizing modification, a low steady-state amount of p53 is present. Once this degradation of p53 is blocked by residue modifications, p53 rapidly increases in the cell [60]. This induction is critical for triggering the effects mentioned previously. The levels of p53 are increased by DNA damage,

hypoxia, and deregulated signals promoting growth [61]. Mdm2 (Hdm2 in human cells) negatively regulates p53 activity by preventing the binding of p53 to target DNA sequences (Fig. 3), but Mdm2 also promotes p53 degradation by conjugating ubiquitin molecules to p53 (the ubiquitin system will be discussed in detail shortly). Stress or damage results in the phosphorylation of p53, making it unable to bind to Mdm2. By preventing this association, p53 is able to avoid destruction and the levels rise rapidly. The levels of p53 can also increase as a result of the actions of the tumor suppressor $p19^{Arf}$ ($p14^{Arf}$ in human cells). $p19^{Arf}$ binds to Mdm2 and sequesters it away from p53, thereby preventing destruction of p53 by its association with Mdm2 (Fig. 3). Because $p21^{Cip1}$ functions primarily as a cyclin-Cdk inhibitor, stabilization of p53 during nearly every phase of the cell cycle results in a stoppage because of subsequent p53-mediated transcription of $p21^{Cip1}$.

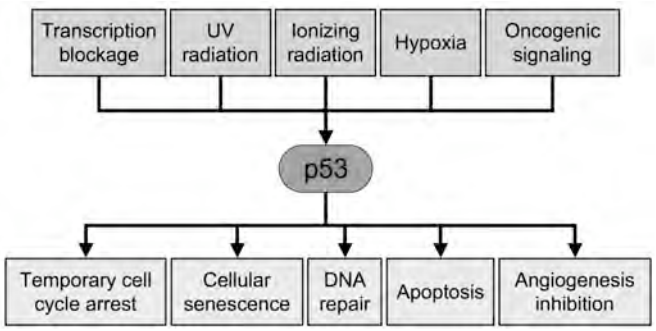

Fig. 4- Activating signals and downstream effects of p53. A variety of stress signals result in the rapid accumulation of p53, which may result in several different outcomes. Stalls of the cell cycle can occur via $p21^{Cip1}$ transient (temporary) or continuous expression (cellular senescence). DNA repair proteins are mobilized in response to active p53, but if they are unable to replace damaged nucleotides, apoptosis may ensue. Additionally, p53 functions to block the formation of new blood vessels (angiogenesis) in other situations.

Molecular changes that affect the pRb-$p16^{Ink4a}$ pathway are one of the most common features of human cancers [5]. Some ways to perturb this pathway include inactivating Rb mutations, high cyclin D activity, and reduced $p16^{Ink4a}$ protein levels. On the other hand, the tumor suppressor p53 is probably the single most frequently mutated gene in human cancer [5]. Tumor cells cleverly employ both of these alterations to avoid the normal regulation of cell growth and induction of apoptosis in order to further propagate themselves to allow for tumor progression. However, these cells still require Cdk activity to transition through the cell cycle, although the regulation of this activity is highly irregular due to aberrancies in Cdk inhibition. An alternative approach to negatively regulate Cdk activity relies on the destruction of the associated cyclin by the proteasome, resulting in dissociation of cyclin-Cdk complexes. Proteins are targeted for degradation by two main families of ubiquitin-conjugating complexes: the APC/C or the SCF.

2.2 THE ANAPHASE PROMOTING COMPLEX (APC/C)

2.2.1 Introduction

Along with cyclin/Cdk complex activity, progression through the eukaryotic cell cycle is mediated by temporally controlled degradation of cell cycle regulatory proteins by the ubiquitin-proteasome system. Proteins degraded by this system are first tagged with a chain of at least four lysine 48-linked ubiquitin molecules. The addition of ubiquitin, a highly conserved 76-amino acid protein, requires the concerted activation of three enzymes: a ubiquitin activating enzyme (E1) [62], a ubiquitin conjugating enzyme (E2) [63], and a ubiquitin ligase (E3) [63, 64]. In a reaction that consumes ATP, E1 functions to create a high-energy thioester bond between its active-site cysteine and the C-terminal glycine residue of ubiquitin, resulting in the activation of ubiquitin [62, 65, 66]. Ubiquitin is then transferred to the active-site cysteine residue of the E2 molecule, with a new thioester linkage [63]. Lastly, ubiquitin is coupled to a lysine side chain of a target substrate via an isopeptide linkage [64]. The final transfer of ubiquitin to a targeted substrate is performed by the joint activities of E2 and one of several E3 ligases, which confers substrate specificity [64, 67]. Two structurally related multiprotein E3 ligases, the APC/C and the Skp1/Cullin/F-box protein (SCF) complexes, drive progression through the eukaryotic cell cycle [2, 68-71]. These complexes differ in that the activity of SCF ligases mainly controls the transition from G1/S and G2/M [68], while APC/C is primarily required for mitotic progression and exit [69, 72-74]. APC/C-mediated ubiquitination of its substrates requires one of two coactivators, Cdc20 (cell division cycle 20) or Cdh1/Hct1, and the recruitment and transient association of one of two specific E2 enzymes; UbcH10 or UbcH5 [2, 75]. APC/C activity needs to be tightly controlled to prevent unscheduled substrate degradation. A variety of APC/C inhibitory mechanisms seem to exist to mediate proper substrate degradation and control the catalytic activity of APC/C.

2.2.2 Components of vertebrate APC/C

The initial discovery of APC/C resulted from observations that certain cyclins are synchronously degraded as cells pass through mitosis [26]. Cdk1 functions to bring cells into mitosis, but its activity needs to be quenched during anaphase and telophase. If Cdk1 remains in its active state, chromosomes will not decondense, the nuclear envelope will not reassemble, and cell division is precluded [2]. Partial inactivation of Cdk1 is also required for the separation of sister chromatids during anaphase [76]. The major mechanism for Cdk1 inactivation is the destruction of its activating cyclins, cyclin A or B [2]. Cyclin A accumulates from late G_1 until mitosis, where it is degraded before metaphase, while cyclin B is degraded slightly later, in anaphase [77-82]. APC/C, the E3 ligase required to target cyclin B for destruction by the ubiquitin-proteasome pathway, was discovered nearly simultaneously in *Saccharomyces cerevisiae* [83], *Xenopus* eggs and clam oocytes [84, 85].

Subsequent work revealed that the vertebrate APC/C is a multiprotein complex consisting of at least 11 core subunits [86-88] (Fig. 5). The largest APC/C subunit is Apc1, which was initially discovered in *Saccharomyces cerevisiae* [89] and *Xenopus* eggs [90]. It is expressed at constant levels throughout the cell cycle but is specifically phosphorylated in mitosis [90, 91]. Although the function of Apc1 is largely unclear, it has been suggested that this subunit acts either as a scaffolding protein or as a protein required for the interaction with polyubiquitinated-proteins [92]. Two APC/C subunits, Apc2 and Apc11, contain cullin [86] and RING-H2 finger domains [93], respectively, which are also found

in subunits of SCF complexes. The cullin domain of Apc2 associates with the RING-H2 finger domain of Apc11 [94]. The RING-H2 finger of Apc11 further mediates interaction with the E2 ligases UbcH10 and UbcH5 [95]. An unexpected finding was that, *in vitro*, Apc11 and UbcH5 are sufficient for polyubiquitination of cyclin B [96]. Apc2/Apc11 along with UbcH10 can catalyze the ubiquitination of securin and cyclin B *in vitro* [97]. Four subunits of APC/C, Apc3/Cdc27, Apc6/Cdc16, Apc7 and Apc8/Cdc23, all contain a 34-residue tetratricopeptide (TPR) motif [98, 99]. This motif, which is found in many other proteins, is known to mediate protein-protein interactions in large multi-protein complexes [100]. Phosphorylation of Apc3/Cdc27, Apc6/Cdc16, Apc7 and Apc8/Cdc23 during mitosis is required for APC/C activation and mitotic progression [90, 101]. Apc3/Cdc27 and Apc7 have increased affinity for the APC/C coactivator Cdc20 when they are phosphorylated [102]. Apc3/Cdc27 and Apc7 bind to Cdc20 and Cdh1 through an isoleucine-arginine (IR) dipeptide motif in the C-terminus of the latter proteins [103, 104]. In addition, a sequence in the N-terminus of both Cdc20 and Cdh1 called the C-box, is necessary for coactivator-APC/C association in yeast [105]. The C-box is not required for Cdc20 binding to APC/C in human cells [106] but is thought to play a role in substrate recognition [107]. Apc10/Doc1 is a subunit of APC/C that contains a Doc domain that is also found in several other proteins of the ubiquitin-proteasome system, including HECT and cullin family members [108, 109]. Apc10 is not required for the stable interaction of other APC/C subunits, which is somewhat surprising because Apc10 directly interacts with Apc3/Cdc27, Apc7, and Apc11 [95, 110]. Mutants of Apc10 are known to prevent substrate binding to APC/C^{Cdh1}, suggesting that this subunit may play a role in substrate recognition [103, 111]. It is not yet clear whether the interaction of the substrate with Cdh1 and APC/C is directly or indirectly linked to Apc10. Currently, little is known about the function of the APC/C subunits Apc4, Apc5, Cdc26, and Apc13. Apc4 and Apc5 bind to Apc2 and Apc11, perhaps mediating the interaction of these proteins with the TPR-motif-containing APC/C subunits [104]. Cdc26 plays a role in maintaining the structure of APC/C [86, 87, 112]. Apc13, which binds to Apc5 and Apc8/Cdc23 [88], presumably plays a more critical role in meiosis than in mitosis, although its exact function is unclear [113].

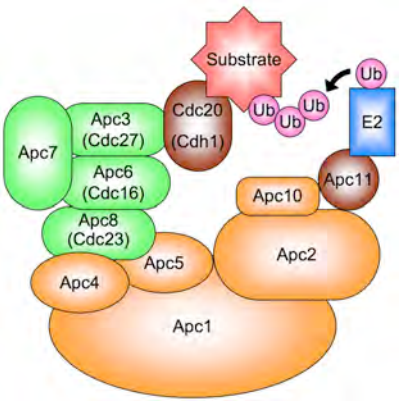

Fig. 5- Composition of the mammalian anaphase promoting complex/cyclosome (APC/C). See text for description of the model.

The fully assembled vertebrate APC/C consists of two large domains [114-116]. These domains, referred to as the "platform" and the "arc lamp", have a large amount of flexibility relative to each other [117]. When APC/C associates with the cofactor Cdh1, a conformational change in the relative positions of the "platform" and "arc lamp" occurs, perhaps mediating the activation of APC/C [116]. It is not yet known where Cdc20 binds to APC/C or if this binding results in a similar change of APC/C conformation.

Disruption of APC/C subunits by genetic manipulation leads to early lethality in every species examined thus far, from simple organisms like fungi to advanced vertebrates like mice [83, 118-120]. It is commonly believed that this lethality is due to the accumulation of securin and mitotic cyclins which inhibits chromosome segregation and mitotic exit [2]. However, APC/C is responsible for degradation of several other proteins as well, and it is entirely possible that overabundance of another substrate may result in cell death [117]. Therefore, it is critical that the activity of this complex be tightly regulated to prevent premature activation, yet also be flexible enough to allow for efficient transfer of ubiquitin when required.

2.2.3 Formation of APC/C and substrate recognition

Phosphorylation of APC/C subunits regulates both the function and the assembly of the mature complex. Three kinases mediate APC/C subunit phosphorylation: Protein Kinase A (PKA), Polo like kinase 1 (Plk1), and cyclin B/Cdk1 [121-124]. Phosphorylation of Apc3/Cdc27, Apc6/Cdc16 and Apc8/Cdc23 by cyclin B/Cdk1, leads to binding of Cdc20 to APC/C [84, 121, 124, 125]. Plk1 also promotes APC/C-mediated ubiquitination, but only in synergy with cyclin B/Cdk1 [121, 122]. In contrast to the activation of APC/C by these two kinases, PKA phosphorylation of APC/C inhibits the destruction of cyclin B, even when all activating cofactors are present [124]. It remains to be established which phosphatase functions to remove these inhibitory modifications.

The coactivators Cdc20 and Cdh1 are only transiently associated with APC/C. Substrates that have a destruction box (D box) or a KEN box are recognized and ubiquitinated by the APC/C [126, 127]. D box recognition elements, with the consensus amino acid sequence of RXXLXXXN, are found in several proteins, including mitotic cyclins, and are essential for ubiquitin-mediated destruction [127]. The KEN box, which contains a consensus KEN amino acid sequence, is found in several APC/C substrates and is preferentially, but not exclusively, recognized by APC/C^{Cdh1} [126]. Most substrates only bind to APC/C when it is activated by Cdc20 or Cdh1 [114]. Binding of Cdc20 to APC/C is tightly regulated to prevent premature APC/C-mediated ubiquitination. Regulation of Cdc20 occurs at various levels, with the protein being transcribed and translated during S and G2 phases, and phosphorylation occurring in a cell cycle dependent fashion [128-130]. Phosphorylation of Cdc20 does not induce the activation of APC/C, but results in coactivator recognition by components of the spindle assembly checkpoint in mitosis, resulting in APC/C inhibition and anaphase prevention [131]. This regulation of APC/C activity is critical to prevent the acquisition of chromosomal aberrations and is discussed in detail below.

2.2.4 Mitotic substrates of APC/C

Current models propose that APC/C^{Cdc20} is active during the early stages of mitosis, whereas APC/C^{Cdh1} is active in late mitosis and G1 (Table 1). In early mitosis, Cdh1 is phosphorylated by cyclin B/Cdk1, which precludes its association with APC/C [132-135]. Cyclin/Cdk1 activity is required to phosphorylate Cdc20, making the APC^{Cdc20} complex completely active [136]. Only after Cdk1 has been inactivated, by APC/C^{Cdc20}-mediated destruction of cyclin A and B, inhibitory phosphates can be removed from Cdh1 by Cdc14,

thereby allowing this coactivator to associate with APC/C [132, 137]. However, recent findings, which will be discussed later, challenge this view. A summary of known mitotic substrates of APC/C mediated ubiquitination can be found in Table 1.

Substrate	Start of degradation	APC/C activity involved	Reference
Cyclin A	Prophase	APC/C^{Cdc20} (early mitosis); APC/C^{Cdh1} (G1)	[82]
Nek2a	Prophase	APC/C^{Cdc20}	[144,145]
Cyclin B	Metaphase	APC/C^{Cdc20} and APC/C^{Cdh1}	[85,146,149]
Securin	Metaphase	APC/C^{Cdc20} and APC/C^{Cdh1}	[146-148]
Xkid	Metaphase	APC/C^{Cdc20} and APC/C^{Cdh1}	[157-159]
Prc1	Metaphase	APC/C^{Cdh1}	[162,163]
Kip1	Metaphase	APC/C^{Cdc20}	[160]
Cin8	Metaphase	APC/C^{Cdh1}	[161]
Geminin	Metaphase	Currently unkown	[165]
Tpx2	Anaphase	APC/C^{Cdh1}	[164]
Plk1	Before mitotic exit	APC/C^{Cdh1}	[167]
Aurora A	Before mitotic exit	APC/C^{Cdh1}	[172-174]
Cdc20	Before mitotic exit	APC/C^{Cdh1}	[126,170,171]
Aurora B	Before mitotic exit	APC/C^{Cdh1}	[168]
Anillin	Before mitotic exit	APC/C^{Cdh1}	[169]

Table 1- Mitotic substrates of APC/C.

Various mechanisms control the catalytic activity of APC/C. Early mitotic inhibitor 1 (Emi1) prevents premature activation of APC/C by interacting with newly synthesized Cdc20 [138-140]. In prophase, Plk1 phosphorylates Emi1. This modification targets Emi1 for destruction by the $SCF^{\beta TrCP}$ E3 ligase [141], which, in turn, leads to formation of active APC/C^{Cdc20}. Overexpression of Emi1 in cells lacking p53 has been shown to promote proliferation, tetraploidy and chromosomal instability [142], underscoring that Emi1 is a key mitotic regulator. A recent study suggests that following the destruction of Emi1 in prophase, Cdc20 continues to be inhibited through prometaphase by the tumor suppressor

protein Ras association domain family 1 (Rassf1A) [143]. At the end of prometaphase, when this inhibition ceases, APC/C^{Cdc20} becomes active and begins to ubiquitinate Nek2a and cyclin A, resulting in the complete destruction of these substrates in metaphase (Table 1) [82, 144, 145]. Nek2a binds to APC/C directly, without any need for adapter proteins or coactivator molecules [145]. Its subsequent destruction can then ensue upon APC/C activation by coactivator binding. Perhaps cyclin A is degraded in a similar fashion, but this remains to be confirmed.

In order for a cell to transit from metaphase to anaphase, several key substrates of APC/C need to be degraded, including cyclin B and securin (Table 1) [2, 85, 146-150]. Anaphase onset is marked by the separation of sister chromatids, which are held together by a large multi-protein complex called cohesin [151, 152]. Separase is the enzyme that mediates cohesin cleavage [151]. Until the metaphase to anaphase transition, securin binding and cyclin B/Cdk1-mediated phosphorylation inhibit the enzymatic activity of separase, thereby preventing premature sister chromatid separation (PMSCS), a hallmark of premature APC/C activation [76, 153, 154]. The phosphatase responsible for the removal of the inhibitory modification of separase is currently unknown [76]. A recent study has demonstrated that cyclin B binding to separase alone, without a requirement for cyclin B/Cdk1-mediated phosphorylation, is sufficient to inhibit separase activity [155]. The view that APC/C^{Cdc20} regulates degradation of both cyclin B and securin at the metaphase/anaphase transition, has been challenged by gene knockout studies showing that premature activation of APC/C^{Cdc20} leads to unscheduled degradation of cyclin B, but not securin [146]. Premature activation of APC/C^{Cdh1}, on the other hand, leads to the precocious degradation of securin, but not cyclin B, *in vivo* [146, 156]. The latter finding has established a critical role for the activity of APC/C^{Cdh1} in mitosis much earlier than originally thought.

In addition to securin and cyclin B, several other proteins need to be degraded to allow for anaphase entry and progression. *Xenopus* Xkid is implicated in generating the polar ejection force that makes the chromosomes align during metaphase [157, 158]. In order for chromosomes to migrate to the poles in anaphase, Xkid needs to be degraded. Both APC/C^{Cdc20} and APC/C^{Cdh1} have been shown to ubiquitinate Xkid *in vitro* [159]. The motor proteins Kip1 and Cin8 are degraded during anaphase by APC/C^{Cdc20} and APC/C^{Cdh1}, respectively, to allow polar movement of chromosomes [160, 161]. Another protein whose degradation is required for progression through anaphase is Prc1. This protein associates with the spindle midzone and is subjected to ubiquitination by APC/C^{Cdh1} [162, 163]. APC/C^{Cdh1} also degrades the microtubule-associated protein Tpx2. Its degradation starts in anaphase and continues through cytokinesis [164]. Geminin, a protein that inhibits DNA replication, is targeted by APC/C beginning at metaphase and continuing until the cell's exit from mitosis [165]. It is currently unclear which APC/C coactivator drives geminin destruction. Complete ablation of geminin results in endoreduplication [166], demonstrating that APC/C-mediated destruction of this protein requires strict temporal regulation. The mitotic kinases Plk1 [167] and Aurora B [168] are also destroyed late in mitosis. Their destruction by APC/C^{Cdh1} allows for entry into G1. Anillin, which controls the spatial contractility of myosin at the cleavage furrow during cytokinesis, is targeted by

APC/C^{Cdh1} for destruction late in cytokinesis and into G1 [169]. However, this destruction is not required for mitotic exit in mammalian cells. The activity of Cdh1 bound APC/C continues through G1, where it regulates the destruction of Cdc20 [126, 170, 171], Aurora A, and mitotic cyclins to prevent the re-accumulation of these proteins [172-174]. Control of APC/C activity during mitosis is controlled by a variety of inhibitory mechanisms, most notable the spindle assembly checkpoint.

2.3 CONTROLLING APC/C FUNCTION DURING MITOSIS

2.3.1 Introduction

The catalytic activity of APC/C during mitosis is mediated by several surveillance mechanisms, most notable the spindle assembly checkpoint. This checkpoint, which is often referred to simply as the mitotic checkpoint, is a molecular system that ensures accurate segregation of mitotic chromosomes by delaying anaphase onset until each kinetochore has properly attached to the mitotic spindle [175-177]. The kinetochore is a highly specialized region of mitotic chromosomes, corresponding to the centromere [178]. Centromeric regions are extremely complex; in that they have very large numbers of tandem repeats existing in arrays [179, 180]. Kinetochores consist of an inner and outer region. A large multiprotein complex can be found at the inner kinetochore. This complex appears as a narrow band of dense chromatin under electron microscopy and can be detected throughout the cell cycle [181, 182]. The outer kinetochore contains many of the proteins responsible for microtubule binding and signal transduction [181]. Trapping of microtubules by the kinetochore is an essential process, yet this capture is relatively fluid, with the microtubules able to grow and shrink at the site of attachment to the kinetochore [182]. The kinetochore complex is also highly dynamic, allowing some of its proteins to leave upon attachment of microtubules or during progression through mitosis [182]. Kinetochores that are not yet attached to mitotic microtubules and chromosome pairs that lack tension across sister chromatids generated by the spindle poles activate the spindle assembly checkpoint [183-187].

2.3.2 The spindle assembly checkpoint

Several proteins participate in the spindle assembly checkpoint-signaling pathway [181, 184]. The established view is that early in mitosis, various mitotic checkpoint proteins, including Bub1, BubR1, Bub3, Mad1, and Mad2 bind to the outer region of kinetochores that lack attachment or tension to generate a “stop anaphase” signal that diffuses into the mitotic cytosol [72, 184, 185, 188-198] (Fig. 6A). This signal is believed to consist of complexes of Bub3, BubR1 and Mad2, which bind and inhibit APC/C^{Cdc20} [2, 95, 199, 200]. As each pair of sister kinetochores attaches to microtubules, and microtubule motors generate tension that stretches them, production of inhibitory “stop anaphase” signals at those kinetochores quenches. Silencing of the “stop anaphase” signal only occurs after the final kinetochore has been captured by spindle microtubules [176, 190, 201], which triggers the release of inhibitory mitotic checkpoint protein complexes from APC/C^{Cdc20} (Fig. 6B). This then allows for APC/C^{Cdc20}-mediated destruction of cyclin B and securin [72, 73, 189, 192, 202, 203]. Separase, which in mammalian cells is inhibited through its association with securin and by cyclin B/Cdk1-mediated phosphorylation, subsequently

triggers sister chromatid disjunction by cleavage of the cohesin subunit Scc1 [151, 204]. This allows cells to progress into anaphase (Fig. 6C).

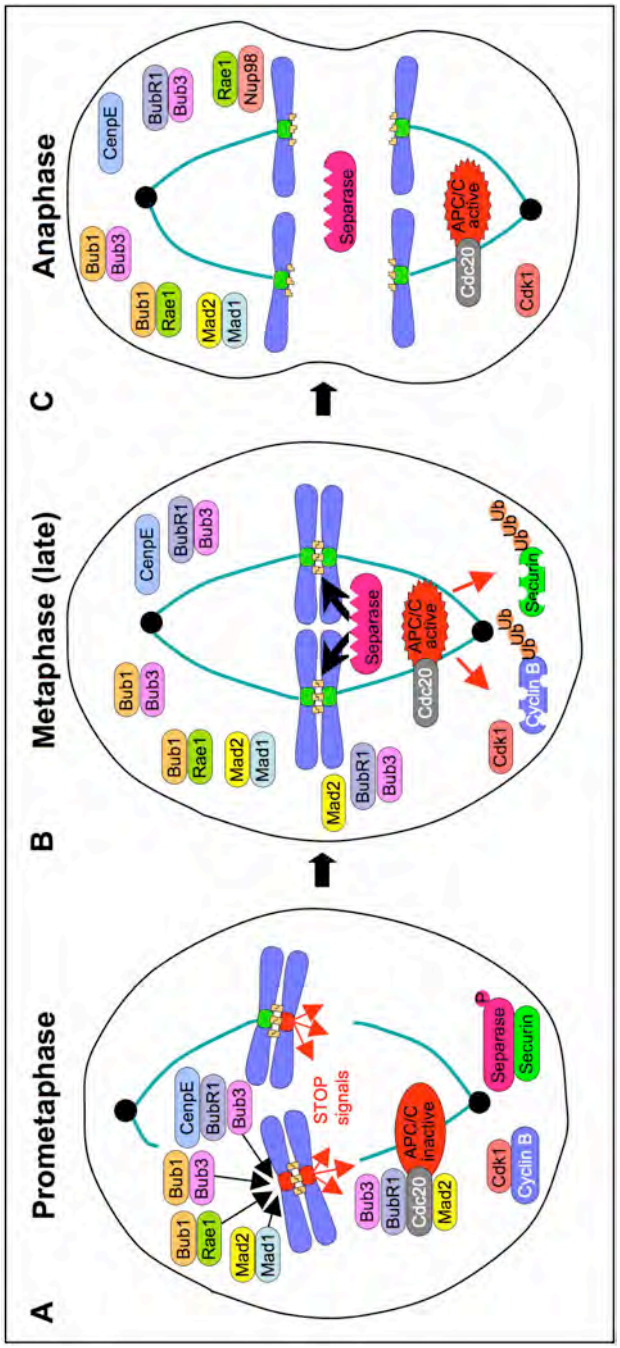

Fig. 6- Established model of APC/C regulation during the metaphase to anaphase transition. For further details, refer to text. Established model for spindle assembly checkpoint control where APC/C^{Cdc20} regulates both securin and cyclin B destruction in a checkpoint-dependent manner.

2.3.3 Other regulatory mechanisms of APC/C activity during mitosis

Recent work involving the nuclear transport factors Nup98 and Rae1 has challenged several aspects of the above model of spindle assembly checkpoint function [146]. Mutant mice that express low levels of both Nup98 and Rae1 exhibit PMSCS and massive aneuploidy. In cells from these mice, securin undergoes ubiquitin-mediated destruction in prometaphase instead of at anaphase onset. On the other hand, the timing of cyclin B destruction is normal in these cells. In prometaphase, Rae1 and Nup98 were observed to interact specifically with APC/C^{Cdh1} to prevent degradation of securin, but not APC/C^{Cdc20} (Fig. 7A), which was surprising as previous studies suggested that the formation of APC/C^{Cdh1} in early mitosis is inhibited through phosphorylation of Cdh1. However, this mechanism does not completely prevent APC/C^{Cdh1} formation in early mitosis. In fact, comparative coimmunoprecipitation experiments suggest that there are very similar amounts of APC/C^{Cdc20} and APC/C^{Cdh1} in early mitosis [156]. Dissociation of Rae1 and Nup98 from APC/C^{Cdh1} coincides with the release of BubR1 from APC/C^{Cdc20} [146]. Because the release of BubR1, and its coinhibitors Bub3 and Mad2, occurs at the metaphase/anaphase transition to activate APC/C^{Cdc20} and drive cells into anaphase, it is likely that the dissociation of Rae1 and Nup98 from APC/C^{Cdh1} also occurs at this mitotic stage and for the same purpose. If APC/C^{Cdc20} promotes anaphase through ubiquitination of both cyclin B and securin, one would expect to observe premature degradation of both of these proteins in cells in which BubR1 is deficient. However, only cyclin B is prematurely degraded in such cells, suggesting that Cdc20 is the primary coactivator for degradation of cyclin B, but not for degradation of securin *in vivo*. Conversely, APC/C^{Cdh1} activated by release of Rae1 and Nup98 might have a more important role in the destruction of securin (Fig. 7B, C). It is currently not understood how the Rae1-Nup98 complex is targeted to Cdh1 in response to lack of attachment at kinetochores and how it senses kinetochore capture to release its inhibition of APC/C^{Cdh1}. Rae1 is known to form a complex with Bub1 and localize to unattached kinetochores [193, 196]. One possibility is that these Bub1-Rae1 complexes regulate Nup98-Rae1 binding to APC/C^{Cdh1}, perhaps in much the same way as other kinetochore-associated mitotic checkpoint proteins promote binding of Bub3-BubR1-Mad2 complexes to APC/C^{Cdc20}.

Additional means of regulating the ubiquitin ligase activity of APC/C during mitosis are beginning to be elucidated. A complex of CBP and p300, two transcription factors, is essential for APC/C activity in mitosis [205, 206]. Through reciprocal immunoprecipitation assays, it has been shown that CBP/p300 interacts with three structural components of APC/C, in addition to the coactivators Cdc20 and Cdh1 [206]. Furthermore, CBP colocalizes with APC/C and siRNA-mediated depletion of CBP leads to reduced APC/C E3 ligase activity and the accumulation of cyclin B and Plk1 [206]. Together these findings implicate CBP/p300 in activation of both coactivator bound forms of APC/C during mitosis. This regulation may be through CBP/p300-mediated acetylation of APC/C subunits and/or the coactivators Cdh1 and Cdc20, although the details are not clearly established currently. It will be interesting to examine in future experiments whether the actions of CBP/p300 in mitosis are regulated by the spindle assembly checkpoint. The implication of Rae1-Nup98 and CBP/p300 complexes in mitotic regulation of APC/C

highlights that controlling APC/C activity in mitosis is far more complex than was once thought.

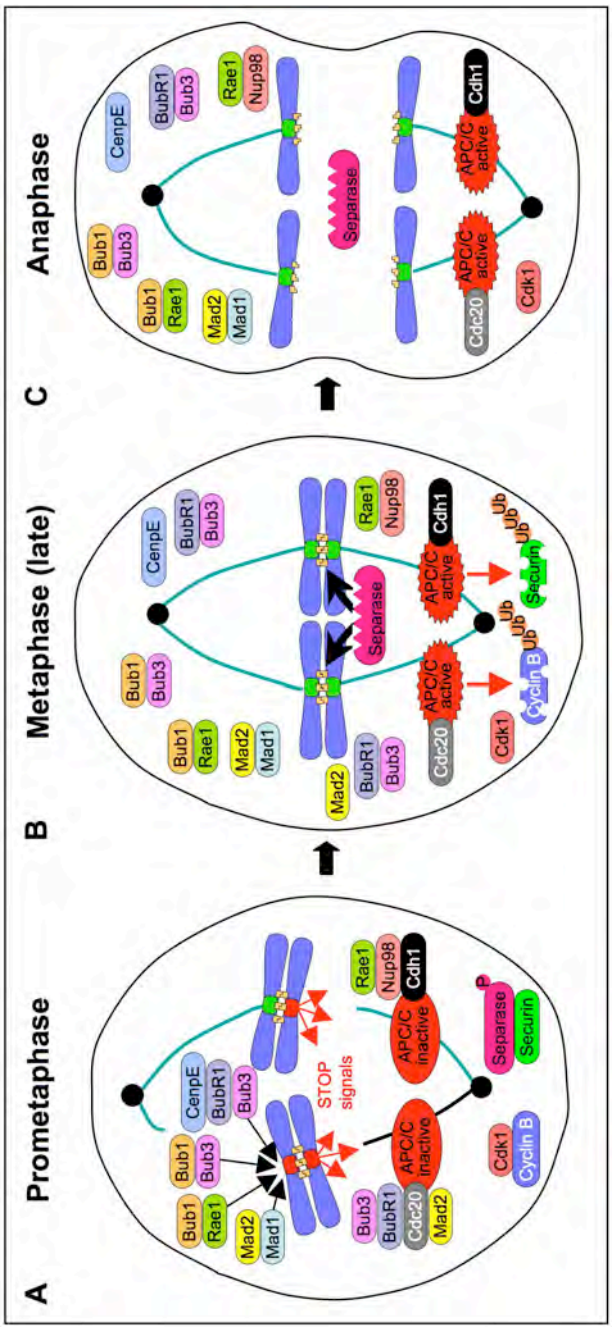

Fig. 7- Modified model of APC/C regulation during the metaphase to anaphase transition that includes the nuclear transport factors. See text for further details. In this model, the degradation of cyclin B and securin is mainly mediated by APC/C^{Cdc20} and APC/C^{Cdh1}, respectively.

2.3.4 Summary

An emerging theme in the regulation of APC/C-mediated degradation of substrates in mitosis is that three key components associate with APC/C (Fig. 8). These three components are: (1) APC/C coactivators; (2) inhibitory protein complexes that prevent unscheduled APC/C-mediated ubiquitination; and (3) the substrate that needs to be degraded. In this way, APC/C is loaded with the target substrate before the transfer of ubiquitin takes place through the association of an E2 enzyme. Once the inhibitory complex is removed from APC/C, swift degradation of bound substrates can ensue because the APC/C is primed for destruction by having the coactivator and the substrate existing in a large complex.

The first example that supports this hypothesis occurs in prophase. Two early mitotic substrates of APC/C are Nek2a and cyclin A. To prevent the unscheduled destruction of these proteins, Emi1 binds to both Cdc20 and Cdh1 before these two coactivators can associate with APC/C [138, 139]. Both Cdc20-Emi1 and Cdh1-Emi1 complexes can associate *in vitro* with APC/C, but only Cdc20-Emi1 loads onto APC/C *in vivo* in early mitosis [139]. Emi1 inhibits APC/C until Plk1 phosphorylates Emi1 and allows it to be recognized and ubiquitinated by the $SCF^{\beta TrCP}$ ubiquitin ligase [141]. Degradation of Emi1 allows Cdc20 activation of preformed APC/C-Nek2a complexes, which in turn leads to prompt destruction of Nek2a [139, 145]. It is therefore possible that Nek2a binds to APC/C while Cdc20-Emi1 complexes are forming and loaded onto APC/C (Fig. 8).

The second example that supports our model occurs during prometaphase. The well-established MCC inhibitory complex consists of Mad2, Bub3, and BubR1 bound to Cdc20. Association of this complex to APC/C^{Cdc20} inhibits the ligase activity until the spindle checkpoint is satisfied. Once the checkpoint is silenced, the inhibitory MCC complex dissociates from APC/C^{Cdc20}, which results in APC/C activation and swift destruction of cyclin B and potentially securin. Importantly, cyclin B already associates with APC/C in prometaphase even though its destruction takes place much later at the metaphase to anaphase transition [156]. Thus, both cyclin B and the MCC may bind to APC/C^{Cdc20} similarly to the way Nek2A and Emi1 associate with APC/C^{Cdc20} (Fig. 8).

The third example that supports our model also occurs during prometaphase. The Rae1-Nup98 inhibitory complex binds to securin-bound APC/C^{Cdh1} complexes [156]. The rapid degradation of securin occurs at a similar rate to cyclin B destruction when the spindle assembly checkpoint is satisfied. Release of Rae1-Nup98 and MCC inhibitory complexes occurs at nearly the same rate, but the mechanism behind the release of Rae1-Nup98 is not known. The rapid synchronous nature of cyclin B and securin degradation suggests that APC/C is primed for the destruction of these two key mitotic regulators. Having the substrate bound to inactivated APC/C could explain this precise regulation.

Currently, the events of late mitosis are not well understood at the mechanistic level. Following the metaphase-anaphase transition, ubiquitin-mediated destruction of substrates primarily occurs through APC/C^{Cdh1}, but it is not known if other inhibitory complexes

prevent the premature degradation of substrates during late mitosis. Perhaps additional complexes associate with APC/C to mediate the destruction of late mitotic substrates, however it is currently an unexplored topic.

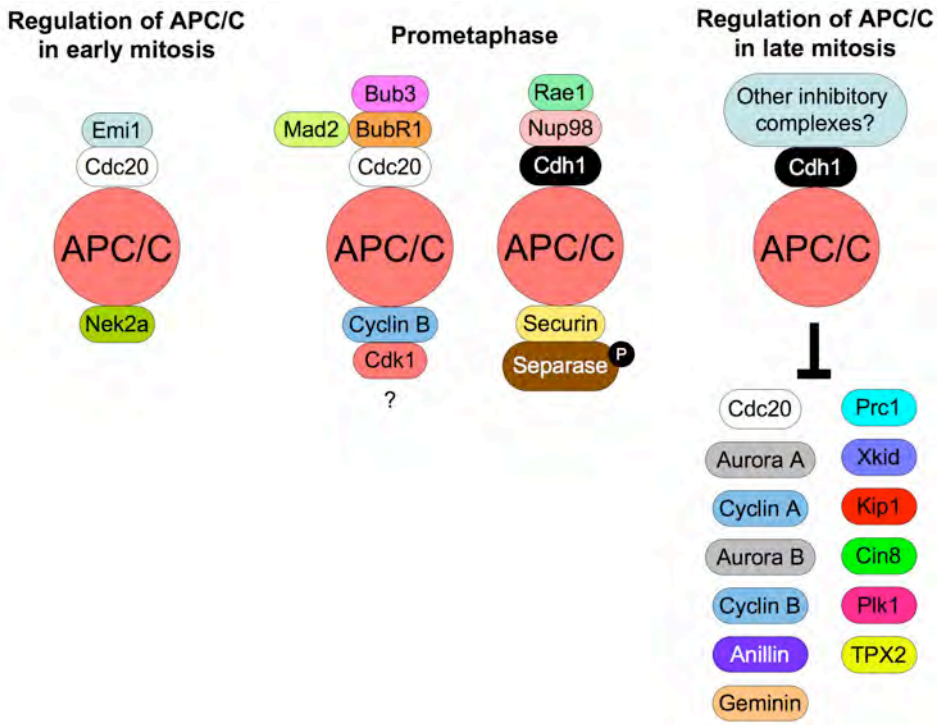

Fig. 8- Inhibitory mechanisms of APC/C catalytic activity during mitosis. In early mitosis, Emi1 regulates the activity of APC/C^{Cdc20}. The well-established MCC and the newly found Nup98-Rae1 complex inhibit the catalytic activity of APC/C during prometaphase, thereby preventing substrate degradation. *In vitro* evidence suggests that APC/C^{Cdc20} also regulates the destruction of securin, but it is not known if MCC also binds to this pool of APC/C. Perhaps additional inhibitory complexes are found later in mitosis to prevent the unscheduled degradation of other key mitotic regulator proteins. The existence of inhibitory complexes may explain how the cell discriminates between early and late mitotic APC/C substrates.

2.4 FUNCTIONAL ANALYSES OF MITOTIC CHECKPOINT PROTEINS

2.4.1 Introduction

Many spindle assembly checkpoint genes have now been disrupted in the mouse, the results of which are summarized in Table 2. Most of them belong to either the Bub (Budding uninhibited by benomyl) or the Mad (Mitotic arrest deficient) gene family. Members of these families were originally identified in yeast, where they are dispensable for survival [207]. It was therefore surprising that homozygous knockout mice all died very early in development. On the other hand, mice that are heterozygous null for these genes are born alive and seem to exhibit no overt phenotypes. Thus, the challenge for studying the function of individual mitotic checkpoint genes in the mouse is to disrupt their function

Table 2 Overview of mutant mouse strains with altered mitotic checkpoint gene expression

Mouse model	Checkpoint defect	Aneuploidy	Main segregation defect(s)	Susceptible to carcinogens	Spontaneous tumorigenesis	Early aging	References
Mad2$^{-/-}$	Yes	ND	Lagging chromosomes	–	–	–	[211]
Mad2$^{+/-}$	Yes	Yes	Lagging chromosomes	ND	Increased	No	[212, 213]
Mad2^{TA}	Yes	Yes	Lagging chrom./Chrom. Bridges(1)	ND	Increased	ND	[214]
Mad1$^{-/-}$	ND	ND	ND	–	–	–	[215]
Mad1$^{+/-}$	Yes	ND	Lagging chrom./Chrom. bridges	ND	Increased	ND	[215]
Bub1$^{-/-}$	Yes	ND	ND	–	–	–	[216, 217]
Bub1$^{+/-}$	Yes	Yes	Lagging chrom./Congression failure	Yes (DMBA)	Normal	No	[216]
Bub1$^{H/H}$	Yes	Yes	Lagging chrom./Congression failure	ND	Increased	No	[216]
Bub1$^{-/H}$	Yes	Yes	Lagging chrom./Congression failure	ND	Increased	No	[216]
BubR1$^{-/-}$	ND	ND	ND	–	–	–	[218, 219]
BubR1$^{+/-}$	Yes	Yes	Lagging chromosomes	Yes (AOM)	Normal	No	[213, 218, 219]
BubR1$^{+/-}$/APC$^{+/min}$	ND	Yes	ND	ND	Decreased(2)	–	[220]
BubR1$^{H/H}$	Yes	Yes	Lagging chromosomes	Yes (DMBA)	Normal	Yes	[213, 218]
Bub3$^{-/-}$	ND	ND	ND	–	–	–	[196, 221]
Bub3$^{+/-}$	Yes	Yes	Lagging chromosomes	Yes (DMBA)(3)	Normal	No	[196]
Bub3$^{+/-}$/p53$^{+/-}$	ND	ND	ND	ND	Normal	ND	[222]
Bub3$^{+/-}$/Rb$^{+/-}$	ND	ND	ND	ND	Normal	ND	[222]
Bub3$^{+/-}$/Rae1$^{+/-}$	Yes	Yes	Lagging chromosomes	Yes (DMBA)	Normal	Yes	[196]
Rae1$^{-/-}$	ND	ND	ND	–	–	–	[196]
Rae1$^{+/-}$	Yes	Yes	Lagging chromosomes	Yes (DMBA)	Normal	No	[196]
Rae1$^{+/-}$/Nup98$^{+/-}$	Yes	Yes	Lagging chromosomes	Yes (DMBA)	Normal	No	[156]
Cenp-E$^{-/-}$	ND	ND	Congression failure	–	–	–	[223]
Cenp-E$^{+/-}$	Yes	Yes	Congression failure	No (DMBA)(4)	Yes/No(5)	No	[224]
Cenp-E$^{+/-}$/p19$^{Arf-/-}$	ND	ND	ND	–	–	–	[224]

Table key: – = not relevant; ND = not determined; (1) = chromosome breaks and gaps were also observed at high frequency (2) = 50% decrease in overall tumor burden in GI tract but increased number of tumors in the colon; (3) = small increase that was not significant; (4) = decreased number of tumors compared to wild-type; (5) = increased in lung and spleen, decreased in liver.

significantly but not so severely that the embryo dies. This goal can be achieved through the use of hypomorphic alleles that express only a small fraction of normal protein levels. Proper spindle assembly checkpoint function and timely activation of APC/C and destruction of its substrates are essential for accurate chromosome segregation. Aberrant checkpoint signaling leads to defects in inhibition of APC/C activity, resulting in untimely entry into anaphase and a high risk of segregation defects (Table 2). PMSCS, which can ultimately contribute to chromosomal instability, is caused by separation of duplicated chromatids before entry into anaphase and is seen in several spindle assembly checkpoint mutant mice [208]. Kinetochores that lack microtubule attachment and/or tension but fail to activate the spindle assembly checkpoint and inhibit APC/C activity will produce lagging chromosomes. Additionally, merotelic kinetochore attachment causes lagging chromosomes [209]. During anaphase, a lagging chromosome does not move towards the spindle poles along with other chromosomes. It is distributed randomly in one of the two daughter cells, which may potentially result in a gain or loss of a whole chromosome. Other missegregation defects, including anaphase bridges may also be present when the spindle checkpoint is defective [208]. Here we will focus on several key players in the spindle checkpoint and the consequences of these genes being disrupted in mice.

2.4.2 Mad2 and Mad1

Information obtained from crystal structure studies demonstrates that Mad2 exists in two natively folded states. One is a less stable monomeric form with what is termed native fold 1 (N1-Mad2) and the other is a more stable homodimeric form with native fold 2 (N2-Mad2). Mad2 is able to switch between these two conformations, but this spontaneous process occurs very slowly [210]. The homodimer of N2-Mad2 is able to inhibit the activity of APC/C^{Cdc20}, whereas N1-Mad2 is unable to interact with Cdc20 [210]. Furthermore, a heterodimer of N1-Mad2 and N2-Mad2 is unable to inhibit APC/C activity as well, demonstrating that either conformation of N1-Mad2 into N2-Mad2 or replacement of N1-Mad2 in heterodimers is required for Cdc20 binding and subsequent inhibition of APC/C-mediated ubiquitination. Mutants of Cdc20 that are unable to bind to Mad2 undergo mitosis independently of Mad2, demonstrating how critical this inhibition by Mad2 is for mitotic progression [225]. Along with being distributed in the mitotic cytosol in early mitosis, Mad2 localizes to unattached kinetochores [226, 227]. This localization is often used as a cellular marker to demonstrate that the spindle assembly checkpoint is engaged. The recruitment of Mad2 to kinetochores is accomplished via its binding to Mad1 [228]. Mad1 stimulates the transition of Mad2 to the N2-Mad2 conformation, resulting in activation of Mad2 [210]. This conformational change causes N2-Mad2 to dissociate from Mad1, and is subsequently replaced by free Mad2 [131, 229]. Mad2 interacts with BubR1 and Bub3 in the mitotic cytosol to inhibit APC/C^{Cdc20} activity as part of the mitotic checkpoint complex or MCC. Upon microtubule attachment to kinetochores, Mad2-Mad1 complexes leave the kinetochore and conformational changes of Mad2 are inhibited [230]. Multiple phosphorylation sites exist on Mad2, but only non-phosphorylated Mad2 binds to

Cdc20 and Mad1 [231]. Transformation/transcription domain-associated protein TRRAP, which has chromatin-remodeling histone-acetlytransferase activity (HAT), specifically regulates the expression of both Mad1 and Mad2 [232]. Members of the E2F family of transcription factors also mediate Mad2 transcription. Mad2 also plays a role in reorienting chromosomes that are incorrectly attached to the spindle during the process of meiosis [233], but it is unknown if Mad2 does this during mitosis as well. A Mad2 related protein, Mad2L2, inhibits APC/C^{Cdh1} in much the same way as Mad2 does for APC/C^{Cdc20} [107].

Mad2 and Mad1 Mouse Studies. Mad2 was the first published mitotic checkpoint gene to be knocked out in mice [211]. Homozygous knockout mice die shortly after implantation around embryonic day E6.5. This lethality is coupled with massive chromosome missegregation and apoptosis [211]. When challenged with nocodazole, a microtubule de-polymerizing agent that triggers the activation of the spindle checkpoint, cells from Mad2 null embryos lack the ability to arrest in prometaphase. [211]. Cells that were post-mitotic however do not require Mad2 to survive. Studies on mouse embryonic fibroblasts (MEFs) suggest that the fidelity of the spindle assembly checkpoint is already affected when a single Mad2 gene copy is lacking, as a substantial proportion of Mad2 heterozygous MEFs develop aneuploidy and show PMSCS [234]. Mad2 haplo-insufficient mice seem to have a normal lifespan without any overt phenotypes. At about 18 months, the incidence of papillary lung adenocarcinomas, a usually very rare tumor, is significantly higher in Mad2 heterozygous mice than in wild-type mice [234]. Being as these tumors developed very late in life, it appears that cooperative mutations of tumor suppressors or oncogenes are required for transformation of checkpoint defective cells [234].

The expression of Mad2 is elevated in cells that lack pRb due to increased E2F transcription factor activity [235]. Mad2 is a direct E2F target, and the overexpression of these two proteins occurs in several tumor types [235]. This overexpression of Mad2 catalyzes the development of aneuploidy, demonstrating that the aberrant expression of this gene at abnormal times during the cell cycle may potentially contribute to the process of tumorigenesis. Transgenic Mad2 expressing mice have been reported very recently [214]. High levels of Mad2 in MEFs results in an initial reduction in growth due to accumulation of cell in mitosis, which similar to what is seen in yeast [225, 236]. However, some of these MEFs escape mitosis without segregation of DNA, resulting in the generation of tetraploid cells. A wide range of mitotic defects are detectable in these MEFs, demonstrating that the aberrant overexpression of Mad2 results in several features of chromosomal instability. Mice overexpressing Mad2 are susceptible to several tumor types, including lung adenomas, hepatomas, intestinal tumors and lymphomas [214]. Interestingly, tumor maintenance does not require the continual overexpression of Mad2. This study demonstrates that the transient overexpression of Mad2 and subsequent chromosome instability can be an important stimulus in the initiation and progression of certain tumor types.

Mad1 has recently been ablated in the mouse [215]. Homozygous null mice die during embryogenesis, although it has not yet been determined at what stage of development Mad1 is essential. Mad1 heterozygous mice are viable and indistinguishable from wild-

type littermates. Mad1 heterozygous MEFs have increased incidence of lagging chromosomes and bridging, two defects that are also seen at increased rates in Mad2 heterozygous null MEFs [215]. The spontaneous tumor incidence of 18-month-old Mad1 heterozygous mice was about two-fold higher than in age-matched wild-type controls, indicating the Mad1 insufficiency promotes the development of spontaneous tumors, just like Mad2. Hemangiosarcomas and lung adenomas/adenocarcinomas were among the most frequently observed tumors in Mad1 haploinsufficient mice. It remains to be established whether Mad1 mutant mice have increased susceptibility to carcinogens. About 40% of nude mice injected with Mad1 heterozygous MEFs develop tumors within 6-10 weeks, compared to 0% for control MEFs, further confirming that partial loss of Mad1 increases the risk of neoplastic transformation.

2.4.3 Bub3

Bub3 is a dispensable protein in yeast that is essential for vertebrate embryogenesis [196, 221, 237]. Bub3 binds to BubR1 and Bub1 through a Gle2-binding sequence (GLEBS motif) and this binding is required for kinetochore localization of these two proteins [238]. When chromosomes are aligned properly at the metaphase plate, Bub3 is undetectable at the kinetochore. Lagging chromosomes that have not attached properly to the mitotic spindle exhibit high levels of Bub3 at the kinetochore, implicating this protein as a sensor of microtubule attachment [239]. The MCC inhibitory complex contains Bub3, BubR1, Mad2, and Cdc20 to specifically inhibit APC/C^{Cdc20} in the mitotic cytotsol. In addition to its role during mitosis, Bub3, like Cdc20, also functions as transcriptional regulator during interphase by associating with histone deacetylases [240].

Bub3 Mouse Studies. Similar to Mad2 knockouts, complete ablation of Bub3 causes mouse embryos to die shortly after implantation in the uterus [196, 221]. Cells from these embryos show features of mitotic disarray, including lagging chromosomes and chromatin bridging. Micronuclei also develop due to lagging chromosomes that do not congregate with the rest of the DNA in the newly formed daughter cell nucleus [221]. In the presence of nocodazole, Bub3 null cells fail to induce a sustained mitotic arrest [221], confirming that their spindle assembly checkpoint is impaired. Heterozygous loss of Bub3 results in a partial loss of spindle assembly checkpoint function, coupled with increased chromosome missegregation and development of moderate aneuploidy in both MEFs and splenocytes [196]. When challenged with the carcinogen DMBA, Bub3 haplo-insufficient mice develop lung adenocarcinomas at a slightly higher incidence than control animals, although the increase is not statistically significant [196]. Bub3 haplo-insufficient mice are not predisposed to spontaneous tumorigenesis, and furthermore, the spectrum of tumor types found in these mice is similar to that of wild-type mice [213, 241]. p53 or Rb1 heterozygous knockout mice bred onto a Bub3 heterozygous background have similar tumor spectrums and tumor incidences as their counterparts that have two intact Bub3 alleles [241]. Thus, despite accumulation of aneuploid cells, Bub3 haplo-insufficient mice do not seem to be prone to spontaneous tumors or to developing tumors on a predisposed genetic background.

2.4.4 Rae1

Rae1, also called Gle2 or mrnp41, is a transport factor that mediates nuclear export of mRNA through nuclear pores during interphase. Rae1 and Bub3 are WD repeat-containing proteins that share remarkable sequence similarity both inside and outside of these repeats [238, 242]. The finding that Rae1 binds to the GLEBS motif of Bub1 at kinetochores during mitosis suggested a mitotic function for this protein [193]. Additionally, the nucleoporin Nup98 contains a GLEBS motif that interacts with Rae1 throughout the cell cycle [243], and this complex was found to be important for regulating the activity of APC/C^{Cdh1} as mentioned previously [146, 156]. Additionally, Rae1 binds to NuMA (Nuclear Mitotic Apparatus) during mitosis, which is a required interaction for normal mitotic spindle formation [244, 245].

Rae1 Mouse Studies. Rae1 null mice exhibit a phenotype that is reminiscent of Bub3 null mice, strengthening the idea that these two proteins are highly related [196]. Furthermore, when challenged with nocodazole, Rae1 haplo-insufficient MEFs fail to arrest in prometaphase, just like Bub3 heterozygous MEFs [196]. These findings, combined with the observation that Rae1 heterozygous mice and MEFs have increased aneuploidy, indicates that Rae1 is a genuine and essential component of the spindle assembly checkpoint [196]. Importantly, the lung tumor incidence and burden are both significantly higher in Rae1 heterozygous mice than in wild-type mice when challenged with DMBA [196], although these mice are not prone to spontaneous tumor formation [213].

Mice that are heterozygous for both Bub3 and Rae1 accumulate many more aneuploid cells than the corresponding single heterozygotes, yet remain viable [196]. PMSCS is also much higher in double mutant mice than in single mutant mice, demonstrating that Rae1 and Bub3 are related proteins with essential, and cooperating roles in the mitotic checkpoint. In carcinogen treated mice, the lung tumor incidence and tumor number of double heterozygous mice is very similar to Rae1 single heterozygous animals. Since the aneuploidy is 3-fold higher in the double heterozygotes, it seems that the aneuploidy might not be the primary cause of increased carcinogen-induced tumorigenesis in mitotic checkpoint defective animals [196]. Also, these mice, despite massive aneuploidy, are not prone to developing spontaneous tumors [213]. However, mice that are double haploinsufficient for Bub3 and Rae1 exhibit several aging-associated phenotypes significantly earlier than wild-type mice (Chapter 6) [213]. These results are discussed in more detail later.

Mice that are haplo-insufficient for Nup98 and Rae1 have substantial PMSCS and aneuploidy [146]. Concordantly, these mice are predisposed to carcinogen induced tumor formation (Chapter 7) [156]. However, as is the case for Bub3/Rae1 double haplo-insufficient animals, the spontaneous tumor incidence remains unchanged in these animals [156]. This model was extremely useful however, as cells from these animals were used to identify a novel regulatory complex of APC/C activity during mitosis [146, 156].

2.4.5 BubR1

The spindle checkpoint protein BubR1 is the mammalian homolog of yeast Mad3 [238]. Protein levels of BubR1 are cyclical, such that it is extremely low in G_1 until late G_2, but rises markedly at mitosis [246]. BubR1 contains a GLEBS motif that results in constitutive binding of BubR1 to Bub3 [193]. This binding is required for recruitment of BubR1 to kinetochores during prometaphase, as mutations in the GLEBS motif ablate the binding and localization of BubR1 [238]. BubR1 mediated inhibition of APC/C does not require the binding of Bub3 however [95], as Cdc20 can be bound directly by BubR1. Cenp-E, a mitotic motor protein, binds to BubR1, and maintains stable microtubule-kinetochore interactions, which are required for proper checkpoint signaling [247]. BubR1 contains a kinase domain, which yeast Mad3 does not, and this kinase is essential for other spindle checkpoint functions other than APC/C inhibition [201]. The kinase activity of BubR1, both for self-phosphorylation and for non-specific targets, is stimulated upon the binding of Cenp-E [201]. Interestingly, p53 can control the transcription of BubR1 [248], although other proteins can compensate for p53 loss.

BubR1 Mouse Studies. Two laboratories have generated mice that lack BubR1. Wang and colleagues disrupted the BubR1 gene through retroviral insertion mutagenesis. They show that complete ablation of BubR1 results in embryonic lethality with massive apoptosis [249]. MEFs that are heterozygous for the retrovirally inactivated BubR1 allele express about 25% of normal protein levels [219, 249]. These MEFs form micronuclei at a high frequency and have the tendency to become hypo- or hyperdiploid [250]. When challenged with nocodazole, these MEFs seem unable to induce a sustained arrest in prometaphase, coupled with impaired BubR1 phosphorylation, premature securin and cyclin B degradation, and early mitotic exit [219, 249, 250]. Mice that are heterozygous for retrovirally inactivated BubR1 exhibit profound splenomegaly, a condition where the spleen is much larger than in normal mice [249]. These mice further show an increased susceptibility to azoxymethane (AOM), a carcinogen that primarily induces intestinal tumors in mice. Surprisingly, BubR1 heterozygotes not only developed intestinal tumors at a higher incidence than wild-type mice, but also lung tumors [219].

Mice carrying the Adenomatous polyposis coli (Apc) Min allele typically develop numerous tumors in the small intestine and an occasional tumor in the colon. When one BubR1 gene copy is inactivated in these mice, the total number of tumors declines significantly due to a dramatic drop in the average number of tumors in the small intestine [250]. Double mutant mice develop 10-fold more colonic polyps than mice that only carry the Apc^{min} mutation [250], although the contribution of colonic polyps to the overall tumor burden remains low. The exact reason for this difference remains unclear. MEFs of double compound mutant mice exhibit increased proliferation potential along with increased genetic instability [250]. These results suggest that BubR1 and Apc functionally interact in regulating the transition of metaphase to anaphase, and deregulation of this may play a role in genomic instability development and the process of colon carcinogenesis.

Recently, we have reported the generation of a series of mice in which the expression of BubR1 is reduced in a graded fashion from normal levels to zero by the use of wild-type, knockout and hypomorphic alleles (Chapter 3) [218]. Hypomorphic alleles can be created

by utilizing a gene targeting strategy that introduces a neomycin resistance cassette carrying a cryptic exon into an intron of the endogenous murine allele [251]. During the processing of RNA, some transcripts will contain the cryptic exon, while others will skip over this exon and create a normal protein. Those with the cryptic exon have premature termination sequences in all three reading frames, leading to premature truncation of the protein. We found that mice with only 5% of normal BubR1 levels are born alive but die on the day of birth, most likely due to the accumulation of vast amounts of aneuploid cells during embryogenesis [218]. On the other hand, mice that express about 10% of normal BubR1 protein are viable and develop into adult mice. 10% BubR1 MEFs have low spindle assembly checkpoint activity, and coincidently are highly aneuploid [218]. These MEFs have high rates of PMSCS and lagging chromosomes [218]. Mice with 10% BubR1 have no detectable aneuploidy at birth, but accumulate more and more cells with abnormal chromosome numbers as they age [218]. For instance, 3% and 33% of their splenocytes are aneuploid at 2 and 12 months, respectively. In contrast, splenocytes from heterozygous BubR1 knockout mice, which express 30% of normal BubR1 protein, have no detectable aneuploidy or PMSCS [218]. $BubR1^{+/-}$ MEFs develop mild but significant aneuploidy, but no significant PMSCS. Only about 3% of mice with 10% of normal BubR1 develop spontaneous tumors [218], but, when treated with DMBA, they develop lung tumors at a significantly higher incidence then their wild-type littermates [213]. We also found that these animals exhibit many features of premature aging, which will be highlighted shortly.

2.4.6 Bub1

Bub1 is a protein kinase that localizes to unattached kinetochores early in prophase, where it plays a role in assisting the mitotic checkpoint apparatus both in response to spindle damage and for mitotic timing [252]. Bub1 is required for recruitment of Mad1-Mad2 protein complexes to unattached kinetochores. These complexes alter the conformation of "free" Mad2, thereby allowing it to interact efficiently and stably with Cdc20. The resulting Mad2-Cdc20 complexes, which may further contain BubR1 and Bub3, then bind and inhibit the APC/C. Bub1, along with BubR1, function in the checkpoint to sense proper microtubule tension [253]. Bub1 also functions to sense microtubule attachment to the kinetochore, thereby functioning at two levels in the checkpoint [197, 254]. Bub1 exists in a complex with Bub3 and Mad1 [255]. Bub1 is a kinase capable of self-phosphorylation that has been demonstrated to also phosphorylate Mad1 *in vitro*, but apparently this is either not important for *in vivo* checkpoint signaling or it does not occur [256]. The localization of Bub3, Mad1, Mad2, BubR1, Cenp-E, Cenp-F and Cenp-I to kinetochores requires Bub1, but not its kinase activity [198, 257, 258]. Phosphorylation of Bub1 at kinetochores, resulting in its activation, has been shown recently to aid in the generation of the spindle checkpoint signal, and is believed to be important during late pro-metaphase when only a few chromatids lack microtubule capture [259]. Bub1 phosphorylates Cdc20, thereby preventing the latter from activating the APC/C [260]. Expression of Cdc20 incapable of phosphorylation by Bub1 or expression of a kinase-dead Bub1 results in premature mitotic exit and defective checkpoint function, indicating the importance of Bub1 kinase activity [261, 262]. Bub1 is cleaved during the process of apoptosis, but whether this is an essential event or if it is just a feature of programmed cell death is debatable [263].

To study the role of Bub1 in chromosome segregation and tumorigenesis at the level of the whole organism, we generated a series of mutant mice in which expression of Bub1 is reduced in graded fashion by the use of wild-type, hypomorphic and knockout alleles [216]. We found that hypomorphic mice with low amounts Bub1 protein are viable, fertile and overtly normal despite low levels of Bub1, severely weakened spindle assembly checkpoint activity, and massive aneuploidy. Bub1 haploinsufficient mice, which express more residual Bub1 protein than Bub1 hypomorphic mice, also exhibit reduced checkpoint activity and increased aneuploidy, but to a lesser extent. Although cells from Bub1 hypomorphic and haploinsufficient mice have remarkably similar rates chromosome missegregation, cell survival after an aberrant separation is shown to increase dramatically with decreasing Bub1 levels. Bub1 hypomorphic mice are prone to a variety of spontaneous tumors, including lymphomas, lung adenocarcinomas, hepatocellular carcinomas and sarcomas. In contrast, Bub1 haploinsufficient mice are somewhat protected against spontaneous tumorigenesis. These findings demonstrate Bub1 drives neoplastic cell transformation when its level of expression drops below a critical threshold, and suggest that besides ensuring proper chromosome segregation, Bub1 is important for mediating cell death when chromosomes happen to be missegregated (Chapter 8).

2.4.7 Cenp-E

Centromere-associated Protein-E (Cenp-E) is an essential, highly conserved, 312 kDa, mitosis specific, cell-cycle regulated kinesin-like motor protein that accumulates in late G2 and mitosis [223, 264-266]. The end of mitosis triggers the rapid destruction of Cenp-E. Both the proteins responsible for this degradation and the mechanism behind its synchronous downregulation is currently unknown [267]. Two main functions are performed by Cenp-E during mitosis. Firstly, Cenp-E participates in making and/or maintaining the interaction between the microtubules of the mitotic spindle and mitotic chromosomes [223, 268]. Secondly, during spindle assembly checkpoint activation, Cenp-E activates the kinase activity of BubR1 [201, 269] and subsequently silences the production of the "stop anaphase" signal that is generated by BubR1 in response to proper attachment to the mitotic spindle [270]. In contrast to other spindle assembly checkpoint proteins, Cenp-E expression and function seems to be narrowly restricted to mitosis. Therefore, downregulations or mutations of this gene may only affect the process of accurate chromosomal separation, and may have no additional consequences.

Cenp-E Mouse Studies. Cells in which Cenp-E is completely depleted by Cre-mediated recombination are characterized by unstable kinetochore-microtubule attachments and high rates of chromosome missegregation [223]. Furthermore, such cells are unable to induce a sustained prometaphase arrest in the presence of spindle damage, indicating that Cenp-E is an essential component of the spindle assembly checkpoint. Cenp-$E^{+/-}$ MEFs, which express 50% of normal protein, rapidly develop aneuploidy [224]. This aneuploidy is also detectable in lymphocytes, splenocytes and colonic epithelial cells from Cenp-$E^{+/-}$ mice [224], demonstrating that disruption of a single allele of Cenp-E results in missegregation of chromosomes during mitosis. These mice also exhibit a predisposition to spontaneous tumor formation in both the spleen and lung, suggesting a link between aneuploidy and

tumor formation. This is not a generalizable conclusion, however, as the number of spontaneous liver tumors decreases in Cenp-E heterozygous mice. In addition, in contrast to all models of defective checkpoint function that have been tested, challenging Cenp-$E^{+/-}$ mice with DMBA also resulted in lower numbers of tumors than in wild-type control mice [224]. In fact, these mice appear to be protected against both carcinogen induced and $p19^{Arf-/-}$ initiated tumor formation. Together, these data suggest that aneuploidy as the result of reduced Cenp-E expression can act both as a promoter and inhibitor of the tumorigenic process in mice.

2.4.8 Summary

In conclusion, with the exception of certain tissues of Cenp-$E^{+/-}$ mice, $Mad1^{+/-}$ mice, Mad2 heterozygous and transgenic mice, and Bub1 hypomorphic mice, a commonality between the distinct mouse models for mitotic checkpoint failure is the lack of an increase in spontaneous tumors. However, with the exception of Cenp-$E^{+/-}$ mice, mouse models with defective spindle assembly checkpoints are prone to carcinogen-induced tumors. Thus, it seems that the kinds of gene mutations introduced by carcinogens do not occur over the normal lifetime of a laboratory mouse. Progress in understanding how mitotic checkpoint failure predisposes cells to transformation appears to depend on the identification of cancer-critical genes targeted by carcinogens such as DMBA and AOM. Mitotic checkpoint failure does not seem to accelerate tumorigenesis in mice heterozygous for tumor suppressor genes such as p53, Rb1 and Apc. This is quite surprising, as one would expect increased chromosome missegregation to increase the frequency with which the remaining wild-type gene copy is lost. One possibility is that the loss of whole chromosomes on which these tumor suppressor genes are located might trigger a cellular response that leads to apoptosis or senescence. Because aneuploidy can exert tumor-suppressive, tumor-promoting, or benign effects depending upon the tissue or cell type and the additional cancer-critical gene mutations that are present in a cell, it is imperative to identify the genetic alterations that synergize with spindle assembly checkpoint mutations in cancer development. Findings revealed from such studies in mice may lead to novel therapeutics that may be able to target human cancers in ways that previously would have been overlooked.

2.5 HUMAN CANCER AND THE MITOTIC CHECKPOINT

2.5.1 Introduction

Because the spindle assembly checkpoint prevents the development of aneuploidy and because the vast majority of human tumors are aneuploid, many efforts have looked for mutations in spindle assembly checkpoint genes in human cancers. Most established tumor cell lines exhibit spindle assembly checkpoint defects [271, 272], but the molecular reason for these aberrancies has been difficult to determine. Using many methods, including direct sequencing and gene expression profiling, have been used to identify the protein that may be responsible. Several studies have reported alterations in various mitotic checkpoint protein genes, including Mad2, Bub1, and BubR1, in human cancers (Table 3 and 4) [175, 273-275], which suggests a potential link between deregulated mitotic checkpoint

inhibition of APC/C and chromosomal instability and cancer. The results of these investigations, both positive and negative, are summarized below.

2.5.2 Mad2

Sequence mutations of Mad2 are rare in human cancer. Established hepatocellular carcinoma (n=8 [271]) and lung cancer cell lines (n=21 [276], n=30 [277]) have no mutations in Mad2. In primary tumors, Mad2 is not mutated in aneuploid colorectal cancers (n=19 [278]), digestive tract tumors (n=32 [279]), soft-tissue sarcomas (n=42 [280]), hepatocellular carcinomas (n=10 [280], n=50 [271]), lung cancers (n=25 [276], n=30 [277]), or breast tumors (n=48 [277]). A small deletion was found in 1 of 22 breast cancer cell lines [281], but additional studies have revealed no additional mutations (n=12 [282]). A point mutation in codon 190 of Mad2 was found in 1 of 44 primary bladder cancers [280], although transfection of this mutant cDNA into cells did not affect mitotic arrest. Conversely, Mad2 is frequently mutated in primary gastric cancers (n=22 of 49 [283]) and cell lines (n=1 of 5 [283]).

Although mutations in Mad2 are rare, differential expression patterns of Mad2 have been found in several tumor types. Hyper-methylation of the Mad2 promoter is correlated with a downregulation in Mad2 and has been seen in hepatocellular carcinomas (n=5 of 10 [284]). Other cancer cell lines that have lower than normal Mad2 expression include ovarian cancer (n=3 of 7 [285]), hepatoma cell lines (n=6 of 11 [286]), adult T-cell leukemia (ATLL, n=2 of 6 [287]), and nasopharyngeal cancer (n=2 of 5 [288]). Patients with Barrett's esophagus, a precancerous condition, may exhibit a downregulation (n=8 of 33) or an upregulation (n=8 of 33) in Mad2 [289]. Esophageal cancers are similar, where lower levels (n=2 of 4) and higher levels (n=1 of 4) of Mad2 have been found [289]. Mad2 is elevated in a high percentage of gastric tumors (n=25 of 34 [290]), but this upregulation does not correlate with any clinicopathological characteristics. Mad2 is also overexpressed in both breast tumor cell lines (n=5 of 12) and primary tumors (n=5 of 9 [282]), as well as primary retinoblastomas [235], colorectal cancers [291, 292], and bladder cancers [235]. Because Mad2 is a direct target of E2F mediated transcription [235], any event that deregulates Rb function (Fig. 3) can lead to aberrant expression of Mad2. Therefore, it is not surprising to find frequent overexpression of Mad2 in human cancers as Rb is often mutated or deleted.

2.5.3 Bub3

Mutations of Bub3 appear to be extremely rare in human cancers. Colorectal cancers do not have reported mutations in the Bub3 coding sequence (n=19, [278]); nor do glioblastomas (n=22 [293]), lung tumors (n=44 [294]) or osteosarcomas (n=32 [295]). Hepatocellular carcinoma (n=8 [271]), bladder cancer [280], breast cancer (n=12 [282]) and osteosarcoma cell lines (n=7 [295]) also have no mutations in Bub3.

Aberrant levels of Bub3 also appear to be rare in human cancers. Lung adenocarcinomas have reduced expression (n=7 of 18 [296]) of Bub3. In the same sample set, Bub3 was overexpressed in certain tumors (n=5 of 18 [296]). Other tumors that also display higher

than normal levels of Bub3 include gastric carcinomas (n=34 of 43 [297]), primary breast tumors (n=7 of 9 [282]), and breast cancer cell lines (n=3 of 12 [282]).

2.5.4 BubR1

Coding sequence mutations in BubR1 are rare in human cancers or established cancer cell lines. BubR1 is not mutated in the following cell lines: breast tumor (n=12 [282], n=19 [298]), hepatocellular carcinoma (n=8 [271]), lung cancer (n=47 [299]), thyroid tumor (n=8 [300]), pancreatic cancer (n=9 [301]), or other various cell lines (n=6 [302]). Missense mutations in BubR1 exist in colorectal carcinoma cell lines (n=2 of 19 [272]). Most primary cancers also have no mutations in BubR1. This includes colorectal tumors (n=19 [278], n=22 [302]), hepatocellular carcinoma (n=7 [302]), lung cancers (n=44 [294]), B-cell lymphomas (n=8 [303]), clear cell renal carcinomas (n=2 [302]), or glioblastomas (n=22 [293]). Primary ATLL have frequent mutations in BubR1 (n=2 missense mutations and one 47bp deletion in 10 ATLL [303]).

Variations in BubR1 expression have been found in several tumor types. Thyroid cancer cell lines have an impaired ability to phosphorylate BubR1, but also have reduced overall protein levels (n=3 of 8 [300]). A greater than 50% reduction in BubR1 was found in colorectal carcinomas (n=10 of 116 [302]). Alternatively, BubR1 is overexpressed in gastric carcinomas (n=29 of 43 [297]), primary breast tumors (n=8 of 9 [282]), breast cancer cell lines (n=8 of 12 [282]), and lung cancer cell lines (n=8 of 8 [304]).

A rare human disorder, called mosaic-variegated aneuploidy (MVA) has recently been shown to have truncating and missense mutations in the coding sequence of BubR1 in 5 of 8 patients (Fig. 9) [305]. In a second study, all 7 Japanese MVA patients had monoallelic BubR1 mutations with polymorphisms in the second allele that correlate with reduced BubR1 expression [306]. MVA was first described in a pigtail macaque monkey that had severe delays in development and apparent mental retardation, as well as abnormal karyotypes of lymphocytes and fibroblasts, that were consistently trisomic, but for varying chromosomes [307]. MVA in humans is characterized by karyotypical abnormalities including aneuploidy and PMSCS, short life-span, severe microcephaly, mental retardation, optical atrophy and cataracts, facial dysmorphisms and heart defects, although the degree of these phenotypes is highly variable [308-314]. Notably, several of these patients developed tumors early in life, most commonly Wilm's tumors, but also rhabdomyosarcomas, nephroblastomas and myelodysplasias [310-312, 315-318]. Out of 22 patients, 11 have had tumors, but many of these individuals died early in life or had no follow-up following early diagnosis [319], suggesting that these figures may under-represent the cancer formation in MVA patients. This is the first disorder that is attributed to germline mutations of a spindle checkpoint protein that also predisposes individuals to tumor development [305]. However, not all cases of MVA correlate with mutant BubR1 alleles, opening the possibility that an alternative mutation or the aberrant expression in other members of the spindle assembly checkpoint machinery may be present. Interestingly, non-MVA related Wilm's tumors (n=30), acute lymphoblastic leukemias (n=10), primary rhabdomyosarcomas (n=9) and rhabdomyosarcomas cell lines (n=11) do not have any mutations in BubR1 [320], demonstrating that these tumors arise

preferentially when BubR1 is mutated, although this step is not essential for the formation of these tumors. It is not known if these tumors that lack mutations in BubR1 express BubR1 at lower than normal levels, which may explain why these tumors develop spontaneously in non-MVA related individuals. Another important point to remember is that every cell of an MVA patient has impaired BubR1 function, yet most individuals develop only one or two tumors. Therefore, at the cellular level, the cancer risk remains low and other events are clearly required for oncogenesis to occur.

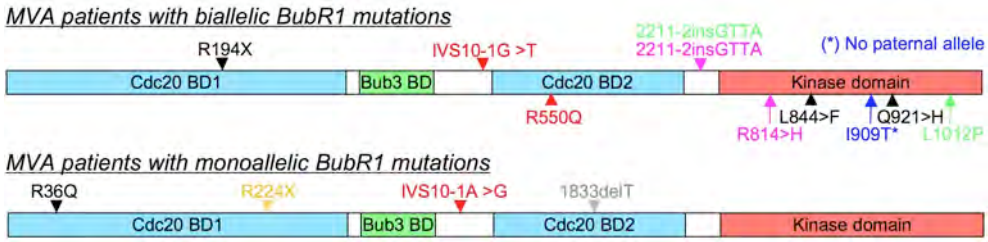

Fig. 9. Overview of BubR1 mutations underlying MVA syndrome. See text for details. Note that BubR1 mutations found in the same patient have the same font color.

2.5.5 Bub1

The spindle assembly checkpoint gene with the most frequent mutations in human tumors occurs in the coding sequence of Bub1. In colorectal cancer cell lines, a dominant negative heterozygous deletion was identified (n=1 of 19 [272]), but mice that carry this mutation are not susceptible to spontaneous tumorigenesis [321]). Additionally, missense mutations of Bub1 are seen in colorectal carcinoma (n=1 of 19 [272]), lung cancer (n=1 of 88 [299]), and pancreatic cancer cell lines (n=1 of 9 [301]). In primary tumors, missense mutations occur in lung adenocarcinomas (n=1 of 30 [322]), colorectal carcinomas (n=1 of 32 [279], n=1 of 22 [302]), and ATLL (n=1 of 10 [303]). Additionally, small deletions have been found in primary thyroid tumors (n=1 of 19 [300]) and leukemia cell lines (n=2 of 7 [323]). These dominant-negative deleted alleles in these leukemia cell lines occur in the kinetochore localization domain of Bub1, thereby inhibiting the proper localization of Bub1 to the kinetochore [323].

Additional studies have not identified any other mutations. Established cell lines from bladder cancer (n=9, [280]), colorectal cancer (n=19 [278], n=8 [324]) hepatocellular carcinoma (n=8 [271]), gastric cancer (n=5 [283]), oral cancer (n=9 [325]), head and neck squamous cell carcinoma (n=6 [326]), lung cancer (n=25 [326], n=30 [322]), breast tumor (n=19 [298], n=12 [282], n=9 [323]), hematopoietic (n=5 [327]), thyroid (n=8 [300]), or various other carcinoma cell lines (n=59 [328], n=6 [302]) have no mutations in Bub1. Primary bladder cancers (n=43, [280]), colorectal cancers (n=32 [324]), hepatocellular carcinomas (n=50 [271], n=7 [302]), gastric cancer (n=49 [283], n=12 [329], n=8 [325]), lung cancers (n=44 [294], n=20 [324]), breast carcinomas (n=20 [330]), glioblastomas (n=40 [293]), clear cell renal carcinomas (n=2 [302]), B-cell lymphomas (n=8 [303]), and acute myeloid leukemia (n=92 [327]) also exhibit no mutations in the sequence in Bub1.

Several types of tumors display aberrant Bub1 expression. In patients with Barrett's esophagus, Bub1 is overexpressed (n=12 of 33) in a subset of patients, while it is repressed in another (n=9 of 33 [289]). A similar profile is also seen in esophageal cancer (n=1 of 4 upregulated, 1 of 4 downregulated [289]). This pattern is also seen in gastric cancers, where a small group exhibits a downregulation of Bub1 (n=4 of 20 [331]) and another displays increased amounts of Bub1 (n=36 of 43 [297], n=8 of 20 [331]). In colorectal carcinomas, Bub1 is silenced below 50% of normal levels in a group of patients (n=10 of 103 [302]). Breast tumors (n=7 of 9) and breast tumor cell lines (n=10 of 12) have Bub1 overexpressed in a majority of cases [282]. In malignant melanoma, Bub1 is highly expressed as well (n=21 of 30 [332]). Bub1 also is expressed highly in leukemia [333] and malignant salivary gland tumors [334]).

2.5.6 Cdc20 and Cdh1

APC/C coactivators have also been observed to be deregulated in human cancers. For instance, the overexpression of Cdc20 is observed in a variety of human malignancies, including pancreatic (n=12 of 20 [335]), lung adenocarcinomas [336], gastric cancer (n=22 of 25 [337]), breast tumors (n=5 of 9 [282]) and breast tumor cell lines (n=10 of 12 [282]). There are no mutations in Cdc20 in colorectal cancer (n=19 [278]), hepatocellular carcinoma (n=8 [271]), lung tumors (n=25 [276]), or lung (n=21 [276]) and breast cancer cell lines (n=12 [282]). Cdh1 downregulation is observed in murine lymphomas, whereas overexpression of Cdh1 acts to suppress B-cell tumorigenesis [338]. In this regard, Cdc20 appears to be a potential oncogene, whereas Cdh1 may more likely be a tumor suppressor.

Protein	Mutation	Frequency*	Tumor type	Reference
Mad2	Missense mutation	1/44 (2%)	Bladder cancer	[280]
	Missense mutation	22/49 (45%)	Gastric cancer	[283]
	Missense mutation	1/5 (20%)	Gastric cancer	[283]
	Heterozygous deletion	1/22 (5%)	Breast cancer	[281]
BubR1	Heterozygous deletion	1/10 (10%)	ATLL	[303]
	Missense mutation	2/10 (20%)	ATLL	[303]
	Missense mutation	2/19 (11%)	Colorectal cancer	[272]
Bub1	Missense mutation	1/32 (3%)	Colorectal cancer	[279]
	Missense mutation	1/22 (5%)	Colorectal cancer	[302]
	Missense mutation	1/30 (3%)	Lung adenocarcinoma	[322]
	Missense mutation	1/10 (10%)	ATLL	[303]
	Heterozygous deletion	1/19 (5%)	Thyroid cancer	[300]
	Heterozygous deletion	2/7 (29%)	Leukemia	[323]
	Heterozygous deletion	1/19 (5%)	Colorectal cancer	[272]
	Missense mutation	1/19 (5%)	Colorectal cancer	[272]
	Missense mutation	1/88 (1%)	Lung cancer	[299]
	Double missense mutation	1/9 (11%)	Pancreatic cancer	[301]

Primary tumors- no shading
Tumor cell lines- shaded boxes

Table 3- Mutational changes in spindle assembly checkpoint genes in human cancer.

Protein	Deregulation	Frequency*	Tumor type	Reference
Mad2	Downregulated	8/33 (24%)	Barrett's esophagus	[289]
	Downregulated	2/4 (50%)	Esophageal	[289]
	Downregulated	5/10 (50%)	Hepatocellular carcinoma	[284]
	Downregulated	3/7 (43%)	Ovarian cancer	[285]
	Downregulated	6/11 (55%)	Hepatoma	[286]
	Downregulated	2/6 (33%)	Leukemia	[287]
	Downregulated	2/5 (40%)	Nasopharyngeal	[288]
	Upregulated	8/33 (24%)	Barrett's esophagus	[289]
	Upregulated	1/4 (25%)	Esophageal	[289]
	Upregulated	23/34 (74%)	Gatric cancer	[300]
	Upregulated	5/9 (56%)	Breast tumor	[282]
	Upregulated	5/12 (42%)	Breast tumor	[282]
Bub3	Downregulated	7/18 (39%)	Lung adenocarcinoma	[296]
	Upregulated	5/18 (28%)	Lung adenocarcinoma	[296]
	Upregulated	34/43 (79%)	Gastric cancer	[297]
	Upregulated	7/9 (78%)	Breast tumor	[282]
	Upregulated	3/12 (25%)	Breast tumor	[282]
BubR1	Downregulated	10/116 (9%)	Colorectal cancer	[302]
	Downregulated	3/8 (38%)	Thyroid cancer	[300]
	Upregulated	29/43 (67%)	Gastric cancer	[297]
	Upregulated	8/9 (89%)	Breast tumor	[282]
	Upregulated	8/12 (67%)	Breast tumor	[282]
	Upregulated	8/8 (100%)	Lung cancer	[304]
Bub1	Downregulated	9/33 (27%)	Barrett's esophagus	[289]
	Downregulated	1/4 (25%)	Esophageal cancer	[289]
	Downregulated	4/20 (20%)	Gastric cancer	[331]
	Downregulated	10/103 (10%)	Colorectal carcinoma	[302]
	Upregulated	12/33 (36%)	Barrett's esophagus	[289]
	Upregulated	1/4 (25%)	Esophageal cancer	[289]
	Upregulated	36/43 (84%)	Gastric cancer	[297]
	Upregulated	8/20 (40%)	Gastric cancer	[331]
	Upregulated	21/30 (70%)	Melanoma	[332]
	Upregulated	7/9 (78%)	Breast tumor	[282]
	Upregulated	10/12 (83%)	Breast tumor	[282]
Cdc20	Upregulated	22/25 (88%)	Gastric cancer	[337]
	Upregulated	12/20 (60%)	Pancreatic cancer	[335]
	Upregulated	5/9 (56%)	Breast tumor	[282]
	Upregulated	10/12 (83%)	Breast tumor	[282]

Primary tumors- no shading
Tumor cell lines- shaded boxes

Table 4- Epigenetic changes in spindle assembly checkpoint genes in human cancer.

2.5.7 Summary

Inactivating mutations in spindle checkpoint genes have been rare to detect in human cancers, which, in retrospect, is not surprising given that homozygous null mutations in murine mitotic checkpoint genes are invariably incompatible with cell viability. Reduced expression of mitotic checkpoint genes, however, is compatible with viability and results, in most cases, in mitotic checkpoint failure, increased chromosome missegregation and increased susceptibility to carcinogens in mice. Mitotic checkpoint genes are expressed at reduced levels in several human cancers, most likely through epigenetic mechanisms. Based on insights from mouse models, it is reasonable to argue that such downregulations could promote malignant cell transformation in humans. Especially, when taken into consideration that humans have a much longer lifespan and a much greater exposure to environmental carcinogens than laboratory mice. Recent evidence of the human mosaic variegated aneuploidy (MVA) syndrome characterized by cancer predisposition caused by germ-line mutations of BubR1 further strengthens the idea that mitotic checkpoint dysfunction promotes carcinogenesis in humans. Several human tumors do have increased levels of spindle checkpoint genes as well, demonstrating that the controlled expression of these proteins needs to be tightly regulated to also prevent chromosomal abnormalities from occurring. The recent evidence of Mad2 overexpression in mice playing a causal role in the establishment of tumorigenesis further strengthens this idea. Whether the overexpression of other mitotic checkpoint genes have similar consequences in animal model systems remains to be determined, making it difficult to generalize that upregulation of spindle assembly checkpoint genes plays a role in the causation or the promotion of cancer formation in humans. It also appears that the genetic context of how aneuploidy develops needs to be taken into account. Bub1 hypomorphic, Mad2 transgenic and Cenp-E mice develop spontaneous tumors, but the locations of these tumors differ. Additionally, within Cenp-E heterozygous mice, there appears to be a protection against certain tumorigenic processes. This demonstrates, that like other types of genetic instability, cancer is a potential, but not obligatory outcome of a situation where there is whole chromosome aneuploidy. Growth-promoting aneuploid cells that could initiate cancer may be offset by cells that acquire a chromosomal content that is incompatible with proliferation or survival. What will be important is to define how different paths that lead to aneuploidy, different genetic contexts, and different cell types when taken together effect whether aneuploidy promotes growth or stimulates apoptosis.

2.6 AGING AND THE SPINDLE ASSEMBLY CHECKPOINT

2.6.1 Introduction

Two recent discoveries have identified the spindle assembly checkpoint BubR1 as a key regulator of aging. First, genetically modified mice that produce reduced amounts of BubR1 have a lifespan that is about 5-fold shorter than normal and develop various aging related disorders at a very young age [218, 339, 340]. Second, during the course of natural aging, BubR1 protein production declines dramatically in many tissues. Various molecular effectors that promote cellular senescence, such as $p16^{Ink4a}$, $p19^{Arf}$, p21 and p53, are

induced in cells from hypomorphic BubR1 mice. Cellular senescence is an important anti-cancer mechanism, as it prevents cell cycle re-entry of potentially neoplastic cells. However, as a consequence of cellular senescence, cells acquire characteristics that promote disruption of normal tissue architecture, thereby promoting pathologies associated with aging and potential oncogenic transformation of pre-neoplastic cells [341, 342]. Along with BubR1 hypomorphic mice, a variety of mouse models have characteristics of premature aging. Here, the similarities and differences between these models will be highlighted.

2.6.2 Aging and pathways of cellular senescence

In contrast to immortal tumor cells, normal cellular proliferation in culture declines after a number of divisions and eventually stops completely when cells enter in to a state known as replicative senescence. The acquisition of a senescent phenotype results in a series of changes in cell morphology and function. These cells spread out as a monolayer and acquire a large cytoplasmic volume. They remain metabolically active and secrete many factors that are not normally secreted, such as degradative enzymes (matrix metalloproteinases), growth factors, and inflammatory cytokines. The secretion of these factors can lead disruption of both normal tissue structure and function [343], which may result in age-related pathology by stimulating chronic inflammation and tissue remodeling. Additionally, senescent cells may promote cancer by stimulating cells with pre-neoplastic lesions in their vicinity [344]. Cells with characteristics of senescence accumulate in multiple tissues of both humans and rodents with age [344]. However, a conclusive demonstration that senescence causes aging has not been shown, as the current published data is entirely correlative. Senescence can be triggered by a variety of intrinsic and extrinsic stresses, including oxidative damage, telomere dysfunction, DNA damage, oncogene activation, and drugs that affect the structure of DNA or microtubules (Fig. 10) [344-346]. The two main cellular pathways that are responsible for the execution senescence are the $p16^{Ink4A}$-Rb and the $p19^{Arf}$-p21-p53 tumor suppressor pathways [344, 347, 348]. Senescence pathways seem to be employed in a cell- and species-specific manner. In both human and mouse cells, direct DNA damage mainly activates p53 through the Atm and Atr kinases [344, 349]. In certain human cells, oxidative stress, attrition of telomeres and loss of telomere function may activate cellular senescence via the same program, but also potentially through $p16^{Ink4a}$ [344, 349]. In mouse cells however, the response to aberrancies in telomere function is dependent on $p19^{Arf}$. Oncogene-induced stress leads to activation of both the $p16^{Ink4a}$-Rb and p19-p53 pathway, although the relative importance of each pathway seems to vary between mouse and human cells. The expression of both $p19^{Arf}$ and $p16^{Ink4A}$ is increased in a variety of tissues with age in mice and rats [350], although it has been difficult to determine what effect these pathways have on normal aging, as disruption in the core components of each pathway results in early tumor formation. Recent studies indicate that $p16^{Ink4A}$ may be responsible for normal aging in certain tissue types, as knockout animals do not display the normal age-related depletion of stem cells in the brain, pancreas, and bone marrow [351-353].

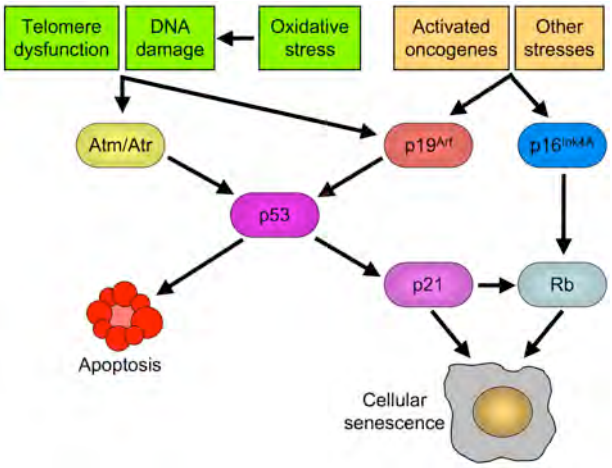

Fig. 10- The p19-p53 and p16-Rb pathways in promotion of cellular senescence. Various intrinsic and extrinsic stresses can activate the cellular senescence program. These stresses engage various cellular signaling cascades, but ultimately activate p53, Rb or both. Activated p53 induces senescence via a complex gene expression program that includes the induction of p21, whereas Rb induces senescence via repression of E2F target genes and alterations in chromatin structure. Once the senescence program is activated, cells withdraw from the cell cycle and a series of changes in cell function and morphology occur.

2.6.3 Spindle assembly checkpoint dysfunction and aging

We generated a series of mice expressing low amounts of BubR1 in an attempt to determine if these animals were susceptible to tumorigenesis, as BubR1 is mutated or expressed at low levels in a variety of tumors. Unexpectedly, mice that express only 10% of normal BubR1 display an array of aging-associated phenotypes much earlier than age-matched controls. These phenotypes include reduced lifespan, cachetic dwarfism, muscle atrophy, lordokyphosis, cataracts, craniofacial dysmorphisms, loss of subcutaneous fat, impaired wound healing, heart arrhtymias, arterial stiffening, gliosis and infertility [218, 339, 340]. Additionally, cells from these mice undergo premature cellular senescence, coupled with a profound induction of $p16^{Ink4a}$, $p19^{Arf}$, $p21^{Cip1}$, and p53. Furthermore, these cells have substantial amounts of lagging chromosomes, aneuploidy, and PMSCS. As mentioned previously, MVA patients display several phenotypes characteristic of old age, including reduced lifespan, cataracts, small stature, and facial dysmorphisms [310, 318], which strengthens the idea that downregulation of BubR1 function is sufficient to drive some cellular processes that result in age-related characteristics. These findings combined with the observation that BubR1 protein levels decline dramatically as normal mice age has suggested the BubR1 functions as a key regulator of the natural aging process. The strong correlation between the onset and progression of the aging-associated phenotypes and the degree and the severity of the chromosome number instability in hypomorphic BubR1 mice suggested a role for aneuploidy in the development of progeroid features. Perhaps, aneuploidy might elicit signals that drive cells into a senescent state and cause early aging-related phenotypes as they accumulate. From this study, it was unclear if this pathology of

aging is unique for hypomorphic BubR1 animals, or if it is a general consequence of impaired spindle checkpoint function. We considered three main possibilities to explain the events that promote the aged phenotype in these animals. One possibility is that a low level of BubR1 protein accelerates the aging process and BubR1 is unique in this function. Alternatively, aging could be a general consequence of defective spindle checkpoint function. Finally, aneuploidy may contribute to these features, as animals demonstrate detectable aneuploidy early and concurrently with the development of aging.

In order rigorously test these possibilities; we used Bub3 and Rae1 haploinsufficient mice (Chapter 6). At 5 months, BubR1 hypomorphic mice have an aged appearance with aneuploidy in 15% of their splenocytes [218]. Aged matched single heterozygous Bub3 and Rae1 mice each have 9% aneuploidy, but no features of aging. One could argue that this may be the result of having aneuploidy that remains below a critical level. However, splenocytes from 5-month-old compound Bub3/Rae1 mice have 36% aneuploidy and a wide spectrum of chromosome losses and gains [196], but show no overt features of aging at this age [213], which further conflicts with the notion that aneuploidy alone is a driving force of aging. We also found that although $Bub3^{+/-}/Rae1^{+/-}$ MEFs are more aneuploid than BubR1 hypomorphic MEFs, they exhibit lower levels of cellular senescence, along with an intermediate induction of p53, p21, $p19^{Arf}$ and $p16^{Ink4A}$. On the other hand, Bub3 and Rae1 single haploinsufficient cells do not display senescence or an induction of these cell cycle arrest-related markers. During the second year of life, which is long after all BubR1 hypomorphic animals have died, progeroid features develop only in double heterozygous Bub3/Rae1 animals, but not in mice with single heterozygous deletions of Bub3 or Rae1. Together, these findings suggest that early onset of age-related phenotypes in mice with spindle assembly checkpoint defects is linked to cellular senescence and the activation of the $p16^{Ink4A}$ and p53 tumor suppressor pathways, rather than to aneuploidy.

As we found common senescence pathway activations in spindle checkpoint defective mice that display hallmarks of early aging, we then asked if disruption of members of the $p16^{Ink4A}$-Rb or $p19^{Arf}$-p53 pathway were able to modulate any phenotypes. We used our BubR1 hypomorphic animals, as these mice age much faster than $p16^{Ink4A}$, $p19^{Arf}$, or p53 null animals die from tumors. As an alternative to possible effects on aging, using this approach allowed us to also evaluate whether aneuploidy resulting from BubR1 insufficiency would synergize with known tumor susceptible models to promote tumorigenesis. Along with an early induction of $p16^{Ink4A}$ in BubR1 hypomorphic cells, we found that a variety tissues from hypomorphic mice also has an elevation of this gene via a quantitative real-time PCR (qRT-PCR) based approach. These tissues include skeletal muscle, subdermal adipose tissue, fat deposits, eye, and kidney. Other tissues, including dermis, heart, testis, ovary, aorta, pancreas, colon and liver, do not have an increased expression, demonstrating that although certain tissues do have an increased amount of $p16^{Ink4A}$ as a result of BubR1 insufficiency, it is not necessarily true that all tissues respond similarly to low amount of BubR1. Interestingly, we found that by knocking out $p16^{Ink4A}$ in these mice, the tissues that had elevated levels of $p16^{Ink4A}$ displayed a delay or attenuation of the aging phenotype of these tissues. Subdermal adipose thickness was maintained in compound mutant mice, whereas BubR1 hypomorphic mice have a decline in adipose with

age. Consistent with an overall improvement in adipose maintenance, BubR1$^{H/H}$/p16$^{-/-}$ mice also had more deposits of visceral and subcutaneous fat than hypomorphic animals. We also found that while BubR1 hypomorphic adipose tissue deposits have a strong staining for β-galactosidase, a feature of senescent cells, BubR1$^{H/H}$/p16$^{-/-}$ mice had marked reduction in β-galactosidase positive cells. It is important to note that although there is not a complete reversal of this aging-associated phenotype, as these animals still had significantly less adipose than wild-type littermates. The development of cataract in compound mutant mice was delayed to small degree, but this phenotype still affected all animals of our cohort. The strongest effect of p16^{Ink4A} disruption was seen in skeletal muscle tissue. Very early in hypomorphic skeletal muscle, p16^{Ink4A} is strongly induced, long before aging appears in this tissue. As hypomorphic mice age, they develop kyphosis which is attributable to muscle atrophy (sarcopenia). This atrophy is severely delayed by disrupting p16^{Ink4A}, as the median time to onset of this disease changes from 15 to 45 weeks, a 3-fold delay. Additionally, not all mice of our compound mutant cohort develop this phenotype, which is in contrast to hypomorphic mice. Several markers of senescence *in vivo* that were upregulated in BubR1 hypomorphic mice are also attenuated by the further disruption of p16^{Ink4A}. Together, these data suggest that tissues that have an induction of p16^{Ink4A} that display characteristics of aging are able to be modulated by abolishing the activation of this gene. Along with an overall improvement in certain age-related disorders, BubR1$^{H/H}$/p16$^{-/-}$ mice also had a 25% extension of median lifespan, going from 20 to 25 weeks. Characteristics of aging in other tissues, which do not have an induction of p16^{Ink4A}, that either have aging related diseases or are unaffected in hypomorphic BubR1 animals, remain unchanged with the disruption of p16^{Ink4A}. However, disrupting this tumor suppressor appears to synergize with low levels of BubR1 in the lung to promote lung tumorigenesis specifically. The incidence of lung tumors, which are not seen in p16^{Ink4A} null animals, increases from <1% in BubR1$^{H/H}$ mice to over 9% in BubR1$^{H/H}$/p16$^{-/-}$ mice. In conclusion, disruption of the p16^{Ink4A} gene in hypomorphic mice delays certain age-related characteristics while promoting lung carcinogenesis when BubR1 levels decline.

We then asked whether disruption of p19^{Arf}-, also encoded by the same locus as p16^{Ink4A}, whose protein levels increases with age in normal animals, was able to modulate any age-related pathologies in our BubR1 hypomorphic animals. Interestingly, most phenotypes of aging, including lordokyphosis, cataract formation, adipose tissue deposition and subdermal adipose tissue thickness were further abrogated by disrupting p19^{Arf}. Additionally, ablation of p19^{Arf} resulted in a significantly increased rate of *in vivo* senescence in our BubR1$^{H/H}$ mice. This is in stark contrast to the tumorigenesis information obtained from the p16^{Ink4A} study. Taken together, these studies suggest that activation of the p16^{Ink4A} acts to promote aging when BubR1 levels decline, versus engagement of the p19^{Arf} acts to delay age-related pathologies in BubR1 hypomorphic mice. In an attempt to understand why there may be such a discrepancy in the outcome of engagement of these pathways, we sought to identify common features of mice that display phenotypes characteristically associated with early aging.

Mutant	Cellular Processes Affected	Tissues affected with age-related pathologies	Accelerated senescence?	Increased tumorigenesis?	Reference
BubR1	Spindle assembly checkpoint	Lens, skin, gonad, muscle	Yes	No	[218]
$Bub3^{+/-}/Rae1^{+/-}$	Spindle assembly checkpoint	Lens, skin, muscle	Yes	No	[213]
$p53^{m/+}$	DNA damage response	Bone, hair, skin, lymphoid tissues	ND	No	[355]
pL53 (p53 Tg)	DNA damage response	Bone, hair, skin, muscle	ND	Yes	[355]
p44 Tg	DNA damage response	Bone, testes	Yes	No	[358]
Atm	DSB repair	Hematopoietic stem cells	Yes	Yes	[361,362]
$Rad50^{S/S}$	DSB repair	Hematopoietic organs, testis	Yes	Yes	[363]
$BRCA1^{Tr/Tr}/p53^{-/-}$	DSB repair	Bone, eye, heart, intestine, liver, testis, + others	Yes	Yes	[364]
Ku86	NHEJ	Bone, skin, liver	Yes	No	[365]
DNA-PKcs	NHEJ	Bone, intestine	No	Yes	[366]
Xpd^{TTD}	NER	Bone, hair, skin, ovary	ND	Yes	[368]
Xpd^{TTD}/XPA	NER	Bone, hair, sking	ND	No	[368]
XPA/CSB	NER	Cerebellum	ND	No	[372]
Ercc1	NER	Brain, kidney, skin, spleen	Yes	No	[373,374]
Terc	TM	Hematopoietic organs, hair, heart, skin, testis, skin	Yes	Yes	[379,380]
Terc/Atm	TM and DSB repair	Hematopoietic organs, bone, brain, hair, intestine	Yes	No	[381]
Terc/Ku86	TM and NHEJ	Various	ND	No	[380]
Terc/DNA-PKcs	TM and NHEJ	Various	ND	No	[380]
Terc/Parp-1	TM and DNA repair	Various	ND	No	[380]
Terc/Wrn	TM and DNA repair	Bone, endocrine, gonad, hair, lens, skin, spleen	Yes	Yes	[382]
PolgA	mtDNA polymerase	Hematopoietic organs, bone, hair, heart, skin, testis	ND	No	[384]
PASG	DNA methylation	Bone, hair, skin, kidney, thymus	Yes	No	[383]

DSB- double strand break, NHEJ- non-homologous end joining, NER- nucleotide excision repair
TM- telomere maintenance, ND- not determined

Table 5- Features of selected premature aging mouse models.

2.6.4 Additional mouse models of aging

Several mouse models that have single gene mutations that do not affect spindle assembly checkpoint function exhibit certain characteristics of premature aging (Table 5). The tumor suppressor p53 responds to a variety of cellular stresses, including DNA damage, to induce apoptosis or senescence depending upon the severity of the damage (Fig. 4) [354]. Mice with a deletion mutation of the first six exons of p53 ($p53^{m/+}$) express a truncated RNA capable of making the carboxy-terminal p53 protein fragment. This mutation results in constitutively activated p53 [355]. This constant supply of active p53 appears to protect $p53^{m/+}$ animals from spontaneous tumor formation, where nearly 50% of wild-type littermates from this cohort develop tumors versus only 6% of $p53^{m/+}$ mice. However, as these mutant animals age, they display several features of premature aging, including reduced stress tolerance, lordokyphosis, osteoporosis, and reduced lifespan, although they are protected from spontaneous tumor formation [355]. Transgenic mice that express a mutant form of p53 that has a alanine to valine change at codon 135 (pL53), a temperature sensitive mutant that makes mutant p53 at normal body temperatures, also display most of these features [355], demonstrating that chronic activation or loss of p53 inhibition promotes the development of aging in certain tissue types. It is however important to note that p53 knock-in mice, which include all promoter regulation sequences, display no overt phenotypes [356]. In fact, these so-called "Super p53" mice are protected from spontaneous tumor formation and live substantially longer than wild-type mice [356]. Additionally, compound "Super p53" and "Super $p19^{Arf}$," knockin mice have a longer lifespan and have a reduced accumulation of cells with aging-associated damage [357]. Transgenic mice expressing the short isoform of p53 (p44), which begins at exon 4 of p53, display premature cellular senescence which results from an upregulation of p21 and an early decline in testis function and bone mass [358], suggesting that chronic activation of the $p19^{Arf}$-p53 senescence pathway promotes age-related phenotypes in these mice.

Werner's syndrome (WS) is a human disorder characterized by genetic instability and premature age-related pathologies. These include short stature, wrinkled skin, baldness, cataracts, muscular atrophy and a tendency to diabetes mellitus. The gene mutated in WS patients is WRN, a DNA helicase which participates in maintaining the integrity of the genome by suppressing illegitimate recombination or by repair of local DNA structural damage [359, 360]. Mice lacking Wrn however do not display early aging or premature senescence [359], illustrating that although WRN mutations in humans have severe ramifications, the genetic ablation of this gene alone in mice is insufficient to establish these phenotypes.

Ataxia telangiectasia (AT) is a human syndrome, which makes some people have a characteristically aged appearance. The gene responsible for this diseases, 'ataxia telangiectasia mutated' (ATM), plays a pivotal role in the activation of cellular responses to DNA damage [361]. ATM senses double strand breaks (DSBs), which is one of the most potentially damaging assaults on DNA. Patients with AT are characterized by neuronal degeneration, immunodeficiency, sterility, genomic instability, and cancer predisposition and have mutations in ATM [362]. Disruption of this gene in mice results in impaired proliferative capacity of hematopoietic stem cells (HSC) due to activation of $p16^{Ink4a}$ and

increased senescence [361]. Disruption of Rad50 or BRCA1, two other key members of the DSB repair machinery, also results in premature age-related phenotypes, along with an increased rate of spontaneous tumor formation and accelerated senescence [363, 364].

Non-homologous end joining (NHEJ) is an error-prone mechanism of repairing DSBs because some DNA is lost when broken strands of DNA are simply pasted back together without the necessity of proofreading. Proteins important for this process include Ku86, Ku70, DNA-PKcs, XRCC4, XLF, and DNA ligase IV [365]. Mice deficient in Ku86 exhibit early death, osteopenia, and skin atrophy, along with an accelerated rate of senescence [365]. However, these animals are not prone to tumor development, perhaps because the cohort died too early from other causes. DNA-PKcs deficient animals also exhibit early death, but have an increased rate of lymphoma development [366]. Interestingly, these mice have kyphosis and reduced body size, but no increased rates of cellular senescence, demonstrating that not all impairments of the NHEJ machinery behave similarly.

The process of nucleotide excision repair (NER) removes damaged bases in DNA stemming from extrinsic factors, such as UV light. Several molecules play a role in this repair pathway and the importance of this repair mechanism is evidenced by the severe human diseases that result from in-born genetic mutations of NER proteins including Xeroderma pigmentosum (XP). Based on the underlying genetic defect, the disease can be divided into the seven complementation groups XPA through XPG [367]. Mice with mutations in XPD that mimic human trichothiodystrophy (Xpd^{TTD}), a brittle hair disorder, exhibit many symptoms of premature aging, including kyphosis, osteosclerosis, early hair graying, cachexia, infertility, and reduced life-span along with a predisposition to tumor formation [368-370]. These mice, when combined with XPA deficient mice, have an even more severe DNA repair defect, as they are more sensitive to oxidative DNA damage [368]. These mice have a greatly accelerated aging phenotype, further strengthening the argument that aging in mice can result from severe damage to DNA that goes unrepaired. Cockayne syndrome (CS), which is very similar to XP, results from mutations in one of two CS genes: CSA or CSB [371]. Compound XPA/CSB null mutant mice, which do not have an accelerated rate of tumor formation, display severe cerebellar abnormalities including apoptosis [372]. Mice deficient in Ercc1, a NER cross complementing gene, die before weaning with substantial aneuploidy and p53 activation in a variety of tissues [373] along with an induction of cellular senescence [374], illustrating that engagement of the p53 pathway is involved in the establishment of a permanent growth arrest.

Along with impaired DNA repair capacity being linked to aging, other defects in overall maintenance of genetic stability also are tied to the early onset of age-related pathologies. Telomeres, which are found on the ends of chromosomes, are necessary to maintain chromosomal integrity and ultimately determine the replicative potential of a cell [375]. Mammalian telomeres are composed of long TTAGGG tandem repeats that become shorter after each cycle of cell division if they are not replaced. If enough of these TTAGGG repeats are lost, the telomere reaches a critically short length and becomes dysfunctional. Critically short telomeres are detected as DSBs and trigger unscheduled repair by NHEJ,

resulting in end-to-end fusions [376, 377]. This erosion of telomeres can be prevented when cells express sufficiently high levels of telomerase. This enzyme is composed of a telomerase RNA component (Terc) and a catalytic telomerase reverse transcriptase (Tert) subunit with the unique capacity to add TTAGGG repeats onto chromosome ends [378]. Ablation of Terc activity in mice leads to a high frequency of end-to-end chromosomal fusions and, at the organismal level, results in loss of fertility, proliferative defects, and symptoms of premature aging affecting the skin, germ line, intestine, immune system and bone marrow, although these mice are protected from carcinogen-induced tumor formation [379, 380]. The disruption of Atm in Terc null mice was also not sufficient to promote tumor formation [381]. However, there appears to be a tradeoff, as these animals display profound cellular senescence and a more severe induction of several phenotypes of early aging, including reduced stem cell precursors, tissue apoptosis, hair graying, hair loss, weight loss and early tumor-free death [381]. Mice lacking Terc along with Ku86 or DNA-PKcs, two members of the NHEJ pathway, have earlier tumor-free death, along with accelerated aging in the germ line and intestine, without the induction of cellular senescence [380]. Alternatively, Parp-1, which recognizes and binds to DSBs, disruption combined with Terc insufficiency has no effect on aging or tumorigenesis [380]. In contrast to these models, disruption of Wrn along with Terc in mice results in cellular senescence, tumor formation, and a phenotype of premature aging that is very similar to WS patients [382]. This demonstrates that $Wrn^{-/-}$ mice do not normally show any of the phenotypes described for human WS patients because of the difference in length between mouse and human telomeres, as mouse telomeres are significantly longer than humans. By removing Terc, erosion of telomeres can occur in these animals and recapitulation of the human disease can be created.

Other modifications of DNA appear to be required to also prevent the accumulation of aged phenotypes. Disruption of PASG, a protein responsible for DNA methylation, results in growth retardation, hair graying, hair loss, osteoporosis, kyphosis, and early death [383]. Cells from these animals also have an induction in $p16^{Ink4a}$ along with cellular senescence. These results are intriguing as it suggests that global hypomethylation of DNA, as the result of disruption of a protein that is involved with transcriptional silencing via promoter methylation is required to prevent these lesions.

In addition to nuclear DNA damage, aberrancies in mitochondrial DNA may also contribute to the biology of aging, as mice that have a defective proofreading capacity in the mitochondrial-specific DNA polymerase, PolgA, exhibit several age-related phenotypes early in life [384]. These mice have a reduced lifespan, weight loss, hair loss, kyphosis, and osteoporosis. These mice are not prone to tumor formation, nor has the senescence phenotype been examined, making this an interesting model for further study. Also, whether other mutations affecting mitochondrial DNA remains an unexplored research venue.

2.6.5 Summary

The process of organismal aging is extremely complex. Several phenotypes occur in multiple mouse models, demonstrating that aging in these tissues can result from a variety

of factors. However, other phenotypes, such as cataracts in spindle assembly checkpoint defective animals, appear to be unique, suggesting that the "lesion" triggering certain aging-related phenotype differs [348, 385]. Also, a common feature of mouse models that exhibit early aging is the engagement of cellular senescence. The proteins responsible for this growth arrest are beginning to be elucidated and appear to include the members of the p53-$p19^{Arf}$ and the $p16^{Ink4A}$-Rb pathway. Interestingly, it seems that DNA damage defective models engage primarily the p53 pathway, while spindle assembly checkpoint mutants engage both pathways. This difference may also explain why some phenotypes are seen commonly in mouse models of aging, while other features, such as cataract, appear to be specific for models with impaired spindle checkpoint function. It will be interesting to determine if disruption of these drivers of senescence results in a modulation of certain age-related pathologies in models that are genetically predisposed to age. Also, with the exception of p53 and p44 transgenic animals, most of the mutants that exhibit premature-aging have mutations that disrupt normal gene function. It will be interesting to examine what is the result of overexpression of these components in mice and if this acts to promote longevity and delay aging.

REFERENCES

1. Schafer, K.A. (1998). The cell cycle: a review. Vet Pathol *35*, 461-478.
2. Peters, J.M. (2002). The anaphase-promoting complex: proteolysis in mitosis and beyond. Mol Cell *9*, 931-943.
3. Deshpande, A., Sicinski, P., and Hinds, P.W. (2005). Cyclins and cdks in development and cancer: a perspective. Oncogene *24*, 2909-2915.
4. Blagosklonny, M.V. (2003). Cell senescence and hypermitogenic arrest. EMBO Rep *4*, 358-362.
5. Hanahan, D., and Weinberg, R.A. (2000). The hallmarks of cancer. Cell *100*, 57-70.
6. Earnshaw, W.C., and Pluta, A.F. (1994). Mitosis. Bioessays *16*, 639-643.
7. Pines, J., and Rieder, C.L. (2001). Re-staging mitosis: a contemporary view of mitotic progression. Nat Cell Biol *3*, E3-6.
8. Wang, H., Oliferenko, S., and Balasubramanian, M.K. (2003). Cytokinesis: relative alignment of the cell division apparatus and the mitotic spindle. Curr Opin Cell Biol *15*, 82-87.
9. Downward, J. (2003). Targeting RAS signalling pathways in cancer therapy. Nat Rev Cancer *3*, 11-22.
10. Rajagopalan, H., and Lengauer, C. (2004). Aneuploidy and cancer. Nature *432*, 338-341.
11. Kaufman, M.H. (1991). New insights into triploidy and tetraploidy, from an analysis of model systems for these conditions. Hum Reprod *6*, 8-16.
12. Atkin, N.B. (2000). Chromosomal doubling: the significance of polyploidization in the development of human tumors: possibly relevant findings on a lymphoma. Cancer Genet Cytogenet *116*, 81-83.
13. Umar, A., and Kunkel, T.A. (1996). DNA-replication fidelity, mismatch repair and genome instability in cancer cells. Eur J Biochem *238*, 297-307.
14. Kastan, M.B., and Bartek, J. (2004). Cell-cycle checkpoints and cancer. Nature *432*, 316-323.
15. Sancar, A., Lindsey-Boltz, L.A., Unsal-Kacmaz, K., and Linn, S. (2004). Molecular mechanisms of mammalian DNA repair and the DNA damage checkpoints. Annu Rev Biochem *73*, 39-85.
16. Fortini, P., Pascucci, B., Parlanti, E., D'Errico, M., Simonelli, V., and Dogliotti, E. (2003). 8-Oxoguanine DNA damage: at the crossroad of alternative repair pathways. Mutat Res *531*, 127-139.

17. Dianov, G.L., Sleeth, K.M., Dianova, II, and Allinson, S.L. (2003). Repair of abasic sites in DNA. Mutat Res *531*, 157-163.
18. Paques, F., and Haber, J.E. (1999). Multiple pathways of recombination induced by double-strand breaks in Saccharomyces cerevisiae. Microbiol Mol Biol Rev *63*, 349-404.
19. Dudas, A., and Chovanec, M. (2004). DNA double-strand break repair by homologous recombination. Mutat Res *566*, 131-167.
20. Kaufmann, W.K., and Paules, R.S. (1996). DNA damage and cell cycle checkpoints. Faseb J *10*, 238-247.
21. Molinari, M. (2000). Cell cycle checkpoints and their inactivation in human cancer. Cell Prolif *33*, 261-274.
22. Deming, P.B., Cistulli, C.A., Zhao, H., Graves, P.R., Piwnica-Worms, H., Paules, R.S., Downes, C.S., and Kaufmann, W.K. (2001). The human decatenation checkpoint. Proc Natl Acad Sci U S A *98*, 12044-12049.
23. Hartwell, L.H., and Kastan, M.B. (1994). Cell cycle control and cancer. Science *266*, 1821-1828.
24. Schang, L.M. (2002). Cyclin-dependent kinases as cellular targets for antiviral drugs. J Antimicrob Chemother *50*, 779-792.
25. Malumbres, M., and Barbacid, M. (2005). Mammalian cyclin-dependent kinases. Trends Biochem Sci *30*, 630-641.
26. Evans, T., Rosenthal, E.T., Youngblom, J., Distel, D., and Hunt, T. (1983). Cyclin: a protein specified by maternal mRNA in sea urchin eggs that is destroyed at each cleavage division. Cell *33*, 389-396.
27. Evans, T. (2004). The discovery of cyclin (II). Cell *116*, S65, 61 p following S65.
28. Hunt, T. (2004). The discovery of cyclin (I). Cell *116*, S63-64, 61 p following S65.
29. Murray, A.W. (2004). Recycling the cell cycle: cyclins revisited. Cell *116*, 221-234.
30. Bartek, J., and Lukas, J. (2001). Pathways governing G1/S transition and their response to DNA damage. FEBS Lett *490*, 117-122.
31. Draetta, G.F. (1997). Cell cycle: will the real Cdk-activating kinase please stand up. Curr Biol *7*, R50-52.
32. Sherr, C.J., and Roberts, J.M. (1999). CDK inhibitors: positive and negative regulators of G1-phase progression. Genes Dev *13*, 1501-1512.
33. Serrano, M., Hannon, G.J., and Beach, D. (1993). A new regulatory motif in cell-cycle control causing specific inhibition of cyclin D/CDK4. Nature *366*, 704-707.
34. Chan, F.K., Zhang, J., Cheng, L., Shapiro, D.N., and Winoto, A. (1995). Identification of human and mouse p19, a novel CDK4 and CDK6 inhibitor with homology to p16ink4. Mol Cell Biol *15*, 2682-2688.
35. Hirai, H., Roussel, M.F., Kato, J.Y., Ashmun, R.A., and Sherr, C.J. (1995). Novel INK4 proteins, p19 and p18, are specific inhibitors of the cyclin D-dependent kinases CDK4 and CDK6. Mol Cell Biol *15*, 2672-2681.
36. Guan, K.L., Jenkins, C.W., Li, Y., Nichols, M.A., Wu, X., O'Keefe, C.L., Matera, A.G., and Xiong, Y. (1994). Growth suppression by p18, a p16INK4/MTS1- and p14INK4B/MTS2-related CDK6 inhibitor, correlates with wild-type pRb function. Genes Dev *8*, 2939-2952.
37. Hannon, G.J., and Beach, D. (1994). p15INK4B is a potential effector of TGF-beta-induced cell cycle arrest. Nature *371*, 257-261.
38. Matsuoka, S., Edwards, M.C., Bai, C., Parker, S., Zhang, P., Baldini, A., Harper, J.W., and Elledge, S.J. (1995). p57KIP2, a structurally distinct member of the p21CIP1 Cdk inhibitor family, is a candidate tumor suppressor gene. Genes Dev *9*, 650-662.

39. Lee, M.H., Reynisdottir, I., and Massague, J. (1995). Cloning of p57KIP2, a cyclin-dependent kinase inhibitor with unique domain structure and tissue distribution. Genes Dev *9*, 639-649.
40. Ho, D.D., Toyoshima, T., Mo, H., Kempf, D.J., Norbeck, D., Chen, C.M., Wideburg, N.E., Burt, S.K., Erickson, J.W., and Singh, M.K. (1994). Characterization of human immunodeficiency virus type 1 variants with increased resistance to a C2-symmetric protease inhibitor. J Virol *68*, 2016-2020.
41. Toyoshima, H., and Hunter, T. (1994). p27, a novel inhibitor of G1 cyclin-Cdk protein kinase activity, is related to p21. Cell *78*, 67-74.
42. Polyak, K., Lee, M.H., Erdjument-Bromage, H., Koff, A., Roberts, J.M., Tempst, P., and Massague, J. (1994). Cloning of p27Kip1, a cyclin-dependent kinase inhibitor and a potential mediator of extracellular antimitogenic signals. Cell *78*, 59-66.
43. Polyak, K., Kato, J.Y., Solomon, M.J., Sherr, C.J., Massague, J., Roberts, J.M., and Koff, A. (1994). p27Kip1, a cyclin-Cdk inhibitor, links transforming growth factor-beta and contact inhibition to cell cycle arrest. Genes Dev *8*, 9-22.
44. Noda, A., Ning, Y., Venable, S.F., Pereira-Smith, O.M., and Smith, J.R. (1994). Cloning of senescent cell-derived inhibitors of DNA synthesis using an expression screen. Exp Cell Res *211*, 90-98.
45. Dulic, V., Kaufmann, W.K., Wilson, S.J., Tlsty, T.D., Lees, E., Harper, J.W., Elledge, S.J., and Reed, S.I. (1994). p53-dependent inhibition of cyclin-dependent kinase activities in human fibroblasts during radiation-induced G1 arrest. Cell *76*, 1013-1023.
46. Zhang, H., Xiong, Y., and Beach, D. (1993). Proliferating cell nuclear antigen and p21 are components of multiple cell cycle kinase complexes. Mol Biol Cell *4*, 897-906.
47. Xiong, Y., Hannon, G.J., Zhang, H., Casso, D., Kobayashi, R., and Beach, D. (1993). p21 is a universal inhibitor of cyclin kinases. Nature *366*, 701-704.
48. el-Deiry, W.S., Tokino, T., Velculescu, V.E., Levy, D.B., Parsons, R., Trent, J.M., Lin, D., Mercer, W.E., Kinzler, K.W., and Vogelstein, B. (1993). WAF1, a potential mediator of p53 tumor suppression. Cell *75*, 817-825.
49. Harper, J.W., Adami, G.R., Wei, N., Keyomarsi, K., and Elledge, S.J. (1993). The p21 Cdk-interacting protein Cip1 is a potent inhibitor of G1 cyclin-dependent kinases. Cell *75*, 805-816.
50. Gu, Y., Turck, C.W., and Morgan, D.O. (1993). Inhibition of CDK2 activity in vivo by an associated 20K regulatory subunit. Nature *366*, 707-710.
51. Weinberg, R.A. (1995). The retinoblastoma protein and cell cycle control. Cell *81*, 323-330.
52. Bartek, J., Bartkova, J., and Lukas, J. (1996). The retinoblastoma protein pathway and the restriction point. Curr Opin Cell Biol *8*, 805-814.
53. Sherr, C.J. (2000). The Pezcoller lecture: cancer cell cycles revisited. Cancer Res *60*, 3689-3695.
54. Giacinti, C., and Giordano, A. (2006). RB and cell cycle progression. Oncogene *25*, 5220-5227.
55. Stevaux, O., and Dyson, N.J. (2002). A revised picture of the E2F transcriptional network and RB function. Curr Opin Cell Biol *14*, 684-691.
56. Frolov, M.V., and Dyson, N.J. (2004). Molecular mechanisms of E2F-dependent activation and pRB-mediated repression. J Cell Sci *117*, 2173-2181.
57. Ohtani, N., Yamakoshi, K., Takahashi, A., and Hara, E. (2004). The p16INK4a-RB pathway: molecular link between cellular senescence and tumor suppression. J Med Invest *51*, 146-153.
58. Cheng, M., Olivier, P., Diehl, J.A., Fero, M., Roussel, M.F., Roberts, J.M., and Sherr, C.J. (1999). The p21(Cip1) and p27(Kip1) CDK 'inhibitors' are essential activators of cyclin D-dependent kinases in murine fibroblasts. Embo J *18*, 1571-1583.
59. Fridman, J.S., and Lowe, S.W. (2003). Control of apoptosis by p53. Oncogene *22*, 9030-9040.

60. Schmitt, C.A., Fridman, J.S., Yang, M., Baranov, E., Hoffman, R.M., and Lowe, S.W. (2002). Dissecting p53 tumor suppressor functions in vivo. Cancer Cell *1*, 289-298.
61. Attardi, L.D., and DePinho, R.A. (2004). Conquering the complexity of p53. Nat Genet *36*, 7-8.
62. Ciechanover, A., Heller, H., Katz-Etzion, R., and Hershko, A. (1981). Activation of the heat-stable polypeptide of the ATP-dependent proteolytic system. Proc Natl Acad Sci U S A *78*, 761-765.
63. Hershko, A., Heller, H., Elias, S., and Ciechanover, A. (1983). Components of ubiquitin-protein ligase system. Resolution, affinity purification, and role in protein breakdown. J Biol Chem *258*, 8206-8214.
64. Hershko, A., and Ciechanover, A. (1998). The ubiquitin system. Annu Rev Biochem *67*, 425-479.
65. Haas, A.L., Warms, J.V., Hershko, A., and Rose, I.A. (1982). Ubiquitin-activating enzyme. Mechanism and role in protein-ubiquitin conjugation. J Biol Chem *257*, 2543-2548.
66. Hershko, A., Ciechanover, A., and Rose, I.A. (1981). Identification of the active amino acid residue of the polypeptide of ATP-dependent protein breakdown. J Biol Chem *256*, 1525-1528.
67. Hershko, A. (1988). Ubiquitin-mediated protein degradation. J Biol Chem *263*, 15237-15240.
68. Deshaies, R.J. (1999). SCF and Cullin/Ring H2-based ubiquitin ligases. Annu Rev Cell Dev Biol *15*, 435-467.
69. Morgan, D.O. (1999). Regulation of the APC and the exit from mitosis. Nat Cell Biol *1*, E47-53.
70. Zachariae, W., and Nasmyth, K. (1999). Whose end is destruction: cell division and the anaphase-promoting complex. Genes Dev *13*, 2039-2058.
71. Harper, J.W., Burton, J.L., and Solomon, M.J. (2002). The anaphase-promoting complex: it's not just for mitosis any more. Genes Dev *16*, 2179-2206.
72. Castro, A., Bernis, C., Vigneron, S., Labbe, J.C., and Lorca, T. (2005). The anaphase-promoting complex: a key factor in the regulation of cell cycle. Oncogene *24*, 314-325.
73. Wasch, R., and Engelbert, D. (2005). Anaphase-promoting complex-dependent proteolysis of cell cycle regulators and genomic instability of cancer cells. Oncogene *24*, 1-10.
74. Rape, M., and Kirschner, M.W. (2004). Autonomous regulation of the anaphase-promoting complex couples mitosis to S-phase entry. Nature *432*, 588-595.
75. Carroll, C.W., and Morgan, D.O. (2002). The Doc1 subunit is a processivity factor for the anaphase-promoting complex. Nat Cell Biol *4*, 880-887.
76. Stemmann, O., Zou, H., Gerber, S.A., Gygi, S.P., and Kirschner, M.W. (2001). Dual inhibition of sister chromatid separation at metaphase. Cell *107*, 715-726.
77. Fung, T.K., and Poon, R.Y. (2005). A roller coaster ride with the mitotic cyclins. Semin Cell Dev Biol *16*, 335-342.
78. Pines, J., and Hunter, T. (1990). Human cyclin A is adenovirus E1A-associated protein p60 and behaves differently from cyclin B. Nature *346*, 760-763.
79. Poon, R.Y., Yamashita, K., Howell, M., Ershler, M.A., Belyavsky, A., and Hunt, T. (1994). Cell cycle regulation of the p34cdc2/p33cdk2-activating kinase p40MO15. J Cell Sci *107 (Pt 10)*, 2789-2799.
80. Erlandsson, F., Linnman, C., Ekholm, S., Bengtsson, E., and Zetterberg, A. (2000). A detailed analysis of cyclin A accumulation at the G(1)/S border in normal and transformed cells. Exp Cell Res *259*, 86-95.
81. den Elzen, N., and Pines, J. (2001). Cyclin A is destroyed in prometaphase and can delay chromosome alignment and anaphase. J Cell Biol *153*, 121-136.
82. Geley, S., Kramer, E., Gieffers, C., Gannon, J., Peters, J.M., and Hunt, T. (2001). Anaphase-promoting complex/cyclosome-dependent proteolysis of human cyclin A starts at the beginning of mitosis and is not subject to the spindle assembly checkpoint. J Cell Biol *153*, 137-148.

83. Irniger, S., Piatti, S., Michaelis, C., and Nasmyth, K. (1995). Genes involved in sister chromatid separation are needed for B-type cyclin proteolysis in budding yeast. Cell *81*, 269-278.
84. Sudakin, V., Ganoth, D., Dahan, A., Heller, H., Hershko, J., Luca, F.C., Ruderman, J.V., and Hershko, A. (1995). The cyclosome, a large complex containing cyclin-selective ubiquitin ligase activity, targets cyclins for destruction at the end of mitosis. Mol Biol Cell *6*, 185-197.
85. King, R.W., Peters, J.M., Tugendreich, S., Rolfe, M., Hieter, P., and Kirschner, M.W. (1995). A 20S complex containing CDC27 and CDC16 catalyzes the mitosis-specific conjugation of ubiquitin to cyclin B. Cell *81*, 279-288.
86. Zachariae, W., Shevchenko, A., Andrews, P.D., Ciosk, R., Galova, M., Stark, M.J., Mann, M., and Nasmyth, K. (1998). Mass spectrometric analysis of the anaphase-promoting complex from yeast: identification of a subunit related to cullins. Science *279*, 1216-1219.
87. Gmachl, M., Gieffers, C., Podtelejnikov, A.V., Mann, M., and Peters, J.M. (2000). The RING-H2 finger protein APC11 and the E2 enzyme UBC4 are sufficient to ubiquitinate substrates of the anaphase-promoting complex. Proc Natl Acad Sci U S A *97*, 8973-8978.
88. Yoon, H.J., Feoktistova, A., Wolfe, B.A., Jennings, J.L., Link, A.J., and Gould, K.L. (2002). Proteomics analysis identifies new components of the fission and budding yeast anaphase-promoting complexes. Curr Biol *12*, 2048-2054.
89. Zachariae, W., Shin, T.H., Galova, M., Obermaier, B., and Nasmyth, K. (1996). Identification of subunits of the anaphase-promoting complex of Saccharomyces cerevisiae. Science *274*, 1201-1204.
90. Peters, J.M., King, R.W., Hoog, C., and Kirschner, M.W. (1996). Identification of BIME as a subunit of the anaphase-promoting complex. Science *274*, 1199-1201.
91. Jorgensen, P.M., Graslund, S., Betz, R., Stahl, S., Larsson, C., and Hoog, C. (2001). Characterisation of the human APC1, the largest subunit of the anaphase-promoting complex. Gene *262*, 51-59.
92. Lupas, A., Baumeister, W., and Hofmann, K. (1997). A repetitive sequence in subunits of the 26S proteasome and 20S cyclosome (anaphase-promoting complex). Trends Biochem Sci *22*, 195-196.
93. Borden, K.L., and Freemont, P.S. (1996). The RING finger domain: a recent example of a sequence-structure family. Curr Opin Struct Biol *6*, 395-401.
94. Ohta, T., Michel, J.J., Schottelius, A.J., and Xiong, Y. (1999). ROC1, a homolog of APC11, represents a family of cullin partners with an associated ubiquitin ligase activity. Mol Cell *3*, 535-541.
95. Tang, Z., Bharadwaj, R., Li, B., and Yu, H. (2001). Mad2-Independent inhibition of APCCdc20 by the mitotic checkpoint protein BubR1. Dev Cell *1*, 227-237.
96. Tang, Z., Li, B., Bharadwaj, R., Zhu, H., Ozkan, E., Hakala, K., Deisenhofer, J., and Yu, H. (2001). APC2 Cullin protein and APC11 RING protein comprise the minimal ubiquitin ligase module of the anaphase-promoting complex. Mol Biol Cell *12*, 3839-3851.
97. Leverson, J.D., Joazeiro, C.A., Page, A.M., Huang, H., Hieter, P., and Hunter, T. (2000). The APC11 RING-H2 finger mediates E2-dependent ubiquitination. Mol Biol Cell *11*, 2315-2325.
98. Sikorski, R.S., Boguski, M.S., Goebl, M., and Hieter, P. (1990). A repeating amino acid motif in CDC23 defines a family of proteins and a new relationship among genes required for mitosis and RNA synthesis. Cell *60*, 307-317.
99. Lamb, J.R., Michaud, W.A., Sikorski, R.S., and Hieter, P.A. (1994). Cdc16p, Cdc23p and Cdc27p form a complex essential for mitosis. Embo J *13*, 4321-4328.
100. D'Andrea, L.D., and Regan, L. (2003). TPR proteins: the versatile helix. Trends Biochem Sci *28*, 655-662.

101. Lahav-Baratz, S., Sudakin, V., Ruderman, J.V., and Hershko, A. (1995). Reversible phosphorylation controls the activity of cyclosome-associated cyclin-ubiquitin ligase. Proc Natl Acad Sci U S A *92*, 9303-9307.
102. Vodermaier, H.C., and Peters, J.M. (2004). APC activators caught by their tails? Cell Cycle *3*, 265-266.
103. Passmore, L.A., McCormack, E.A., Au, S.W., Paul, A., Willison, K.R., Harper, J.W., and Barford, D. (2003). Doc1 mediates the activity of the anaphase-promoting complex by contributing to substrate recognition. Embo J *22*, 786-796.
104. Vodermaier, H.C., Gieffers, C., Maurer-Stroh, S., Eisenhaber, F., and Peters, J.M. (2003). TPR subunits of the anaphase-promoting complex mediate binding to the activator protein CDH1. Curr Biol *13*, 1459-1468.
105. Schwab, M., Neutzner, M., Mocker, D., and Seufert, W. (2001). Yeast Hct1 recognizes the mitotic cyclin Clb2 and other substrates of the ubiquitin ligase APC. Embo J *20*, 5165-5175.
106. Zhang, Y., and Lees, E. (2001). Identification of an overlapping binding domain on Cdc20 for Mad2 and anaphase-promoting complex: model for spindle checkpoint regulation. Mol Cell Biol *21*, 5190-5199.
107. Pfleger, C.M., Salic, A., Lee, E., and Kirschner, M.W. (2001). Inhibition of Cdh1-APC by the MAD2-related protein MAD2L2: a novel mechanism for regulating Cdh1. Genes Dev *15*, 1759-1764.
108. Grossberger, R., Gieffers, C., Zachariae, W., Podtelejnikov, A.V., Schleiffer, A., Nasmyth, K., Mann, M., and Peters, J.M. (1999). Characterization of the DOC1/APC10 subunit of the yeast and the human anaphase-promoting complex. J Biol Chem *274*, 14500-14507.
109. Kominami, K., Seth-Smith, H., and Toda, T. (1998). Apc10 and Ste9/Srw1, two regulators of the APC-cyclosome, as well as the CDK inhibitor Rum1 are required for G1 cell-cycle arrest in fission yeast. Embo J *17*, 5388-5399.
110. Wendt, K.S., Vodermaier, H.C., Jacob, U., Gieffers, C., Gmachl, M., Peters, J.M., Huber, R., and Sondermann, P. (2001). Crystal structure of the APC10/DOC1 subunit of the human anaphase-promoting complex. Nat Struct Biol *8*, 784-788.
111. Carroll, C.W., Enquist-Newman, M., and Morgan, D.O. (2005). The APC subunit Doc1 promotes recognition of the substrate destruction box. Curr Biol *15*, 11-18.
112. Yamada, H., Kumada, K., and Yanagida, M. (1997). Distinct subunit functions and cell cycle regulated phosphorylation of 20S APC/cyclosome required for anaphase in fission yeast. J Cell Sci *110 (Pt 15)*, 1793-1804.
113. Hall, M.C., Torres, M.P., Schroeder, G.K., and Borchers, C.H. (2003). Mnd2 and Swm1 are core subunits of the Saccharomyces cerevisiae anaphase-promoting complex. J Biol Chem *278*, 16698-16705.
114. Passmore, L.A., and Barford, D. (2005). Coactivator functions in a stoichiometric complex with anaphase-promoting complex/cyclosome to mediate substrate recognition. EMBO Rep *6*, 873-878.
115. Gieffers, C., Dube, P., Harris, J.R., Stark, H., and Peters, J.M. (2001). Three-dimensional structure of the anaphase-promoting complex. Mol Cell *7*, 907-913.
116. Dube, P., Herzog, F., Gieffers, C., Sander, B., Riedel, D., Muller, S.A., Engel, A., Peters, J.M., and Stark, H. (2005). Localization of the coactivator Cdh1 and the cullin subunit Apc2 in a cryo-electron microscopy model of vertebrate APC/C. Mol Cell *20*, 867-879.
117. Peters, J.M. (2006). The anaphase promoting complex/cyclosome: a machine designed to destroy. Nat Rev Mol Cell Biol *7*, 644-656.

118. Wirth, K.G., Ricci, R., Gimenez-Abian, J.F., Taghybeeglu, S., Kudo, N.R., Jochum, W., Vasseur-Cognet, M., and Nasmyth, K. (2004). Loss of the anaphase-promoting complex in quiescent cells causes unscheduled hepatocyte proliferation. Genes Dev *18*, 88-98.

119. Furuta, T., Tuck, S., Kirchner, J., Koch, B., Auty, R., Kitagawa, R., Rose, A.M., and Greenstein, D. (2000). EMB-30: an APC4 homologue required for metaphase-to-anaphase transitions during meiosis and mitosis in Caenorhabditis elegans. Mol Biol Cell *11*, 1401-1419.

120. Golden, A., Sadler, P.L., Wallenfang, M.R., Schumacher, J.M., Hamill, D.R., Bates, G., Bowerman, B., Seydoux, G., and Shakes, D.C. (2000). Metaphase to anaphase (mat) transition-defective mutants in Caenorhabditis elegans. J Cell Biol *151*, 1469-1482.

121. Kraft, C., Herzog, F., Gieffers, C., Mechtler, K., Hagting, A., Pines, J., and Peters, J.M. (2003). Mitotic regulation of the human anaphase-promoting complex by phosphorylation. Embo J *22*, 6598-6609.

122. Golan, A., Yudkovsky, Y., and Hershko, A. (2002). The cyclin-ubiquitin ligase activity of cyclosome/APC is jointly activated by protein kinases Cdk1-cyclin B and Plk. J Biol Chem *277*, 15552-15557.

123. Rudner, A.D., and Murray, A.W. (2000). Phosphorylation by Cdc28 activates the Cdc20-dependent activity of the anaphase-promoting complex. J Cell Biol *149*, 1377-1390.

124. Kotani, S., Tugendreich, S., Fujii, M., Jorgensen, P.M., Watanabe, N., Hoog, C., Hieter, P., and Todokoro, K. (1998). PKA and MPF-activated polo-like kinase regulate anaphase-promoting complex activity and mitosis progression. Mol Cell *1*, 371-380.

125. Hershko, A., Ganoth, D., Sudakin, V., Dahan, A., Cohen, L.H., Luca, F.C., Ruderman, J.V., and Eytan, E. (1994). Components of a system that ligates cyclin to ubiquitin and their regulation by the protein kinase cdc2. J Biol Chem *269*, 4940-4946.

126. Pfleger, C.M., and Kirschner, M.W. (2000). The KEN box: an APC recognition signal distinct from the D box targeted by Cdh1. Genes Dev *14*, 655-665.

127. Glotzer, M., Murray, A.W., and Kirschner, M.W. (1991). Cyclin is degraded by the ubiquitin pathway. Nature *349*, 132-138.

128. Chung, E., and Chen, R.H. (2003). Phosphorylation of Cdc20 is required for its inhibition by the spindle checkpoint. Nat Cell Biol *5*, 748-753.

129. Weinstein, J. (1997). Cell cycle-regulated expression, phosphorylation, and degradation of p55Cdc. A mammalian homolog of CDC20/Fizzy/slp1. J Biol Chem *272*, 28501-28511.

130. Lorca, T., Castro, A., Martinez, A.M., Vigneron, S., Morin, N., Sigrist, S., Lehner, C., Doree, M., and Labbe, J.C. (1998). Fizzy is required for activation of the APC/cyclosome in Xenopus egg extracts. Embo J *17*, 3565-3575.

131. Chung, E., and Chen, R.H. (2002). Spindle checkpoint requires Mad1-bound and Mad1-free Mad2. Mol Biol Cell *13*, 1501-1511.

132. Jaspersen, S.L., Charles, J.F., and Morgan, D.O. (1999). Inhibitory phosphorylation of the APC regulator Hct1 is controlled by the kinase Cdc28 and the phosphatase Cdc14. Curr Biol *9*, 227-236.

133. Kramer, E.R., Scheuringer, N., Podtelejnikov, A.V., Mann, M., and Peters, J.M. (2000). Mitotic regulation of the APC activator proteins CDC20 and CDH1. Mol Biol Cell *11*, 1555-1569.

134. Bembenek, J., and Yu, H. (2001). Regulation of the anaphase-promoting complex by the dual specificity phosphatase human Cdc14a. J Biol Chem *276*, 48237-48242.

135. Zachariae, W., Schwab, M., Nasmyth, K., and Seufert, W. (1998). Control of cyclin ubiquitination by CDK-regulated binding of Hct1 to the anaphase promoting complex. Science *282*, 1721-1724.

136. Kotani, S., Tanaka, H., Yasuda, H., and Todokoro, K. (1999). Regulation of APC activity by phosphorylation and regulatory factors. J Cell Biol *146*, 791-800.

137. Visintin, R., Craig, K., Hwang, E.S., Prinz, S., Tyers, M., and Amon, A. (1998). The phosphatase Cdc14 triggers mitotic exit by reversal of Cdk-dependent phosphorylation. Mol Cell *2*, 709-718.
138. Reimann, J.D., Gardner, B.E., Margottin-Goguet, F., and Jackson, P.K. (2001). Emi1 regulates the anaphase-promoting complex by a different mechanism than Mad2 proteins. Genes Dev *15*, 3278-3285.
139. Reimann, J.D., Freed, E., Hsu, J.Y., Kramer, E.R., Peters, J.M., and Jackson, P.K. (2001). Emi1 is a mitotic regulator that interacts with Cdc20 and inhibits the anaphase promoting complex. Cell *105*, 645-655.
140. Miller, J.J., Summers, M.K., Hansen, D.V., Nachury, M.V., Lehman, N.L., Loktev, A., and Jackson, P.K. (2006). Emi1 stably binds and inhibits the anaphase-promoting complex/cyclosome as a pseudosubstrate inhibitor. Genes Dev *20*, 2410-2420.
141. Hansen, D.V., Loktev, A.V., Ban, K.H., and Jackson, P.K. (2004). Plk1 regulates activation of the anaphase promoting complex by phosphorylating and triggering SCFbetaTrCP-dependent destruction of the APC Inhibitor Emi1. Mol Biol Cell *15*, 5623-5634.
142. Lehman, N.L., Verschuren, E.W., Hsu, J.Y., Cherry, A.M., and Jackson, P.K. (2006). Overexpression of the anaphase promoting complex/cyclosome inhibitor Emi1 leads to tetraploidy and genomic instability of p53-deficient cells. Cell Cycle *5*, 1569-1573.
143. Song, M.S., Song, S.J., Ayad, N.G., Chang, J.S., Lee, J.H., Hong, H.K., Lee, H., Choi, N., Kim, J., Kim, H., Kim, J.W., Choi, E.J., Kirschner, M.W., and Lim, D.S. (2004). The tumour suppressor RASSF1A regulates mitosis by inhibiting the APC-Cdc20 complex. Nat Cell Biol *6*, 129-137.
144. Hames, R.S., Wattam, S.L., Yamano, H., Bacchieri, R., and Fry, A.M. (2001). APC/C-mediated destruction of the centrosomal kinase Nek2A occurs in early mitosis and depends upon a cyclin A-type D-box. Embo J *20*, 7117-7127.
145. Hayes, M.J., Kimata, Y., Wattam, S.L., Lindon, C., Mao, G., Yamano, H., and Fry, A.M. (2006). Early mitotic degradation of Nek2A depends on Cdc20-independent interaction with the APC/C. Nat Cell Biol *8*, 607-614.
146. Jeganathan, K.B., Malureanu, L., and van Deursen, J.M. (2005). The Rae1-Nup98 complex prevents aneuploidy by inhibiting securin degradation. Nature *438*, 1036-1039.
147. Hagting, A., Den Elzen, N., Vodermaier, H.C., Waizenegger, I.C., Peters, J.M., and Pines, J. (2002). Human securin proteolysis is controlled by the spindle checkpoint and reveals when the APC/C switches from activation by Cdc20 to Cdh1. J Cell Biol *157*, 1125-1137.
148. Zur, A., and Brandeis, M. (2001). Securin degradation is mediated by fzy and fzr, and is required for complete chromatid separation but not for cytokinesis. Embo J *20*, 792-801.
149. Peters, J.M. (1999). Subunits and substrates of the anaphase-promoting complex. Exp Cell Res *248*, 339-349.
150. Sudo, T., Ota, Y., Kotani, S., Nakao, M., Takami, Y., Takeda, S., and Saya, H. (2001). Activation of Cdh1-dependent APC is required for G1 cell cycle arrest and DNA damage-induced G2 checkpoint in vertebrate cells. Embo J *20*, 6499-6508.
151. Uhlmann, F., Lottspeich, F., and Nasmyth, K. (1999). Sister-chromatid separation at anaphase onset is promoted by cleavage of the cohesin subunit Scc1. Nature *400*, 37-42.
152. Darwiche, N., Freeman, L.A., and Strunnikov, A. (1999). Characterization of the components of the putative mammalian sister chromatid cohesion complex. Gene *233*, 39-47.
153. Stemmann, O., Boos, D., and Gorr, I.H. (2005). Rephrasing anaphase: separase FEARs shugoshin. Chromosoma *113*, 409-417.

154. Zou, H., McGarry, T.J., Bernal, T., and Kirschner, M.W. (1999). Identification of a vertebrate sister-chromatid separation inhibitor involved in transformation and tumorigenesis. Science *285*, 418-422.
155. Holland, A.J., and Taylor, S.S. (2006). Cyclin-B1-mediated inhibition of excess separase is required for timely chromosome disjunction. J Cell Sci *119*, 3325-3336.
156. Jeganathan, K.B., Baker, D.J., and van Deursen, J.M. (2006). Securin associates with APCCdh1 in prometaphase but its destruction is delayed by Rae1 and Nup98 until the metaphase/anaphase transition. Cell Cycle *5*, 366-370.
157. Antonio, C., Ferby, I., Wilhelm, H., Jones, M., Karsenti, E., Nebreda, A.R., and Vernos, I. (2000). Xkid, a chromokinesin required for chromosome alignment on the metaphase plate. Cell *102*, 425-435.
158. Funabiki, H., and Murray, A.W. (2000). The Xenopus chromokinesin Xkid is essential for metaphase chromosome alignment and must be degraded to allow anaphase chromosome movement. Cell *102*, 411-424.
159. Castro, A., Vigneron, S., Bernis, C., Labbe, J.C., and Lorca, T. (2003). Xkid is degraded in a D-box, KEN-box, and A-box-independent pathway. Mol Cell Biol *23*, 4126-4138.
160. Gordon, D.M., and Roof, D.M. (2001). Degradation of the kinesin Kip1p at anaphase onset is mediated by the anaphase-promoting complex and Cdc20p. Proc Natl Acad Sci U S A *98*, 12515-12520.
161. Hildebrandt, E.R., and Hoyt, M.A. (2001). Cell cycle-dependent degradation of the Saccharomyces cerevisiae spindle motor Cin8p requires APC(Cdh1) and a bipartite destruction sequence. Mol Biol Cell *12*, 3402-3416.
162. Juang, Y.L., Huang, J., Peters, J.M., McLaughlin, M.E., Tai, C.Y., and Pellman, D. (1997). APC-mediated proteolysis of Ase1 and the morphogenesis of the mitotic spindle. Science *275*, 1311-1314.
163. Visintin, R., Prinz, S., and Amon, A. (1997). CDC20 and CDH1: a family of substrate-specific activators of APC-dependent proteolysis. Science *278*, 460-463.
164. Stewart, S., and Fang, G. (2005). Anaphase-promoting complex/cyclosome controls the stability of TPX2 during mitotic exit. Mol Cell Biol *25*, 10516-10527.
165. McGarry, T.J., and Kirschner, M.W. (1998). Geminin, an inhibitor of DNA replication, is degraded during mitosis. Cell *93*, 1043-1053.
166. Gonzalez, M.A., Tachibana, K.E., Adams, D.J., van der Weyden, L., Hemberger, M., Coleman, N., Bradley, A., and Laskey, R.A. (2006). Geminin is essential to prevent endoreduplication and to form pluripotent cells during mammalian development. Genes Dev *20*, 1880-1884.
167. Lindon, C., and Pines, J. (2004). Ordered proteolysis in anaphase inactivates Plk1 to contribute to proper mitotic exit in human cells. J Cell Biol *164*, 233-241.
168. Stewart, S., and Fang, G. (2005). Destruction box-dependent degradation of aurora B is mediated by the anaphase-promoting complex/cyclosome and Cdh1. Cancer Res *65*, 8730-8735.
169. Zhao, W.M., and Fang, G. (2005). Anillin is a substrate of anaphase-promoting complex/cyclosome (APC/C) that controls spatial contractility of myosin during late cytokinesis. J Biol Chem *280*, 33516-33524.
170. Prinz, S., Hwang, E.S., Visintin, R., and Amon, A. (1998). The regulation of Cdc20 proteolysis reveals a role for APC components Cdc23 and Cdc27 during S phase and early mitosis. Curr Biol *8*, 750-760.
171. Shirayama, M., Zachariae, W., Ciosk, R., and Nasmyth, K. (1998). The Polo-like kinase Cdc5p and the WD-repeat protein Cdc20p/fizzy are regulators and substrates of the anaphase promoting complex in Saccharomyces cerevisiae. Embo J *17*, 1336-1349.
172. Littlepage, L.E., and Ruderman, J.V. (2002). Identification of a new APC/C recognition domain, the A box, which is required for the Cdh1-dependent destruction of the kinase Aurora-A during mitotic exit. Genes Dev *16*, 2274-2285.

173. Castro, A., Vigneron, S., Bernis, C., Labbe, J.C., Prigent, C., and Lorca, T. (2002). The D-Box-activating domain (DAD) is a new proteolysis signal that stimulates the silent D-Box sequence of Aurora-A. EMBO Rep *3*, 1209-1214.
174. Castro, A., Arlot-Bonnemains, Y., Vigneron, S., Labbe, J.C., Prigent, C., and Lorca, T. (2002). APC/Fizzy-Related targets Aurora-A kinase for proteolysis. EMBO Rep *3*, 457-462.
175. Kops, G.J., Weaver, B.A., and Cleveland, D.W. (2005). On the road to cancer: aneuploidy and the mitotic checkpoint. Nat Rev Cancer *5*, 773-785.
176. Rieder, C.L., Cole, R.W., Khodjakov, A., and Sluder, G. (1995). The checkpoint delaying anaphase in response to chromosome monoorientation is mediated by an inhibitory signal produced by unattached kinetochores. J Cell Biol *130*, 941-948.
177. Rieder, C.L., Schultz, A., Cole, R., and Sluder, G. (1994). Anaphase onset in vertebrate somatic cells is controlled by a checkpoint that monitors sister kinetochore attachment to the spindle. J Cell Biol *127*, 1301-1310.
178. Nasmyth, K. (2005). How do so few control so many? Cell *120*, 739-746.
179. Henikoff, S., Ahmad, K., and Malik, H.S. (2001). The centromere paradox: stable inheritance with rapidly evolving DNA. Science *293*, 1098-1102.
180. Fukagawa, T. (2004). Assembly of kinetochores in vertebrate cells. Exp Cell Res *296*, 21-27.
181. Cleveland, D.W., Mao, Y., and Sullivan, K.F. (2003). Centromeres and kinetochores: from epigenetics to mitotic checkpoint signaling. Cell *112*, 407-421.
182. Maiato, H., DeLuca, J., Salmon, E.D., and Earnshaw, W.C. (2004). The dynamic kinetochore-microtubule interface. J Cell Sci *117*, 5461-5477.
183. Logarinho, E., Bousbaa, H., Dias, J.M., Lopes, C., Amorim, I., Antunes-Martins, A., and Sunkel, C.E. (2004). Different spindle checkpoint proteins monitor microtubule attachment and tension at kinetochores in Drosophila cells. J Cell Sci *117*, 1757-1771.
184. Yu, H. (2002). Regulation of APC-Cdc20 by the spindle checkpoint. Curr Opin Cell Biol *14*, 706-714.
185. Musacchio, A., and Hardwick, K.G. (2002). The spindle checkpoint: structural insights into dynamic signalling. Nat Rev Mol Cell Biol *3*, 731-741.
186. Millband, D.N., Campbell, L., and Hardwick, K.G. (2002). The awesome power of multiple model systems: interpreting the complex nature of spindle checkpoint signaling. Trends Cell Biol *12*, 205-209.
187. Rieder, C.L., and Maiato, H. (2004). Stuck in division or passing through: what happens when cells cannot satisfy the spindle assembly checkpoint. Dev Cell *7*, 637-651.
188. Acquaviva, C., Herzog, F., Kraft, C., and Pines, J. (2004). The anaphase promoting complex/cyclosome is recruited to centromeres by the spindle assembly checkpoint. Nat Cell Biol *6*, 892-898.
189. Bharadwaj, R., and Yu, H. (2004). The spindle checkpoint, aneuploidy, and cancer. Oncogene *23*, 2016-2027.
190. Hoyt, M.A. (2001). A new view of the spindle checkpoint. J Cell Biol *154*, 909-911.
191. Tan, A.L., Rida, P.C., and Surana, U. (2005). Essential tension and constructive destruction: the spindle checkpoint and its regulatory links with mitotic exit. Biochem J *386*, 1-13.
192. Taylor, S.S., Scott, M.I., and Holland, A.J. (2004). The spindle checkpoint: a quality control mechanism which ensures accurate chromosome segregation. Chromosome Res *12*, 599-616.
193. Wang, X., Babu, J.R., Harden, J.M., Jablonski, S.A., Gazi, M.H., Lingle, W.L., de Groen, P.C., Yen, T.J., and van Deursen, J.M. (2001). The mitotic checkpoint protein hBUB3 and the mRNA export

factor hRAE1 interact with GLE2p-binding sequence (GLEBS)-containing proteins. J Biol Chem *276*, 26559-26567.

194. Meraldi, P., Draviam, V.M., and Sorger, P.K. (2004). Timing and checkpoints in the regulation of mitotic progression. Dev Cell *7*, 45-60.

195. Howell, B.J., Moree, B., Farrar, E.M., Stewart, S., Fang, G., and Salmon, E.D. (2004). Spindle checkpoint protein dynamics at kinetochores in living cells. Curr Biol *14*, 953-964.

196. Babu, J.R., Jeganathan, K.B., Baker, D.J., Wu, X., Kang-Decker, N., and van Deursen, J.M. (2003). Rae1 is an essential mitotic checkpoint regulator that cooperates with Bub3 to prevent chromosome missegregation. J Cell Biol *160*, 341-353.

197. Taylor, S.S., Hussein, D., Wang, Y., Elderkin, S., and Morrow, C.J. (2001). Kinetochore localisation and phosphorylation of the mitotic checkpoint components Bub1 and BubR1 are differentially regulated by spindle events in human cells. J Cell Sci *114*, 4385-4395.

198. Sharp-Baker, H., and Chen, R.H. (2001). Spindle checkpoint protein Bub1 is required for kinetochore localization of Mad1, Mad2, Bub3, and CENP-E, independently of its kinase activity. J Cell Biol *153*, 1239-1250.

199. Fang, G., Yu, H., and Kirschner, M.W. (1998). The checkpoint protein MAD2 and the mitotic regulator CDC20 form a ternary complex with the anaphase-promoting complex to control anaphase initiation. Genes Dev *12*, 1871-1883.

200. Sudakin, V., Chan, G.K., and Yen, T.J. (2001). Checkpoint inhibition of the APC/C in HeLa cells is mediated by a complex of BUBR1, BUB3, CDC20, and MAD2. J Cell Biol *154*, 925-936.

201. Mao, Y., Abrieu, A., and Cleveland, D.W. (2003). Activating and silencing the mitotic checkpoint through CENP-E-dependent activation/inactivation of BubR1. Cell *114*, 87-98.

202. Draviam, V.M., Xie, S., and Sorger, P.K. (2004). Chromosome segregation and genomic stability. Curr Opin Genet Dev *14*, 120-125.

203. Craig, J.M., and Choo, K.H. (2005). Kiss and break up-a safe passage to anaphase in mitosis and meiosis. Chromosoma, 1-11.

204. Nasmyth, K., and Haering, C.H. (2005). The structure and function of smc and kleisin complexes. Annu Rev Biochem *74*, 595-648.

205. Liu, J., and Fuchs, S.Y. (2006). Cross-Talk Between APC/C and CBP/p300. Cancer Biol Ther *5*, 760-762.

206. Turnell, A.S., Stewart, G.S., Grand, R.J., Rookes, S.M., Martin, A., Yamano, H., Elledge, S.J., and Gallimore, P.H. (2005). The APC/C and CBP/p300 cooperate to regulate transcription and cell-cycle progression. Nature *438*, 690-695.

207. Wells, W.A. (1996). The spindle-assembly checkpoint: aiming for a perfect mitosis, every time. Trends Cell Biol *6*, 228-234.

208. Baker, D.J., Chen, J., and van Deursen, J.M. (2005). The mitotic checkpoint in cancer and aging: what have mice taught us? Curr Opin Cell Biol *17*, 583-589.

209. Salmon, E.D., Cimini, D., Cameron, L.A., and DeLuca, J.G. (2005). Merotelic kinetochores in mammalian tissue cells. Philos Trans R Soc Lond B Biol Sci *360*, 553-568.

210. Luo, X., Tang, Z., Xia, G., Wassmann, K., Matsumoto, T., Rizo, J., and Yu, H. (2004). The Mad2 spindle checkpoint protein has two distinct natively folded states. Nat Struct Mol Biol *11*, 338-345.

211. Dobles, M., Liberal, V., Scott, M.L., Benezra, R., and Sorger, P.K. (2000). Chromosome missegregation and apoptosis in mice lacking the mitotic checkpoint protein Mad2. Cell *101*, 635-645.

212. Michel, L.S., Liberal, V., Chatterjee, A., Kirchwegger, R., Pasche, B., Gerald, W., Dobles, M., Sorger, P.K., Murty, V.V., and Benezra, R. (2001). MAD2 haplo-insufficiency causes premature anaphase and chromosome instability in mammalian cells. Nature *409*, 355-359.

213. Baker, D.J., Jeganathan, K.B., Malureanu, L., Perez-Terzic, C., Terzic, A., and van Deursen, J.M. (2006). Early aging-associated phenotypes in Bub3/Rae1 haploinsufficient mice. J Cell Biol *172*, 529-540.

214. Sotillo, R., Hernando, E., Diaz-Rodriguez, E., Teruya-Feldstein, J., Cordon-Cardo, C., Lowe, S.W., and Benezra, R. (2007). Mad2 overexpression promotes aneuploidy and tumorigenesis in mice. Cancer Cell *11*, 9-23.

215. Iwanaga, Y., Chi, Y.H., Miyazato, A., Sheleg, S., Haller, K., Peloponese, J.M., Jr., Li, Y., Ward, J.M., Benezra, R., and Jeang, K.T. (2007). Heterozygous deletion of mitotic arrest-deficient protein 1 (MAD1) increases the incidence of tumors in mice. Cancer Res *67*, 160-166.

216. Jeganathan, K., Malureanu, L., Baker, D.J., Abraham, S.C., and van Deursen, J.M. (2007). Bub1 mediates cell death in response to chromosome missegregation and acts to suppress spontaneous tumorigenesis. J Cell Biol *179*, 255-267.

217. Perera, D., Tilston, V., Hopwood, J.A., Barchi, M., Boot-Handford, R.P., and Taylor, S.S. (2007). Bub1 maintains centromeric cohesion by activation of the spindle checkpoint. Dev Cell *13*, 566-579.

218. Baker, D.J., Jeganathan, K.B., Cameron, J.D., Thompson, M., Juneja, S., Kopecka, A., Kumar, R., Jenkins, R.B., de Groen, P.C., Roche, P., and van Deursen, J.M. (2004). BubR1 insufficiency causes early onset of aging-associated phenotypes and infertility in mice. Nat Genet *36*, 744-749.

219. Dai, W., Wang, Q., Liu, T., Swamy, M., Fang, Y., Xie, S., Mahmood, R., Yang, Y.M., Xu, M., and Rao, C.V. (2004). Slippage of mitotic arrest and enhanced tumor development in mice with BubR1 haploinsufficiency. Cancer Res *64*, 440-445.

220. Rao, C.V., Yang, Y.M., Swamy, M.V., Liu, T., Fang, Y., Mahmood, R., Jhanwar-Uniyal, M., and Dai, W. (2005). Colonic tumorigenesis in BubR1+/-ApcMin/+ compound mutant mice is linked to premature separation of sister chromatids and enhanced genomic instability. Proc Natl Acad Sci U S A *102*, 4365-4370.

221. Kalitsis, P., Earle, E., Fowler, K.J., and Choo, K.H. (2000). Bub3 gene disruption in mice reveals essential mitotic spindle checkpoint function during early embryogenesis. Genes Dev *14*, 2277-2282.

222. Kalitsis, P., Fowler, K.J., Griffiths, B., Earle, E., Chow, C.W., Jamsen, K., and Choo, K.H. (2005). Increased chromosome instability but not cancer predisposition in haploinsufficient Bub3 mice. Genes Chromosomes Cancer *44*, 29-36.

223. Putkey, F.R., Cramer, T., Morphew, M.K., Silk, A.D., Johnson, R.S., McIntosh, J.R., and Cleveland, D.W. (2002). Unstable kinetochore-microtubule capture and chromosomal instability following deletion of CENP-E. Dev Cell *3*, 351-365.

224. Weaver, B.A., Silk, A.D., Montagna, C., Verdier-Pinard, P., and Cleveland, D.W. (2007). Aneuploidy acts both oncogenically and as a tumor suppressor. Cancer Cell *11*, 25-36.

225. Kim, S.H., Lin, D.P., Matsumoto, S., Kitazono, A., and Matsumoto, T. (1998). Fission yeast Slp1: an effector of the Mad2-dependent spindle checkpoint. Science *279*, 1045-1047.

226. Chen, R.H., Waters, J.C., Salmon, E.D., and Murray, A.W. (1996). Association of spindle assembly checkpoint component XMAD2 with unattached kinetochores. Science *274*, 242-246.

227. Li, Y., and Benezra, R. (1996). Identification of a human mitotic checkpoint gene: hsMAD2. Science *274*, 246-248.

228. Chen, R.H., Shevchenko, A., Mann, M., and Murray, A.W. (1998). Spindle checkpoint protein Xmad1 recruits Xmad2 to unattached kinetochores. J Cell Biol *143*, 283-295.

229. De Antoni, A., Pearson, C.G., Cimini, D., Canman, J.C., Sala, V., Nezi, L., Mapelli, M., Sironi, L., Faretta, M., Salmon, E.D., and Musacchio, A. (2005). The Mad1/Mad2 complex as a template for Mad2 activation in the spindle assembly checkpoint. Curr Biol *15*, 214-225.
230. Howell, B.J., Hoffman, D.B., Fang, G., Murray, A.W., and Salmon, E.D. (2000). Visualization of Mad2 dynamics at kinetochores, along spindle fibers, and at spindle poles in living cells. J Cell Biol *150*, 1233-1250.
231. Wassmann, K., Liberal, V., and Benezra, R. (2003). Mad2 phosphorylation regulates its association with Mad1 and the APC/C. Embo J *22*, 797-806.
232. Li, H., Cuenin, C., Murr, R., Wang, Z.Q., and Herceg, Z. (2004). HAT cofactor Trrap regulates the mitotic checkpoint by modulation of Mad1 and Mad2 expression. Embo J *23*, 4824-4834.
233. Shonn, M.A., Murray, A.L., and Murray, A.W. (2003). Spindle checkpoint component Mad2 contributes to biorientation of homologous chromosomes. Curr Biol *13*, 1979-1984.
234. Michel, L.S., Liberal, V., Chatterjee, A., Kirchwegger, R., Pasche, B., Gerald, W., Dobles, M., Sorger, P.K., Murty, V.V., and Benezra, R. (2001). MAD2 haplo-insufficiency causes premature anaphase and chromosome instability in mammalian cells. Nature *409*, 355-359.
235. Hernando, E., Nahle, Z., Juan, G., Diaz-Rodriguez, E., Alaminos, M., Hemann, M., Michel, L., Mittal, V., Gerald, W., Benezra, R., Lowe, S.W., and Cordon-Cardo, C. (2004). Rb inactivation promotes genomic instability by uncoupling cell cycle progression from mitotic control. Nature *430*, 797-802.
236. Hwang, L.H., Lau, L.F., Smith, D.L., Mistrot, C.A., Hardwick, K.G., Hwang, E.S., Amon, A., and Murray, A.W. (1998). Budding yeast Cdc20: a target of the spindle checkpoint. Science *279*, 1041-1044.
237. Hoyt, M.A., Totis, L., and Roberts, B.T. (1991). S. cerevisiae genes required for cell cycle arrest in response to loss of microtubule function. Cell *66*, 507-517.
238. Taylor, S.S., Ha, E., and McKeon, F. (1998). The human homologue of Bub3 is required for kinetochore localization of Bub1 and a Mad3/Bub1-related protein kinase. J Cell Biol *142*, 1-11.
239. Martinez-Exposito, M.J., Kaplan, K.B., Copeland, J., and Sorger, P.K. (1999). Retention of the BUB3 checkpoint protein on lagging chromosomes. Proc Natl Acad Sci U S A *96*, 8493-8498.
240. Yoon, Y.M., Baek, K.H., Jeong, S.J., Shin, H.J., Ha, G.H., Jeon, A.H., Hwang, S.G., Chun, J.S., and Lee, C.W. (2004). WD repeat-containing mitotic checkpoint proteins act as transcriptional repressors during interphase. FEBS Lett *575*, 23-29.
241. Kalitsis, P., Fowler, K.J., Griffiths, B., Earle, E., Chow, C.W., Jamsen, K., and Choo, K.H. (2005). Increased chromosome instability but not cancer predisposition in haploinsufficient Bub3 mice. Genes Chromosomes Cancer.
242. Larsen, N.A., and Harrison, S.C. (2004). Crystal structure of the spindle assembly checkpoint protein Bub3. J Mol Biol *344*, 885-892.
243. Pritchard, C.E., Fornerod, M., Kasper, L.H., and van Deursen, J.M. (1999). RAE1 is a shuttling mRNA export factor that binds to a GLEBS-like NUP98 motif at the nuclear pore complex through multiple domains. J Cell Biol *145*, 237-254.
244. Blower, M.D., Nachury, M., Heald, R., and Weis, K. (2005). A Rae1-containing ribonucleoprotein complex is required for mitotic spindle assembly. Cell *121*, 223-234.
245. Wong, R.W., Blobel, G., and Coutavas, E. (2006). Rae1 interaction with NuMA is required for bipolar spindle formation. Proc Natl Acad Sci U S A *103*, 19783-19787.
246. Davenport, J.W., Fernandes, E.R., Harris, L.D., Neale, G.A., and Goorha, R. (1999). The mouse mitotic checkpoint gene bub1b, a novel bub1 family member, is expressed in a cell cycle-dependent manner. Genomics *55*, 113-117.

247. Abrieu, A., Kahana, J.A., Wood, K.W., and Cleveland, D.W. (2000). CENP-E as an essential component of the mitotic checkpoint in vitro. Cell *102*, 817-826.
248. Oikawa, T., Okuda, M., Ma, Z., Goorha, R., Tsujimoto, H., Inokuma, H., and Fukasawa, K. (2005). Transcriptional control of BubR1 by p53 and suppression of centrosome amplification by BubR1. Mol Cell Biol *25*, 4046-4061.
249. Wang, Q., Liu, T., Fang, Y., Xie, S., Huang, X., Mahmood, R., Ramaswamy, G., Sakamoto, K.M., Darzynkiewicz, Z., Xu, M., and Dai, W. (2004). BUBR1 deficiency results in abnormal megakaryopoiesis. Blood *103*, 1278-1285.
250. Rao, C.V., Yang, Y.M., Swamy, M.V., Liu, T., Fang, Y., Mahmood, R., Jhanwar-Uniyal, M., and Dai, W. (2005). Colonic tumorigenesis in BubR1+/-ApcMin/+ compound mutant mice is linked to premature separation of sister chromatids and enhanced genomic instability. Proc Natl Acad Sci U S A.
251. Meyers, E.N., Lewandoski, M., and Martin, G.R. (1998). An Fgf8 mutant allelic series generated by Cre- and Flp-mediated recombination. Nat Genet *18*, 136-141.
252. Taylor, S.S., and McKeon, F. (1997). Kinetochore localization of murine Bub1 is required for normal mitotic timing and checkpoint response to spindle damage. Cell *89*, 727-735.
253. Skoufias, D.A., Andreassen, P.R., Lacroix, F.B., Wilson, L., and Margolis, R.L. (2001). Mammalian mad2 and bub1/bubR1 recognize distinct spindle-attachment and kinetochore-tension checkpoints. Proc Natl Acad Sci U S A *98*, 4492-4497.
254. Warren, C.D., Brady, D.M., Johnston, R.C., Hanna, J.S., Hardwick, K.G., and Spencer, F.A. (2002). Distinct chromosome segregation roles for spindle checkpoint proteins. Mol Biol Cell *13*, 3029-3041.
255. Brady, D.M., and Hardwick, K.G. (2000). Complex formation between Mad1p, Bub1p and Bub3p is crucial for spindle checkpoint function. Curr Biol *10*, 675-678.
256. Seeley, T.W., Wang, L., and Zhen, J.Y. (1999). Phosphorylation of human MAD1 by the BUB1 kinase in vitro. Biochem Biophys Res Commun *257*, 589-595.
257. Johnson, V.L., Scott, M.I., Holt, S.V., Hussein, D., and Taylor, S.S. (2004). Bub1 is required for kinetochore localization of BubR1, Cenp-E, Cenp-F and Mad2, and chromosome congression. J Cell Sci *117*, 1577-1589.
258. Liu, S.T., Hittle, J.C., Jablonski, S.A., Campbell, M.S., Yoda, K., and Yen, T.J. (2003). Human CENP-I specifies localization of CENP-F, MAD1 and MAD2 to kinetochores and is essential for mitosis. Nat Cell Biol *5*, 341-345.
259. Chen, R.H. (2004). Phosphorylation and activation of Bub1 on unattached chromosomes facilitate the spindle checkpoint. Embo J *23*, 3113-3121.
260. Tang, Z., Shu, H., Oncel, D., Chen, S., and Yu, H. (2004). Phosphorylation of Cdc20 by Bub1 provides a catalytic mechanism for APC/C inhibition by the spindle checkpoint. Mol Cell *16*, 387-397.
261. Margolis, R.L. (2004). Bub1, a gatekeeper for Cdc20-dependent mitotic exit. Dev Cell *7*, 634-635.
262. Vanoosthuyse, V., and Hardwick, K.G. (2005). Bub1 and the multilayered inhibition of Cdc20-APC/C in mitosis. Trends Cell Biol *15*, 231-233.
263. Perera, D., and Freire, R. (2005). Human spindle checkpoint kinase Bub1 is cleaved during apoptosis. Cell Death Differ.
264. Wood, K.W., Sakowicz, R., Goldstein, L.S., and Cleveland, D.W. (1997). CENP-E is a plus end-directed kinetochore motor required for metaphase chromosome alignment. Cell *91*, 357-366.
265. Yen, T.J., Compton, D.A., Wise, D., Zinkowski, R.P., Brinkley, B.R., Earnshaw, W.C., and Cleveland, D.W. (1991). CENP-E, a novel human centromere-associated protein required for progression from metaphase to anaphase. Embo J *10*, 1245-1254.

266. Yucel, J.K., Marszalek, J.D., McIntosh, J.R., Goldstein, L.S., Cleveland, D.W., and Philp, A.V. (2000). CENP-meta, an essential kinetochore kinesin required for the maintenance of metaphase chromosome alignment in Drosophila. J Cell Biol *150*, 1-11.

267. Brown, K.D., Coulson, R.M., Yen, T.J., and Cleveland, D.W. (1994). Cyclin-like accumulation and loss of the putative kinetochore motor CENP-E results from coupling continuous synthesis with specific degradation at the end of mitosis. J Cell Biol *125*, 1303-1312.

268. McEwen, B.F., Chan, G.K., Zubrowski, B., Savoian, M.S., Sauer, M.T., and Yen, T.J. (2001). CENP-E is essential for reliable bioriented spindle attachment, but chromosome alignment can be achieved via redundant mechanisms in mammalian cells. Mol Biol Cell *12*, 2776-2789.

269. Weaver, B.A., Bonday, Z.Q., Putkey, F.R., Kops, G.J., Silk, A.D., and Cleveland, D.W. (2003). Centromere-associated protein-E is essential for the mammalian mitotic checkpoint to prevent aneuploidy due to single chromosome loss. J Cell Biol *162*, 551-563.

270. Mao, Y., Desai, A., and Cleveland, D.W. (2005). Microtubule capture by CENP-E silences BubR1-dependent mitotic checkpoint signaling. J Cell Biol *170*, 873-880.

271. Saeki, A., Tamura, S., Ito, N., Kiso, S., Matsuda, Y., Yabuuchi, I., Kawata, S., and Matsuzawa, Y. (2002). Frequent impairment of the spindle assembly checkpoint in hepatocellular carcinoma. Cancer *94*, 2047-2054.

272. Cahill, D.P., Lengauer, C., Yu, J., Riggins, G.J., Willson, J.K., Markowitz, S.D., Kinzler, K.W., and Vogelstein, B. (1998). Mutations of mitotic checkpoint genes in human cancers. Nature *392*, 300-303.

273. Yuen, K.W., Montpetit, B., and Hieter, P. (2005). The kinetochore and cancer: what's the connection? Curr Opin Cell Biol *17*, 576-582.

274. Weaver, B.A., and Cleveland, D.W. (2005). Decoding the links between mitosis, cancer, and chemotherapy: The mitotic checkpoint, adaptation, and cell death. Cancer Cell *8*, 7-12.

275. Weaver, B.A., and Cleveland, D.W. (2006). Does aneuploidy cause cancer? Curr Opin Cell Biol *18*, 658-667.

276. Takahashi, T., Haruki, N., Nomoto, S., Masuda, A., Saji, S., Osada, H., and Takahashi, T. (1999). Identification of frequent impairment of the mitotic checkpoint and molecular analysis of the mitotic checkpoint genes, hsMAD2 and p55CDC, in human lung cancers. Oncogene *18*, 4295-4300.

277. Gemma, A., Hosoya, Y., Seike, M., Uematsu, K., Kurimoto, F., Hibino, S., Yoshimura, A., Shibuya, M., Kudoh, S., and Emi, M. (2001). Genomic structure of the human MAD2 gene and mutation analysis in human lung and breast cancers. Lung Cancer *32*, 289-295.

278. Cahill, D.P., da Costa, L.T., Carson-Walter, E.B., Kinzler, K.W., Vogelstein, B., and Lengauer, C. (1999). Characterization of MAD2B and other mitotic spindle checkpoint genes. Genomics *58*, 181-187.

279. Imai, Y., Shiratori, Y., Kato, N., Inoue, T., and Omata, M. (1999). Mutational inactivation of mitotic checkpoint genes, hsMAD2 and hBUB1, is rare in sporadic digestive tract cancers. Jpn J Cancer Res *90*, 837-840.

280. Hernando, E., Orlow, I., Liberal, V., Nohales, G., Benezra, R., and Cordon-Cardo, C. (2001). Molecular analyses of the mitotic checkpoint components hsMAD2, hBUB1 and hBUB3 in human cancer. Int J Cancer *95*, 223-227.

281. Percy, M.J., Myrie, K.A., Neeley, C.K., Azim, J.N., Ethier, S.P., and Petty, E.M. (2000). Expression and mutational analyses of the human MAD2L1 gene in breast cancer cells. Genes Chromosomes Cancer *29*, 356-362.

282. Yuan, B., Xu, Y., Woo, J.H., Wang, Y., Bae, Y.K., Yoon, D.S., Wersto, R.P., Tully, E., Wilsbach, K., and Gabrielson, E. (2006). Increased expression of mitotic checkpoint genes in breast cancer cells with chromosomal instability. Clin Cancer Res *12*, 405-410.

283. Kim, H.S., Park, K.H., Kim, S.A., Wen, J., Park, S.W., Park, B., Gham, C.W., Hyung, W.J., Noh, S.H., Kim, H.K., and Song, S.Y. (2005). Frequent mutations of human Mad2, but not Bub1, in gastric cancers cause defective mitotic spindle checkpoint. Mutat Res *578*, 187-201.

284. Jeong, S.J., Shin, H.J., Kim, S.J., Ha, G.H., Cho, B.I., Baek, K.H., Kim, C.M., and Lee, C.W. (2004). Transcriptional abnormality of the hsMAD2 mitotic checkpoint gene is a potential link to hepatocellular carcinogenesis. Cancer Res *64*, 8666-8673.

285. Wang, X., Jin, D.Y., Ng, R.W., Feng, H., Wong, Y.C., Cheung, A.L., and Tsao, S.W. (2002). Significance of MAD2 expression to mitotic checkpoint control in ovarian cancer cells. Cancer Res *62*, 1662-1668.

286. Sze, K.M., Ching, Y.P., Jin, D.Y., and Ng, I.O. (2004). Association of MAD2 expression with mitotic checkpoint competence in hepatoma cells. J Biomed Sci *11*, 920-927.

287. Kasai, T., Iwanaga, Y., Iha, H., and Jeang, K.T. (2002). Prevalent loss of mitotic spindle checkpoint in adult T-cell leukemia confers resistance to microtubule inhibitors. J Biol Chem *277*, 5187-5193.

288. Wang, X., Jin, D.Y., Wong, Y.C., Cheung, A.L., Chun, A.C., Lo, A.K., Liu, Y., and Tsao, S.W. (2000). Correlation of defective mitotic checkpoint with aberrantly reduced expression of MAD2 protein in nasopharyngeal carcinoma cells. Carcinogenesis *21*, 2293-2297.

289. Doak, S.H., Jenkins, G.J., Parry, E.M., Griffiths, A.P., Baxter, J.N., and Parry, J.M. (2004). Differential expression of the MAD2, BUB1 and HSP27 genes in Barrett's oesophagus-their association with aneuploidy and neoplastic progression. Mutat Res *547*, 133-144.

290. Wu, C.W., Chi, C.W., and Huang, T.S. (2004). Elevated level of spindle checkprotein MAD2 correlates with cellular mitotic arrest, but not with aneuploidy and clinicopathological characteristics in gastric cancer. World J Gastroenterol *10*, 3240-3244.

291. Li, G.Q., and Zhang, H.F. (2004). Mad2 and p27 expression profiles in colorectal cancer and its clinical significance. World J Gastroenterol *10*, 3218-3220.

292. Li, G.Q., Li, H., and Zhang, H.F. (2003). Mad2 and p53 expression profiles in colorectal cancer and its clinical significance. World J Gastroenterol *9*, 1972-1975.

293. Reis, R.M., Nakamura, M., Masuoka, J., Watanabe, T., Colella, S., Yonekawa, Y., Kleihues, P., and Ohgaki, H. (2001). Mutation analysis of hBUB1, hBUBR1 and hBUB3 genes in glioblastomas. Acta Neuropathol (Berl) *101*, 297-304.

294. Haruki, N., Saito, H., Harano, T., Nomoto, S., Takahashi, T., Osada, H., Fujii, Y., and Takahashi, T. (2001). Molecular analysis of the mitotic checkpoint genes BUB1, BUBR1 and BUB3 in human lung cancers. Cancer Lett *162*, 201-205.

295. Mendoza, S., David, H., Gaylord, G.M., and Miller, C.W. (2005). Allelic loss at 10q26 in osteosarcoma in the region of the BUB3 and FGFR2 genes. Cancer Genet Cytogenet *158*, 142-147.

296. Miura, K., Bowman, E.D., Simon, R., Peng, A.C., Robles, A.I., Jones, R.T., Katagiri, T., He, P., Mizukami, H., Charboneau, L., Kikuchi, T., Liotta, L.A., Nakamura, Y., and Harris, C.C. (2002). Laser capture microdissection and microarray expression analysis of lung adenocarcinoma reveals tobacco smoking- and prognosis-related molecular profiles. Cancer Res *62*, 3244-3250.

297. Grabsch, H., Takeno, S., Parsons, W.J., Pomjanski, N., Boecking, A., Gabbert, H.E., and Mueller, W. (2003). Overexpression of the mitotic checkpoint genes BUB1, BUBR1, and BUB3 in gastric cancer--association with tumour cell proliferation. J Pathol *200*, 16-22.

298. Myrie, K.A., Percy, M.J., Azim, J.N., Neeley, C.K., and Petty, E.M. (2000). Mutation and expression analysis of human BUB1 and BUB1B in aneuploid breast cancer cell lines. Cancer Lett *152*, 193-199.

299. Sato, M., Sekido, Y., Horio, Y., Takahashi, M., Saito, H., Minna, J.D., Shimokata, K., and Hasegawa, Y. (2000). Infrequent mutation of the hBUB1 and hBUBR1 genes in human lung cancer. Jpn J Cancer Res *91*, 504-509.

300. Ouyang, B., Knauf, J.A., Ain, K., Nacev, B., and Fagin, J.A. (2002). Mechanisms of aneuploidy in thyroid cancer cell lines and tissues: evidence for mitotic checkpoint dysfunction without mutations in BUB1 and BUBR1. Clin Endocrinol (Oxf) *56*, 341-350.

301. Hempen, P.M., Kurpad, H., Calhoun, E.S., Abraham, S., and Kern, S.E. (2003). A double missense variation of the BUB1 gene and a defective mitotic spindle checkpoint in the pancreatic cancer cell line Hs766T. Hum Mutat *21*, 445.

302. Shichiri, M., Yoshinaga, K., Hisatomi, H., Sugihara, K., and Hirata, Y. (2002). Genetic and epigenetic inactivation of mitotic checkpoint genes hBUB1 and hBUBR1 and their relationship to survival. Cancer Res *62*, 13-17.

303. Ohshima, K., Haraoka, S., Yoshioka, S., Hamasaki, M., Fujiki, T., Suzumiya, J., Kawasaki, C., Kanda, M., and Kikuchi, M. (2000). Mutation analysis of mitotic checkpoint genes (hBUB1 and hBUBR1) and microsatellite instability in adult T-cell leukemia/lymphoma. Cancer Lett *158*, 141-150.

304. Seike, M., Gemma, A., Hosoya, Y., Hosomi, Y., Okano, T., Kurimoto, F., Uematsu, K., Takenaka, K., Yoshimura, A., Shibuya, M., Ui-Tei, K., and Kudoh, S. (2002). The promoter region of the human BUBR1 gene and its expression analysis in lung cancer. Lung Cancer *38*, 229-234.

305. Hanks, S., Coleman, K., Reid, S., Plaja, A., Firth, H., Fitzpatrick, D., Kidd, A., Mehes, K., Nash, R., Robin, N., Shannon, N., Tolmie, J., Swansbury, J., Irrthum, A., Douglas, J., and Rahman, N. (2004). Constitutional aneuploidy and cancer predisposition caused by biallelic mutations in BUB1B. Nat Genet *36*, 1159-1161.

306. Matsuura, S., Matsumoto, Y., Morishima, K., Izumi, H., Matsumoto, H., Ito, E., Tsutsui, K., Kobayashi, J., Tauchi, H., Kajiwara, Y., Hama, S., Kurisu, K., Tahara, H., Oshimura, M., Komatsu, K., Ikeuchi, T., and Kajii, T. (2006). Monoallelic BUB1B mutations and defective mitotic-spindle checkpoint in seven families with premature chromatid separation (PCS) syndrome. Am J Med Genet A *140*, 358-367.

307. Vigfusson, N.V., Dawson, R.J., Jones, J.F., Shaw, K.J., Lloyd, M.A., Ruppenthal, G.C., and Sackett, G.P. (1986). Mosaic variegated trisomy (42,XY/43,XY, + variable) in a male pigtail macaque monkey. Cytogenet Cell Genet *42*, 154-158.

308. Warburton, D., Anyane-Yeboa, K., Taterka, P., Yu, C.Y., and Olsen, D. (1991). Mosaic variegated aneuploidy with microcephaly: a new human mitotic mutant? Ann Genet *34*, 287-292.

309. Bitoun, P., Martin-Pont, B., Tamboise, E., and Gaudelus, J. (1994). Optic atrophy, microcephaly, mental retardation and mosaic variegated aneuploidy: a human mitotic mutation. Ann Genet *37*, 75-77.

310. Kajii, T., Kawai, T., Takumi, T., Misu, H., Mabuchi, O., Takahashi, Y., Tachino, M., Nihei, F., and Ikeuchi, T. (1998). Mosaic variegated aneuploidy with multiple congenital abnormalities: homozygosity for total premature chromatid separation trait. Am J Med Genet *78*, 245-249.

311. Limwongse, C., Schwartz, S., Bocian, M., and Robin, N.H. (1999). Child with mosaic variegated aneuploidy and embryonal rhabdomyosarcoma. Am J Med Genet *82*, 20-24.

312. Kawame, H., Sugio, Y., Fuyama, Y., Hayashi, Y., Suzuki, H., Kurosawa, K., and Maekawa, K. (1999). Syndrome of microcephaly, Dandy-Walker malformation, and Wilms tumor caused by mosaic variegated aneuploidy with premature centromere division (PCD): report of a new case and review of the literature. J Hum Genet *44*, 219-224.

313. Lane, A.H., Aijaz, N., Galvin-Parton, P., Lanman, J., Mangano, R., and Wilson, T.A. (2002). Mosaic variegated aneuploidy with growth hormone deficiency and congenital heart defects. Am J Med Genet *110*, 273-277.

314. Bower, K.L., Dennis, N.R., Wellesley, D., Williams, C.P., Hodgkins, P., Tyreman, C., Browne, C.E., and Barber, J.C. (2003). New case of "apple-peel" intestinal atresia and ocular anomalies with mosaic variegated aneuploidy. Am J Med Genet A *117*, 200-201.

315. Matsuura, S., Ito, E., Tauchi, H., Komatsu, K., Ikeuchi, T., and Kajii, T. (2000). Chromosomal instability syndrome of total premature chromatid separation with mosaic variegated aneuploidy is defective in mitotic-spindle checkpoint. Am J Hum Genet *67*, 483-486.

316. Kajii, T., Ikeuchi, T., Yang, Z.Q., Nakamura, Y., Tsuji, Y., Yokomori, K., Kawamura, M., Fukuda, S., Horita, S., and Asamoto, A. (2001). Cancer-prone syndrome of mosaic variegated aneuploidy and total premature chromatid separation: report of five infants. Am J Med Genet *104*, 57-64.

317. Jacquemont, S., Boceno, M., Rival, J.M., Mechinaud, F., and David, A. (2002). High risk of malignancy in mosaic variegated aneuploidy syndrome. Am J Med Genet *109*, 17-21; discussion 16.

318. Furukawa, T., Azakami, S., Kurosawa, H., Ono, Y., Ueda, Y., and Konno, Y. (2003). Cystic partially differentiated nephroblastoma, embryonal rhabdomyosarcoma, and multiple congenital anomalies associated with variegated mosaic aneuploidy and premature centromere division: a case report. J Pediatr Hematol Oncol *25*, 896-899.

319. Hunter, A. (2003). High risk of malignancy in mosaic variegated aneuploidy syndrome. Am J Med Genet A *117*, 199.

320. Hanks, S., Coleman, K., Summersgill, B., Messahel, B., Williamson, D., Pritchard-Jones, K., Strefford, J., Swansbury, J., Plaja, A., Shipley, J., and Rahman, N. (2006). Comparative genomic hybridization and BUB1B mutation analyses in childhood cancers associated with mosaic variegated aneuploidy syndrome. Cancer Lett *239*, 234-238.

321. Cowley, D.O., Muse, G.W., and Van Dyke, T. (2005). A dominant interfering Bub1 mutant is insufficient to induce or alter thymic tumorigenesis in vivo, even in a sensitized genetic background. Mol Cell Biol *25*, 7796-7802.

322. Gemma, A., Seike, M., Seike, Y., Uematsu, K., Hibino, S., Kurimoto, F., Yoshimura, A., Shibuya, M., Harris, C.C., and Kudoh, S. (2000). Somatic mutation of the hBUB1 mitotic checkpoint gene in primary lung cancer. Genes Chromosomes Cancer *29*, 213-218.

323. Ru, H.Y., Chen, R.L., Lu, W.C., and Chen, J.H. (2002). hBUB1 defects in leukemia and lymphoma cells. Oncogene *21*, 4673-4679.

324. Jaffrey, R.G., Pritchard, S.C., Clark, C., Murray, G.I., Cassidy, J., Kerr, K.M., Nicolson, M.C., and McLeod, H.L. (2000). Genomic instability at the BUB1 locus in colorectal cancer, but not in non-small cell lung cancer. Cancer Res *60*, 4349-4352.

325. Nakagawa, H., Yokozaki, H., Oue, N., Sugiyama, M., Ishikawa, T., Tahara, E., and Yasui, W. (2002). No mutations of the Bub1 gene in human gastric and oral cancer cell lines. Oncol Rep *9*, 1229-1232.

326. Yamaguchi, K., Okami, K., Hibi, K., Wehage, S.L., Jen, J., and Sidransky, D. (1999). Mutation analysis of hBUB1 in aneuploid HNSCC and lung cancer cell lines. Cancer Lett *139*, 183-187.

327. Lin, S.F., Lin, P.M., Yang, M.C., Liu, T.C., Chang, J.G., Sue, Y.C., and Chen, T.P. (2002). Expression of hBUB1 in acute myeloid leukemia. Leuk Lymphoma *43*, 385-391.

328. Mimori, K., Inoue, H., Alder, H., Ueo, H., Tanaka, Y., and Mori, M. (2001). Mutation analysis of hBUB1, human mitotic checkpoint gene in multiple carcinomas. Oncol Rep *8*, 39-42.

329. Shigeishi, H., Yokozaki, H., Kuniyasu, H., Nakagawa, H., Ishikawa, T., Tahara, E., and Yasui, W. (2001). No mutations of the Bub1 gene in human gastric carcinomas. Oncol Rep *8*, 791-794.

330. Langerod, A., Stromberg, M., Chin, K., Kristensen, V.N., and Borresen-Dale, A.L. (2003). BUB1 infrequently mutated in human breast carcinomas. Hum Mutat *22*, 420.
331. Shigeishi, H., Oue, N., Kuniyasu, H., Wakikawa, A., Yokozaki, H., Ishikawa, T., and Yasui, W. (2001). Expression of Bub1 gene correlates with tumor proliferating activity in human gastric carcinomas. Pathobiology *69*, 24-29.
332. Lewis, T.B., Robison, J.E., Bastien, R., Milash, B., Boucher, K., Samlowski, W.E., Leachman, S.A., Dirk Noyes, R., Wittwer, C.T., Perreard, L., and Bernard, P.S. (2005). Molecular classification of melanoma using real-time quantitative reverse transcriptase-polymerase chain reaction. Cancer *104*, 1678-1686.
333. Qian, Z., Fernald, A.A., Godley, L.A., Larson, R.A., and Le Beau, M.M. (2002). Expression profiling of CD34+ hematopoietic stem/ progenitor cells reveals distinct subtypes of therapy-related acute myeloid leukemia. Proc Natl Acad Sci U S A *99*, 14925-14930.
334. Shigeishi, H., Yoneda, S., Taki, M., Nobumori, T., Ohta, K., Higashikawa, K., Yasui, W., and Kamata, N. (2006). Correlation of human Bub1 expression with tumor-proliferating activity in salivary gland tumors. Oncol Rep *15*, 933-938.
335. Li, D., Zhu, J., Firozi, P.F., Abbruzzese, J.L., Evans, D.B., Cleary, K., Friess, H., and Sen, S. (2003). Overexpression of oncogenic STK15/BTAK/Aurora A kinase in human pancreatic cancer. Clin Cancer Res *9*, 991-997.
336. Singhal, S., Amin, K.M., Kruklitis, R., DeLong, P., Friscia, M.E., Litzky, L.A., Putt, M.E., Kaiser, L.R., and Albelda, S.M. (2003). Alterations in cell cycle genes in early stage lung adenocarcinoma identified by expression profiling. Cancer Biol Ther *2*, 291-298.
337. Kim, J.M., Sohn, H.Y., Yoon, S.Y., Oh, J.H., Yang, J.O., Kim, J.H., Song, K.S., Rho, S.M., Yoo, H.S., Kim, Y.S., Kim, J.G., and Kim, N.S. (2005). Identification of gastric cancer-related genes using a cDNA microarray containing novel expressed sequence tags expressed in gastric cancer cells. Clin Cancer Res *11*, 473-482.
338. Wang, C.X., Fisk, B.C., Wadehra, M., Su, H., and Braun, J. (2000). Overexpression of murine fizzy-related (fzr) increases natural killer cell-mediated cell death and suppresses tumor growth. Blood *96*, 259-263.
339. Matsumoto, T., Baker, D.J., d'Uscio, L.V., Mozammel, G., Katusic, Z.S., and van Deursen, J.M. (2007). Aging-associated vascular phenotype in mutant mice with low levels of BubR1. Stroke *38*, 1050-1056.
340. Hartman, T.K., Wengenack, T.M., Poduslo, J.F., and van Deursen, J.M. (2007). Mutant mice with small amounts of BubR1 display accelerated age-related gliosis. Neurobiol Aging *28*, 921-927.
341. Campisi, J. (2003). Cellular senescence and apoptosis: how cellular responses might influence aging phenotypes. Exp Gerontol *38*, 5-11.
342. Kirkwood, T.B., and Austad, S.N. (2000). Why do we age? Nature *408*, 233-238.
343. Krtolica, A., and Campisi, J. (2002). Cancer and aging: a model for the cancer promoting effects of the aging stroma. Int J Biochem Cell Biol *34*, 1401-1414.
344. Campisi, J. (2005). Senescent cells, tumor suppression, and organismal aging: good citizens, bad neighbors. Cell *120*, 513-522.
345. Ben-Porath, I., and Weinberg, R.A. (2005). The signals and pathways activating cellular senescence. Int J Biochem Cell Biol *37*, 961-976.
346. Collado, M., and Serrano, M. (2006). The power and the promise of oncogene-induced senescence markers. Nat Rev Cancer *6*, 472-476.

347. Ben-Porath, I., and Weinberg, R.A. (2004). When cells get stressed: an integrative view of cellular senescence. J Clin Invest *113*, 8-13.
348. Lombard, D.B., Chua, K.F., Mostoslavsky, R., Franco, S., Gostissa, M., and Alt, F.W. (2005). DNA repair, genome stability, and aging. Cell *120*, 497-512.
349. Itahana, K., Campisi, J., and Dimri, G.P. (2004). Mechanisms of cellular senescence in human and mouse cells. Biogerontology *5*, 1-10.
350. Krishnamurthy, J., Torrice, C., Ramsey, M.R., Kovalev, G.I., Al-Regaiey, K., Su, L., and Sharpless, N.E. (2004). Ink4a/Arf expression is a biomarker of aging. J Clin Invest *114*, 1299-1307.
351. Molofsky, A.V., Slutsky, S.G., Joseph, N.M., He, S., Pardal, R., Krishnamurthy, J., Sharpless, N.E., and Morrison, S.J. (2006). Increasing p16INK4a expression decreases forebrain progenitors and neurogenesis during ageing. Nature *443*, 448-452.
352. Janzen, V., Forkert, R., Fleming, H.E., Saito, Y., Waring, M.T., Dombkowski, D.M., Cheng, T., DePinho, R.A., Sharpless, N.E., and Scadden, D.T. (2006). Stem-cell ageing modified by the cyclin-dependent kinase inhibitor p16INK4a. Nature *443*, 421-426.
353. Krishnamurthy, J., Ramsey, M.R., Ligon, K.L., Torrice, C., Koh, A., Bonner-Weir, S., and Sharpless, N.E. (2006). p16INK4a induces an age-dependent decline in islet regenerative potential. Nature *443*, 453-457.
354. Levine, A.J. (1997). p53, the cellular gatekeeper for growth and division. Cell *88*, 323-331.
355. Tyner, S.D., Venkatachalam, S., Choi, J., Jones, S., Ghebranious, N., Igelmann, H., Lu, X., Soron, G., Cooper, B., Brayton, C., Hee Park, S., Thompson, T., Karsenty, G., Bradley, A., and Donehower, L.A. (2002). p53 mutant mice that display early ageing-associated phenotypes. Nature *415*, 45-53.
356. Garcia-Cao, I., Garcia-Cao, M., Martin-Caballero, J., Criado, L.M., Klatt, P., Flores, J.M., Weill, J.C., Blasco, M.A., and Serrano, M. (2002). "Super p53" mice exhibit enhanced DNA damage response, are tumor resistant and age normally. Embo J *21*, 6225-6235.
357. Matheu, A., Maraver, A., Klatt, P., Flores, I., Garcia-Cao, I., Borras, C., Flores, J.M., Vina, J., Blasco, M.A., and Serrano, M. (2007). Delayed ageing through damage protection by the Arf/p53 pathway. Nature *448*, 375-379.
358. Maier, B., Gluba, W., Bernier, B., Turner, T., Mohammad, K., Guise, T., Sutherland, A., Thorner, M., and Scrable, H. (2004). Modulation of mammalian life span by the short isoform of p53. Genes Dev *18*, 306-319.
359. Lebel, M., and Leder, P. (1998). A deletion within the murine Werner syndrome helicase induces sensitivity to inhibitors of topoisomerase and loss of cellular proliferative capacity. Proc Natl Acad Sci U S A *95*, 13097-13102.
360. Lombard, D.B., Beard, C., Johnson, B., Marciniak, R.A., Dausman, J., Bronson, R., Buhlmann, J.E., Lipman, R., Curry, R., Sharpe, A., Jaenisch, R., and Guarente, L. (2000). Mutations in the WRN gene in mice accelerate mortality in a p53-null background. Mol Cell Biol *20*, 3286-3291.
361. Ito, K., Hirao, A., Arai, F., Matsuoka, S., Takubo, K., Hamaguchi, I., Nomiyama, K., Hosokawa, K., Sakurada, K., Nakagata, N., Ikeda, Y., Mak, T.W., and Suda, T. (2004). Regulation of oxidative stress by ATM is required for self-renewal of haematopoietic stem cells. Nature *431*, 997-1002.
362. Shiloh, Y., and Kastan, M.B. (2001). ATM: genome stability, neuronal development, and cancer cross paths. Adv Cancer Res *83*, 209-254.
363. Cao, L., Li, W., Kim, S., Brodie, S.G., and Deng, C.X. (2003). Senescence, aging, and malignant transformation mediated by p53 in mice lacking the Brca1 full-length isoform. Genes Dev *17*, 201-213.

364. Bender, C.F., Sikes, M.L., Sullivan, R., Huye, L.E., Le Beau, M.M., Roth, D.B., Mirzoeva, O.K., Oltz, E.M., and Petrini, J.H. (2002). Cancer predisposition and hematopoietic failure in Rad50(S/S) mice. Genes Dev *16*, 2237-2251.

365. Vogel, H., Lim, D.S., Karsenty, G., Finegold, M., and Hasty, P. (1999). Deletion of Ku86 causes early onset of senescence in mice. Proc Natl Acad Sci U S A *96*, 10770-10775.

366. Espejel, S., Martin, M., Klatt, P., Martin-Caballero, J., Flores, J.M., and Blasco, M.A. (2004). Shorter telomeres, accelerated ageing and increased lymphoma in DNA-PKcs-deficient mice. EMBO Rep *5*, 503-509.

367. de Laat, W.L., Jaspers, N.G., and Hoeijmakers, J.H. (1999). Molecular mechanism of nucleotide excision repair. Genes Dev *13*, 768-785.

368. de Boer, J., Andressoo, J.O., de Wit, J., Huijmans, J., Beems, R.B., van Steeg, H., Weeda, G., van der Horst, G.T., van Leeuwen, W., Themmen, A.P., Meradji, M., and Hoeijmakers, J.H. (2002). Premature aging in mice deficient in DNA repair and transcription. Science *296*, 1276-1279.

369. de Boer, J., van Steeg, H., Berg, R.J., Garssen, J., de Wit, J., van Oostrum, C.T., Beems, R.B., van der Horst, G.T., van Kreijl, C.F., de Gruijl, F.R., Bootsma, D., Hoeijmakers, J.H., and Weeda, G. (1999). Mouse model for the DNA repair/basal transcription disorder trichothiodystrophy reveals cancer predisposition. Cancer Res *59*, 3489-3494.

370. de Boer, J., de Wit, J., van Steeg, H., Berg, R.J., Morreau, H., Visser, P., Lehmann, A.R., Duran, M., Hoeijmakers, J.H., and Weeda, G. (1998). A mouse model for the basal transcription/DNA repair syndrome trichothiodystrophy. Mol Cell *1*, 981-990.

371. Nance, M.A., and Berry, S.A. (1992). Cockayne syndrome: review of 140 cases. Am J Med Genet *42*, 68-84.

372. Murai, M., Enokido, Y., Inamura, N., Yoshino, M., Nakatsu, Y., van der Horst, G.T., Hoeijmakers, J.H., Tanaka, K., and Hatanaka, H. (2001). Early postnatal ataxia and abnormal cerebellar development in mice lacking Xeroderma pigmentosum Group A and Cockayne syndrome Group B DNA repair genes. Proc Natl Acad Sci U S A *98*, 13379-13384.

373. McWhir, J., Selfridge, J., Harrison, D.J., Squires, S., and Melton, D.W. (1993). Mice with DNA repair gene (ERCC-1) deficiency have elevated levels of p53, liver nuclear abnormalities and die before weaning. Nat Genet *5*, 217-224.

374. Weeda, G., Donker, I., de Wit, J., Morreau, H., Janssens, R., Vissers, C.J., Nigg, A., van Steeg, H., Bootsma, D., and Hoeijmakers, J.H. (1997). Disruption of mouse ERCC1 results in a novel repair syndrome with growth failure, nuclear abnormalities and senescence. Curr Biol *7*, 427-439.

375. Blasco, M.A. (2003). Telomeres in cancer and aging: lessons from the mouse. Cancer Lett *194*, 183-188.

376. Goytisolo, F.A., and Blasco, M.A. (2002). Many ways to telomere dysfunction: in vivo studies using mouse models. Oncogene *21*, 584-591.

377. d'Adda di Fagagna, F., Reaper, P.M., Clay-Farrace, L., Fiegler, H., Carr, P., Von Zglinicki, T., Saretzki, G., Carter, N.P., and Jackson, S.P. (2003). A DNA damage checkpoint response in telomere-initiated senescence. Nature *426*, 194-198.

378. Blasco, M.A., and Hahn, W.C. (2003). Evolving views of telomerase and cancer. Trends Cell Biol *13*, 289-294.

379. Lee, H.W., Blasco, M.A., Gottlieb, G.J., Horner, J.W., 2nd, Greider, C.W., and DePinho, R.A. (1998). Essential role of mouse telomerase in highly proliferative organs. Nature *392*, 569-574.

380. Espejel, S., Klatt, P., Menissier-de Murcia, J., Martin-Caballero, J., Flores, J.M., Taccioli, G., de Murcia, G., and Blasco, M.A. (2004). Impact of telomerase ablation on organismal viability, aging,

and tumorigenesis in mice lacking the DNA repair proteins PARP-1, Ku86, or DNA-PKcs. J Cell Biol *167*, 627-638.

381. Wong, K.K., Maser, R.S., Bachoo, R.M., Menon, J., Carrasco, D.R., Gu, Y., Alt, F.W., and DePinho, R.A. (2003). Telomere dysfunction and Atm deficiency compromises organ homeostasis and accelerates ageing. Nature *421*, 643-648.

382. Chang, S., Multani, A.S., Cabrera, N.G., Naylor, M.L., Laud, P., Lombard, D., Pathak, S., Guarente, L., and DePinho, R.A. (2004). Essential role of limiting telomeres in the pathogenesis of Werner syndrome. Nat Genet *36*, 877-882.

383. Sun, L.Q., Lee, D.W., Zhang, Q., Xiao, W., Raabe, E.H., Meeker, A., Miao, D., Huso, D.L., and Arceci, R.J. (2004). Growth retardation and premature aging phenotypes in mice with disruption of the SNF2-like gene, PASG. Genes Dev *18*, 1035-1046.

384. Trifunovic, A., Wredenberg, A., Falkenberg, M., Spelbrink, J.N., Rovio, A.T., Bruder, C.E., Bohlooly, Y.M., Gidlof, S., Oldfors, A., Wibom, R., Tornell, J., Jacobs, H.T., and Larsson, N.G. (2004). Premature ageing in mice expressing defective mitochondrial DNA polymerase. Nature *429*, 417-423.

385. Hasty, P., Campisi, J., Hoeijmakers, J., van Steeg, H., and Vijg, J. (2003). Aging and genome maintenance: lessons from the mouse? Science *299*, 1355-1359.

Chapter 3

BubR1 insufficiency causes early onset of aging-associated phenotypes and infertility in mice

Nature Genetics 36, 744-749
Reprinted with permission

BubR1 insufficiency causes early onset of aging-associated phenotypes and infertility in mice

Darren J Baker[1,2], Karthik B Jeganathan[1,2], J Douglas Cameron[3], Michael Thompson[1,2], Subhash Juneja[2], Alena Kopecka[1], Rajiv Kumar[2,4], Robert B Jenkins[5], Piet C de Groen[4], Patrick Roche[5] & Jan M van Deursen[1,2]

Faithful segregation of replicated chromosomes is essential for maintenance of genetic stability and seems to be monitored by several mitotic checkpoints. Various components of these checkpoints have been identified in mammals, but their physiological relevance is largely unknown. Here we show that mutant mice with low levels of the spindle assembly checkpoint protein BubR1 develop progressive aneuploidy along with a variety of progeroid features, including short lifespan, cachectic dwarfism, lordokyphosis, cataracts, loss of subcutaneous fat and impaired wound healing. Graded reduction of BubR1 expression in mouse embryonic fibroblasts causes increased aneuploidy and senescence. Male and female mutant mice have defects in meiotic chromosome segregation and are infertile. Natural aging of wild-type mice is marked by decreased expression of BubR1 in multiple tissues, including testis and ovary. These results suggest a role for BubR1 in regulating aging and infertility.

In humans, aueuploidy is a hallmark of spontaneous abortions, birth defects and most cancers[1–3]. Accurate separation of duplicated chromosomes is ensured by the spindle assembly checkpoint, which prevents anaphase onset until each kinetochore has attached to mitotic spindle microtubules[4–6]. To determine the physiological role of the spindle assembly checkpoint protein BubR1, encoded by *Bub1b*, we produced a series of mice in which expression of BubR1 is reduced in graded fashion from normal levels to zero by the use of wild-type ($Bub1b^{+}$), knockout ($Bub1b^{-}$) and hypomorphic ($Bub1b^{H}$) alleles (**Fig. 1a,b** and **Supplementary Methods** and **Supplementary Fig. 1** online). As previously described[7], complete loss of BubR1 caused early embryonic lethality (data not shown). $Bub1b^{-/H}$ mice died within several hours of birth, seemingly due to respiratory insufficiency, whereas $Bub1b^{H/H}$ mice survived to adulthood. $Bub1b^{H/H}$ mice were normal in appearance and size at birth but had slow postnatal growth (**Fig. 1c**). $Bub1b^{+/-}$ and $Bub1b^{+/H}$ mice had no overtly abnormal phenotypes

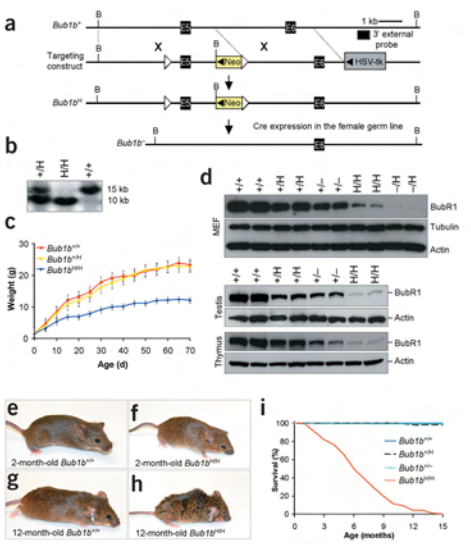

Figure 1 Cachectic dwarfism and short lifespan in BubR1-insufficient mice. (**a**) Schematic representation of the *Bub1b* gene-targeting strategy. Part of the *Bub1b* locus (+), the targeting vector with *lox*P sites (open triangles), the hypomorphic (H) and knockout (–) *Bub1b* alleles, *Bam*HI restriction sites (B) and the Southern blot probe are indicated. (**b**) Southern-blot analysis of mice with indicated *Bub1b* genotypes. The 15-kb and 10-kb fragments represent the wild-type and hypomorphic alleles, respectively. (**c**) Growth curves of $Bub1b^{+/+}$, $Bub1b^{+/H}$ and $Bub1b^{H/H}$ mice. (**d**) Western-blot analysis of MEFs, testis and thymus from mice carrying the indicated *Bub1b* alleles with antibodies against BubR1 (α-tubulin and β-actin were used for loading control). (**e–h**) Photographs of $Bub1b^{H/H}$ and $Bub1b^{+/+}$ mice at indicated ages. (**i**) Survival analysis of $Bub1b^{H/H}$ ($n = 212$), $Bub1b^{+/H}$ ($n = 108$, two animals died before 15 months), $Bub1b^{+/-}$ ($n = 43$) and $Bub1b^{+/+}$ ($n = 50$) mice.

Departments of [1]Pediatric and Adolescent Medicine, [2]Biochemistry and Molecular Biology, [3]Ophthalmology, [4]Medicine and [5]Pathology, Mayo Clinic, 200 First Street SW, Rochester, Minnesota 55905, USA. Correspondence should be addressed to J.M.v.D. (vandeursen.jan@mayo.edu).

(**Supplementary Fig. 2** online). Decreased expression of BubR1 was confirmed by western-blot analysis (**Fig. 1d**). BubR1 signals from *Bub1b*$^{+/H}$, *Bub1b*$^{+/-}$, *Bub1b*$^{H/H}$ and *Bub1b*$^{-/H}$ mouse embryonic fibroblasts (MEFs) were 42% (± 15%), 29% (± 9%), 11% (± 3%) and 4% (± 2%), respectively, of those from *Bub1b*$^{+/+}$ MEFs.

We monitored 50 *Bub1b*$^{+/+}$, 108 *Bub1b*$^{+/H}$, 43 *Bub1b*$^{+/-}$ and 230 *Bub1b*$^{H/H}$ mice to 15–16 months of age. One *Bub1b*$^{H/H}$ mouse developed a life-threatening tumor. Six of 116 moribund or deceased *Bub1b*$^{H/H}$ mice had solitary tumors at autopsy. *Bub1b*$^{H/H}$ mice had a normal appearance until 2–3 months of age (**Fig. 1f**; compare with wild-type mouse in **Fig. 1e**) but typically developed cachexia and lordokyphosis at 3–6 months of age (**Fig. 1h** and **Supplementary Fig. 2** online; compare with wild-type mouse in **Fig. 1g**). The median lifespan of *Bub1b*$^{H/H}$ mice was ~6 months, compared with more than 15 months for *Bub1b*$^{+/-}$, *Bub1b*$^{+/H}$ and *Bub1b*$^{+/+}$ mice (**Fig. 1i**). At age 2 months and older, *Bub1b*$^{H/H}$ mice developed progressive bilateral cataracts with features reminiscent of age-related human cataracts (**Fig. 2a**). No cataracts were observed in *Bub1b*$^{+/-}$, *Bub1b*$^{+/H}$ or *Bub1b*$^{+/+}$ mice. Histological analysis of skin showed that the dermis and subcutaneous fat cell layers were significantly thinner in 12-month-old *Bub1b*$^{H/H}$ mice than in control mice (**Fig. 2b,c** and **Supplementary Fig. 2** online). Skinning of *Bub1b*$^{H/H}$ mice confirmed substantial loss of subdermal adipose tissue and highlighted their severe spinal kyphosis and muscle atrophy (**Fig. 2d**). Dual-energy X-ray absorptiometry measurements confirmed that total body fat of *Bub1b*$^{H/H}$ mice declined prematurely (**Fig. 2e**). *Bub1b*$^{H/H}$ mice also had less ability to repair wounds at an early age (**Fig. 2f**). Taken together, these results (**Supplementary Table 1** online) suggest that multiple aging-associated phenotypes develop early in mice expressing BubR1 below a threshold level.

To investigate whether the progeroid phenotypes could be due to a defective spindle assembly checkpoint, we measured the ability of *Bub1b*-mutant MEFs to induce a sustained preanaphase arrest in the presence of nocodazole. Approximately 11–12% of *Bub1b*$^{+/+}$, *Bub1b*$^{+/H}$ and *Bub1b*$^{+/-}$ MEFs were arrested by 12 h (**Fig. 3a**). In

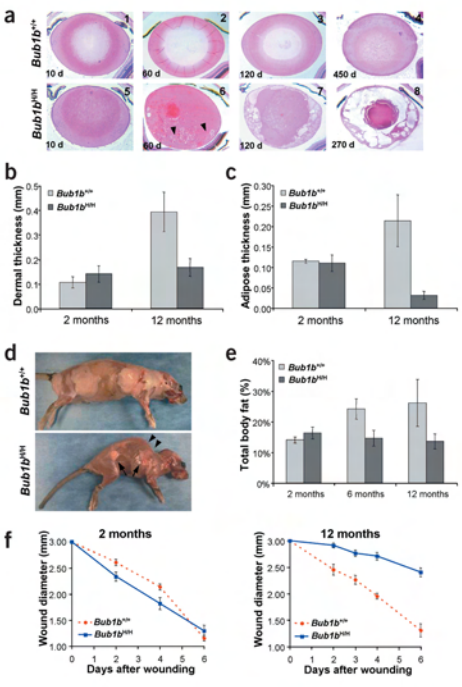

Figure 2 Aging phenotypes in *Bub1b*$^{H/H}$ mice. (**a**) Cross-sections of lenses from *Bub1b*$^{H/H}$ and *Bub1b*$^{+/+}$ mice at various ages stained with hematoxylin and eosin. *Bub1b*$^{H/H}$ lenses were normal at day 10 but showed Morgagnian globules at day 60 (arrowheads), overt cataracts at day 120 and advanced stage nuclear cataracts at day 270. (**b**) Dermal layer thickness of *Bub1b*$^{H/H}$ and *Bub1b*$^{+/+}$ mice at indicated ages ($n = 3$ mice per group). (**c**) Subcutaneous adipose layer thickness of *Bub1b*$^{H/H}$ and *Bub1b*$^{+/+}$ mice at indicated ages ($n = 3$ mice per group). (**d**) Skinned 9-month-old *Bub1b*$^{+/+}$ (top) and *Bub1b*$^{H/H}$ (bottom) females. The *Bub1b*$^{H/H}$ mouse had little subcutaneous fat (arrows) and pronounced kyphosis (arrowheads). (**e**) Analysis of total body fat of *Bub1b*$^{+/+}$ and *Bub1b*$^{H/H}$ females at indicated ages ($n = 3$ mice per genotype and age group). (**f**) Closure of 3-mm punch biopsy wounds in *Bub1b*$^{+/+}$ and *Bub1b*$^{H/H}$ mice at 2 months (left panel) and 12 months (right panel) of age.

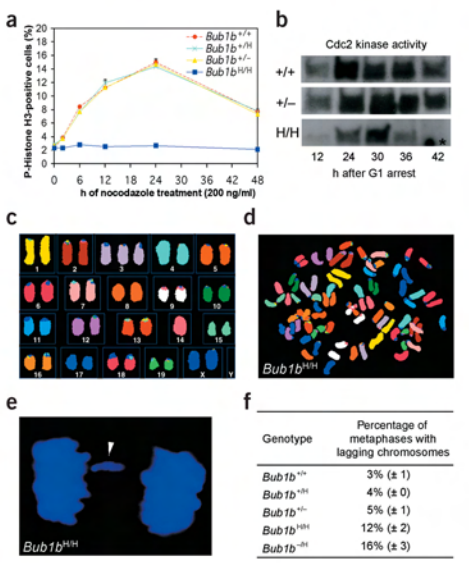

Genotype	Percentage of metaphases with lagging chromosomes
Bub1b$^{+/+}$	3% (± 1)
Bub1b$^{+/H}$	4% (± 0)
Bub1b$^{+/-}$	5% (± 1)
Bub1b$^{H/H}$	12% (± 2)
Bub1b$^{-/H}$	16% (± 3)

Figure 3 *Bub1b*$^{H/H}$ cells have mitotic checkpoint defects. (**a**) Mitotic index (defined as the percentage of mitotic cells) of nocodazole-treated MEF lines of indicated genotypes ($n = 3$ for each genotype). The growth rates of these MEF lines were similar (growth curves not shown). (**b**) Cyclin B–associated Cdc2 kinase activity of synchronized MEF cells at indicated time points after release into medium with high serum and nocodazole. The asterisk marks an aspecific spot on the autoradiogram. (**c**) Spectral karyotype of a numerically normal *Bub1b*$^{H/H}$ metaphase with a gain of chromosome 3 and a loss of chromosome 14. (**d**) Spectral image of a *Bub1b*$^{H/H}$ metaphase (MEF) that shows PMSCS. (**e**) *Bub1b*$^{H/H}$ MEF cell with a lagging chromosome in anaphase. DNA was stained with Hoechst. The arrowhead highlights a lagging chromosome. (**f**) The average percentage of anaphases with lagging chromosomes per genotype.

contrast, only 2.5% of *Bub1b*$^{H/H}$ MEFs were arrested by 12 h, suggesting that spindle assembly checkpoint function was severely compromised. We confirmed this result by flow cytometry (**Supplementary Fig. 3** online). Next, we synchronized MEFs in G1 and analyzed their cyclin B–associated Cdc2 kinase activity after releasing them into medium with nocodazole. *Bub1b*$^{H/H}$ cells had high Cdc2 kinase activity by 24–30 h after release, similar to *Bub1b*$^{+/+}$ cells (**Fig. 3b**). *Bub1b*$^{+/+}$ cells sustained high levels of Cdc2 activity until 42 h after restimulation, but *Bub1b*$^{H/H}$ cells did not maintain activity after 30 h, consistent with a spindle assembly checkpoint defect[8,9].

The average percentage of aneuploid metaphases was much higher in passage 5 (P5) *Bub1b*$^{H/H}$ MEFs than in P5 *Bub1b*$^{+/-}$, *Bub1b*$^{+/H}$ and *Bub1b*$^{+/+}$ MEFs (**Table 1a**). We observed even more profound aneuploidy in P5 *Bub1b*$^{-/H}$ MEFs. We also carried out spectral karyotype analysis on metaphase spreads from *Bub1b*$^{+/+}$ and *Bub1b*$^{H/H}$ MEFs. *Bub1b*$^{+/+}$ metaphases ($n = 9$) were karyotypically normal. In contrast, five of ten *Bub1b*$^{H/H}$ metaphases had numerical abnormalities. Furthermore, two numerically normal *Bub1b*$^{H/H}$ metaphases showed loss of one chromosome and gain of another (**Fig. 3c**). We observed premature sister chromatid separation (PMSCS), a hallmark of a defective spindle assembly checkpoint[8,9], in 38% and 15% of mitotic figures from *Bub1b*$^{-/H}$ and *Bub1b*$^{H/H}$ MEFs, respectively, but in only 1–3% of *Bub1b*$^{+/-}$, *Bub1b*$^{+/H}$ and *Bub1b*$^{+/+}$ MEFs (**Table 1a** and **Fig. 3d**). As expected, we observed more anaphase figures with lagging chromosomes in *Bub1b*$^{-/H}$ and *Bub1b*$^{H/H}$ cells than in *Bub1b*$^{+/-}$, *Bub1b*$^{+/H}$ or *Bub1b*$^{+/+}$ cells (**Fig. 3e,f**). Together, these data suggest that the accuracy of chromosome segregation is greatly affected when BubR1 levels drop below a certain level.

Bub1b$^{-/H}$ pups showed substantial aneuploidy at birth, but *Bub1b*$^{H/H}$ mice did not (**Table 1b**). At age 2 months, however, *Bub1b*$^{H/H}$ mice had developed mild aneuploidy that increased in both degree and severity as mice aged further. *Bub1b*$^{+/-}$ and *Bub1b*$^{+/H}$ mice did not have detectable aneuploidy. We observed no genome maintenance defects other than chromosome number instability in *Bub1b*$^{H/H}$ and *Bub1b*$^{-/H}$ cells (**Table 1a** and **Supplementary Fig. 4** online). The strong correlation between the onset and progression of the aging-associated phenotypes and the degree and the severity of the chromosome number instability in *Bub1b*$^{H/H}$ mice are suggestive of a role for aneuploidy stemming from BubR1 dysfunction in the development of progeroid features.

We next determined whether BubR1 deficiency triggers apoptosis or cellular senescence, two responses that have been linked to aging[10,11]. We found similar numbers of apoptotic cells in kidney, liver and lung sections from 1-year-old *Bub1b*$^{H/H}$ and *Bub1b*$^{+/+}$ mice, and in *Bub1b*$^{H/H}$ and *Bub1b*$^{+/+}$ MEF cultures (data not shown). Senescence-associated β-galactosidase activity was high in kidney sections from 5-month-old *Bub1b*$^{H/H}$ mice, but not in those from age-matched *Bub1b*$^{+/+}$ mice and 2-month-old *Bub1b*$^{H/H}$ mice (**Fig. 4a**). P3 *Bub1b*$^{H/H}$ MEFs had comparable growth rates (**Fig. 4d**) and numbers of cells positive for senescence-associated β-galactosidase activity to those of *Bub1b*$^{+/+}$ MEFs (**Fig. 4b**). At P7, however,

Table 1 Gradual reduction of BubR1 causes progressively more aneuploidy in MEFs and mice

(**a**)

Mitotic MEF genotype (*n*)	Percent figures inspected	Aneuploid figures	s.d.	Karyotypes with indicated chromosome number								Percent mitotic figures with PMSCS	s.d.	Percent mitotic figures with breaks	Percent mitotic figures with fusions
				38	39	40	41	42	43	44	45				
Bub1b$^{+/+}$ (6)	300	9 (11)[a]	2 (3)		4	137	9					2 (2)[a]	1 (1)	1	0
Bub1b$^{+/H}$ (3)	150	8	2		4	138	8		1			1	1	ND	ND
Bub1b$^{+/-}$ (6)	300	14	2		9	128	12		1			3	1	ND	ND
Bub1b$^{H/H}$ (3)	125	36 (35)[a]	6 (1)	5	13	80	20	6	1			15 (18)[a]	3 (3)	2	0
Bub1b$^{-/H}$ (3)	100	72	4	3	11	28	20	17	14	5	2	43	4	0	0

(**b**)

Mouse genotype	Age (*n*)	Mitotic figures inspected	Percent aneuploid figures	s.d.	Karyotypes with indicated chromosome number					Percent mitotic figures with PMSCS	s.d.
					38	39	40	41	42		
Bub1b$^{+/+}$	1 day (5)[b]	250	0	0			250			1	1
	2 months (5)	250	0	0			250			0	0
	5 months (4)	200	0	0			200			0	0
	1 year (3)	150	0	0			150			1	1
Bub1b$^{+/H}$	1 day (3)[b]	150	0	0			150			0	0
	1 year (3)	150	0	0			150			0	0
Bub1b$^{+/-}$	1 day (4)[b]	200	0	0			200			2	2
	1 year (3)	150	0	0			150			5	5
Bub1b$^{H/H}$	1 day (3)[b]	150	0	0			150			30	7
	2 months (7)	315	3	2		3	310	2		38	7
	3 months (3)	125	9	2		4	114	6	1	35	2
	5 months (4)	200	15	4	2	12	170	16		35	4
	12 months (5)	250	33	4	9	22	168	44	7	24	4
Bub1b$^{-/H}$	1 day (3)[b]	150	21	1	1	10	117	21	1	43	2

[a]Values in parentheses were derived from independently generated MEF lines cultured in 3% oxygen (instead of 20% oxygen). [b]Spleens did not contain sufficient cells for karyotyping at day 1 and livers were used at this age.

(**a**) Analysis of numerical and structural chromosomal abnormalities in P5 MEFs of indicated genotypes. Spectral karyotype analysis showed that the incidence of chromosomal translocations in *Bub1b*$^{+/+}$ and *Bub1b*$^{H/H}$ MEFs was similar (data not shown). ND, not done. (**b**) Aneuploidy and PMSCS in liver cells from newborn pups and splenocytes from adult mice of indicated genotypes and ages.

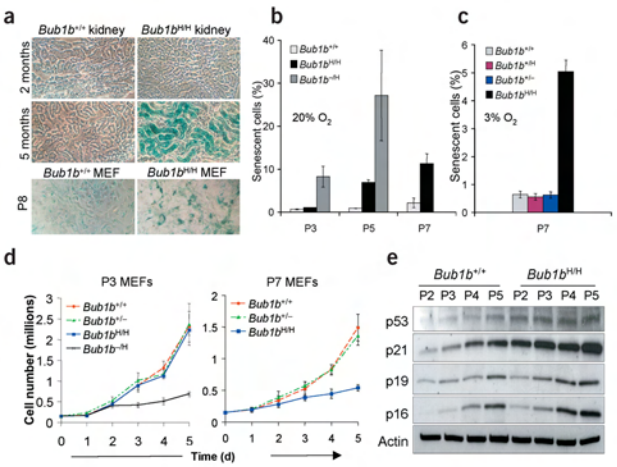

Figure 4 BubR1 insufficiency causes early onset of senescence. (**a**) Senescence-associated β-galactosidase activity in kidney sections of 2- and 5-month-old *Bub1b*$^{H/H}$ and *Bub1b*$^{+/+}$ mice, and in P8 *Bub1b*$^{H/H}$ and *Bub1b*$^{+/+}$ MEFs. (**b**) Percentages of *Bub1b*$^{-/H}$, *Bub1b*$^{H/H}$ and *Bub1b*$^{+/+}$ MEF cells cultured in 20% oxygen that were positive for senescence-associated β-galactosidase activity. Passages at which measurements were made are indicated. (**c**) Percentages of MEF cells of indicated genotypes cultured in 3% oxygen that were positive for senescence-associated β-galactosidase activity. (**d**) Growth curves of P3 (left panel) and P7 (right panel) MEF cells of indicated genotypes. (**e**) Expression of senescence-associated markers in *Bub1b*$^{H/H}$ and *Bub1b*$^{+/+}$ MEF cells at P2–P5.

Bub1b$^{H/H}$ MEF cultures had substantially slower growth rates and more cells positive for senescence-associated β-galactosidase activity than *Bub1b*$^{+/+}$ cultures (**Fig. 4b**,**d**). *Bub1b*$^{-/H}$ MEFs had even more profound growth inhibition and senescence-associated β-galactosidase activity (**Fig. 4b**,**d**), suggesting that the rate of senescence correlates with the degree of aneuploidy. *Bub1b*$^{H/H}$ MEFs senesced quickly in both 20% and 3% oxygen (**Fig. 4c**), indicating that oxidative DNA damage[12] is an unlikely cause of the senescence phenotype. *Bub1b*$^{H/H}$ MEFs showed early accumulation of the senescence markers p53, p21, p16 and p19 (**Fig. 4e**). Taken together, these results suggest that aneuploidy in cells from BubR1-insufficient mice might elicit signals that drive them into a senescent state and cause early aging-related phenotypes as they accumulate.

Bub1b$^{H/H}$ mice did not produce any pregnancies. Testicular weight of *Bub1b*$^{H/H}$ males (0.088 g ± 0.009; $n = 8$ testes) was slightly below that of *Bub1b*$^{+/+}$ males (0.106 g ± 0.006; $n = 8$ testes). Testes of 4-month-old *Bub1b*$^{H/H}$ mice were histologically normal (data not shown), but sperm counts of *Bub1b*$^{H/H}$ mice ($9.3 \times 10^6 \pm 2.6 \times 10^6$; $n = 3$) were about four times lower than those of *Bub1b*$^{+/+}$ mice ($37.1 \times 10^6 \pm 8 \times 10^6$; $n = 3$). *Bub1b*$^{H/H}$ spermatozoa had normal motility and morphology (data not shown) and were able to attach to and fertilize *Bub1b*$^{+/+}$ eggs *in vitro*, but they produced 2-cell-stage embryos at 13 times less frequently than *Bub1b*$^{+/+}$ spermatozoa (**Fig. 5a**). Chromosome counts on metaphases of spermatocytes in meiosis II showed that 5% of *Bub1b*$^{H/H}$ karyotypes had abnormal chromosome numbers compared with 0% of *Bub1b*$^{+/+}$ karyotypes (**Fig. 5b**). Thus, reduced expression of BubR1 seems to affect male fertility at the levels of meiotic chromosome segregation, sperm number and fertilization.

Ovaries from 4-month-old *Bub1b*$^{H/H}$ mice appeared histologically normal (data not shown) and were capable of producing mature eggs that arrested at metaphase of meiosis II. But we observed highly abnormal metaphase II configurations in 9 of 13 arrested *Bub1b*$^{H/H}$ oocytes (**Fig. 5c**). Oocytes from age-matched *Bub1b*$^{+/+}$ mice ($n = 14$) yielded normal metaphase II configurations. We conclude that infertility in female mice expressing low levels of BubR1 is caused, at least in part, by meiotic chromosome segregation defects.

To determine whether reduced expression of BubR1 might have a role in natural aging, we measured BubR1 levels in wild-type mice of various ages. BubR1 was high in testes of 4-month-old mice but gradually decreased to very low levels as mice aged up to 32 months (**Fig. 5d**). In contrast, the spindle assembly checkpoint proteins Bub3 and Rae1 remained highly expressed as mice aged (**Fig. 5d**). Reductions in BubR1 expression were also seen in ovaries and spleens of 22-month-old mice, but not in lungs (**Fig. 5e**,**f** and data not shown). Overall, these data are consistent with the idea that BubR1 might have a role in normal aging.

The finding that very few *Bub1b*$^{H/H}$ mice had detectable tumors when they died, despite substantial chromosome number instability, is unexpected because aneuploidy is a hallmark of most human cancers[3,13,14], and because *Bub1b* is mutated or expressed at low levels in a subset of colorectal carcinomas with chromosomal instability[15,16]. Instead, BubR1-deficient mice have early onset of several aging-associated phenotypes and have severely shortened lifespans. This, together with the demonstration that BubR1 expression declines in several tissues as wild-type mice age, suggests that this checkpoint protein may be a key regulator of normal aging. Reproductive aging in female mammals occurs relatively early in life and is characterized by the production of increasing numbers of aneuploid oocytes. In humans, this leads to increased abortions and birth defects, such as Down syndrome[1]. Chromosomal segregation defects associated with reproductive aging are reminiscent of those seen in oocytes of mutant mice expressing low levels of BubR1. Given this age-dependent decline in ovarian BubR1, we propose that downregulation of BubR1 might be a mechanism that contributes to age-related female infertility and certain birth defects. Paternal fertility also declines with advancing age[17,18], and a regulatory role for BubR1 is certainly conceivable, given the decline in BubR1 levels in testes of aging normal mice and the negative impact of BubR1-deficiency on fertility of male mutant mice.

METHODS

Generation of BubR1 mutant mice. We used a previously reported gene targeting strategy to create a hypomorphic *Bub1b* allele in mouse embryonic stem cells[19] (for details, see **Supplementary Methods** and **Supplementary Fig. 1**

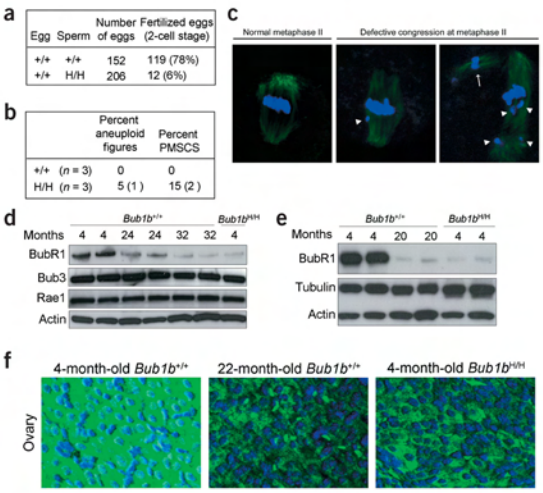

Figure 5 Analysis of BubR1 in testis and ovary of mutant and normal mice. (**a**) *In vitro* fertilization experiments with eggs from $Bub1b^{+/+}$ females and sperm from $Bub1b^{+/+}$ or $Bub1b^{H/H}$ males. (**b**) Karyotype analysis of $Bub1b^{+/+}$ and $Bub1b^{H/H}$ spermatocytes at prometaphase of meiotic division II. Abnormal $Bub1b^{H/H}$ karyotypes showed either a gain or loss of one duplicated chromosome. (**c**) Oocytes from $Bub1b^{H/H}$ mice arrested at metaphase II stained with α-tubulin and Hoechst. Normal metaphase configuration (left panel), metaphase with misaligned chromosomes (middle panel) and metaphase with an extra spindle (arrow) and misaligned chromosomes (arrowheads; right panel) are shown. (**d**) Western-blot analyses of BubR1 levels in testis of young and old $Bub1b^{+/+}$ mice. (**e**) Western-blot analyses of BubR1 levels in ovary of young and old $Bub1b^{+/+}$ mice. (**f**) Cross-sections through ovary from young and old $Bub1b^{+/+}$ mice immunostained for BubR1 (green) and DNA (blue). Representative corpora lutea are shown.

online). $Bub1b^{H/H}$ mice obtained from four independently targeted embryonic stem cell clones had identical phenotypes. We monitored body weight in ten females of each genotype for 70 d. All mice were housed in a pathogen-free barrier environment for the duration of the study. Experimental procedures involving laboratory mice were reviewed and approved by the Institutional Animal Care and Use Committee of the Mayo Clinic.

Western-blot analysis. We carried out western-blot analyses as previously described[20]. We used affinity-purified rabbit antibody against mouse BubR1 (382–420) to detect BubR1. We quantified BubR1 signals ($n = 6$ per genotype) by the use of Bio-Rad Quantity One Software (version 4.1.0) and normalized them to β-actin (AC-151, Sigma; 1:40,000 dilution). We also probed some blots with α-tubulin (T-9026, Sigma; 1:2,000 dilution) as a loading control. We used antibody against human BubR1 (1–350) to exclude production of truncated BubR1 products by $Bub1b^{H}$ and $Bub1b^{-}$ alleles. To quantify senescence-associated proteins in various MEF lysates, we used the following antibodies at 1:200 dilution (purchased from Santa Cruz unless noted otherwise): p16 (M-156; sc-1207), p19 (NB200-106; Novus Biologicals), p21 (M-19; sc-471), p53 (FI-393-G, sc-6243-G). We detected Bub3 and Rae1 as previously described[8].

Histopathology. We screened all major organs for overt tumors using a dissection microscope and processed the collected tumors routinely for histopathological confirmation. We fixed dissected tissues for histology in 10% formalin, processed them and embedded them in paraffin. We cut 5-μm sections of all tissues and stained them with hematoxylin and eosin using standard procedures. We stained dorsal skin sections and determined the thickness of the dermal and adipose layers by taking 40 random measurements of each mouse for each genotype and age group ($n = 3$). Calculations were done using a calibrated computer program (Spot Advanced by BioSpot). We stained ovary sections with affinity-purified antibody against BubR1 (382-420) as previously described[21].

Bone and fat analyses by dual-energy X-ray absorptiometry. We analyzed bone mineral content, bone mineral density and total body adipose using a LUNAR PIXI-mus small animal densitometer (LUNAR Corporate Headquarters) as described[22] in three anesthetized mice (with avertin) of each genotype and age.

Wound healing analysis. We analyzed the ability of mice to repair wounds as previously described[23]. We introduced 3-mm punch biopsy wounds into dorsal skin of anesthetized mice. For a period of 6 d, we measured wound diameters using a digital caliper. $Bub1b^{H/H}$ mice did not survive at a standard anesthetic dose of 375 μg of avertin per g body weight but did survive with half that dose.

Generation and culture of MEFs. We intercrossed $Bub1b^{+/H}$ mice to derive $Bub1b^{+/+}$, $Bub1b^{+/H}$ and $Bub1b^{H/H}$ MEFs from individual 13.5-d-old fetuses. We intercrossed $Bub1b^{+/-}$ and $Bub1b^{+/+}$ mice to generate $Bub1b^{+/+}$ and $Bub1b^{+/-}$ MEFs, and $Bub1b^{+/-}$ and $Bub1b^{+/H}$ mice to generate $Bub1b^{-/H}$ MEFs. They were cultured in 20% oxygen, frozen at P2 and P3 and used for experimentation at indicated passages. For the studies described, we examined at least three $Bub1b^{H/H}$, $Bub1b^{+/+}$ and $Bub1b^{+/-}$ clones. We generated growth curves using P3 and P7 MEFs. At day 0, we plated 1.5×10^5 MEFs per 35-mm dish and counted duplicate cultures at 24-h intervals thereafter ($n = 3$ MEF lines per genotype). In certain experiments, we wanted to limit senescence due to oxidative stress[12], and so we used MEFs that were generated and cultured in 3% oxygen. MEFs were synchronized as previously described[8]. We washed confluent cultures three times with phosphate-buffered saline and then cultured them in Dulbecco's modified Eagle medium containing 0.1% fetal bovine serum and 0.04% bovine serum albumin for 18 h. We treated quiescent MEFs with trypsin and reseeded them in Dulbecco's modified Eagle medium with 10% fetal bovine serum to allow their reentry into the cell cycle.

Spindle assembly checkpoint analyses. We measured mitotic index ($n = 3$ MEF lines per genotype) and carried out FACS-based analysis of spindle assembly checkpoint activity as previously described[8]. We carried out Cdc2-kinase assays as previously described[24].

Karyotype analyses. We prepared metaphase spreads from MEFs and splenocytes and analyzed them for aneuploidy and PMSCS as previously described[8]. For chromosome number analysis of spermatocytes, we minced testes between two microscope slides and instantly prepared metaphase spreads from the resulting cell suspensions. We carried out spectral karyotypic analysis of MEFs using the protocol, reagents, instrumentation and software from Applied Spectral Imaging.

Analysis of DNA repair functions. We carried out DNA damage MEF survival experiments as described[25,26]. For mitomycin C (Sigma) and paraquat (Sigma) survival experiments, we seeded 10^4 P2 MEFs in triplicate in a 96-well flat-bottom tissue culture dish. The next day, we replaced the medium

with drug-containing medium and allowed cells to grow for 72 h. For ultraviolet-B and γ-irradiation experiments, we exposed 2×10^4 P2 MEFs to various doses of ultraviolet-B or ionizing irradiation, seeded them in triplicate and cultured them for 72 h. We measured cell survival by the use of the MTS assay (Promega). Data represent three independent MEF lines of each genotype. For γ-irradiation colony forming assays, we seeded 4×10^4 MEF cells in duplicate in 10-cm tissue culture dishes and exposed them to various doses of ionizing radiation at P2. We grew cells in 3% oxygen for 14 d and counted colonies. In the colony-forming assay after treatment with mitomycin C, we seeded 4×10^4 P2 MEF cells in duplicate in 10-cm tissue culture dishes and allowed them to grow for 24 h. The indicated concentration of medium containing mitomycin C was added and cells were allowed to grow for 14 d in 3% oxygen. For the highest doses of γ-irradiation and mitomycin C, we used five times as many cells. We counted colonies containing >20 cells after staining with Coomassie blue.

Senescence-associated β-galactosidase staining. We stained cryosections of mouse kidney for senescence-associated β-galactosidase activity according to manufacturer's protocol (Cell Signaling Technology). To quantify MEFs stained for senescence-associated β-galactosidase activity, we counterstained cells with Hoechst to visualize nuclei. The percentage of senescent cells was the total number of senescent cells divided by the total number of cells counted using immunofluorescence ($n = 3$ MEF lines per genotype).

Collection and analysis of metaphase II oocytes and *in vitro* fertilization. We collected ovulated oocytes and instantly fixed them as previously described[27]. We stained fixed oocytes with α-tubulin (1:1,000 dilution of T-9026, Sigma) and Hoechst and analyzed them by confocal microscopy. We carried out *in vitro* fertilization experiments as previously described[28]. We obtained aged testes from the aged rodent tissue bank maintained by the National Institute of Aging (Bethesda).

Note: Supplementary information is available on the Nature Genetics website.

ACKNOWLEDGMENTS

We thank J. Harden, R. Babu, M. Gazi, S. Guyse, M. Pittelkow, R. Goorha, J. Davenport, D. Pearson, K. Hafner (Cytogenetics Shared Resource), J. van Ree and S. Kaufman for supporting this project; R. Bram for critically reviewing the manuscript and for discussions; and T. Yen for providing BubR1 antibody. This work was supported by a grant from the US National Institutes of Health.

COMPETING INTERESTS STATEMENT

The authors declare that they have no competing financial interests.

Received 30 March; accepted 7 May 2004
Published online at http://www.nature.com/naturegenetics/

1. Hassold, T. & Hunt, P. To err (meiotically) is human: the genesis of human aneuploidy. *Nat. Rev. Genet.* **2**, 280–291 (2001).
2. Thomas, N.S. *et al.* Maternal sex chromosome non-disjunction: evidence for X chromosome-specific risk factors. *Hum. Mol. Genet.* **10**, 243–250 (2001).
3. Jallepalli, P.V. & Lengauer, C. Chromosome segregation and cancer: cutting through the mystery. *Nat. Rev. Cancer* **1**, 109–117 (2001).
4. Wassmann, K. & Benezra, R. Mitotic checkpoints: from yeast to cancer. *Curr. Opin. Genet. Dev.* **11**, 83–90 (2001).
5. Yu, H. Regulation of APC-Cdc20 by the spindle checkpoint. *Curr. Opin. Cell Biol.* **14**, 706–714 (2002).
6. Cleveland, D.W., Mao, Y. & Sullivan, K.F. Centromeres and kinetochores: from epigenetics to mitotic checkpoint signaling. *Cell* **112**, 407–421 (2003).
7. Wang, Q. *et al.* BUBR1 deficiency results in abnormal megakaryopoiesis. *Blood* **103**, 1278–1285 (2004).
8. Babu, J.R. *et al.* Rae1 is an essential mitotic checkpoint regulator that cooperates with Bub3 to prevent chromosome missegregation. *J. Cell Biol.* **160**, 341–353 (2003).
9. Michel, L.S. *et al.* MAD2 haplo-insufficiency causes premature anaphase and chromosome instability in mammalian cells. *Nature* **409**, 355–359 (2001).
10. Hasty, P., Campisi, J., Hoeijmakers, J., van Steeg, H. & Vijg, J. Aging and genome maintenance: lessons from the mouse? *Science* **299**, 1355–1359 (2003).
11. Campisi, J. Cancer and ageing: rival demons? *Nat. Rev. Cancer* **3**, 339–349 (2003).
12. Parrinello, S. *et al.* Oxygen sensitivity severely limits the replicative lifespan of murine fibroblasts. *Nat. Cell Biol.* **5**, 741–747 (2003).
13. Lengauer, C., Kinzler, K.W. & Vogelstein, B. Genetic instabilities in human cancers. *Nature* **396**, 643–649 (1998).
14. Li, R., Sonik, A., Stindl, R., Rasnick, D. & Duesberg, P. Aneuploidy vs. gene mutation hypothesis of cancer: recent study claims mutation but is found to support aneuploidy. *Proc. Natl. Acad. Sci. USA* **97**, 3236–3241 (2000).
15. Cahill, D.P. *et al.* Mutations of mitotic checkpoint genes in human cancers. *Nature* **392**, 300–303 (1998).
16. Shichiri, M., Yoshinaga, K., Hisatomi, H., Sugihara, K. & Hirata, Y. Genetic and epigenetic inactivation of mitotic checkpoint genes hBUB1 and hBUBR1 and their relationship to survival. *Cancer Res.* **62**, 13–17 (2002).
17. Ford, W.C. *et al.* Increasing paternal age is associated with delayed conception in a large population of fertile couples: evidence for declining fecundity in older men. The ALSPAC Study Team (Avon Longitudinal Study of Pregnancy and Childhood). *Hum. Reprod.* **15**, 1703–1708 (2000).
18. Eskenazi, B. *et al.* The association of age and semen quality in healthy men. *Hum. Reprod.* **18**, 447–454 (2003).
19. Meyers, E.N., Lewandoski, M. & Martin, G.R. An Fgf8 mutant allelic series generated by Cre- and Flp-mediated recombination. *Nat. Genet.* **18**, 136–141 (1998).
20. Kasper, L.H. *et al.* CREB binding protein interacts with nucleoporin-specific FG repeats that activate transcription and mediate NUP98-HOXA9 oncogenicity. *Mol. Cell. Biol.* **19**, 764–776 (1999).
21. Feldmann, K.A., Pittelkow, M.R., Roche, P.C., Kumar, R. & Grande, J.P. Expression of an immediate early gene, IEX-1, in human tissues. *Histochem. Cell Biol.* **115**, 489–497 (2001).
22. Nagy, T.R. & Clair, A.L. Precision and accuracy of dual-energy X-ray absorptiometry for determining in vivo body composition of mice. *Obes. Res.* **8**, 392–398 (2000).
23. Tyner, S.D. *et al.* p53 mutant mice that display early ageing-associated phenotypes. *Nature* **415**, 45–53 (2002).
24. Wassmann, K. & Benezra, R. Mad2 transiently associates with an APC/p55Cdc complex during mitosis. *Proc. Natl. Acad. Sci. USA* **95**, 11193–11198 (1998).
25. Koomen, M. *et al.* Reduced fertility and hypersensitivity to mitomycin C characterize Fancg/Xrcc9 null mice. *Hum. Mol. Genet.* **11**, 273–281 (2002).
26. de Boer, J. *et al.* Premature aging in mice deficient in DNA repair and transcription. *Science* **296**, 1276–1279 (2002).
27. Woods, L.M. *et al.* Chromosomal influence on meiotic spindle assembly: abnormal meiosis I in female Mlh1 mutant mice. *J. Cell Biol.* **145**, 1395–1406 (1999).
28. Kang-Decker, N., Mantchev, G.T., Juneja, S.C., McNiven, M.A. & van Deursen, J.M. Lack of acrosome formation in Hrb-deficient mice. *Science* **294**, 1531–1533 (2001).

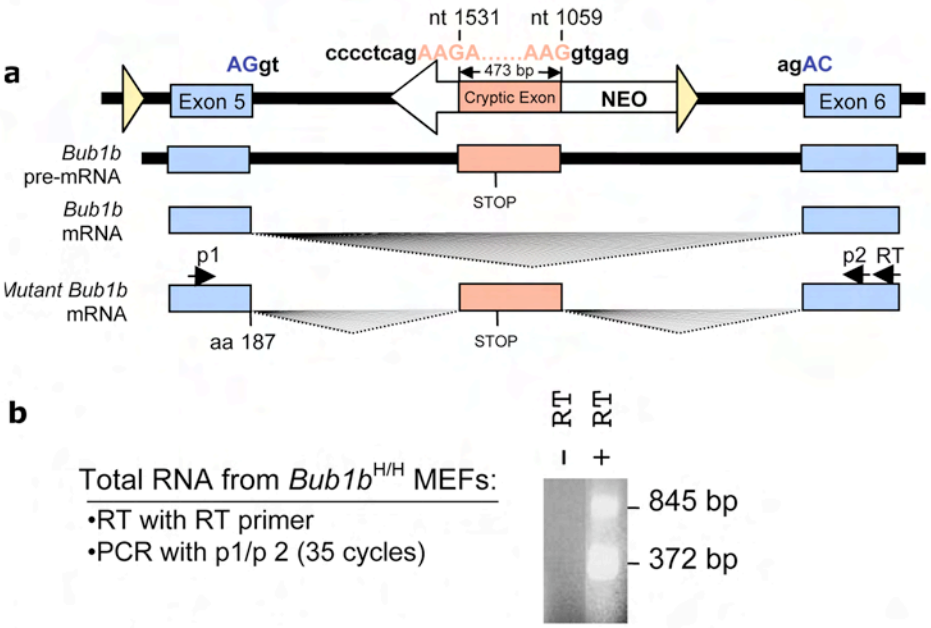

Supplementary Figure 1

Alternative RNA splicing mechanism underlying hypomophic BubR1 expression. (**a**) The pMC1neo cassette contains a cryptic splice acceptor as well as a cryptic splice donor site in the 3'>5' orientation. They create a 473 bp cryptic exon[1,2]. Insertion of pMC1neo between exons 5 and 6 leads to synthesis of mutant *Bub1b* pre-mRNAs. Normal splicing of pre-mRNAs yields wild-type mRNAs that translate into full-length BubR1 protein. However, part of the pre-mRNAs will be spliced abnormally, creating mutant *Bub1b* mRNAs that cannot generate BubR1 protein, thereby reducing cellular BubR1 protein levels. (**b**) RT-PCR on total RNA from $Bub1b^{H/H}$ MEFs confirming that the predicted wild-type (represented by the 372 bp fragment) and mutant *Bub1b* mRNAs (845 bp fragment) are indeed produced.

Supplementary Figure 2

Photograph of newborn pups from a $Bub1b^{+/-}$ x $Bub1b^{+/H}$ intercross. $Bub1b^{-/H}$ pups (top) were always much smaller than $Bub1b^{+/H}$ and $Bub1b^{+/+}$ control mice (bottom). $Bub1b^{-/H}$ pups display massive aneuploidy and die within 24 h after birth.

a

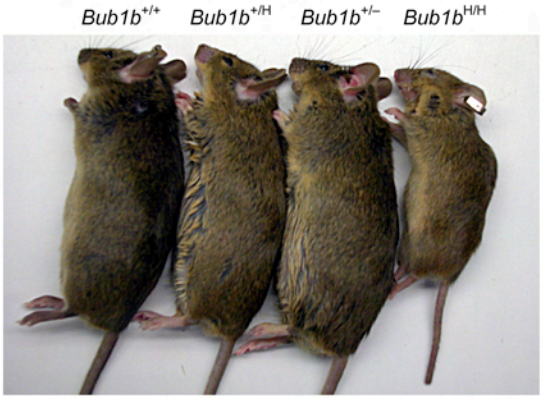

b

	Bub1b $^{+/+}$	*Bub1b* $^{+/-}$
Body weight (g)	47.44	49.37
SD	5.53	11.63
Spleen weight (mg)	129.4	88.7
SD	3.1	1.7

c

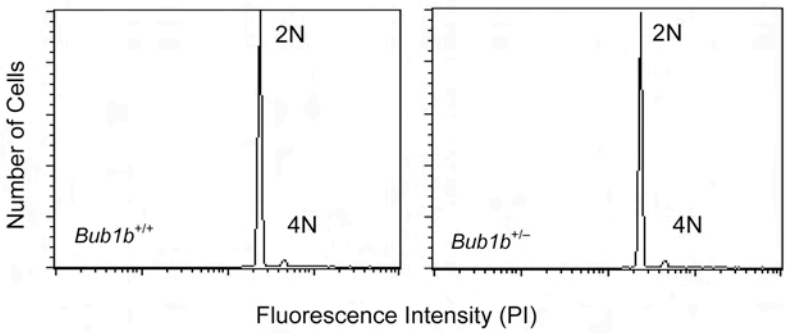

Supplementary Figure 3

Bub1b-haploinsufficient mice display no overt phenotypes (**a**) Images of representative 4-month-old male mice of indicated genotypes. Note that the *Bub1b*$^{H/H}$ mouse is growth retarded and displays kyphosis. (**b** and **c**) Analyses of *Bub1b*$^{+/-}$ mice for extramedullary hematopoiesis in spleen. (**b**) Comparison of spleen weights of 7 month-old *Bub1b*$^{+/+}$ and *Bub1b*$^{+/-}$ male mice. Note that our *Bub1b*$^{+/-}$ mice do no display splenomegaly. (**c**) Splenocytes from 7 month-old *Bub1b*$^{+/+}$ and *Bub1b*$^{+/-}$ male mice stained with propidium iodide and analyzed for DNA content by FACS. Note that there is no evidence for extramedullary megakaryopoiesis in the *Bub1b*$^{+/-}$ spleen.

Supplementary Figure 4

X-rays of *Bub1b*$^{+/+}$ and *Bub1b*$^{H/H}$ mice at 2 and 6 months of age (arrows mark the abnormal curvature of the spine).

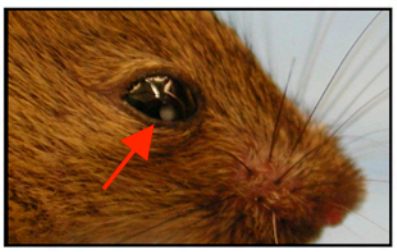

Supplementary Figure 5

Lens (arrow) of 4-month-old *Bub1b*$^{H/H}$ mouse with nuclear cataract.

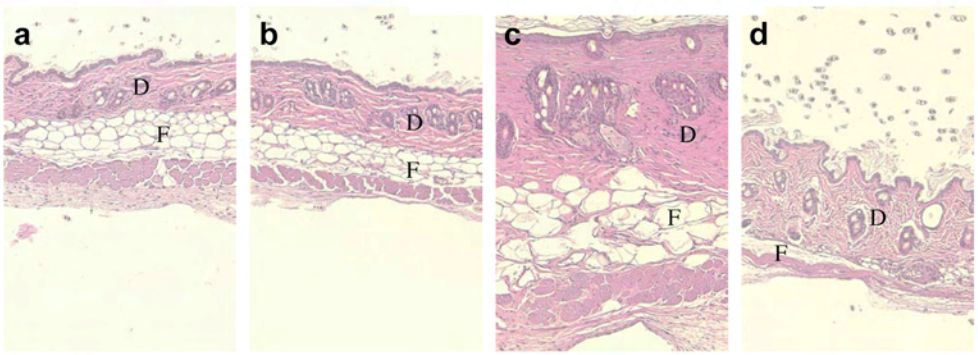

Supplementary Figure 6

Haematoxylin and eosin-stained cross-sections of dorsal skin from a 2-month-old *Bub1b*$^{+/+}$ mouse (**a**), a 2-month-old *Bub1b*$^{H/H}$ mouse (**b**), a 12-month-old *Bub1b*$^{+/+}$ mouse (**c**) and a 12-month-old *Bub1b*$^{H/H}$ mouse (**d**). Note that the dermis (D) as well as the subcutaneous fat layer (F) in skin from 12-month-old *Bub1b*$^{H/H}$ mice is much thinner than in skin from 12-month-old *Bub1b*$^{+/+}$.

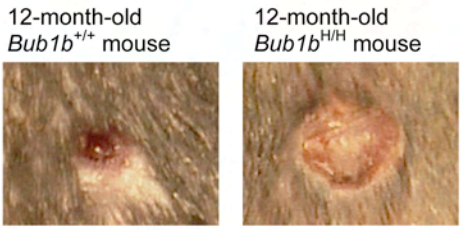

Supplementary Figure 7

Photographs of wounds 6 days after 3-mm punch biopsies.

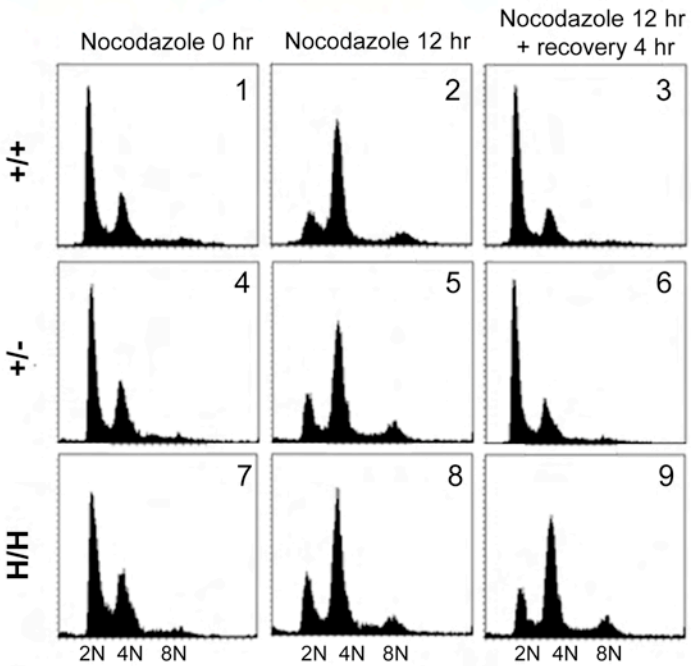

Supplementary Figure 8

Analysis of spindle assembly checkpoint activity by flow cytometry. *Bub1b*$^{+/+}$, *Bub1b*$^{+/-}$ and *Bub1b*$^{H/H}$ MEFs were treated with nocodazole for 12 h and then allowed to recover in nocodazole-free medium for 4 h. In all cultures, the population of cells with 4N DNA content increased dramatically after the nocodazole treatment (panels 2, 5 and 8). The 4N populations of *Bub1b*$^{+/+}$ and *Bub1b*$^{+/-}$ cultures returned to normal size shortly after removal of nocodazole (panels 3 and 6), indicating that these populations consisted of prometaphase-arrested cells that, after repair of the spindle, successfully completed mitosis and entered into G1 with a DNA content of 2N. The DNA profile of *Bub1b*$^{H/H}$ MEFs showed little-to-no recovery (panel 9), which is typical for cells that are unable to induce a sustained prometaphase arrest in nocodazole.

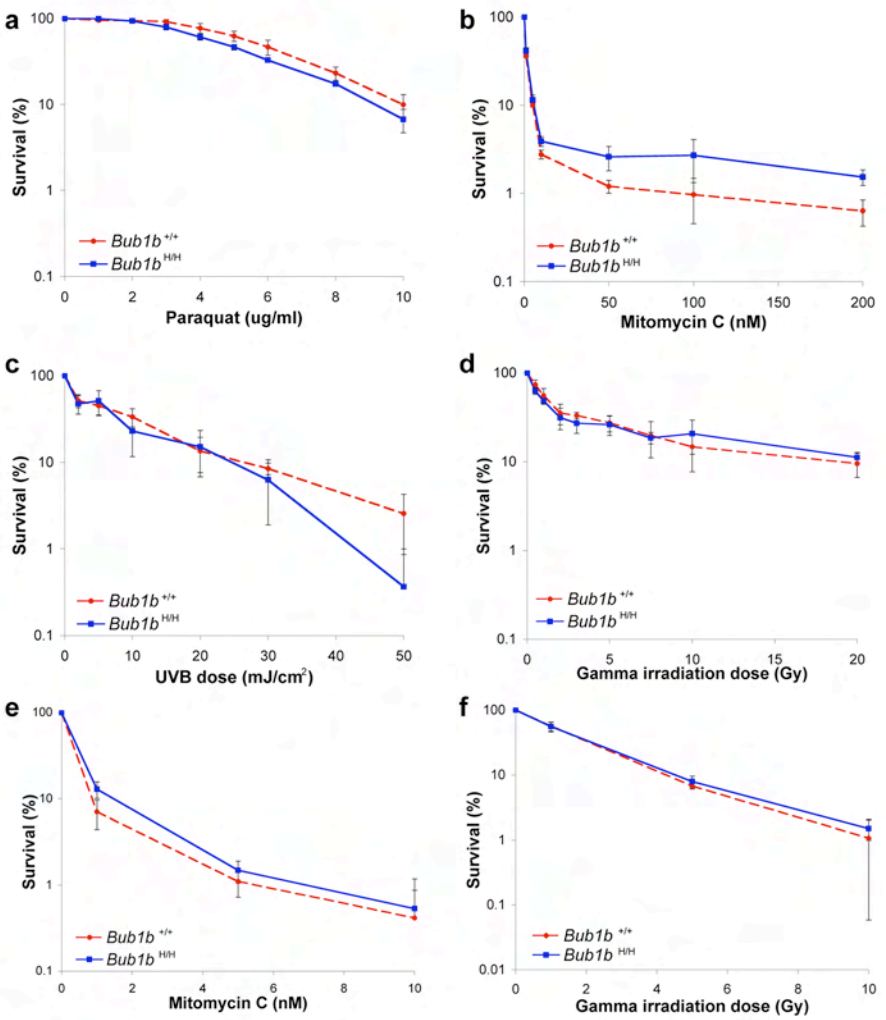

Supplementary Figure 9

Analysis of the fidelity of distinct DNA damage repair pathways by measuring cell survival and colony formation ability after exposing early-passage MEFs to various kinds of DNA damaging agents. (**a-d**) Survival curves of *Bub1b*$^{+/+}$ and *Bub1b*$^{H/H}$ MEFs after DNA damage by paraquat (**a**), mitomycin C (**b**), UVB (**c**) or gamma-irradiation (**d**). (**e-f**) Colony-forming assay of *Bub1b*$^{+/+}$ and *Bub1b*$^{H/H}$ MEFs after DNA damage by mitomycin C (**e**) or gamma-irradiation (**f**). Note that *Bub1b*$^{H/H}$ and *Bub1b*$^{+/+}$ MEFs responded similarly to ionizing radiation, ultraviolet light (UV), mitomycin C or paraquat, indicating that there are no significant differences in DNA repair ability between *Bub1b*$^{+/+}$ and *Bub1b*$^{H/H}$ cells. Thus, although premature ageing has previously been linked to defects in genome maintenance systems that lead to accumulation of base changes, single- or double-strand DNA breaks, interstrand crosslinks and/or telomere shortening, such defects are not likely to cause premature ageing in *Bub1b*$^{H/H}$ mice.

Phenotype	*Bub1b*$^{+/+}$ *Bub1b*$^{+/H}$ *Bub1b*$^{+/-}$	*Bub1b*$^{H/H}$
Median life span	>16 months	~6 months
Maximum life span	>30 months*	15 months
Cancer incidence	0%	2-3%
Body weight	Increase in body fat	Reduced body size after postnatal growth phase; loss of fat and cachetic appearance in last 4-12 weeks of life.
Kyphosis	Normal	Pronounced
Osteoporosis	Normal*	Normal
Muscle atrophy	Normal	Pronounced
Cataracts	None between 12 -16 months	100% bilateral >4-6 months
Dermal thickness	Normal*	Reduced
Thickness subcutaneous adipose layer	Normal*	Reduced
Wound healing	Normal*	Delayed
Hair regeneration	Normal*	Normal
Hair graying	Normal	Slightly increased
Anesthetic stress tolerance	Normal	Reduced
Peripheral RBC/WBC counts	Normal*	Normal

Supplementary Table 1

Summary of aging-related phenotypes. Phenotypes were assessed during the first 15-16 months of post-natal life, except for the maximum life span. *Analyzed in *Bub1b*$^{+/+}$ mice but not in *Bub1b*$^{+/H}$ and *Bub1b*$^{+/-}$ mice.

Supplementary Methods

Generation of *Bub1b* mutant mice

A pMC1neo cassette containing a single loxP site was inserted in the reverse orientation into an intronic XbaI site between exons 5 and 6 of the murine *Bub1b* gene. By reversing the orientation of the cassette, a cryptic splice acceptor and donor site was introduced which led to mutant *Bub1b* pre-mRNA. This pre-mRNA will be spliced abnormally, creating *Bub1b* mRNA that cannot generate BubR1 protein, thereby reducing cellular levels of BubR1. A second loxP recombination site was inserted into a unique intronic NheI site 5' of exon 5 (Fig. 1A). This strategy allowed us to create both a hypomorphic allele as well as a null allele by using Cre-mediated recombination at the loxP sites flanking exon 5. Cre recombination will result in the out-frame fusion of exons 4 and 6. This event truncates BubR1 protein after amino acid 187. We electroporated the targeting vector into TL1 ES cells and screened 192 drug-resistant clones for homologous recombination by Southern blotting. Nine targeted embryonic stem cell clones were isolated and shown to have the incorporation of the pMC1neo cassette. Four of these clones were amplified and used to generate chimeric mice. F1 heterozygote mice derived from each clone were intercrossed to produce homozygous mutant offspring (termed $Bub1b^{H/H}$), as well as $Bub1b^{+/+}$ and $Bub1b^{+/H}$ mice. By RT-PCR, we confirmed that the expected wild-type and mutant *Bub1b* mRNAs were indeed produced by $Bub1b^{H/H}$ cells (see fig. 1B). By breeding $Bub1b^{+/H}$ males with MMTV-LTR-Cre-transgenic female mice (purchased from the Jackson Laboratories), we generated $Bub1b^{+/-}$ mice. Mouse genotypes were routinely determined by PCR. Primer sequences and reaction conditions are available on request.

References

1. Jacks, T. et al. Tumour predisposition in mice heterozygous for a targeted mutation in Nf1. *Nat Genet* 7, 353-61. (1994).
2. Meyers, E. N., Lewandoski, M. & Martin, G. R. An Fgf8 mutant allelic series generated by Cre- and Flp-mediated recombination. *Nat Genet* 18, 136-41. (1998).

Chapter 4

Aging-associated vascular phenotype in mutant mice with low levels of BubR1

Stroke 38, 1050-1056
Reprinted with permission

Aging-Associated Vascular Phenotype in Mutant Mice With Low Levels of BubR1

Takuya Matsumoto, MD; Darren J. Baker, MSc; Livius V. d'Uscio, PhD; Gazi Mozammel, PhD; Zvonimir S. Katusic, MD, PhD; Jan M. van Deursen, PhD

Background and Purpose—Aging is a major risk for stroke and a highly complex biological process believed to involve multiple mechanisms. Mutant mice that express low levels of the spindle assembly checkpoint protein BubR1 are known to develop several aging-associated phenotypes at a very young age, including cataracts, lordokyphosis, loss of subcutaneous fat, and impaired wound healing. However, whether BubR1 acts to prevent vascular aging has not yet been established. The present study was designed to investigate the vascular phenotype of mutant mice with low levels of BubR1.

Methods—Morphological, functional, and biochemical analyses were performed on aortas and carotid arteries of 3- to 5-month-old BubR1 mutant mice and wild-type littermates.

Results—Arterial wall thickness and inner diameter were significantly reduced in BubR1 mutant mice. Arterial walls of BubR1 mutant mice had low numbers of medial smooth muscle cells. Masson trichrome staining showed profound fibrosis in arterial walls of BubR1 mutant. In agreement with these morphological changes, functional analysis of pressurized isolated carotid arteries of BubR1 mutant mice demonstrated reduced elastic properties. Endothelium-dependent relaxations to acetylcholine and endothelium-independent relaxations to the nitric oxide donor DEA-NONOate were significantly reduced in carotid arteries of BubR1 mutant mice. Furthermore, enzymatic activity of nitric oxide synthase and levels of cyclic GMP were significantly reduced in aortas of mutant mice, but production of superoxide anions was significantly increased.

Conclusions—These findings demonstrate that BubR1 insufficiency in mice results in phenotypic changes reminiscent of vascular aging in humans and suggest a role for BubR1 in suppressing the vascular aging process. **(*Stroke*. 2007; 38:1050-1056.)**

Key Words: aging ■ carotid arteries ■ endothelium ■ nitric oxide ■ nitric oxide synthase

Evidence continues to accumulate on the importance of aging as a risk factor for development of cardiovascular disease and stroke.[1] A large number of published studies demonstrated that endothelial dysfunction is one of the major phenotypic changes in aged arteries.[2–8] Loss of nitric oxide (NO) biological activity is a central mechanism responsible for dysfunction of the vascular endothelium. Aging-induced increase in formation of oxygen-derived free radicals, including superoxide anion, appears to be the most likely explanation for the loss of NO.[9] Indeed, superoxide anion chemically inactivates NO, thereby decreasing local bioavailability of NO in the vascular wall.[7,8,10] This in turn may stimulate smooth muscle cells proliferation, thereby contributing in part to lesion formation in early stages of atherosclerosis.[11–13] However, the proliferative capacity of smooth muscle cells declines with aging, which ultimately contributes to plaque destabilization and subsequent vessel occlusion.[14–16]

Previous studies have demonstrated that mouse mutants defective in genome maintenance mechanisms display symptoms of accelerated aging.[17] Most notably, commonly described human syndromes of accelerated aging are also caused by genome maintenance defects.[17] Thus, it seems that DNA maintenance and repair pathways play an important role in aging processes. Consistent with this concept, a study by Baker et al[18] demonstrated that mice that express only 10% of normal levels of the mitotic spindle assembly checkpoint protein BubR1 leads to progressive aneuploidy and development of specific early aging-associated phenotypes, including short life span, cachectic dwarfism, lordokyphosis, cataracts, loss of subcutaneous fat, and impaired wound healing.[18] In addition, natural aging of wild-type mice is marked by decreased BubR1 expression is multiple tissues, further suggesting that this protein may be a regulator of normal aging.[18] The physiological relevance of BubR1 to the

Received September 21, 2006; final revision received October 12, 2006; accepted October 13, 2006.

From the Departments of Anesthesiology, Molecular Pharmacology & Experimental Therapeutics (T.M., L.V.d'U., Z.S.K.) and Pediatric & Adolescent Medicine (D.J.B., G.M., J.M.v.D.), Mayo Clinic College of Medicine, Rochester, Minn.

Correspondence to Zvonimir S. Katusic, MD, PhD, Department of Anesthesiology, Mayo Clinic College of Medicine, 200 First St SW, Rochester, MN 55905. E-mail katusic.zvonimir@mayo.edu, or Jan M. van Deursen, Department of Pediatrics and Adolescent Medicine, Mayo Clinic College of Medicine, 200 First St SW, Rochester, MN 55905. E-mail vandeursen.jan@mayo.edu

vascular system has not yet been studied. Here we present the major characteristics of vascular phenotype caused by BubR1 insufficiency.

Materials and Methods

Experimental Animals

Hypomorphic BubR1 mutant ($BubR1^{H/H}$) mice were generated in Dr van Deursen's laboratory as previously described.[18] Male $BubR1^{H/H}$ mice (3 to 5 months of age) and their age-matched wild-type littermates on mixed 129 and C57BL/6 background ($BubR1^{+/+}$) were used for all experiments. The mice were fed regular pellet diet and housed in facilities with a 12:12 hour light–dark cycle. Experimental protocols and housing facilities were approved by the Institutional Animal Care and Use Committee.

The mice were killed with a 60 mg/kg intraperitoneal injection of pentobarbital. Blood samples were obtained through puncture of the right ventricle. The blood was mixed with heparin and centrifuged at 4°C for 10 minutes at 2000 rpm. The plasma was aspirated and stored at −80°C. The aorta and carotid arteries were removed and placed immediately in ice-cold modified Krebs-Ringer solution (in mmol/L: NaCl 118.6; KCl 4.7; $CaCl_2$ 2.5; $MgSO_4$ 1.2; KH_2PO_4 1.2; $NaHCO_3$ 25.1; $Ca^{2+}Na^{+}2$ versenate 0.026; glucose 11.1). Arteries were dissected and connective tissue was removed under a microscope (Carl Zeiss). Because of the small size of the BubR1 arteries, we used carotid artery for analysis of vasomotor function and mechanical properties, whereas the largest conduit vessel, aorta, was used for biochemical and morphological analysis.

Morphological Analyses

Thoracic aortas were carefully dissected, fixed in 4% formalin, and embedded in paraffin. Serial sections (5-μm-thick) were cut for analysis by hematoxylin-eosin, elastica van Gieson, and Masson trichrome staining. The arterial segments were cut into 5 serial sections at 5-mm intervals. The medial area was quantified using Image-Pro PLUS (Media Cybernetics).

Vasomotor Reactivity

Carotid arteries were studied as previously described.[19,20] Briefly, both sites of the artery were sutured onto microcannulae and placed in a vessel chamber (Living Systems Instrumentation) filled with aerated (94% O_2, 6% CO_2) Krebs-Ringer solution (37°C). A pressure of 50 mm Hg was maintained in the artery through the microcannulae. The arteries were equilibrated 45 minutes before each of the experiments. The arteries were submaximally contracted with 9,11-dideoxy-11α,9α-epoxymethanoprostaglandin $F_2\alpha$ (U46619; 10^{-7}–3×10^{-7} mol/L), a thromboxane analog, and then endothelium-dependent relaxation was obtained by cumulative addition of acetylcholine (10^{-9} to 10^{-5} mol/L). After washout, equilibration, and submaximal contraction with U46619, endothelium-independent relations were determined using diethylammonium (Z)-1-(*N*,*N*-diethylamino)diazen-1-IM1,2-diolate (DEA-NONOate; 10^{-9} to 10^{-5} mol/L). Relaxation was determined as a percent of relaxation to a high concentration of papaverine (3×10^{-4} mol/L). In a separate protocol, diameter changes were measured during stepwise increments in intraluminal pressure from 25 to 150 mm Hg. At the end of each experiment, arteries were incubated in Ca^{2+}-free control solution containing EGTA (2×10^{-3} mol/L) and sodium nitroprusside (10^{-4} mol/L) for 45 minutes. Stepwise increase in intraluminal pressure was repeated to determine the passive diameter of the arteries.[21,22]

Mechanical Properties of Arterial Wall

Passive diameter is defined as the inner diameter of carotid artery measured in Ca^{2+}-free control solution. Cross-sectional compliance (C) is defined by the change in luminal cross-sectional area (δS) for a given change in intravascular pressure (δP), ie, $C=\delta S/\delta P$ (μm^2/mm Hg). Distensibility is the compliance value normalized for the luminal cross-sectional area and defined by distensibility$=(1/S)\times(\delta S/\delta P)$ (mm $Hg^{-1}\times1000$).[23]

Western Blot Analysis

We performed Western blot analysis as previously described.[24] Aortas from wild-type and BubR1 hypomorphs were isolated and all surrounding material was removed. After preparing lysates, blots were probed with antibody for BubR1 as previously described.[18] Equal loading was confirmed by using α-tubulin (T-9026, Sigma; 1:2000 dilution). Results are representative for 3 independent males of each genotype at each age.

Nitric Oxide Synthase Enzymatic Activity

Total enzymatic activity of nitric oxide synthase (NOS) was assayed in aorta with L-arginine to L-citrulline conversion as described previously.[25] Briefly, 2 aortas (n=1 experiment) were homogenized on ice in lysis buffer (pH 7.5). Total protein was determined using the BioRad DC Protein assay kit. Equal amounts of total protein homogenates prepared as described were applied. [^{14}C]-L-citrulline was measured in a scintillation counter (LS 5000TD; Beckman Instruments). NOS activity was expressed as fmol of [^{14}C]-citrulline produced per mg of protein per min.

Measurement of cGMP Levels in Aorta

A radioimmunoassay technique was used to determine the levels of cGMP as reported previously.[25] Briefly, aortic tissue was initially incubated in minimal essential media with 0.1% albumin and 1% penicillin-streptomycin (GIBCO) in a 5% CO_2 incubator at 37°C for 30 minutes. Then, 3-isobutyl-1-methylxanthnine (10^{-4} mol/L; Sigma) was added and aortas were incubated for additional 30 minutes to inhibit the degradation of cyclic nucleotides by phosphodiesterases. The aortic tissue was then removed from the media and quickly frozen in N_2. cGMP levels were measured by a radioimmunoassay kit (Amersham). The results were expressed as pmol/mg protein.

Detection of Vascular Superoxide Anion Production

Superoxide anion production was measured by lucigenin-enhanced chemiluminescence as previously described.[25] Briefly, aortas were opened length-wise and equilibrated for 30 minutes at 37°C in the modified Krebs-HEPES buffer (pH 7.4, composition in mmol/L: NaCl 118.3, KCl 4.7, $CaCl_2$ 2.5, $MgSO_4$ 1.2, KH_2PO_4 1.2, $Ca^{2+}Na^{+}2$ versenate 0.026, glucose 11.1, and HEPES 20). Scintillation vials containing 2 mL Krebs-HEPES buffer with 5 μmol/L lucigenin were placed into a scintillation counter (LS 5000; Beckman Instruments, Inc.) switched to the out-of-coincidence mode. Background signals were recorded, and vascular segments were then added to each vial. The results were expressed as counts/min per mg dry weight.

Drugs

Acetylcholine hydrochloride, EGTA, and sodium nitroprusside were purchased from Sigma Chemical Co. DEA-NONOate and U46619 were from Cayman Chemical. DEA-NONOate was prepared as stock solutions in 1.5 mol/L Tris buffer pH 8.8. U46619 was dissolved in 1 part of 100% ethanol and then diluted with 9 parts of water. The remaining drugs were dissolved in distilled water. All drugs were then diluted in Krebs solution and concentrations were expressed as final molar concentration (mol/L) in the organ bath.

Statistical Analysis

Results are expresses as means±SEM for number of animals used for each experimental protocol. An unpaired Student *t* test was used to detect significant differences when 2 groups were compared. Factorial ANOVA followed by a Bonferroni/Dunn hoc test was used to detect significant differences in multiple comparisons. The concentration-response curves were analyzed by ANOVA for repeated measures followed by a Bonferroni/Dunn hoc test. Statistical significance was accepted at a level of $P<0.05$.

Characteristics of BubR1$^{H/H}$ Mice and Age-Matched Littermates (BubR1$^{+/+}$)

	BubR1$^{+/+}$	BubR1$^{H/H}$
Body weight (g)	25.3±0.8 (20)	14.4±0.5* (22)
Total cholesterol (mg/dL)	57.8±4.5 (4)	43.5±13.8 (4)
Glucose (mg/gL)	193±16 (4)	138±32 (4)
Aorta		
Weight (mg)	18.7±1.2 (15)	8.1±0.7* (8)
Protein content (μg)	347±37 (15)	111±12* (8)
Medial area ×10^4 (μm^2)	9.49±0.35 (6)	3.44±0.38* (5)
Medial cell number	330±13 (6)	124±6.4* (5)
Endothelial cell number	25.0±1.7 (6)	32.8±4.3 (5)
Carotid artery		
Internal diameter (μm)	411±6 (12)	257±4* (12)
Diameter (μm) of contraction to U46619 (10^{-7}−3×10^{-7} mol/L)	84±19 (8)	244±5* (7)
Wall thickness (μm)	44.5±1.6 (12)	31.2±1.6* (12)
Wall to lumen ratio ×10	1.08±0.1 (12)	1.21±0.1 (12)

Values are mean±SEM. Numbers of mice are shown in chambers.
*P<0.05 vs BubR1$^{+/+}$ mice (unpaired t test).

Results

Animal Characteristics

The average body weight of BubR1$^{H/H}$ mice was significantly lower than that of age-matched BubR1$^{+/+}$ littermates (P<0.05; Table). No difference was detected in plasma concentration of cholesterol and glucose between both groups of mice (Table). Aorta weight and total protein were significantly lower in BubR1$^{H/H}$ mice as compared with littermates (P<0.05; Table). The medial surface area of the aorta was significantly smaller in BubR1$^{H/H}$ mice (P<0.05; Table). This is consistent with the reduced number of vascular smooth muscle cells of BubR1$^{H/H}$ mice (P<0.05; Table). In contrast, numbers of endothelial cells per circumference were not different between BubR1$^{+/+}$ and BubR1$^{H/H}$ mice (Table).

Vascular Morphology

Histological analysis of aorta sections revealed significant reductions in arterial wall thickness and diameter in BubR1$^{H/H}$ mice (Figure 1a and 1b, respectively). The decline in arterial wall thickness was associated with a profound reduction in smooth muscle cells (Figure 1c and d). Elastica van Gieson staining of aorta sections revealed that the elastic laminas were intact but flat in BubR1$^{H/H}$ mice. Intervals between elastic laminas were much smaller in BubR1$^{H/H}$ aortas than in BubR1$^{+/+}$ aortas (Figure 1e and 1f). Aorta sections from BubR1$^{H/H}$ mice stained with Masson trichrome showed evidence of fibrosis (Figure 1g and 1h).

Mechanical Properties of the Vascular Wall

The average internal diameter of common carotid arteries was significantly smaller in BubR1$^{H/H}$ mice than in littermates, but the wall-to-lumen ratio was not different (Table). Carotid arteries were dissected from BubR1$^{H/H}$ and BubR1$^{+/+}$ mice and incubated in a calcium-free solution. BubR1$^{+/+}$ arteries greatly expanded when the pressure in the arterial lumen was stepwise increased, but BubR1$^{H/H}$ arteries barely expanded under these conditions (Figure 2a). In addition, compliance and distensibility of BubR1$^{H/H}$ carotid arteries were significantly reduced as compared with carotid arteries of BubR1$^{+/+}$ mice (Figure 2b and 2c).

Vascular Reactivity

Absolute values of vasoconstriction to thromboxane analog U46619 were reduced in BubR1$^{H/H}$ mice carotid arteries (Table). However, when normalized to percent of maximal contractions to U46619, contractions were not significantly different between the 2 groups of mice (Figure 3a). During submaximal contractions to U46619 (10^{-7}−3×10^{-7} mol/L) endothelium-dependent relaxations to acetylcholine were significantly impaired in the carotid artery of BubR1$^{H/H}$ mice (Figure 3b). Endothelium-independent relaxations to DEA-NONOate were also significantly impaired in carotid arteries of BubR1$^{H/H}$ mice as compared with BubR1$^{+/+}$ mice (Figure 3c).

Expression of BubR1 Protein

Expression of BubR1 protein was detectable in aortas of wild type mice but not in aortas of BubR1$^{H/H}$ mice (Figure 4). Aging caused significant reduction in BubR1 protein expression in aortas of wild type mice (Figure 4).

cGMP Levels

Basal cGMP levels were significantly lower in aortas of BubR1$^{H/H}$ mice than in those of BubR1$^{+/+}$ mice (Figure 5a).

NOS Enzyme Activity

Aortas from BubR1$^{H/H}$ mice had significantly lower NOS enzyme activity than aortas from BubR1$^{+/+}$ mice (Figure 5b).

Vascular Superoxide Anion Production

Formation of superoxide anion was increased ≈5-fold in BubR1$^{H/H}$ aortas (199 653±33 637 counts/min per mg versus BubR1$^{+/+}$ mice: 41 928±17 504 counts/min per mg; P<0.05; n=3 to 7).

Discussion

Cells are equipped with surveillance mechanisms that detect various kinds of genome-destabilizing events (such as incompletely replicated or damaged DNA or unaligned metaphase chromosomes) and prevent cell cycle progression until DNA damage has been repaired. The spindle checkpoint protein BubR1 plays an essential role in the maintenance of genetic stability by ensuring proper microtubule–kinetochore attachment and sister chromatid segregation during mitosis.[26] Efforts designed to characterize the physiological relevance of BubR1 have been hindered by the fact that null mutant mice die during embryogenesis soon after implantation. To bypass this problem, hypomorphic BubR1 mice were created.[18] These animals are viable despite having only ≈10% of normal levels of BubR1.[18] As anticipated, reduced expression of BubR1 caused chromosome number instability but no other genome maintenance defects.[18] The results of our morphological, biochemical, and functional analyses described here demonstrate that BubR1 insufficiency in mice results in phenotypic changes reminiscent of vascular aging in humans and rodents, and suggest a role for BubR1 in

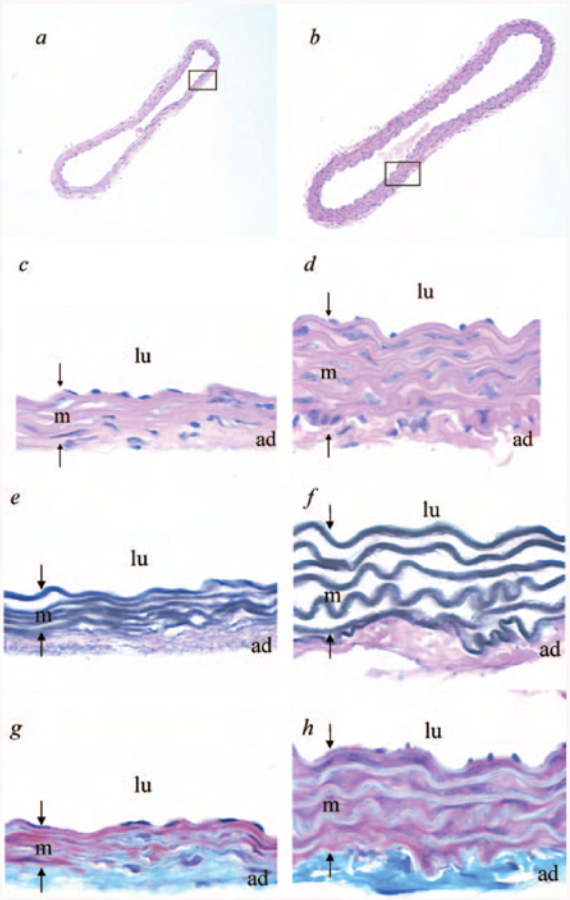

Figure 1. Hematoxylin-eosin–stained cross-sections of aortas of BubR1$^{H/H}$ mice (a, c, e, g) and BubR1$^{+/+}$ mice (b, d, f, h). Original magnification 200× is shown in (a and b). High-power view (400×) of sections presented in (a) and (b) are shown in (c) and (d), respectively. Elastica van Gieson stainings of aortas are presented in (e) and (f). Masson tricrome staining of aortas are presented in (g) and (h). Original magnification 400×. Lu, lumen; m, media; ad, adventitia. Area between arrows indicates media.

suppressing vascular aging. Reduced expression of BubR1 did not affect circulating levels of cholesterol or glucose, ruling out the possibility that hypercholesterolemia or hyperglycemia contributes to alterations of vascular phenotype in BubR1$^{H/H}$ mice.

Morphological analyses of arteries from BubR1$^{H/H}$ mice demonstrated reduced numbers of smooth muscle cells and diffuse medial fibrosis. This observation is consistent with reported age-related decline in proliferative capacity of vascular smooth muscle cells derived from humans and mice.[27–30] As the number of smooth muscle cells in arterial media decreases, major changes may occur in extracellular matrix, including increased content of collagen and decreased levels of elastin leading to fibrosis of vascular wall, a phenomenon observed in aged arteries of humans and rats.[1,31,32] Most notably, changes in vascular structure of BubR1$^{H/H}$ mice were in agreement with alterations in mechanical properties of arterial wall. Aortas of BubR1$^{H/H}$ mice exhibited impaired elasticity and compliance, a typical characteristic of aged arteries.[1] The molecular mechanism underlying loss of smooth muscle cells and increased rigidity of vascular wall in BubR1$^{H/H}$ mice is unknown and remains to be determined.

A large number of published studies demonstrated that endothelial dysfunction in aged arteries is caused by the loss of NO biological activity.[2–8] In a recent mouse study, we have shown that aging impairs NO-mediated endothelium-dependent relaxations in carotid artery.[8] This phenomenon was explained by an age-induced increase in production of superoxide anion and subsequent chemical inactivation of NO.[8] Consistent with these reports, endothelium-dependent relaxations to acetylcholine were impaired in carotid arteries of BubR1$^{H/H}$ mice. Furthermore, we detected increased formation of superoxide anion in arteries of genetically altered mice suggesting that consumption of NO by superoxide anion plays a role in the impairment of endothelial function. In agreement with elevated superoxide anion production, relax-

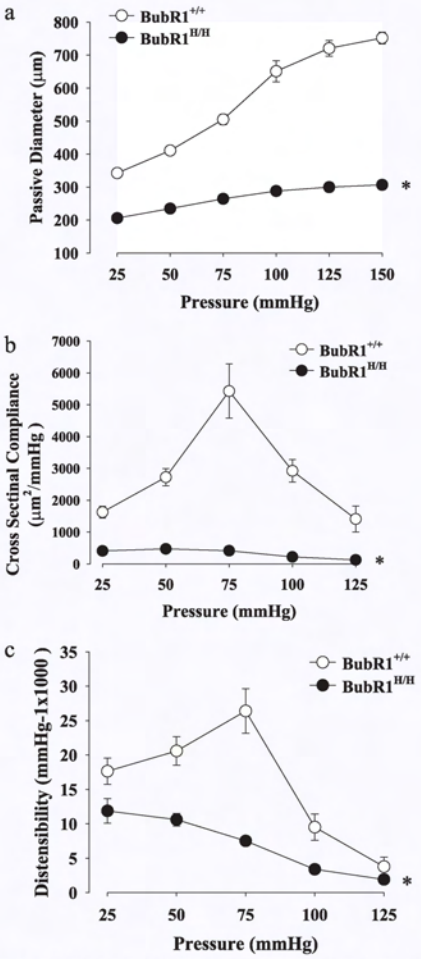

Figure 2. Passive arterial diameter (a), cross-sectional compliance (b), and distensibility (c) of isolated common carotid arteries of wild-type (BubR1$^{+/+}$) and BubR1$^{H/H}$ mice. *P<0.05 vs wild-type mice (n=6).

ations of BubR1$^{H/H}$ mice carotid arteries to exogenous NO were also reduced.

Biochemical analysis of BubR1$^{H/H}$ mice aortas demonstrated significantly reduced levels of cyclic GMP, a second messenger for NO. Decrease in arterial cGMP content is most likely caused by reduced availability of NO. In addition to chemical inactivation of NO by superoxide anion, measurements of NOS enzymatic activity indicated that reduced production of NO contributes to loss of NO in BubR1$^{H/H}$ mice. Previous studies detected decreased enzymatic activity of eNOS in aged rats,[9,33] rabbits,[34] and humans,[35] further supporting our conclusion that reduced expression of BubR1 causes phenotypic alterations resembling vascular aging. The

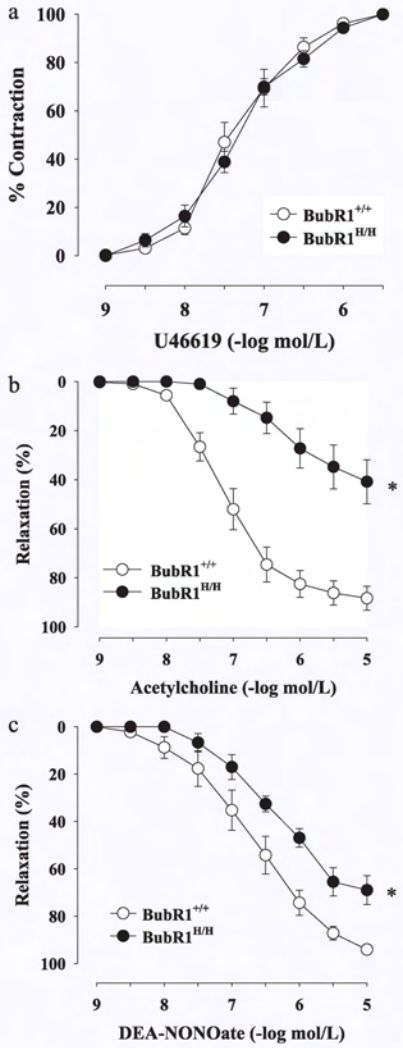

Figure 3. Concentration-dependent contractions to U46619 (a) obtained in common carotid arteries of BubR1$^{+/+}$ and BubR1$^{H/H}$ mice. Contractions to U46619 (normalized as %) were not significantly difference between both groups (n=7 to 9). Concentration-dependent relaxations to acetylcholine (b) obtained in common carotid arteries of BubR1$^{+/+}$ and BubR1$^{H/H}$ mice. Endothelium-dependent relaxations to acetylcholine were reduced in BubR1$^{H/H}$ mice as compared with wild-type mice (*P<0.05; n=6 to 9). Concentration-dependent relaxations to DEA-NONOate (c) obtained in common carotid arteries of BubR1$^{+/+}$ and BubR1$^{H/H}$ mice. Endothelium-independent relaxations to DEA-NONOate were reduced in BubR1$^{H/H}$ mice as compared with BubR1$^{+/+}$ mice (*P<0.05; n=7 to 12).

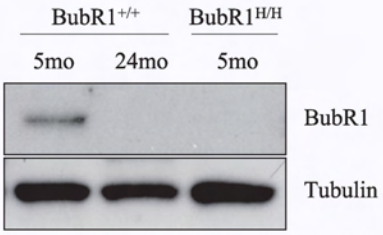

Figure 4. Representative western blot analysis of BubR1 protein expression in aortas of BubR1$^{H/H}$ and BubR1$^{+/+}$ mice; mo indicates months.

molecular mechanisms responsible for downregulation of NO production and its biological activity in BubR1$^{H/H}$ mice arteries are unknown and remain to be studied.

In summary, we demonstrated that mice with low levels of the mitotic checkpoint protein BubR1 develop, early in life, phenotypic changes reminiscent of vascular aging in humans, suggesting that BubR1 acts to prevent onset of vascular aging. We speculate that impairment of BubR1 function may enhance development of carotid artery disease, thereby increasing risk of stroke. In the future studies it will be important to determine whether mouse strains in which DNA damage repair or telomere maintenance defects cause premature aging also exhibit early vascular aging or whether this phenotype is specific for deficiency of BubR1.

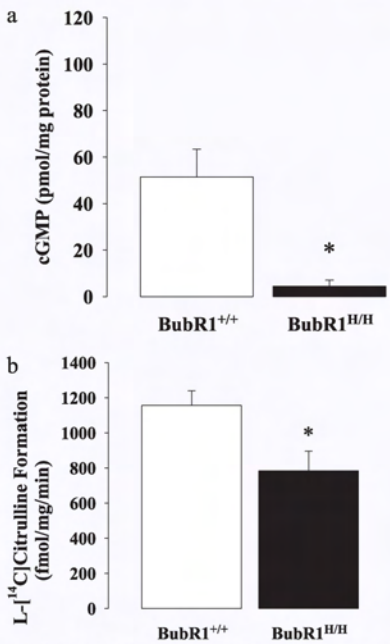

Figure 5. Bar graphs showing basal cGMP levels (a) and NOS enzymatic activity (b) in aorta of BubR1$^{+/+}$ and BubR1$^{H/H}$ mice. Values are means±SEM (n=5 to 9 for cGMP and n=5 to 10 for NOS activity). *P<0.05 vs BubR1$^{+/+}$ mice.

Acknowledgments

The authors thank Leslie Smith, Darcy Richardson, and Mike Thompson for technical assistance, and Janet Beckman for help in preparing the manuscript.

Sources of Funding

This work was supported in part by National Institute of Health Grants to J.M.v.D. (CA96985) and Z.S.K. (HL-53524, HL-58080, HL-66958), and the Mayo Foundation.

Disclosures

None.

References

1. Lakatta EG, Levy D. Arterial and cardiac aging: major shareholders in cardiovascular disease enterprises: Part I: aging arteries: a "set up" for vascular disease. *Circulation*. 2003;107:139–146.
2. Hongo K, Nakagomi T, Kassell NF, Sasaki T, Lehman M, Vollmer DG, Tsukahara T, Ogawa H, Torner J. Effects of aging and hypertension on endothelium-dependent vascular relaxation in rat carotid artery. *Stroke*. 1988;19:892–897.
3. Hatake K, Kakishita E, Wakabayashi I, Sakiyama N, Hishida S. Effect of aging on endothelium-dependent vascular relaxation of isolated human basilar artery to thrombin and bradykinin. *Stroke*. 1990;21:1039–1043.
4. Paterno R, Faraci FM, Heistad DD Age-related changes in release of endothelium-derived relaxing factor from the carotid artery. *Stroke*. 1994; 25:2457–2460; discussion 2461–2.
5. Egashira K, Inou T, Hirooka Y, Kai H, Sugimachi M, Suzuki S, Kuga T, Urabe Y, Takeshita A. Effects of age on endothelium-dependent vasodilation of resistance coronary artery by acetylcholine in humans. *Circulation*. 1993;88:77–81.
6. Hoffmann J, Haendeler J, Aicher A, Rossig L, Vasa M, Zeiher AM, Dimmeler S. Aging enhances the sensitivity of endothelial cells toward apoptotic stimuli: important role of nitric oxide. *Circ Res*. 2001;89: 709–715.
7. Francia P, delli Gatti C, Bachschmid M, Martin-Padura I, Savoia C, Migliaccio E, Pelicci PG, Schiavoni M, Lüscher TF, Volpe M, Cosentino F. Deletion of p66shc gene protects against age-related endothelial dysfunction. *Circulation*. 2004;110:2889–2895.
8. Blackwell KA, Sorenson JP, Richardson DM, Smith LA, Suda O, Nath K, Katusic ZS. Mechanisms of aging-induced impairment of endothelium-dependent relaxation: role of tetrahydrobiopterin. *Am J Physiol Heart Circ Physiol*. 2004;287:H2448–H2453.
9. Tschudi MR, Barton M, Bersinger NA, Moreau P, Cosentino F, Noll G, Malinski T, Lüscher TF. Effect of age on kinetics of nitric oxide release in rat aorta and pulmonary artery. *J Clin Invest*. 1996;98:899–905.
10. van der Loo B, Labugger R, Skepper JN, Bachschmid M, Kilo J, Powell JM, Palacios-Callender M, Erusalimsky JD, Quaschning T, Malinski T, Gygi D, Ullrich V, Lüscher TF. Enhanced peroxynitrite formation is associated with vascular aging. *J Exp Med*. 2000;192:1731–1744.
11. Clowes AW, Reidy MA, Clowes MM. Kinetics of cellular proliferation after arterial injury. I. Smooth muscle growth in the absence of endothelium. *Lab Invest*. 1983;49:327–333.
12. Schwartz SM, Reidy MR, Clowes A. Kinetics of atherosclerosis: a stem cell model. *Ann N Y Acad Sci*. 1985;454:292–304.
13. Newby AC, Zaltsman AB. Fibrous cap formation or destruction–the critical importance of vascular smooth muscle cell proliferation, migration and matrix formation. *Cardiovasc Res*. 1999;41:345–360.
14. van der Wal AC, Becker AE, Das PK. Medial thinning and atherosclerosis-evidence for involvement of a local inflammatory effect. *Atherosclerosis*. 1993;103:55–64.
15. Davies MJ, Richardson PD, Woolf N, Katz DR, Mann J. Risk of thrombosis in human atherosclerotic plaques: role of extracellular lipid, macrophage, and smooth muscle cell content. *Br Heart J*. 1993;69: 377–381.
16. Tracy RE. Declining density of intimal smooth muscle cells and age as preconditions for atheronecrosis in the basilar artery. *Virchows Arch*. 1995;427:131–138.

17. Hasty P, Campisi J, Hoeijmakers J, van Steeg H, Vijg J. Aging and genome maintenance: lessons from the mouse? *Science*. 2003;299: 1355–1359.
18. Baker DJ, Jeganathan KB, Cameron JD, Thompson M, Juneja S, Kopecka A, Kumar R, Jenkins RB, de Groen PC, Roche P, van Deursen JM. BubR1 insufficiency causes early onset of aging-associated phenotypes and infertility in mice. *Nat Genet*. 2004;36:744–749.
19. Matsumoto T, d'Uscio LV, Eguchi D, Akiyama M, Smith LA, Katusic ZS. Protective effect of chronic vitamin C treatment on endothelial function of apolipoprotein E-deficieint mouse carotid artery. *J Pharmacol Exp Ther*. 2003;306:103–108.
20. d'Uscio LV, Smith LA, Katusic ZS. Hypercholesterolemia impairs endothelium-dependent relaxations in common carotid arteries of apolipoprotein E-deficient mice. *Stroke*. 2001;32:2658–2664.
21. Henrion D, Terzi F, Matrougui K, Duriez M, Boulanger CM, Colucci-Guyon E, Babinet C, Briand P, Friedlander G, Poitevin P, Levy BI. Impaired flow-induced dilation in mesenteric resistance arteries from mice lacking vimentin. *J Clin Invest*. 1997;100:2909–2914.
22. Loufrani L, Matrougui K, Gorny D, Duriez M, Blanc I, Levy BI, Henrion D. Flow (shear stress)-induced endothelium-dependent dilation is altered in mice lacking the gene encoding for dystrophin. *Circulation*. 2001;103: 864–870.
23. Laurent S, Caviezel B, Beck L, Girerd X, Billaud E, Boutouyrie P, Hoeks A, Safar M. Carotid artery distensibility and distending pressure in hypertensive humans. *Hypertension*. 1994;23:878–883.
24. Kasper LH, Brindle PK, Schnabel CA, Pritchard CE, Cleary ML, van Deursen JM. CREB binding protein interacts with nucleoporin-specific F-G repeats that activate transcription and mediate NUP98-HOXA9 oncogenicity. *Mol Cell Biol*. 1999;19:764–776.
25. d'Uscio LV, Baker TA, Mantilla CB, Smith L, Weiler D, Sieck GC, Katusic ZS. Mechanism of endothelial dysfunction in apolipoprotein E–deficient mice. *Arterioscler Thromb Vasc Biol*. 2001;21:1017–1022.
26. Chan GK, Jablonski SA, Sudakin V, Hittle JC, Yen TJ. Human BUBR1 is a mitotic checkpoint kinase that monitors CENP-E functions at kinetochores and binds the cyclosome/APC. *J Cell Biol*. 1999;146:941–954.
27. Bennett MR, Macdonald K, Chan SW, Boyle JJ, Weissberg PL. Cooperative interactions between RB and p53 regulate cell proliferation, cell senescence, and apoptosis in human vascular smooth muscle cells from atherosclerotic plaques. *Circ Res*. 1998;82:704–712.
28. Ruiz-Torres A, Gimeno A, Melon J, Mendez L, Munoz FJ, Macia M. Age-related loss of proliferative activity of human vascular smooth muscle cells in culture. *Mech Ageing Dev*. 1999;110:49–55.
29. Liao S, Curci JA, Kelley BJ, Sicard GA, Thompson RW. Accelerated replicative senescence of medial smooth muscle cells derived from abdominal aortic aneurysms compared to the adjacent inferior mesenteric artery. *J Surg Res*. 2000;92:85–95.
30. Moon SK, Thompson LJ, Madamanchi N, Ballinger S, Papaconstantinou J, Horaist C, Runge MS, Patterson C. Aging, oxidative responses, and proliferative capacity in cultured mouse aortic smooth muscle cells. *Am J Physiol Heart Circ Physiol*. 2001;280:H2779–H2788.
31. Hajdu MA, Heistad DD, Siems JE, Baumbach GL. Effects of aging on mechanics and composition of cerebral arterioles in rats. *Circ Res*. 1990; 66:1747–1754.
32. Fornieri C, Quaglino D, Jr., Mori G. Role of the extracellular matrix in age-related modifications of the rat aorta. Ultrastructural, morphometric, and enzymatic evaluations. *Arterioscler Thromb*. 1992;12:1008–1016.
33. Cernadas MR, Sanchez de Miguel L, Garcia-Duran M, Gonzalez-Fernandez F, Millas I, Monton M, Rodrigo J, Rico L, Fernandez P, de Frutos T, Rodriguez-Feo JA, Guerra J, Caramelo C, Casado S, Lopez-Farre AJ. Expression of constitutive and inducible nitric oxide synthases in the vascular wall of young and aging rats. *Circ Res*. 1998; 83:279–286.
34. Orlandi A, Marcellini M, Spagnoli LG. Aging influences development and progression of early aortic atherosclerotic lesions in cholesterol-fed rabbits. *Arterioscler Thromb Vasc Biol*. 2000;20:1123–1136.
35. Oemar BS, Tschudi MR, Godoy N, Brovkovich V, Malinski T, Lüscher TF. Reduced endothelial nitric oxide synthase expression and production in human atherosclerosis. *Circulation*. 1998;97:2494–2498.

Chapter 5

Opposing roles for $p16^{Ink4a}$ and $p19^{Arf}$ in senescence and aging caused by BubR1 insufficiency

Nature Cell Biology (In press)

Opposing roles for $p16^{Ink4a}$ and $p19^{Arf}$ in senescence and aging caused by BubR1 insufficiency

Darren J. Baker[1], Carmen Perez-Terzic[2], Fang Jin[1], Kevin Pitel[1], Nicolas J. Niederlander[3], Karthik Jeganathan[1], Satsuki Yamada[3], Santiago Reyes[3], Lois Rowe[3], H. Jay Hiddinga[4], Norman L. Eberhardt[4], Andre Terzic[3] and Jan M. van Deursen[1,4,*]

[1]Department of Pediatric and Adolescent Medicine, [2]Department of Physical Medicine and Rehabilitation, [3]Department of Medicine, and [4]Department of Biochemistry and Molecular Biology Mayo Clinic College of Medicine, Rochester, MN 55905

*Corresponding author: Jan M. A. van Deursen, Mayo Clinic, 200 First Street SW, Rochester, MN 55905 USA. Telephone: 507-284-2524. Fax: 507-284-9759
Email: vandeursen.jan@mayo.edu

Abstract
Expression of *p16*^{Ink4a} and *p19*^{Arf} increases with age in both rodent and human tissues. However, whether these tumor suppressors are effectors of aging remains unclear, mainly because knockout mice lacking *p16*^{Ink4a} or *p19*^{Arf} die early of tumors. Here, we show that two tissues that develop early aging-associated phenotypes in response to BubR1 insufficiency, skeletal muscle and fat, have high levels of $p16^{Ink4a}$ and $p19^{Arf}$. Inactivation of *p16*^{Ink4a} in BubR1 insufficient mice attenuates both cellular senescence and premature aging in these same tissues. Conversely, *p19*^{Arf} inactivation exacerbates senescence and aging in BubR1 mutant mice. Thus, we identify BubR1 insufficiency as a trigger for activation of the *Cdkn2a* locus in certain mouse tissues, and demonstrate that $p16^{Ink4a}$ is an effector and $p19^{Arf}$ an attenuator of senescence and aging in these tissues.

Introduction
Cellular senescence is a state of irreversible growth arrest that can be induced by various cellular stressors[1, 2]. The *Cdkn2a* locus encodes two separate tumor suppressors, $p16^{Ink4a}$, a cyclin-dependent kinase (Cdk) inhibitor that can block G_1/S progression when present above a certain level, and $p19^{Arf}$, a positive regulator of the transcription factor p53 that integrates and responds to a wide variety of cellular stresses[1, 3-5]. Both $p16^{Ink4a}$ and $p19^{Arf}$ are effectors of senescence in cultured cells[6] and increase with aging in many tissues[7, 8], leading to speculation that their induction is causally implicated in *in vivo* senescence and organismal aging. However, rigorous testing of this notion has been difficult because mice that lack *p16*^{Ink4a} or *p19*^{Arf} die of cancer long before they reach the age at which normal mice start to develop age-related disorders[1, 2]. Recent evidence in middle-aged *p16*^{Ink4a} knockout mice indicates that the age-induced expression of *p16*^{Ink4a} limits the proliferative

and regenerative capacity of progenitor populations[9-11]. Yet, whether increased stem-cell proliferation and tissue regeneration seen in *p16*^{Ink4a} knockouts actually delays onset of age-related pathologies remains unknown due to the limited animal lifespan[1, 12].

One approach to study the role of *p16*^{Ink4a} and *p19*^{Arf} in aging would be to determine whether their respective inactivation in mouse models that develop aging-associated pathologies at an early age, due to single gene mutations, would prevent or delay premature aging. Mutant mice with low levels of the mitotic checkpoint protein BubR1 (called BubR1 hypomorphic or *BubR1*$^{H/H}$ mice) undergo premature sister chromosome separation and develop progressive aneuploidy along with various progeroid phenotypes that include short lifespan, cachectic dwarfism, lordokyphosis (abnormal curvature of the spine), sarcopenia (age-related skeletal muscle atrophy), cataracts, craniofacial dysmorphisms, arterial stiffening, loss of (subcutaneous) fat, reduced stress tolerance and impaired wound healing[13-15]. During the course of natural aging, several mouse tissues show a dramatic decline in BubR1 protein expression, which, combined with the observation that *BubR1*$^{H/H}$ mice age prematurely, suggests a possible role for BubR1 in regulating natural aging[13-15]. Here we show that certain mouse tissues induce *p16*^{Ink4a} and *p19*^{Arf} in response to BubR1 hypomorphism. Using *BubR1*$^{H/H}$ mice in which these tumor suppressors are lacking, we demonstrate that p16^{Ink4a} is an effector of cellular senescence and aging, while, conversely, p19^{Arf} acts to suppress cellular senescence and aging.

Results

p16^{Ink4a} inactivation increases the lifespan of *BubR1*$^{H/H}$ mice

To determine the requirement for p16^{Ink4a} in the development of progeroid phenotypes in BubR1-insufficient mice, we bred *BubR1*$^{H/H}$ mice onto a *p16*^{Ink4a} homozygous null genetic background. In total, 86 *BubR1*$^{H/H}$/*p16*$^{Ink4a-/-}$, 192 *BubR1*$^{H/H}$, 160 *BubR1*$^{+/+}$ and 44 *p16*$^{Ink4a-/-}$ mice were generated and monitored for development of age-related phenotypes for a period of one year. Inactivation of *p16*^{Ink4a} offered *BubR1*$^{H/H}$ mice a 25% extension of lifespan (Fig. 1a). Although the median lifespan of *BubR1*$^{H/H}$ mice was extended in the absence of p16^{Ink4a}, the maximum lifespan was not, suggesting that the condition(s) that cause(s) death was not rescued by *p16*^{Ink4a} inactivation.

p16^{Ink4a} loss blunts sarcopenia induced by BubR1 insufficiency

A prominent aging-associated phenotype of *BubR1*$^{H/H}$ mice is the development of lordokyphosis[13]. The incidence of this phenotype was dramatically reduced in *BubR1*$^{H/H}$/*p16*$^{Ink4a-/-}$ animals in comparison to *BubR1*$^{H/H}$ mice (Fig. 1b, c). Furthermore, the median time to onset of lordokyphosis was three times longer in *BubR1*$^{H/H}$/*p16*$^{Ink4a-/-}$ mice than in *BubR1*$^{H/H}$ mice (Fig. 1b). Lordokyphosis is associated with both osteoporosis and

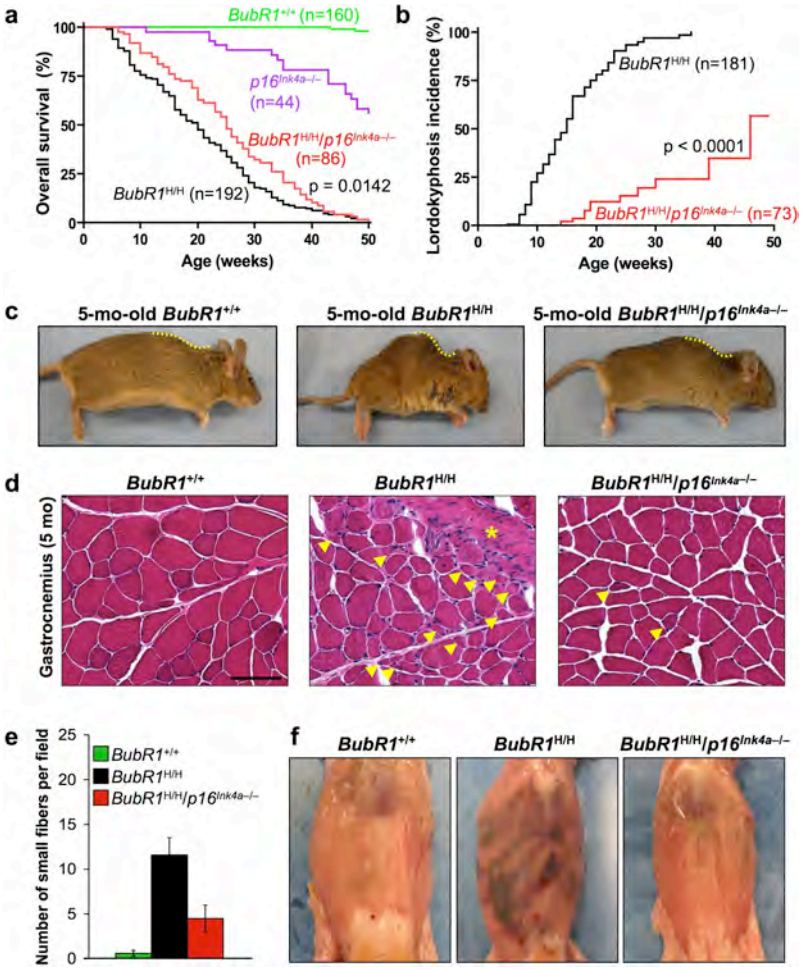

Figure 1 Ablation of p16^{Ink4a} in *BubR1*$^{H/H}$ mice extends lifespan and attenuates sarcopenia. (**a**) Overall survival curves for wild-type, *p16*$^{Ink4a–/–}$, *BubR1*$^{H/H}$ and *BubR1*$^{H/H}$/*p16*$^{Ink4a–/–}$ mice. The median overall survival of combined *BubR1*$^{H/H}$/*p16*$^{Ink4a–/–}$ mice is 25 weeks, a 25% extension in lifespan compared to *BubR1*$^{H/H}$ animals. We note that the *p16*$^{Ink4a–/–}$, *BubR1*$^{H/H}$ and *BubR1*$^{H/H}$/*p16*$^{Ink4a–/–}$ curves are all statistically different from the wild-type curve by log-rank tests ($p < 0.0001$). Moreover, the *BubR1*$^{H/H}$/*p16*$^{Ink4a–/–}$ curve is statistically different from the *BubR1*$^{H/H}$ curve ($p = 0.0142$). **(b)** Incidence and latency of lordokyphosis in *BubR1*$^{H/H}$ and *BubR1*$^{H/H}$/*p16*$^{Ink4a–/–}$ mice. The curves are statistically different by use of a log-rank test ($p < 0.0001$). We note that no wild-type or *p16*$^{Ink4a–/–}$ mice developed lordokyphosis during our one-year observation period (data not shown). (**c**) Images of 5-month-old wild-type, *BubR1*$^{H/H}$ and *BubR1*$^{H/H}$/*p16*$^{Ink4a–/–}$ mice. Note the profound difference in the curvature of the spine in the *BubR1*$^{H/H}$/*p16*$^{Ink4a–/–}$ mouse. (**d**) Cross sections of gastrocnemius muscles of 5-month-old wild-type, *BubR1*$^{H/H}$, and *BubR1*$^{H/H}$/*p16*$^{Ink4a–/–}$ mice. Arrowheads mark degenerated fibers and asterisks mark areas of connective tissue infiltration. Scale bar = 100 µm. (**e**) Quantitation of the number of deteriorating (atrophic) muscle fibers in gastrocnemius muscles shown in d. Note that *BubR1*$^{H/H}$/*p16*$^{Ink4a–/–}$ muscles have three-fold less atrophic fibers than *BubR1*$^{H/H}$ muscles. Error bars are s.d. (**f**) Skinned 5-month-old wild-type, *BubR1*$^{H/H}$ and *BubR1*$^{H/H}$/*p16*$^{Ink4a–/–}$ mice demonstrating that abdominal wall thickness is visually increased in *BubR1*$^{H/H}$/*p16*$^{Ink4a–/–}$ mice when compared with *BubR1*$^{H/H}$ animals.

age-related degenerative loss of muscle mass and strength (sarcopenia) in wild-type mice of extremely advanced age[16]. Histological evaluation of longitudinal femur sections from kyphotic *BubR1*$^{H/H}$ mice revealed no evidence for osteoporosis (Supplementary Information, Fig. S1a, b). Histopathology on gastrocnemius and paraspinal muscles of 5-month-old *BubR1*$^{H/H}$ mice, however, revealed clear signs of skeletal muscle atrophy and degeneration (Fig. 1d and data not shown). Muscle degeneration was greatly reduced in *BubR1*$^{H/H}$ muscles lacking p16^{Ink4a} (Fig. 1d, e). In addition, abdominal muscles of *BubR1*$^{H/H}$ mice were poorly developed, as revealed by macroscopic analysis and magnetic resonance imaging (Fig. 1f and Supplementary Information, Fig. S1c). Depletion of p16^{Ink4a} resulted in substantial correction of this defect. These data demonstrate that p16^{Ink4a} plays a major role in establishing sarcopenia in *BubR1*$^{H/H}$ mice.

p16^{Ink4a} limits the regenerative capacity of beta cells and has been linked to pancreatic islet atrophy and development of diabetes[9, 17, 18], which, in turn, can cause muscle atrophy through accelerated muscle protein degradation[19]. This prompted us to test whether the sarcopenia observed in *BubR1*$^{H/H}$ mice might be due to beta cell failure. *BubR1*$^{H/H}$ mice showed highly efficient glucose clearance in a glucose tolerance test (Supplementary Information, Fig. S2a). Complementary blood insulin measurements indicated that insulin sensitivity was not impaired in *BubR1*$^{H/H}$ mice and revealed no evidence for insulin resistance (Supplementary Information, Fig. S2b). Furthermore, overall pancreatic morphology as well as islet size, shape and abundance were similar in 12-month-old *BubR1*$^{H/H}$ and control mice, as verified by histology (Supplementary Information, Fig. S2c). Consistent with this, *p16^{Ink4a}* expression in pancreas was not significantly elevated in *BubR1*$^{H/H}$ mice compared with *BubR1*$^{+/+}$ counterparts (Fig. 3c). Thus, sarcopenia in *BubR1*$^{H/H}$ mice is unlikely to be the result of p16^{Ink4a}-mediated beta cell degeneration or insulin resistance.

BubR1 and p16^{Ink4a} levels are inversely linked in skeletal muscle

To determine if BubR1 might play a role in the normal skeletal muscle aging, we measured BubR1 protein levels in skeletal muscle of young and old wild-type mice by western blot analysis. Gastrocnemius muscles had considerably higher levels of BubR1 protein at two months than at 35 months of age (Fig. 2a and Supplementary Information, Fig. S6a). *BubR1* transcripts were undetectable by quantitative (q)RT-PCR in the gastrocnemius of 35-month-old mice but readily present at two months (data not shown), suggesting that reduced *BubR1* transcriptional activity contributes to the decline in BubR1 protein levels at advanced age. In contrast to *BubR1* transcription, *p16^{Ink4a}* transcription dramatically increased with age in gastrocnemius muscles of old wild-type mice (Fig. 2b). Gastrocnemius of 2- and 5-month-old *BubR1*$^{H/H}$ mice also had high *p16^{Ink4a}* transcript levels (Fig. 2b), providing evidence for an inverse relationship between *BubR1* and *p16^{Ink4a}*

expression. To characterize this relationship further, we measured *p16*^{Ink4a} expression in gastrocnemius of 3-week-old *BubR1*$^{H/H}$ mice, when skeletal muscle atrophy is histologically undetectable (Supplementary Information, Fig. S2d). *p16*^{Ink4a} transcript levels were similarly elevated for 3-week-old, and 2- and 5-month-old mice (Fig. 2b), indicating that *p16*^{Ink4a} induction is an early response to BubR1 hypomorphism that precedes histological signs of sarcopenia.

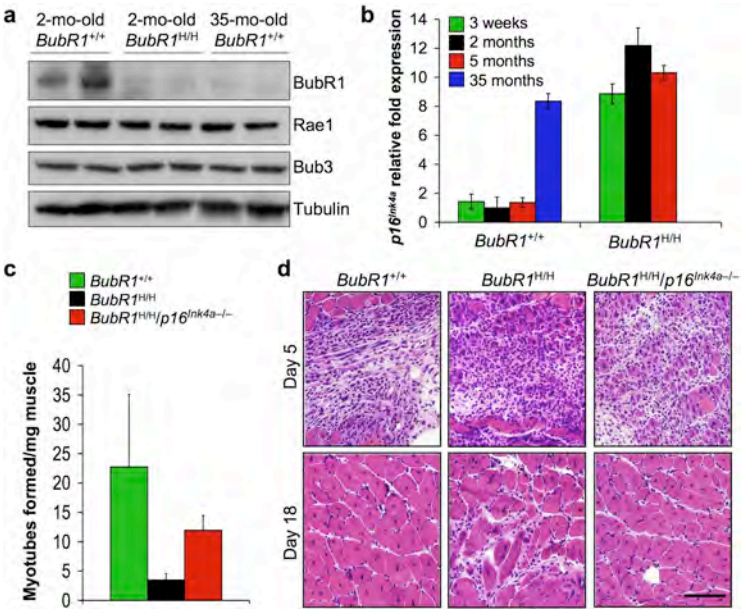

Figure 2 Inverse correlation between BubR1 and p16^{Ink4a} expression levels with aging. (**a**) Western blot analysis of gastrocnemius muscle in young wild-type and *BubR1*$^{H/H}$ mice and old wild-type mice. Blots were probed with antibodies against BubR1, Bub3 and Rae1. Anti-tubulin was used as a loading control. Note that the mitotic checkpoint proteins Bub3 and Rae1 remain highly expressed as wild-type mice age. Uncropped images of the scans are shown in Supplementary Information, Fig. S6a. (**b**) *p16*^{Ink4a} expression in wild-type and *BubR1*$^{H/H}$ gastrocnemius muscles at various ages analyzed by qRT-PCR (n = 3 males per genotype and age group, with triplicate measurements taken). Values were normalized to *GAPDH*. Relative fold expression is to 2-month-old wild-type values. Error bars are s.d. **(c)** Myotube formation potential of gastrocnemius muscles from 5-month-old mice of the indicated genotypes analyzed by a well-standardized *in vitro* assay. Error bars are s.d. **(d)** Cardiotoxin treated gastrocnemius muscle of 5-month-old wild-type, *BubR1*$^{H/H}$ and *BubR1*$^{H/H}$/*p16*$^{Ink4a-/-}$ mice at five days (top) or 18 days (bottom) after injection. Note that all gastrocnemius muscles exhibit an extensive hypercellular response to cardiotoxin injection by day 5 regardless of genotype. Wild-type and *BubR1*$^{H/H}$/*p16*$^{Ink4a-/-}$ mice have complete restoration of muscle architecture by myofibers with central nuclei by day 18, while *BubR1*$^{H/H}$ mice have been unable to restore normal tissue structure. Scale bar = 100 µm.

Increased expression of *p16*^{Ink4a} with age in adult stem cells is associated with reduced tissue repair and regeneration in several mouse tissues[9-12]. To explore whether p16^{Ink4a}-mediated exhaustion of myogenic stem cell potential might contribute to premature

sarcopenia in *BubR1*$^{H/H}$ mice, *in vitro* myoblast-to-myofiber differentiation assays were performed on gastrocnemius muscles from 5-month-old wild-type, *BubR1*$^{H/H}$ and *BubR1*$^{H/H}$/*p16*$^{Ink4a-/-}$ mice. In these assays, the average number of myotubes obtained per milligram muscle tissue was about 7-fold lower in *BubR1*$^{H/H}$ mice than in wild-type mice (Fig. 2c). By contrast, only a 2-fold reduction in myotube formation was observed in *BubR1*$^{H/H}$ mice lacking p16^{Ink4a}. To confirm these data, 5-month-old wild-type, *BubR1*$^{H/H}$ and *BubR1*$^{H/H}$/*p16*$^{Ink4a-/-}$ mice were challenged to regenerate muscle fibers by injection of cardiotoxin, a sixty amino-acid polypeptide that causes acute injury by rapidly destroying muscle fibers[20]. Consistent with our *in vitro* data, muscle regeneration was overtly delayed in *BubR1*$^{H/H}$ mice, but not in *BubR1*$^{H/H}$/*p16*$^{Ink4a-/-}$ counterparts (Fig. 2d). Collectively, these data indicate that p16^{Ink4a} promotes sarcopenia in *BubR1*$^{H/H}$ mice, at least in part, by impairing muscle regeneration.

p16^{Ink4a} loss attenuates aging in selective BubR1 hypomorphic tissues

Loss of p16^{Ink4a} further caused a modest, yet significant, delay in the latency of cataract formation in *BubR1*$^{H/H}$ mice (Fig. 3a). Aged skin is characterized by reduced dermal thickness and subcutaneous adipose tissue, both of which are observed in *BubR1*$^{H/H}$ mice at young ages[13]. At two months of age, *BubR1*$^{H/H}$, *BubR1*$^{H/H}$/*p16*$^{Ink4a-/-}$, and *p16*$^{Ink4a-/-}$ mice had similar amounts of subdermal adipose tissue (Fig. 3b). As expected, the mean thickness of the subcutaneous adipose layer notably decreased in 5-month-old *BubR1*$^{H/H}$ mice. This decline was not accompanied by increased fat storage in liver tissue (Supplementary Information, Fig. S2e). The decrease in subcutaneous fat was much less severe in age-matched *BubR1*$^{H/H}$/*p16*$^{Ink4a-/-}$ mice (Fig. 3b), indicating that p16^{Ink4a} is, at least in part, responsible for loss of subcutaneous adipose tissue in *BubR1*$^{H/H}$ mice. Tolerance of anesthetic stress was also greatly improved in *BubR1*$^{H/H}$/*p16*$^{Ink4a-/-}$ mice (Supplementary Information, Table S1), as was adipose tissue deposition (Supplementary Information, Fig. S2f). However, several progeroid symptoms seen in *BubR1*$^{H/H}$ mice remained unchanged following loss of p16^{Ink4a}, including dwarfism, dermis thinning, arterial wall stiffening, and infertility (Supplementary Information, Table S1 and data not shown). No progeroid phenotypes of *BubR1*$^{H/H}$ mice were aggravated by p16^{Ink4a} loss.

The differential corrective effects of *p16*^{Ink4a} disruption on individual progeroid phenotypes infers tissue-specific differences in engagement of the p16^{Ink4a} pathway in the cellular response to BubR1 deficiency. *BubR1*$^{H/H}$ tissues in which p16^{Ink4a} loss causes a significant delay of premature aging, such as eye and (subdermal) adipose tissue, showed strong induction of *p16*^{Ink4a} expression in response to BubR1 hypomorphism (Fig. 3c, d and Supplementary Information, Fig. S6b, c). *BubR1*$^{H/H}$ tissues in which *p16*^{Ink4a} inactivation has no discernible corrective effect, such as dermis, brain, aorta, testis and ovary, did not exhibit significant *p16*^{Ink4a} induction (Fig. 3c, and data not shown). Furthermore, mutant

tissues that are not subjected to premature aging, including lung, pancreas, colon and liver[13], maintained low *p16*^{Ink4a} expression levels. Together, these data demonstrate that *p16*^{Ink4a} is activated in a subset of tissues in *BubR1*$^{H/H}$ mice, where it contributes to progeroid phenotypes.

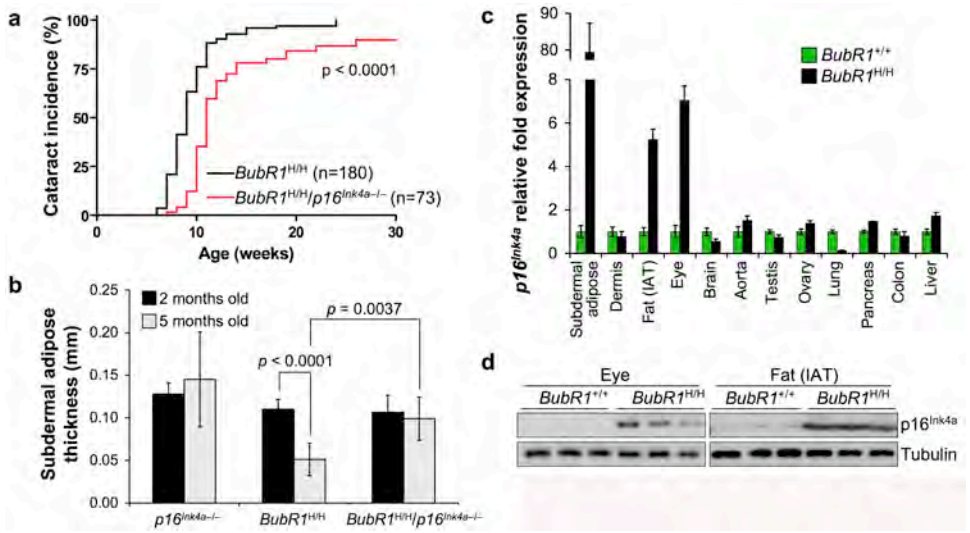

Figure 3 *p16*^{Ink4a} disruption attenuates selective progeroid features of BubR1 hypomorphic mice. (**a**) Incidence and latency of cataract formation in *BubR1*$^{H/H}$ and *BubR1*$^{H/H}$/*p16*$^{Ink4a-/-}$ mice as detected by the use of slit light after dilation of eyes. The curves are statistically different using a log-rank test ($p < 0.0001$). We note that no wild-type or *p16*$^{Ink4a-/-}$ mice developed cataracts during this observation period. (**b**) Subcutaneous adipose layer thickness of *p16*$^{Ink4a-/-}$, *BubR1*$^{H/H}$, and *BubR1*$^{H/H}$/*p16*$^{Ink4a-/-}$ mice at two and five months of age (n = 4 male mice for each age per genotype). Error bars are s.d. A two-tailed Mann-Whitney test was used for statistical analyses (**c**) qRT-PCR analysis for relative expression of *p16*^{Ink4a} in a variety of 2-month-old tissues from *BubR1*$^{H/H}$ and wild-type mice. Values were normalized to *GAPDH*, and relative fold is to 2-month-old wild-type samples (n = 3 male mice for each tissue, with triplicate measurements taken). Error bars are s.d. (**d**) Western blots of eye and fat extracts from 2-month-old *BubR1*$^{+/+}$ and *BubR1*$^{H/H}$ mice probed with anti-p16^{Ink4a} antibody. Anti-tubulin antibody served as loading control. Uncropped images of the scans are shown in Supplementary Information, Fig. S6b, c.

p16^{Ink4a} loss attenuates *in vivo* senescence

BubR1 is a putative E2F-regulated gene[21] and loss of p16^{Ink4a} leads to increased E2F transcriptional activity[22]. Accordingly, attenuation of aging in skeletal muscle, fat and eye might be the result of increased *BubR1* gene expression. However, this is unlikely as *BubR1* transcript levels in these tissues were not impacted by loss of p16^{Ink4a} (Fig. 4a). As p16^{Ink4a} is an effector of cellular senescence, *p16*^{Ink4a} deletion might delay aging in hypomorphic mice by decreasing senescense. As shown in Fig. 4b, *BubR1*$^{H/H}$ adipose

tissue expresses high levels of senescence-associated (SA) beta-galactosidase, a marker of cellular senescence[23]. SA-beta-galactosidase staining was much lower in adipose tissue of *BubR1*$^{H/H}$/*p16*$^{Ink4a-/-}$ mice (Fig. 4b). Skeletal muscles of 2-month-old *BubR1*$^{H/H}$ mice did not stain positive for SA-beta-galactosidase but expressed high levels of several other senescence-associated genes, including *Igfbp2*, *Nrg1*, *Mmp13* and *PAI-1*[24-27] (Fig. 4c). Expression of these markers was markedly decreased in skeletal muscles of age-matched *BubR1*$^{H/H}$/*p16*$^{Ink4a-/-}$ mice. A key feature of senescence is loss of proliferative potential. *In vivo* 5-bromo-2-deoxyuridine (BrdU) labeling showed that 2-month-old *BubR1*$^{H/H}$ mice had much lower percentages of cycling cells in skeletal muscle and fat than wild-type mice (Fig. 4d). These reductions were less profound in *BubR1*$^{H/H}$/*p16*$^{Ink4a-/-}$ mice. Collectively, these data suggest that BubR1 hypomorphism causes cellular senescence in adipose tissue and skeletal muscle through a p16^{Ink4a}-dependent mechanism. As *p16*^{Ink4a} inactivation

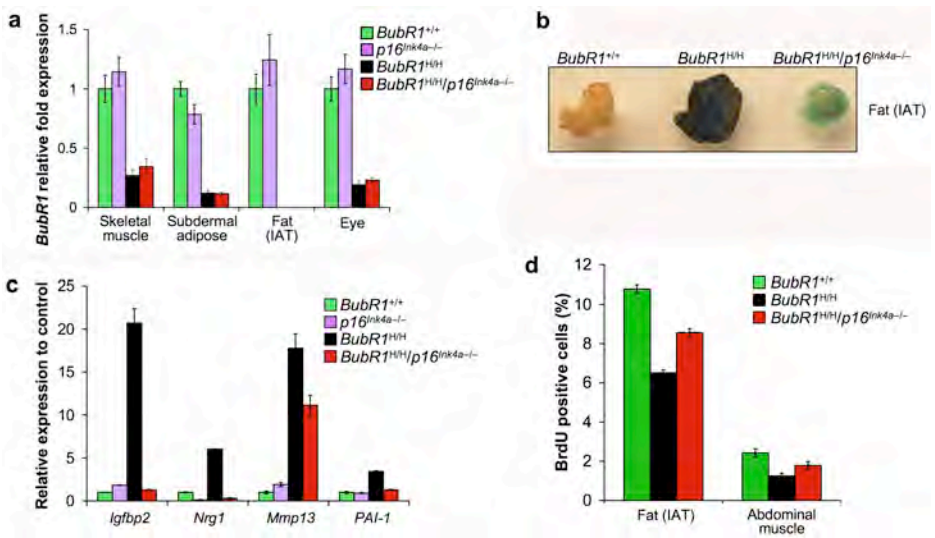

Figure 4 *p16*^{Ink4a} induction in *BubR1*$^{H/H}$ mice promotes cellular senescence. (**a**) Relative expression of BubR1 in gastrocnemius, subdermal adipose, fat deposit, and eye from 2-month-old wild-type, *p16*$^{Ink4a-/-}$, *BubR1*$^{H/H}$ and *BubR1*$^{H/H}$/*p16*$^{Ink4a-/-}$ mice as determined by qRT-PCR. Values were normalized to GAPDH. Relative fold is to 2-month-old wild-type samples (n = 3 male mice per genotype, with triplicate measurements taken per sample). Error bars are s.d. We note that ablation of p16^{Ink4a} was unable to increase the amount of BubR1 present in either wild-type or BubR1 hypomorphic mice. (**b**) IAT of 5-month-old wild-type, *BubR1*$^{H/H}$ and *BubR1*$^{H/H}$/*p16*$^{Ink4a-/-}$ mice stained for SA-beta-galactosidase activity. (**c**) Relative expression of senescence markers in gastrocnemius muscles of 2-month-old wild-type, *p16*$^{Ink4a-/-}$, *BubR1*$^{H/H}$ and *BubR1*$^{H/H}$/*p16*$^{Ink4a-/-}$ mice analyzed by qRT-PCR (n = 3 male mice per genotype). Values were normalized to *GAPDH*. Relative fold expression is to 2-month-old wild-type muscle. Error bars are s.d. (**d**) Analysis of replicative senescence in skeletal muscle and fat of 2-month-old wild-type, *BubR1*$^{H/H}$ and *BubR1*$^{H/H}$/*p16*$^{Ink4a-/-}$ mice by analyzing *in vivo* BrdU incorporation (n = 3 males per genotype). Error bars are s.d.

attenuates both senescence and aging in these tissues, the mechanism by which BubR1 hypomorphism accelerates the aging phenotypes may involve $p16^{Ink4a}$-induced senescence.

$p19^{Arf}$ is elevated in *BubR1*$^{H/H}$ tissues with high $p16^{Ink4a}$

Besides *p16*^{Ink4a}, *p19*^{Arf} is expressed at increased levels in many tissues of wild-type mice with advanced age[7], including skeletal muscle (Fig. 5a). Although $p19^{Arf}$ is an established effector of senescence in cultured MEFs, its role in senescence and aging in the context of the whole organism has not been clarified[1, 2]. To explore the role of $p19^{Arf}$ in BubR1-

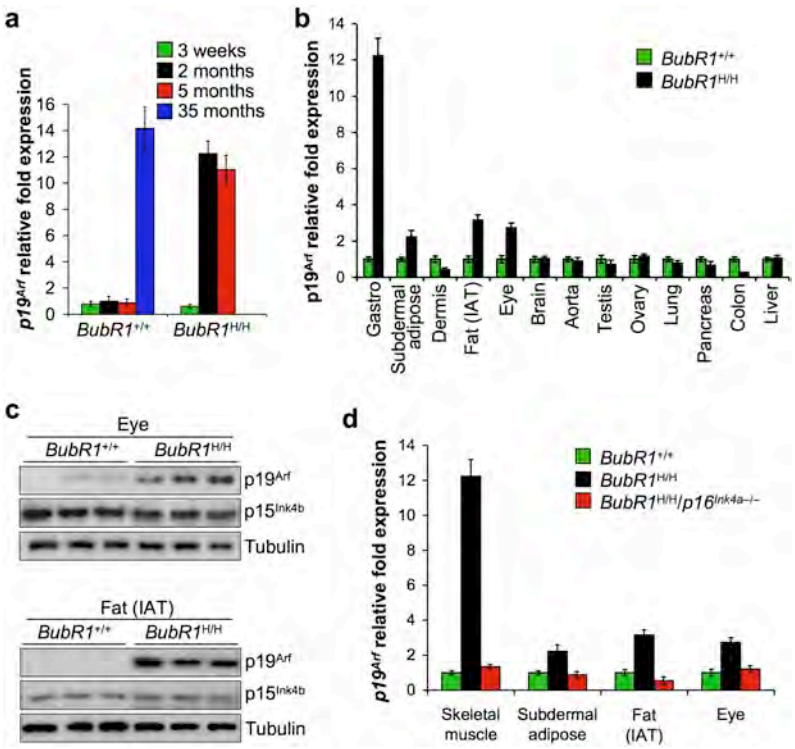

Figure 5 $p19^{Arf}$ is elevated in BubR1 hypomorphic tissues with high $p16^{Ink4a}$. (**a**) Skeletal muscles of wild-type and *BubR1*$^{H/H}$ mice of various ages were analyzed for *p19*^{Arf} expression by qRT-PCR. All values were normalized to *GAPDH*. Three mice were used per genotype and age group. Error bars are s.d. (**b**) Relative expression of *p19*^{Arf} in various tissues of 2-month-old *BubR1*$^{H/H}$ and *BubR1*$^{+/+}$ mice as measured by qRT-PCR (n = 3 males per genotype). All values were normalized to *GAPDH*. Relative expression is to wild-type samples. Error bars are s.d. (**c**) Western blots of eye and fat extracts from 2-month-old *BubR1*$^{+/+}$ and *BubR1*$^{H/H}$ mice probed with anti-$p19^{Arf}$ and $p15^{Ink4b}$ antibodies. Anti-tubulin antibody served as loading control. Uncropped images of the scans are shown in Supplementary Information, Fig. S6b, c. (**d**) Relative expression of *p19*^{Arf} in skeletal muscle (gastrocnemius), subdermal adipose, fat deposit, and eye of 2-month-old wild-type, *BubR1*$^{H/H}$ and *BubR1*$^{H/H}$/*p16*$^{Ink4a-/-}$ mice as determined by qRT-PCR (n = 3 males per genotype). All values were normalized to *GAPDH*. Relative expression is to wild-type samples. Error bars are s.d.

mediated aging, we analyzed its relative expression in tissues from 2-month-old *BubR1*$^{H/H}$ and *BubR1*$^{+/+}$ mice. Increased *p19*^{Arf} expression was consistently observed in *BubR1*$^{H/H}$ tissues that are subjected to premature aging and have high p16^{Ink4a} levels, including skeletal muscle, (subdermal) adipose and eye, but not in tissues that develop age-related pathology in a p16^{Ink4a}-independent fashion or have no age-related phenotypes (Fig. 5b, c and Supplementary Information, Fig. S6b, c and data not shown). Skeletal muscle, (subdermal) adipose and eye from *BubR1*$^{H/H}$ mice lacking p16^{Ink4a} had normal *p19*^{Arf} transcript levels (Fig. 5d), suggesting that the observed increase in *p19*^{Arf} expression is dependent on high p16^{Ink4a} levels. *p15*^{Ink4b}, encoding a Cdk inhibitor that has been linked to aging in some tissues[7], was neither increased in *BubR1*$^{H/H}$ tissues with increased *p16*^{Ink4a} and *p19*^{Arf} expression, nor in any other tissue of *BubR1*$^{H/H}$ mice (Supplementary Information, Fig. S3a and Fig. S6b, c). Unlike *p16*^{Ink4a} and *p19*^{Arf}, *p15*^{Ink4b} was not expressed at increased levels in skeletal muscles of aged wild-type mice (Supplementary Information, Fig. S3b).

p19^{Arf} disruption accelerates aging in *BubR1*$^{H/H}$ mice

To determine whether p19^{Arf} also acts as an effector of aging in *BubR1*$^{H/H}$ mice, 41 *BubR1*$^{H/H}$/*p19*$^{Arf-/-}$ mice were generated and monitored for development of age-related phenotypes. Surprisingly, lordokyphosis developed significantly faster in *BubR1*$^{H/H}$/*p19*$^{Arf-/-}$ mice than in *BubR1*$^{H/H}$ mice (Fig. 6a and b). Six-week-old *BubR1*$^{H/H}$/*p19*$^{Arf-/-}$ mice had significantly smaller fibers in gastrocnemius and abdominal muscles than age-matched *BubR1*$^{H/H}$ mice (Fig. 6c and Supplementary Information, Fig. S4a), indicating that muscle wasting was accelerated in the absence of p19^{Arf}. Cataract formation was also significantly accelerated when p19^{Arf} was lacking (Fig. 6d). Skinned 6-week-old *BubR1*$^{H/H}$/*p19*$^{Arf-/-}$ mice showed overt reductions in adipose tissue deposition (Fig. 6b). This was confirmed by weighing inguinal adipose tissue (IAT, Fig. 6e). Furthermore, the mean thickness of the subcutaneous adipose layer was significantly smaller in *BubR1*$^{H/H}$/*p19*$^{Arf-/-}$ mice than in *BubR1*$^{H/H}$ mice (0.07 versus 0.11 mm; $p < 0.0001$ using a two-tailed Mann-Whitney test). Other progeroid features of *BubR1*$^{H/H}$ mice appeared unchanged by *p19*^{Arf} inactivation (Supplementary Information, Fig. S4b and Table S1). Taken together, these data indicate that p19^{Arf} acts to delay aging in response to BubR1 hypomorphism.

One possible explanation for the pro-aging effect of *p19*^{Arf} inactivation in *BubR1*$^{H/H}$ mice might involve increased expression of p16^{Ink4a}. Consistent with this idea, p16^{Ink4a} levels in skeletal muscle, fat and eye markedly increased when *p19*^{Arf} was knocked out in *BubR1*$^{H/H}$ mice (Fig. 6f, g and Supplementary Information, Fig. S6d). A potential explanation for these results might be that genetic manipulation of *p19*^{Arf} sequences changes the normal regulatory balance in the *Cdkn2* locus, thereby increasing *p16*^{Ink4a} expression. However, disruption of *p19*^{Arf} had no appreciable effect on p16^{Ink4a} levels in tissues undergoing

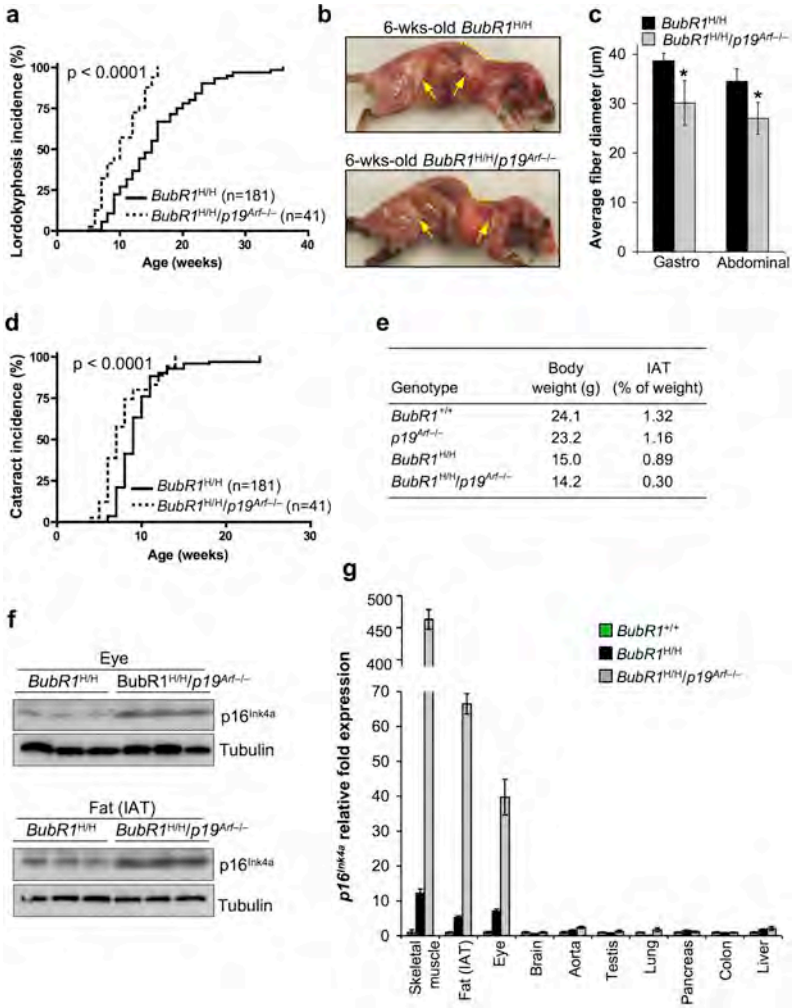

Figure 6 Accelerated aging in *BubR1*$^{H/H}$ mouse tissues with increased p16^{Ink4a} expression when p19^{Arf} is lacking. (**a**) Incidence and latency of lordokyphosis in *BubR1*$^{H/H}$ and *BubR1*$^{H/H}$/*p19*$^{Arf-/-}$ mice. The curves are statistically different by use of a log-rank test ($p < 0.0001$). (**b**) Skinned 6-week-old *BubR1*$^{H/H}$ and *BubR1*$^{H/H}$/*p19*$^{Arf-/-}$ males. Note that the *BubR1*$^{H/H}$/*p19*$^{Arf-/-}$ mouse has more profound lordokyphosis (dotted line) and reduced subcutaneous fat deposits (arrows). (**c**) Average muscle fiber size of gastrocnemius and abdominal muscles of *BubR1*$^{H/H}$ and *BubR1*$^{H/H}$/*p19*$^{Arf-/-}$ males (n = 3 mice per genotype). Error bars are s.d. A two-tailed Mann-Whitney test was used for statistics. P values for both comparisons are < 0.0001. (**d**) Incidence and latency of cataract formation in *BubR1*$^{H/H}$ and *BubR1*$^{H/H}$/*p19*$^{Arf-/-}$ mice. The curves are statistically different as calculated by a log-rank test ($p < 0.0001$). (**e**) Amount of inguinal adipose tissue in 6-week-old mice of the indicated genotypes. IAT is expressed as percentage of total body weight. Three male mice of each genotype were used. (**f**) Western blots of eye and fat extracts from 2-month-old *BubR1*$^{H/H}$ and *BubR1*$^{H/H}$/*p19*$^{Arf-/-}$ mice probed with anti-p16^{Ink4a} and anti-tubulin antibody. Uncropped images of the scans are shown in Supplementary Information, Fig. S6d. (**g**) Relative expression of *p16*^{Ink4a} in various tissues of 2-month-old *BubR1*$^{+/+}$, *BubR1*$^{H/H}$ and *BubR1*$^{H/H}$/*p19*$^{Arf-/-}$ mice as measured by qRT-PCR (n = 3 males per genotype). All values were normalized to *GAPDH*. Relative expression is to wild-type samples. Error bars are s.d.

p16^{Ink4a}-independent aging or lacking age-related pathologies (Fig. 6g), which argues against this possibility.

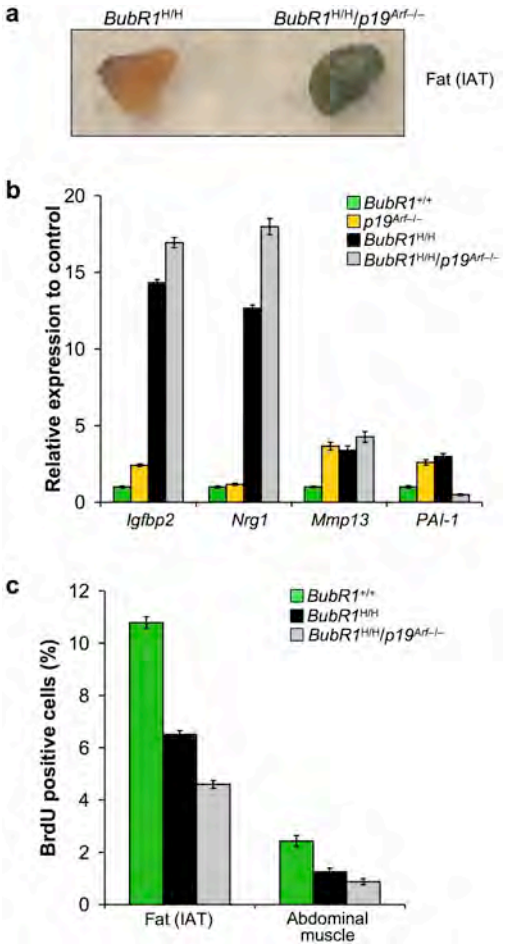

Figure 7 Senescence increases in *BubR1*$^{H/H}$ tissues with high p16^{Ink4a} when p19^{Arf} is lacking. (**a**) IAT of 2-month-old *BubR1*$^{H/H}$ and *BubR1*$^{H/H}$/*p19*$^{Arf-/-}$ mice stained for SA-beta-galactosidase activity. (**b**) Relative expression of senescence markers in gastrocnemius muscles of 6-week-old wild-type, *p19*$^{Arf-/-}$, *BubR1*$^{H/H}$ and *BubR1*$^{H/H}$/*p19*$^{Arf-/-}$ mice. All values were normalized to *GAPDH*. Relative fold expression is to wild-type gastrocnemius. Three male mice were evaluated per genotype. Error bars are s.d. (**c**) Replicative senescence in skeletal muscle and fat of 2-month-old wild-type, *BubR1*$^{H/H}$ and *BubR1*$^{H/H}$/*p19*$^{Arf-/-}$ mice as analyzed by *in vivo* BrdU incorporation. Three male mice per genotype were used for this experiment. Error bars are s.d.

Inactivation of *p19*^{Arf} increases cellular senescence

Next, we investigated whether p19^{Arf} loss accelerates aging in *BubR1*$^{H/H}$ mice through increased senescence. Adipose tissue of 6-week-old *BubR1*$^{H/H}$/*p19*$^{Arf-/-}$ mice indeed showed

much higher SA-beta-galactosidase activity than that of corresponding *BubR1*$^{H/H}$ mice (Fig. 7a). Furthermore, two senescence-associated genes, *Igfbp2* and *Nrg1*, which are expressed at increased levels in gastrocnemius muscles of 6-week-old *BubR1*$^{H/H}$ mice, were further elevated in corresponding muscles of age-matched *BubR1*$^{H/H}$/*p19*$^{Arf-/-}$ mice (Fig. 7b). *In vivo* BrdU incorporation showed that cell proliferation in skeletal muscle and fat was considerably lower in *BubR1*$^{H/H}$/*p19*$^{Arf-/-}$ mice than in *BubR1*$^{H/H}$ mice (Fig. 7c). Collectively, these data indicate that p19^{Arf} induction in *BubR1*$^{H/H}$ mice functions to prevent or delay senescence and provide further evidence for the notion that *in vivo* senescence promotes aging.

Distinct *in vivo* and *in vitro* effects of *p16*^{Ink4a} and *19*^{Arf} inactivation on senescence

Previously, we have shown that *BubR1*$^{H/H}$ MEFs express high p16^{Ink4a} and p19^{Arf} levels and senesce early[13]. To determine the effects p16^{Ink4a} and p19^{Arf} on cellular senescence in these MEFs, we stained *BubR1*$^{H/H}$/p*16*$^{Ink4a-/-}$ and *BubR1*$^{H/H}$/*p19*$^{Arf-/-}$ MEFs for SA-beta-galactosidase. Inactivation of *p19*^{Arf} strongly decreased senescence in *BubR1*$^{H/H}$ MEFs, whereas inactivation of *p16*^{Ink4a} had no effect (Supplementary Information, Fig. S5a, b). Consistently, the percentage of cycling cells was greatly increased in *BubR1*$^{H/H}$/*p19*$^{Arf-/-}$ MEFs, but not in *BubR1*$^{H/H}$/*p16*$^{Ink4a-/-}$ MEFs (Supplementary Information, Fig. S5c, d). Furthermore, *BubR1*$^{H/H}$/*p19*$^{Arf-/-}$ MEFs grew considerably faster than *BubR1*$^{H/H}$ MEFs, but *BubR1*$^{H/H}$/*p16*$^{Ink4a-/-}$ MEFs did not (Supplementary Information, Fig. S5e, f). Immunoblotting showed that the p19^{Arf}-p53 pathway remained highly active in *BubR1*$^{H/H}$/*p16*$^{Ink4a-/-}$ MEFs, similar to *BubR1*$^{H/H}$ MEFs, while it was inactive in *BubR1*$^{H/H}$/*p19*$^{Arf-/-}$ MEFs (Supplementary Information, Fig. S5h, g). Together, these data demonstrate that the effects of p16^{Ink4a} and 19^{Arf} ablation on *in vivo* senescence in skeletal muscle and fat of *BubR1*$^{H/H}$ mice are not recapitulated by their effects on *in vitro* senescence in *BubR1*$^{H/H}$ MEFs.

p16^{Ink4a} loss synergizes with BubR1 insufficiency in lung tumorigenesis

BubR1$^{H/H}$ mice exhibit progressive and severe aneuploidy but rarely develop tumors[13]. Activation of *p16*^{Ink4a} or *p19*^{Arf} in response to BubR1 hypomorphism might act to suppress tumorigenesis. To test for this possibility, *BubR1*$^{H/H}$ mice lacking p16^{Ink4a} or p19^{Arf} were monitored for tumor formation. Live *BubR1*$^{H/H}$/*p16*$^{Ink4a-/-}$ and *BubR1*$^{H/H}$ mice showed no overt tumors, but upon biopsy of moribund or dead animals, *BubR1*$^{H/H}$/*p16*$^{Ink4a-/-}$ mice had significantly more tumors than *BubR1*$^{H/H}$ mice (Fig. 8a). Eight out of nine *BubR1*$^{H/H}$/*p16*$^{Ink4a-/-}$ tumors were lung adenocarcinomas, a tumor type observed in only one *BubR1*$^{H/H}$ mouse and zero *p16*$^{Ink4a-/-}$ mice (Fig. 8b). Sarcomas, the most prevalent tumor type in *p16*$^{Ink4a-/-}$ mice, were rare in *BubR1*$^{H/H}$/*p16*$^{Ink4a-/-}$ mice and not present in *BubR1*$^{H/H}$ mice. Thus, BubR1 insufficiency synergizes with p16^{Ink4a} loss during tumorigenesis in lung epithelial cells, but not in other cell types (see Supplementary Discussion).

BubR1$^{H/H}$/*p19*$^{Arf-/-}$ and *p19*$^{Arf-/-}$ mice, however, had overlapping tumor-free survival curves (Fig. 8c), indicating that BubR1 insufficiency and p19^{Arf} loss do not synergize in tumorigenesis.

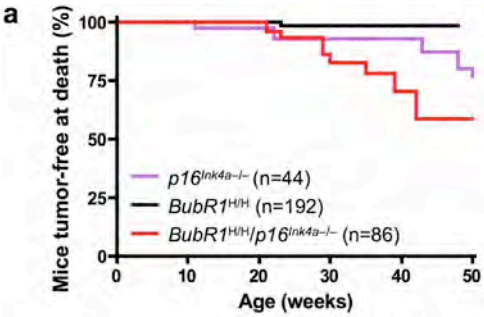

b

Mouse genotype	*BubR1*$^{H/H}$	*BubR1*$^{H/H}$/*p16*$^{Ink4a-/-}$	*p16*$^{Ink4a-/-}$
Tumor type			
Lymphoma	-	-	2%
Lung adenocarcinoma	<1%	9%	-
Hepatocellular carcinoma	-	-	5%
Sarcoma	-	1%	9%

Percentages of tumors from total mice (n=44 p16$^{Ink4a-/-}$ *mice; n=192 BubR1*$^{H/H}$*; n= 86 BubR1*$^{H/H}$*/p16*$^{Ink4a-/-}$ *mice).*

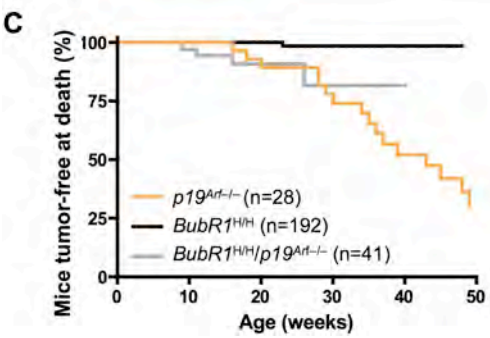

Figure 8 Ablation of p16^{Ink4a} accelerates lung tumorigenesis in BubR1 insufficient mice. (**a**) Percentage of mice which had a tumor at time of death as a function of time for *p16*$^{Ink4a-/-}$, *BubR1*$^{H/H}$ and *BubR1*$^{H/H}$/*p16*$^{Ink4a-/-}$ mice. Upon biopsy of moribund animals, all tissues were screened for tumors. Tumor tissues were collected and processed for histological confirmation. The *BubR1*$^{H/H}$/*p16*$^{Ink4a-/-}$ curve is statistically different from the *BubR1*$^{H/H}$ curve with p = 0.0027 (calculated using a log-rank test). (**b**) Tumor spectra of *p16*$^{Ink4a-/-}$, *BubR1*$^{H/H}$ and *BubR1*$^{H/H}$/*p16*$^{Ink4a-/-}$ mice. (**c**) As in a but now for *p19*$^{Arf-/-}$, *BubR1*$^{H/H}$ and *BubR1*$^{H/H}$/*p19*$^{Arf-/-}$ mice. There is no statistical difference between the curves of *BubR1*$^{H/H}$/*p19*$^{Arf-/-}$ and *p19*$^{Arf-/-}$ mice using a log-rank test.

Discussion

Here, we report that inactivation of p16^{Ink4a} attenuates the development of age-related pathologies in *BubR1*$^{H/H}$ tissues with elevated p16^{Ink4a}. This shows that induction of *p16*^{Ink4a} by cellular stress resulting from BubR1-insufficiency drives the development of aging-associated phenotypes, and provides direct evidence for a causal involvement of this tumor suppressor in organismal aging. Importantly, two tissues that are subject to p16^{Ink4a}-dependent aging when BubR1 levels are low, skeletal muscle and fat, have higher numbers of replicating cells and show decreased expression of senescence-associated proteins in the absence of p16^{Ink4a}. These observations support the notion that p16^{Ink4a} contributes to aging-associated pathologies through accumulation of senescent cells. This is a significant finding as evidence that cellular senescence promotes aging has thus far been largely circumstantial[2, 6].

BubR1$^{H/H}$ mouse tissues in which p16^{Ink4a} is elevated also have increased p19^{Arf}. However, *p19*^{Arf} inactivation accelerates instead of delays aging in these tissues, indicating that this tumor suppressor provides anti-aging activity. This seems surprising, considering that p19^{Arf} is an effector of senescence in cultured cells[2, 6]. However, the recent observation that transgenic mice carrying an extra copy of both p19^{Arf} and p53 are protected from aging-associated damage and live longer than normal mice[28], is consistent with our finding that p19^{Arf} has anti-aging activity in *BubR1*$^{H/H}$ mice. It has been proposed that the p19^{Arf}-p53 pathway in response to low, chronic stress, may primarily induce genes that promote cell survival and repair, thereby extending lifespan[5, 28, 29]. High, acute kinds of stress, on the other hand, may accelerate aging by triggering a more robust p53 response causing irreversible cell-cycle arrest and/or apoptosis[5, 29-31]. Therefore, one possibility is that p19^{Arf} may elicit a p53 transcriptional response that provides protection against cellular stress resulting from BubR1 hypomorphism, thus delaying the onset of cellular senescence. The observation that skeletal muscle and fat from *BubR1*$^{H/H}$ mice lacking p19^{Arf} accumulate more senescent cells is consistent with this idea. Strong additional support for the conclusion that p19^{Arf} has anti-aging activity is provided by our unpublished observations indicating that *BubR1*$^{H/H}$ mice lacking p53 phenocopy those lacking p19^{Arf}. Two observations reported here suggest that p19^{Arf} might exert its anti-aging effect, at least in part, through negative regulation of p16^{Ink4a} expression. First, inactivation of *p19*^{Arf} in *BubR1*$^{H/H}$ mice resulted in increased p16^{Ink4a} expression in skeletal muscle, fat and eye, three tissues that have high p19^{Arf} levels and are subjected to accelerated aging. Second, inactivation of *p16*^{Ink4a} prevented the induction of *p19*^{Arf} in these same *BubR1*$^{H/H}$ tissues. How p19^{Arf} might attenuate *p16*^{Ink4a} expression remains to be addressed.

Although inactivation of *p16*^{Ink4a} significantly delays the development of certain aging-associated phenotypes in *BubR1*$^{H/H}$ mice, it does not completely prevent them. Furthermore, other progeroid phenotypes are not impacted by loss of p16^{Ink4a}. These findings imply that BubR1 hypomorphism engages other progeroid effectors in addition to p16^{Ink4a}. The identity of these effectors is currently unclear and remains to be established. Striking similarities exist between the progeroid phenotypes of *BmalI* knockout and *BubR1*$^{H/H}$ mice[32]. The molecular basis of this similarity is unclear, although it is unlikely, based on the known functions of each protein, that BubR1 and BmalI are functionally connected. However, it is possible that the downstream pathways that respond to stress resulting from Bmal1 loss and BubR1 hypomorphism are shared.

Methods

Generation of compound mutant mice

BubR1$^{H/H}$ mice were generated as previously described[13]. *p16*^{Ink4a} and *p19*^{Arf} knockout mice have been previously generated and were acquired from the Mouse Models of Human Cancers Consortium located at the National Cancer Institute-Frederick[33, 34]. All mice were on a mixed 129 x C57BL/6 genetic background. They were housed in a pathogen-free barrier environment throughout the duration of the study. Experimental procedures involving the use of these laboratory mice were reviewed and approved by the Institutional Animal Care and Use Committee of the Mayo Clinic. Prism software (GraphPad Software, Inc.) was used for generation of all survival curves and for statistical analyses.

Collection and analysis of tumors

Moribund mice were killed and all major organs were screened for overt tumors using a dissection microscope. Tumors that were collected were processed by standard procedures for histopathology. A Fisher's exact test was used to compare tumor incidence proportions across the genotypes for mice that developed tumors. Board-certified pathologists assisted in the histological evaluation of tumor sections.

Analysis of progeroid phenotypes

Biweekly, mice were screened for the development of overt cataracts by examining dilated eyes with a slit-light. Incidence of lordokyphosis was checked biweekly. Mice that exhibited lordokyphosis for three consecutive monitoring periods were determined to have this condition. Various skeletal muscles were collected and processed for histology as described[35, 36]. Fiber diameter measurements were done on cross sections of gastrocnemius and abdominal muscles from 6-week-old male mice (n = 3 mice per genotype). A total of 50 fibers were measured per muscle using a calibrated computer program (Olympus MicroSuite Five). Dissection, histology and measurements of dermal and adipose layers of dorsal skin were performed as described[16]. Values represent an average of four males. Analysis of arterial wall stiffening was performed as described[14]. Measurements of body weight and IAT were performed on 6-week-old males (n = 3 per genotype). Oral glucose tolerance tests were performed on 5-month-old male mice (n = 5 per genotype) as described by the Jackson Laboratory (www.jax.org). Insulin measurements were as described[37].

Quantitative real-time PCR

Total RNA was extracted from tissues using a Qiagen RNeasy RNA isolation kit according to the manufacturer's protocol. Transcription into cDNA was performed using random hexamers and SuperScript III reverse transcriptase (Invitrogen Corp.) according to

manufacturer's instructions. All PCR reactions used SYBR green PCR Master Mix (Applied Biosystems) to a final volume of 12 µl, with each cDNA sample performed in triplicate in the ABI PRISM 7900 Sequence Detection System (Applied Biosystems) according to the protocol of the manufacturer. All experiments were done on organs/tissues from at least three different animals in each age group and genotype. The expression of genes was normalized to *GAPDH*. Sequences of primers used for qRT-PCR of *p15*^{Ink4b} [38], *p16*^{Ink4a} [39], *p19*^{Arf} [28], *BubR1*[40], *Mmp-13*[41], *PAI-1*[42], *Igfbp-2*[43], and *GAPDH*[44] were as published. Additionally, sequences for *Nrg1*: forward, CATGGTGAACATAGCGAATGGCC; reverse, CCACAATATGCTCACTGGAGATG A. Statistical differences were determined by using an un-paired two-tailed t test.

Analysis of satellite cell function

Analyses of *in vivo* satellite cell function were carried out as described[20]. Briefly, anesthetized mice were given a single 50-µl injection of cardiotoxin (10 µM; Calbiochem, San Diego, CA) into the gastrocnemius muscle. After this injection, the skin incision was closed with a nylon suture. Mice were allowed to recover and then were analyzed at both 5 and 18 days post-injection by routine histology. Isolation and culture of skeletal muscle satellite cells was performed as described[45]. Briefly, hind-limb muscles of 5-month-old mice were removed and trimmed of excess connective tissue and fat. Minced muscles were subjected to several 15-min rounds of digestion at 37ºC in incubation medium (50% DMEM high glucose (GIBCO)/50% F-12K (CellGro)/168U/mL collagenase type II (Worthington)/0.04% Trypsin (GIBCO)). Once fully digested, cells were successively filtered through 70 and 40 µm strainers, collected by centrifugation at 300 x *g* for 5 min and resuspended in propagation medium (DMEM high glucose/15% FCS (GIBCO)/glutamine (CellGro)/penicillin-streptomycin (CellGro)). After seven days in culture, differentiation medium (propagation medium with 2% FCS) was applied and cells were fixed seven days after the switch in medium. Myotube formation was quantified using the total number of myotubes for each sample normalized to the muscle mass extracted.

Magnetic resonance imaging

Magnetic resonance images with a 7-tesla scanner (Bruker, Billerica, MA) were obtained in 2%-isofluorane anesthetized mice using a spin-echo method as previously described[46]. Digital images were analyzed with the Metamorph software (Visitron, Universal Imaging, Downingtown, PA). The ratio of muscle area (paraspinal and chest or abdominal wall muscles) to total body cross-section was measured at the distal thorax and mid-abdomen levels.

***In vivo* BrdU incorporation**

At 24 and 6 h before tissue collection, male mice of various genotypes were injected intraperitoneally with 200 μl of 10 mg/ml BrdU (Sigma) in PBS. Mice were anesthetized and successively perfused (transcardially) with PBS and 10% formalin. Organs were collected and embedded in paraffin. Five μm sections were prepared and stained for BrdU according to the manufacturer's protocol (BD Pharmingen). The percentage of BrdU positive cells was determined by counting total and BrdU positive nuclei in 10 non-overlapping fields at 40-x magnification. N = 3 mice per genotype.

Generation and culture of MEFs

MEFs were generated as described[47]. BrdU incorporation assays on MEFs were performed according to the protocol of the manufacturer (BD Bioscience). Growth curves were generated as described[13]. Three independent MEF lines for each genotype were analyzed in both experiments.

SA-beta-galactosidase staining

Adherent MEFs were stained with a SA-beta-galactosidase activity kit according to manufacturer's protocol (Cell Signaling). Nuclei were stained with Hoechst to determine percentages of cells positive for SA-beta-galactosidase activity. The percentage of SA-beta-galactosidase-positive cells was the total number of cells positive for SA-beta-galactosidase activity divided by the total number of cells (n = 3 independent MEF lines for each genotype at each passage). Adipose tissue depositions were stained for SA-beta-galactosidase activity as described previously[13].

Western blot analysis

Western-blot analyses were carried out as described[48]. Antibodies for senescence-associated proteins were as described[13, 16]. Antibody for $p15^{Ink4b}$ was a gift from Dr. M. Barbacid[49].

Acknowledgements

We thank Drs. Paul Galardy, Rick Bram, Randy Faustino, Amy Tang, Robin Ricke and Jim Kirkland for critical reading of the manuscript or helpful discussions. We would like to thank Dr. Mariano Barbacid for the generous gift of $p15^{Ink4b}$ antibody. This work was supported by grants from the National Institutes of Health, the Ted Nash Foundation and the Ellison Medical Foundation to JvD.

References

1. Collado, M., Blasco, M.A. & Serrano, M. Cellular senescence in cancer and aging. *Cell* **130**, 223-233 (2007).
2. Campisi, J. & d'Adda di Fagagna, F. Cellular senescence: when bad things happen to good cells. *Nat Rev Mol Cell Biol* **8**, 729-740 (2007).
3. Sharpless, N.E. & DePinho, R.A. The INK4A/ARF locus and its two gene products. *Curr Opin Genet Dev* **9**, 22-30 (1999).
4. Sherr, C.J. & Weber, J.D. The ARF/p53 pathway. *Curr Opin Genet Dev* **10**, 94-99 (2000).
5. Vousden, K.H. & Lane, D.P. p53 in health and disease. *Nat Rev Mol Cell Biol* **8**, 275-283 (2007).
6. Kim, W.Y. & Sharpless, N.E. The regulation of INK4/ARF in cancer and aging. *Cell* **127**, 265-275 (2006).
7. Krishnamurthy, J. *et al.* Ink4a/Arf expression is a biomarker of aging. *J Clin Invest* **114**, 1299-1307 (2004).
8. Zindy, F., Quelle, D.E., Roussel, M.F. & Sherr, C.J. Expression of the p16INK4a tumor suppressor versus other INK4 family members during mouse development and aging. *Oncogene* **15**, 203-211 (1997).
9. Krishnamurthy, J. *et al.* p16INK4a induces an age-dependent decline in islet regenerative potential. *Nature* **443**, 453-457 (2006).
10. Janzen, V. *et al.* Stem-cell ageing modified by the cyclin-dependent kinase inhibitor p16INK4a. *Nature* **443**, 421-426 (2006).
11. Molofsky, A.V. *et al.* Increasing p16INK4a expression decreases forebrain progenitors and neurogenesis during ageing. *Nature* **443**, 448-452 (2006).
12. Beausejour, C.M. & Campisi, J. Ageing: balancing regeneration and cancer. *Nature* **443**, 404-405 (2006).
13. Baker, D.J. *et al.* BubR1 insufficiency causes early onset of aging-associated phenotypes and infertility in mice. *Nat Genet* **36**, 744-749 (2004).
14. Matsumoto, T. *et al.* Aging-Associated Vascular Phenotype in Mutant Mice With Low Levels of BubR1. *Stroke* (2007).
15. Hartman, T.K., Wengenack, T.M., Poduslo, J.F. & van Deursen, J.M. Mutant mice with small amounts of BubR1 display accelerated age-related gliosis. *Neurobiol Aging* **28**, 921-927 (2007).
16. Baker, D.J. *et al.* Early aging-associated phenotypes in Bub3/Rae1 haploinsufficient mice. *J Cell Biol* **172**, 529-540 (2006).
17. Rane, S.G. *et al.* Loss of Cdk4 expression causes insulin-deficient diabetes and Cdk4 activation results in beta-islet cell hyperplasia. *Nat Genet* **22**, 44-52 (1999).

18. Sharpless, N.E. & DePinho, R.A. How stem cells age and why this makes us grow old. *Nat Rev Mol Cell Biol* **8**, 703-713 (2007).
19. Price, S.R. & Mitch, W.E. Mechanisms stimulating protein degradation to cause muscle atrophy. *Curr Opin Clin Nutr Metab Care* **1**, 79-83 (1998).
20. Koh, T.J., Bryer, S.C., Pucci, A.M. & Sisson, T.H. Mice deficient in plasminogen activator inhibitor-1 have improved skeletal muscle regeneration. *Am J Physiol Cell Physiol* **289**, C217-223 (2005).
21. Fridlyand, J. *et al.* Breast tumor copy number aberration phenotypes and genomic instability. *BMC Cancer* **6**, 96 (2006).
22. Hengstschlager, M. *et al.* Loss of the p16/MTS1 tumor suppressor gene causes E2F-mediated deregulation of essential enzymes of the DNA precursor metabolism. *DNA Cell Biol* **15**, 41-51 (1996).
23. Dimri, G.P. *et al.* A biomarker that identifies senescent human cells in culture and in aging skin in vivo. *Proc Natl Acad Sci U S A* **92**, 9363-9367 (1995).
24. West, M.D., Pereira-Smith, O.M. & Smith, J.R. Replicative senescence of human skin fibroblasts correlates with a loss of regulation and overexpression of collagenase activity. *Exp Cell Res* **184**, 138-147 (1989).
25. Wang, S., Moerman, E.J., Jones, R.A., Thweatt, R. & Goldstein, S. Characterization of IGFBP-3, PAI-1 and SPARC mRNA expression in senescent fibroblasts. *Mech Ageing Dev* **92**, 121-132 (1996).
26. Shelton, D.N., Chang, E., Whittier, P.S., Choi, D. & Funk, W.D. Microarray analysis of replicative senescence. *Curr Biol* **9**, 939-945 (1999).
27. Linskens, M.H. *et al.* Cataloging altered gene expression in young and senescent cells using enhanced differential display. *Nucleic Acids Res* **23**, 3244-3251 (1995).
28. Matheu, A. *et al.* Delayed ageing through damage protection by the Arf/p53 pathway. *Nature* **448**, 375-379 (2007).
29. Serrano, M. & Blasco, M.A. Cancer and ageing: convergent and divergent mechanisms. *Nat Rev Mol Cell Biol* **8**, 715-722 (2007).
30. Varela, I. *et al.* Accelerated ageing in mice deficient in Zmpste24 protease is linked to p53 signalling activation. *Nature* **437**, 564-568 (2005).
31. Cao, L., Li, W., Kim, S., Brodie, S.G. & Deng, C.X. Senescence, aging, and malignant transformation mediated by p53 in mice lacking the Brca1 full-length isoform. *Genes & development* **17**, 201-213 (2003).
32. Kondratov, R.V., Kondratova, A.A., Gorbacheva, V.Y., Vykhovanets, O.V. & Antoch, M.P. Early aging and age-related pathologies in mice deficient in BMAL1, the core componentof the circadian clock. *Genes Dev* **20**, 1868-1873 (2006).
33. Sharpless, N.E. *et al.* Loss of p16Ink4a with retention of p19Arf predisposes mice to tumorigenesis. *Nature* **413**, 86-91. (2001).

34. Sharpless, N.E., Ramsey, M.R., Balasubramanian, P., Castrillon, D.H. & DePinho, R.A. The differential impact of p16(INK4a) or p19(ARF) deficiency on cell growth and tumorigenesis. *Oncogene* **23**, 379-385 (2004).
35. Engel, W.K. & Cunningham, G.G. Rapid Examination of Muscle Tissue. an Improved Trichrome Method for Fresh-Frozen Biopsy Sections. *Neurology* **13**, 919-923 (1963).
36. Kane, G.C. *et al.* ATP-sensitive K+ channel knockout compromises the metabolic benefit of exercise training, resulting in cardiac deficits. *Diabetes* **53 Suppl 3**, S169-175 (2004).
37. Baur, J.A. *et al.* Resveratrol improves health and survival of mice on a high-calorie diet. *Nature* **444**, 337-342 (2006).
38. Krimpenfort, P. *et al.* p15Ink4b is a critical tumour suppressor in the absence of p16Ink4a. *Nature* **448**, 943-946 (2007).
39. Edwards, M.G. *et al.* Gene expression profiling of aging reveals activation of a p53-mediated transcriptional program. *BMC Genomics* **8**, 80 (2007).
40. Yuan, B. *et al.* Increased expression of mitotic checkpoint genes in breast cancer cells with chromosomal instability. *Clin Cancer Res* **12**, 405-410 (2006).
41. Maes, C. *et al.* Soluble VEGF isoforms are essential for establishing epiphyseal vascularization and regulating chondrocyte development and survival. *J Clin Invest* **113**, 188-199 (2004).
42. Asahi, M. *et al.* Protective effects of statins involving both eNOS and tPA in focal cerebral ischemia. *J Cereb Blood Flow Metab* **25**, 722-729 (2005).
43. Ohlson, N., Bergh, A., Persson, M.L. & Wikstrom, P. Castration rapidly decreases local insulin-like growth factor-1 levels and inhibits its effects in the ventral prostate in mice. *Prostate* **66**, 1687-1697 (2006).
44. Jeong, Y.J. *et al.* Optimization of real time RT-PCR methods for the analysis of gene expression in mouse eggs and preimplantation embryos. *Mol Reprod Dev* **71**, 284-289 (2005).
45. Beauchamp, J.R., Morgan, J.E., Pagel, C.N. & Partridge, T.A. Dynamics of myoblast transplantation reveal a discrete minority of precursors with stem cell-like properties as the myogenic source. *J Cell Biol* **144**, 1113-1122 (1999).
46. Yamada, S. *et al.* Protection conferred by myocardial ATP-sensitive K+ channels in pressure overload-induced congestive heart failure revealed in KCNJ11 Kir6.2-null mutant. *J Physiol* **577**, 1053-1065 (2006).
47. Babu, J.R. *et al.* Rae1 is an essential mitotic checkpoint regulator that cooperates with Bub3 to prevent chromosome missegregation. *J Cell Biol* **160**, 341-353 (2003).

48. Kasper, L.H. *et al.* CREB binding protein interacts with nucleoporin-specific FG repeats that activate transcription and mediate NUP98-HOXA9 oncogenicity. *Mol Cell Biol* **19**, 764-776 (1999).
49. Latres, E. *et al.* Limited overlapping roles of P15(INK4b) and P18(INK4c) cell cycle inhibitors in proliferation and tumorigenesis. *Embo J* **19**, 3496-3506 (2000).

Supplementary Discussion

The only discernible adverse effect of $p16^{Ink4a}$ inactivation in BubR1 hypomorphic mice was an acceleration of lung tumorigenesis. The simplest explanation for this effect would be that $p16^{Ink4a}$ is induced in BubR1 hypomorphic lung tissue as part of a tumor-suppressive mechanism triggering senescence of cells that are at risk for neoplastic transformation. We extensively screened BubR1 hypomorphic lungs for the presence of premalignant lesions, but none were found (data not shown). This precluded us from testing whether $p16^{Ink4a}$ levels are indeed elevated in such lesions. Alternatively, as aneuploidy has been shown to promote tumorigenesis in certain mouse tissues[1], it is conceivable that the numerical chromosome instability resulting from BubR1 insufficiency cooperates with $p16^{Ink4a}$ loss in lung tumorigenesis. Our data demonstrating that $p16^{Ink4a}$ inactivation accelerates lung tumorigenesis in BubR1 hypomorphic mice provides a first example of synergy between a mitotic checkpoint gene defect and a cancer gene mutation. Our observation that BubR1 insufficiency does not cooperate with $p19^{Arf}$ loss in tumorigenesis, suggests that the genetic context or microenvironment in which mitotic checkpoint gene defects promote tumorigenesis is limited.

Reference

1. Weaver, B.A., Silk, A.D., Montagna, C., Verdier-Pinard, P. & Cleveland, D.W. Aneuploidy acts both oncogenically and as a tumor suppressor. *Cancer cell* **11**, 25-36 (2007).

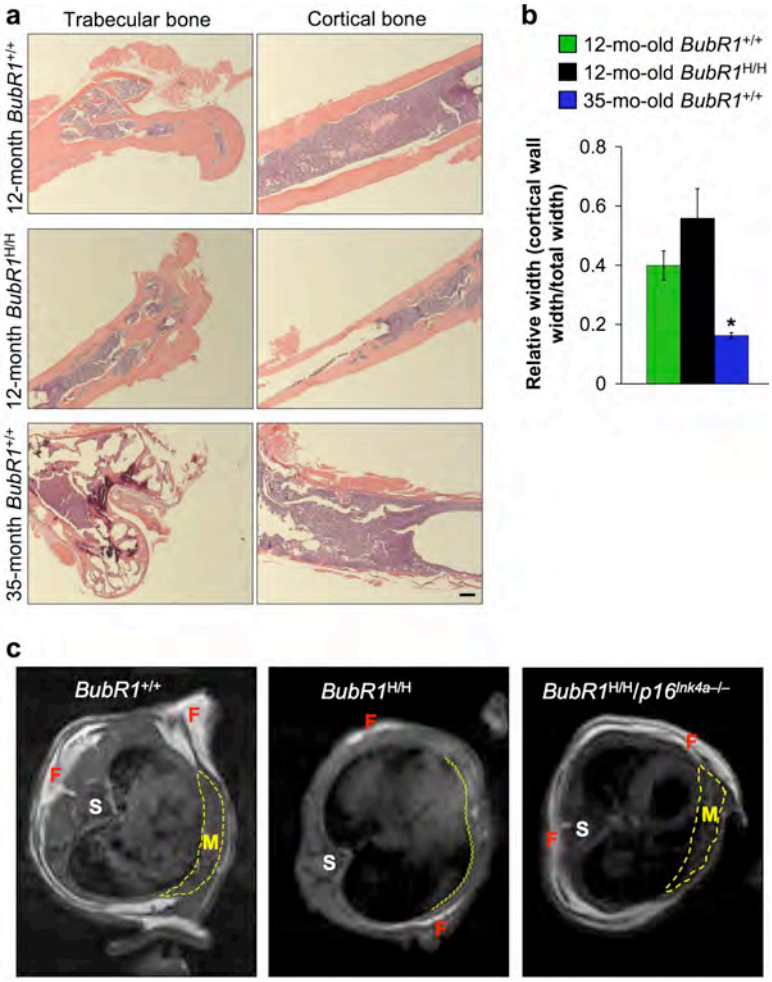

Figure S1 Screening of *BubR1*$^{+/+}$ and *BubR1*$^{H/H}$ mice for osteoporosis and analysis of *BubR1*$^{+/+}$, *BubR1*$^{H/H}$ and *BubR1*$^{H/H}$/*p16*$^{Ink4a-/-}$ mice for abdominal muscle volume and fat disposition. (**a**) Haematoxylin and eosin-stained longitudinal sections of femurs from a 1-year-old wild-type, a 1-year-old BubR1 hypomorphic and a 35-month-old wild-type mouse. Scale bar = 100 µm. (**b**) Quantitation of relative width of the cortical wall to total bone width in sections from a. For each genotype, three male mice were used and 40 random measurements were taken. Note the clear reduction in bone mass and density in the old wild-type animal, while there is no difference between the 1-year-old samples. Asterisks indicates p value of < 0.0001 compared to 12-month-old wild-type using a two-tailed Mann-Whitney test. Error bars are s.d. (**c**) Analysis of abdominal muscle and fat tissue of 5-month-old wild-type, *BubR1*$^{H/H}$, and *BubR1*$^{H/H}$/*p16*$^{Ink4a-/-}$ mice by MRI. Representative cross-sectional MRI images are shown. Areas of muscle (M), fat (F), and the spinal cord (S) are indicated. Note the substantial increase in fat and muscle in *BubR1*$^{H/H}$/*p16*$^{Ink4a-/-}$ mice.

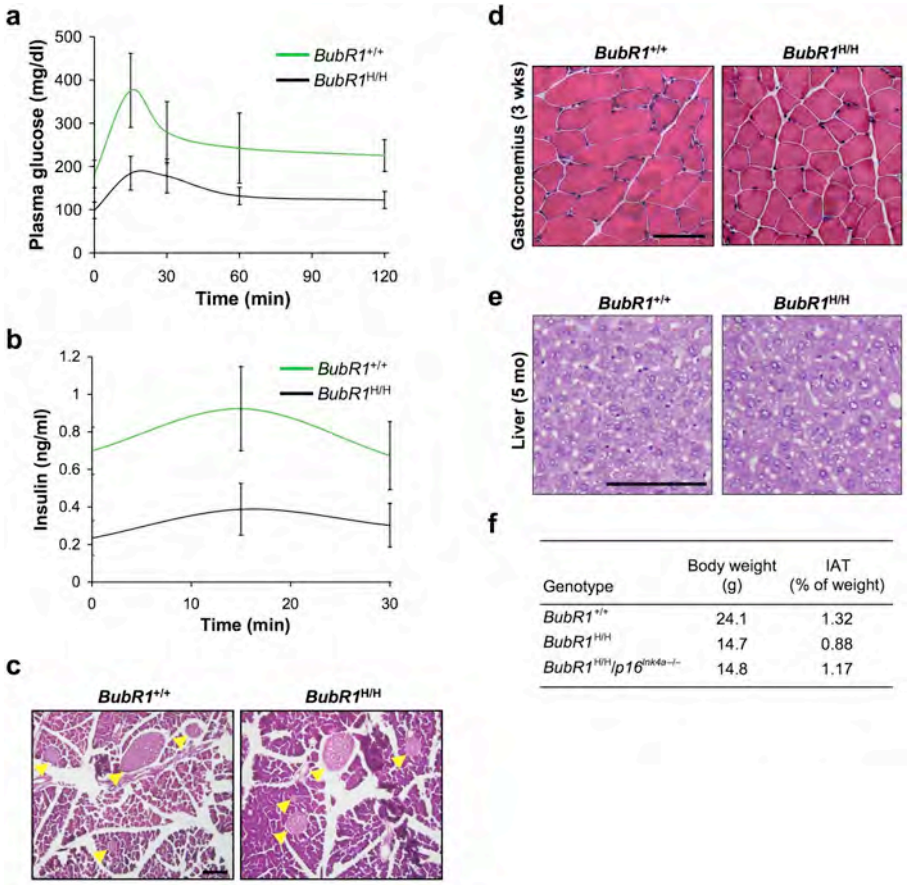

Figure S2 Analysis of pancreatic beta-cell function, young skeletal muscle histology, and fat deposition of BubR1 hypomorphic mice (**a**-**c**) BubR1 hypomorphic mice have normal pancreatic beta-cell function. Changes in blood glucose (**a**) and insulin (**b**) levels after oral glucose administration to 5-month-old *BubR1*$^{+/+}$ and *BubR1*$^{H/H}$ mice (n = 5 males for each genotype). Error bars are s.d. (**c**) Hematoxylin and eosin stained pancreas sections of 1-year-old *BubR1*$^{+/+}$ and *BubR1*$^{H/H}$ mice. Arrowheads mark beta-cell islets. Scale bar = 100 µm. (**d**) Muscles of 3-week-old *BubR1*$^{H/H}$ appear normal. Cross-sections of gastrocnemius muscles from 3-week-old wild-type and *BubR1*$^{H/H}$ mice stained with hematoxylin and eosin. Scale bar = 100 µm. (**e**) BubR1 hypomorphic mice do not have fatty livers. Hematoxylin and eosin stained liver sections of 5-month-old *BubR1*$^{+/+}$ and *BubR1*$^{H/H}$ mice. Scale bar = 100 µm. (**f**) Quantitation of inguinal adipose tissue in 6-week-old *BubR1*$^{+/+}$, *BubR1*$^{H/H}$ and *BubR1*$^{H/H}$/*p16*$^{Ink4a-/-}$ mice. IAT is expressed as percentage of total body weight. Three males of each genotype were used. Note that *BubR1*$^{H/H}$ mice lacking p16^{Ink4a} have improved fat disposition.

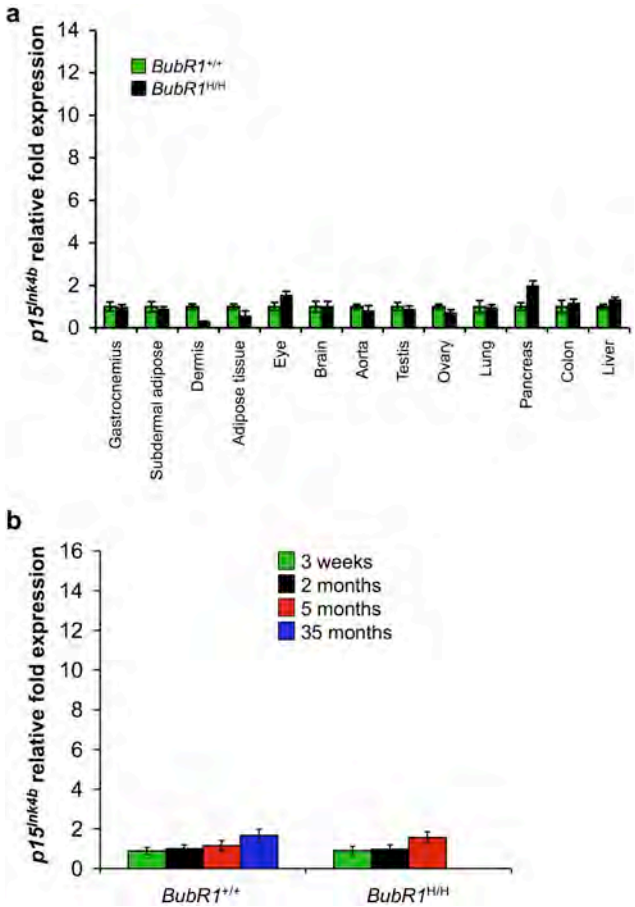

Figure S3 *p15*^{Ink4b} is not induced in response to BubR1 hypomorphism. (**a**) Relative expression of *p15*^{Ink4b} in different tissues of 2-month-old *BubR1*$^{H/H}$ and *BubR1*$^{+/+}$ mice as determined by qRT-PCR (n = 3 males for each genotype). All values were normalized to *GAPDH*. Relative expression is to wild-type samples. Error bars are s.d. (**b**) Relative expression of *p15*^{Ink4b} in gastrocnemius muscles of wild-type and *BubR1*$^{H/H}$ males at various ages as measured by qRT-PCR (n = three muscles per genotype and age group). Values were normalized to *GAPDH*. Relative fold expression is to 2-month-old wild-type values. Error bars are s.d.

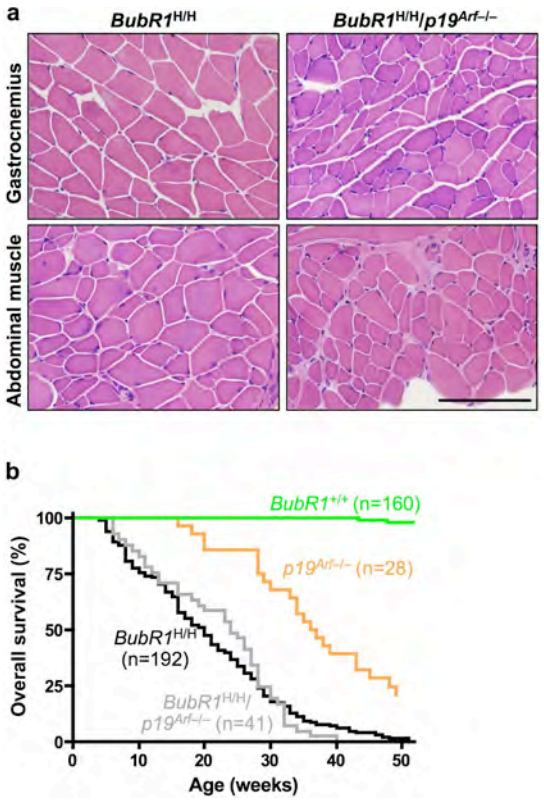

Figure S4 Ablation of p19^{Arf} in BubR1 hypomorphic mice increases muscle wasting but has no impact on lifespan. (**a**) Cross sections of gastrocnemius and abdominal muscles from 6-week-old *BubR1*$^{H/H}$ and *BubR1*$^{H/H}$/*p19*$^{Arf-/-}$ mice. Sections were stained with hematoxylin and eosin. Note that fibers diameters are typically smaller when p19^{Arf} is lacking. Scale bar = 100 µm. (**b**) Overall survival curves for wild-type, *p19*$^{Arf-/-}$, *BubR1*$^{H/H}$, and *BubR1*$^{H/H}$/*p19*$^{Arf-/-}$ mice. We note that *BubR1*$^{H/H}$ and *BubR1*$^{H/H}$/*p19*$^{Arf-/-}$ curves are not statistically different using a log-rank test.

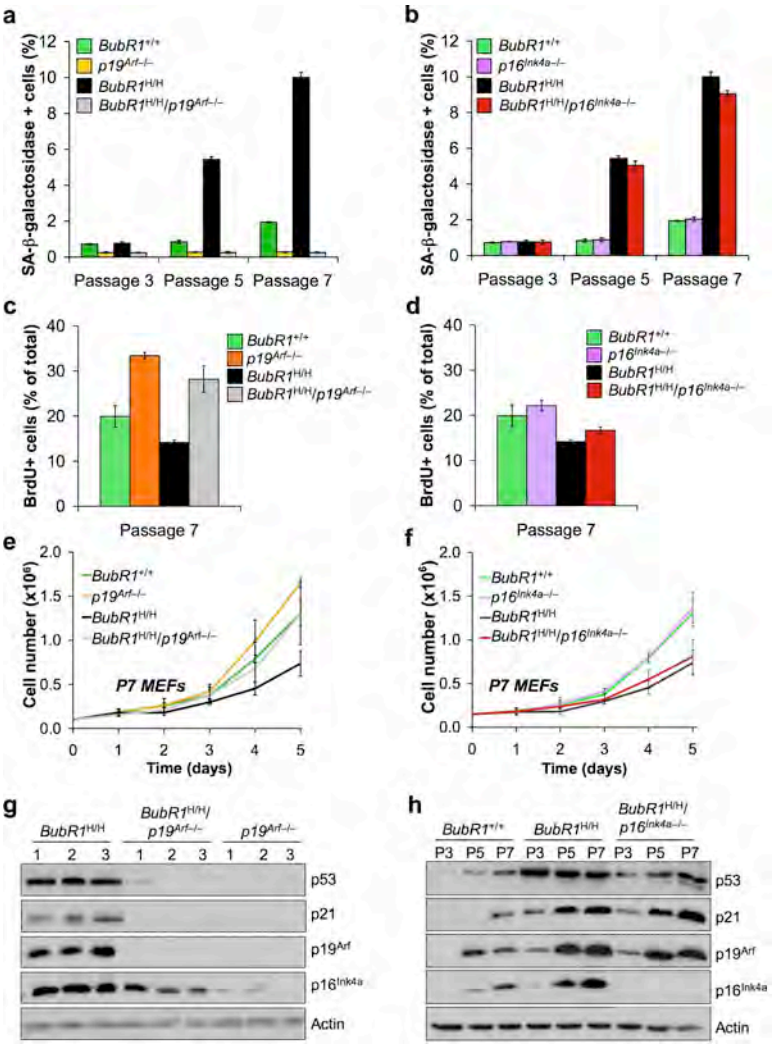

Figure S5 *In vivo* and *in vitro* effects of $p16^{Ink4a}$ and 19^{Arf} ablation on cellular senescence are dissimilar. (**a** and **b**) Percentages of SA-beta-galactosidase positive cells in P3, P5 and P7 MEF cultures of the indicated genotypes. For each genotype and passage, three independent MEF lines were scored for SA-beta-galactosidase staining. Error bars are s.d. (**c** and **d**) Percentages of cycling cells in P7 MEF cultures of the indicated genotypes as measured by BrdU incorporation. Three independent MEF lines were used for each genotype. Error bars are s.d. (**e** and **f**) *In vitro* growth curves of P7 MEF cultures of the indicated genotypes. On day 0, 1.5 x 10^5 cells were seeded in duplicate and counted for five consecutive days thereafter in three independent lines of each genotype. Compared to wild-type MEFs, the proliferative capacity of both $BubR1^{H/H}$ and $BubR1^{H/H}/p16^{Ink4a-/-}$ MEFs was greatly reduced but that of $BubR1^{H/H}/p19^{Arf-/-}$ was not. Lines represent three independent MEF lines per genotype. Error bars are s.d. (**g**) Western blots of extracts from P7 MEFs of the indicated genotypes probed for $p16^{Ink4a}$, $p19^{Arf}$, p53 and p21. Extracts from three independent MEF lines (1-3) were loaded for each genotype. (**h**) Western blots of extracts from P3, P5, and P7 MEFs of the indicated genotypes were probed for $p16^{Ink4a}$, $p19^{Arf}$, p53 and p21. Blots are representative of three independent MEF lines of each genotype. Actin was used as a loading control.

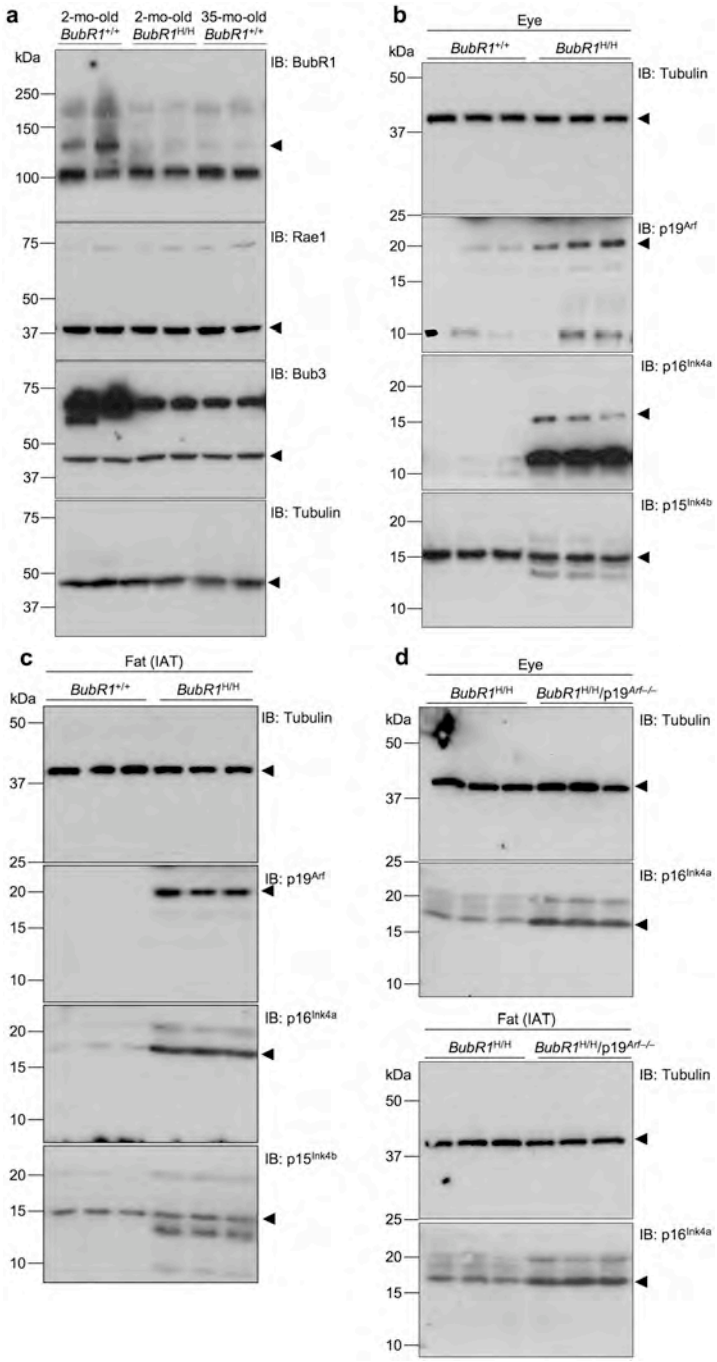

Figure S6 Uncropped images of the western blots shown in: (**a**) Fig. 2a, (**b** and **c**) Fig. 3d and Fig. 5c, (**d**) Fig. 6f. Blots were cut horizontally into two portions prior to antibody incubations. Arrowheads indicate specific bands shown in cropped images.

Table S1

Analysis of progeroid phenotypes in *BubR1*$^{H/H}$ mice lacking p16^{Ink4a} or p19^{Arf}

Aging Characteristic	Effect in *BubR1*$^{H/H}$/*p16*$^{Ink4a-/-}$ mice compared with *BubR1*$^{H/H}$ mice [p value]	Effect in *BubR1*$^{H/H}$/*p19*$^{Arf-/-}$ mice compared with *BubR1*$^{H/H}$ mice [p value]
Survival	Improved (+) [p = 0.0142]	Unchanged
Lordokyphosis	Improved (+++) [p < 0.0001]	Worsened (++) [p < 0.0001]
Abdominal wall integrity	Improved (+++)	Worsened (++)
Respiratory function	Improved (++) [p < 0.05]	N.D.
Cataract formation	Improved (+) [p < 0.0001]	Worsened (+) [p < 0.0001]
Subdermal adipose	Improved (++) [p = 0.0037]	Worsened (++) [p < 0.0001]
Adipose deposition	Increased (++) [p = 0.003]	Reduced (++) [p = 0.0008]
Anaesthesia tolerance	Improved (+++)	Worsened (+)
Dermal thickness	Unchanged	Unchanged
Dwarfism	Unchanged	Unchanged
Infertility	Unchanged	Unchanged
Arterial wall stiffening	Unchanged	Unchanged

Chapter 6

Early aging-associated phenotypes in Bub3/Rae1 haplo-insufficient mice

Journal of Cell Biology 172, 529-540
Reprinted with permission

Early aging–associated phenotypes in Bub3/Rae1 haploinsufficient mice

Darren J. Baker,[1,2] Karthik B. Jeganathan,[1,2] Liviu Malureanu,[1,2] Carmen Perez-Terzic,[3,4] Andre Terzic,[3,4] and Jan M.A. van Deursen[1,2]

[1]Department of Pediatric and Adolescent Medicine, [2]Department of Biochemistry and Molecular Biology, [3]Department of Medicine, and [4]Department of Molecular Pharmacology and Experimental Therapeutics, Mayo Clinic, Rochester, MN 55905

Aging is a highly complex biological process that is believed to involve multiple mechanisms. Mice that have small amounts of the mitotic checkpoint protein BubR1 age much faster than normal mice, but whether other mitotic checkpoint genes function to prevent the early onset of aging is unknown. In this study, we show that several aging-associated phenotypes appear early in mice that are double haploinsufficient for the mitotic checkpoint genes Bub3 and Rae1 but not in mice that are single haploinsufficient for these genes. Mouse embryonic fibroblasts (MEFs) from Bub3/Rae1 haploinsufficient mice undergo premature senescence and accumulate high levels of p19, p53, p21, and p16, whereas MEFs from single haploinsufficient mice do not. Furthermore, although BubR1 hypomorphic mice have less aneuploidy than Bub3/Rae1 haploinsufficient mice, they age much faster. Our findings suggest that early onset of aging-associated phenotypes in mice with mitotic checkpoint gene defects is linked to cellular senescence and activation of the p53 and p16 pathways rather than to aneuploidy.

Introduction

Maintenance of genetic stability requires faithful segregation of duplicated chromosomes during mitosis. Most human cancers consist of cells that have an abnormal chromosome content, which is also known as aneuploidy. However, how the aneuploidy develops remains poorly understood (Jallepalli and Lengauer, 2001; Draviam et al., 2004; Weaver and Cleveland, 2005). The spindle assembly checkpoint, commonly referred to as the mitotic checkpoint, is a surveillance mechanism that ensures accurate segregation of mitotic chromosomes by delaying metaphase-to-anaphase progression until each kinetochore has properly attached to the mitotic spindle (Kops et al., 2005). Kinetochores that are not yet attached to mitotic microtubules and chromosome pairs that lack tension across sister chromatids generated by the spindle poles activate the spindle assembly checkpoint (Yu, 2002; Rieder and Maiato, 2004). Various mitotic checkpoint proteins, including Bub3, Bub1, BubR1, Mad1, and Mad2, bind to kinetochores that lack attachment or tension and generate a "stop anaphase" signal that diffuses into the mitotic cytosol (Shah and Cleveland, 2000). This signal is believed to consist of Bub3, BubR1, and Mad2 protein complexes (Fang et al., 1998; Sudakin et al., 2001; Tang et al., 2001). These complexes bind to Cdc20 to prevent premature ubiquitination of cyclin B and securin by the anaphase-promoting complex (APC; Peters, 2002; Nasmyth and Haering, 2005). Checkpoint inactivation occurs after proper alignment of the mitotic chromosomes at the metaphase plate. This triggers release of Bub3, BubR1, and Mad2 protein complexes from Cdc20 and subsequent destruction of cyclin B and securin by the APC. Separase, which in mammalian cells is inhibited through association with securin and also by cyclin B/Cdk1-mediated phosphorylation, triggers sister chromatid disjunction by cleavage of the cohesin subunit Scc1 (Nasmyth and Haering, 2005). Various studies have addressed the physiological relevance of the spindle assembly checkpoint by deleting Mad or Bub genes in the mouse (for review see Baker et al., 2005). Mice that are homozygous null for Mad2, Bub3, or BubR1 die during the early stages of embryogenesis (Dobles et al., 2000; Kalitsis et al., 2000; Babu et al., 2003; Baker et al., 2004; Wang et al., 2004), with a small subset of Mad2-null embryos remaining viable until embryonic day 10.5 (Burds et al., 2005). On the other hand, mice that are heterozygous null for these genes are born alive and seem to exhibit no overt phenotypes. Thus, the challenge for studying the function of individual mitotic checkpoint genes in the mouse is to disrupt their function significantly but not so severely that the embryo dies.

Correspondence to Jan M.A. van Deursen: vandeursen.jan@mayo.edu

Abbreviations used in this paper: APC, anaphase-promoting complex; DMBA, dimethylbenzanthrene; MEF, mouse embryonic fibroblast; MVA, mosaic variegated aneuploidy; NEBD, nuclear envelope breakdown; PI, propidium iodide; PMSCS, premature sister chromatid separation; SA, senescence associated.

The online version of this article contains supplemental material.

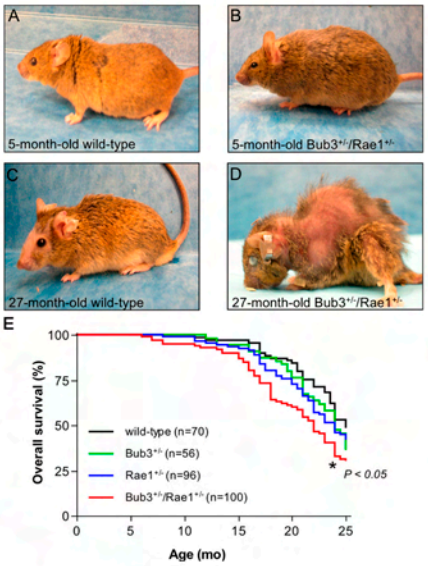

Figure 1. **Combined Bub3 and Rae1 haploinsufficiency reduces lifespan.** (A–D) Representative photographs of wild-type and Bub3$^{+/-}$/Rae1$^{+/-}$ mice at 5 (A and B) and 27 mo (C and D). These animals were not moribund at the time of the picture. Note the overt cataract, severe lordokyphosis, and cachetic appearance of the 27-mo-old Bub3$^{+/-}$/Rae1$^{+/-}$ mouse pictured in D. (E) Overall survival curves for wild-type, Bub3$^{+/-}$, Rae1$^{+/-}$, and Bub3$^{+/-}$/Rae1$^{+/-}$ mice. The curve marked with an asterisk is significantly different from that of wild-type mice using a log-rank test. We note that the lifespan of Bub3$^{+/-}$ and Rae1$^{+/-}$ mice is not statistically different from that of Bub3$^{+/-}$/Rae1$^{+/-}$ mice.

A

Genotype	wild-type	Bub3$^{+/-}$	Rae1$^{+/-}$	Bub3$^{+/-}$/Rae1$^{+/-}$
Mice in study	70	56	96	100
Mice with tumors	20	19	28	24
Tumor incidence	29%	34%	29%	24%
Tumor latency	782 days	768 days	779 days	653 days
Tumor type				
Lymphoma	2	1	1	1
Lung adenocarcinoma	12	8	11	14
Hepatocellular carcinoma	11	12	15	8
Sarcoma	1	3	5	3
Other[1]				4
Mice with multiple tumors	6	4	3	6

Other[1] - 3 ovarian carcinoma, 1 pancreatic adenocarcinoma

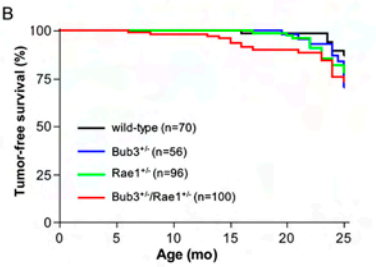

Figure 2. **Bub3$^{+/-}$/Rae1$^{+/-}$ mice develop spontaneous tumors at normal rates despite severe aneuploidy.** (A) Spontaneous tumor incidence, latency, and spectrum of wild-type and Bub3$^{+/-}$/Rae1$^{+/-}$ mice. Upon biopsy of moribund animals, all tissues were screened for tumors. Tumorous tissues were collected and processed for histological evaluation. (B) Tumor-free survival curves of wild-type, Bub3$^{+/-}$, Rae1$^{+/-}$, and Bub3$^{+/-}$/Rae1$^{+/-}$ mice.

Recently, we have reported the generation of a series of mice in which the expression of BubR1 is reduced in a graded fashion from normal levels to zero by the use of wild-type, knockout, and hypomorphic alleles (Baker et al., 2004). Of this series, mice with BubR1 levels as low as 10% of normal (BubR1$^{H/H}$ mice) are born alive and develop into adult mice. Remarkably, despite having severe aneuploidy, these animals do not have an escalated spontaneous tumor burden (Baker et al., 2004). Instead, these mice develop a variety of progeroid (resembling old age) features. In addition, mouse embryonic fibroblasts (MEFs) from BubR1$^{H/H}$ mice show profound premature cellular senescence. These observations, combined with the demonstration that BubR1 levels decline in ovary, testis, and spleen tissue as wild-type mice age, have suggested that this mitotic checkpoint protein is a key regulator of the normal aging process. However, whether aging is a general feature of spindle assembly checkpoint dysfunction remains unknown.

The mitotic checkpoint protein Bub3 is a seven-blade β propeller that has substantial sequence similarity with the mRNA export factor protein Rae1; the two proteins have 34% identity and 52% similarity in humans (Larsen and Harrison, 2004). Like Bub3 (Kalitsis et al., 2000), Rae1 is essential for early mouse embryogenesis, but mice that are haploinsufficient for Bub3 or Rae1 are viable and have a normal appearance (Babu et al., 2003). These heterozygous mice show remarkably similar mitotic defects, including spindle assembly checkpoint impairment and chromosome missegregation (Babu et al., 2003). Mice that are haploinsufficient for both Bub3 and Rae1 are also viable but develop much more severe mitotic phenotypes than single haploinsufficient mice. In this study, we have investigated the long-term phenotypes of mice in which the mitotic checkpoint proteins Bub3 and Rae1 are disrupted individually or in combination. We find that phenotypes associated with aging appear early in double haploinsufficient mice but not in single haploinsufficient mice. We also find that single and double haploinsufficient mice are not predisposed to spontaneous tumor development despite the accumulation of substantial numbers of aneuploid cells.

Results

Combined Bub3 and Rae1 haploinsufficiency reduces lifespan

To examine the long-term biological consequences of impaired spindle assembly checkpoint function, we generated cohorts of mice in which the mitotic checkpoint genes Bub3 and Rae1 were haploinsufficient individually or in combination (Babu et al., 2003). We monitored 70 wild-type, 56 Bub3$^{+/-}$, 96 Rae1$^{+/-}$, and 100 Bub3$^{+/-}$/Rae1$^{+/-}$ mice daily for spontaneous tumor development or ill health for a period of >2 yr. During the first

Table I. **Mice that are single or double haploinsufficient for Bub3 and Rae1 develop progressive aneuploidy**

Mouse genotype	Age (*n*)	Mitotic figures inspected	Percent aneuploid figures (SD)	Karyotypes with indicated chromosome number											Percent mitotic figures with PMSCS (SD)	Percent mitotic figures with breaks	Percent mitotic figures with fusions
				37	38	39	40	41	42	43	44	45	46	47			
Wild type	5 mo (3)	150	0 (0)				150								0 (0)	ND	ND
	22 mo (3)	150	0 (0)				150								0 (0)	ND	ND
	27 mo (3)	150	0 (0)				150								0 (0)	0	0
	35 mo (3)	150	3 (1)			1	145	3	1						4 (1)	ND	ND
Bub3$^{+/-}$	5 mo (3)	150	9 (1)		2	3	136	7	2						0 (0)	ND	ND
	27 mo (3)	150	29 (3)	2	3	5	106	20	9	5					11 (2)	0	0
Rae1$^{+/-}$	5 mo (3)	150	9 (1)		3	2	136	6	3						0 (0)	ND	ND
	24 mo (3)	150	33 (5)	1	5	10	101	19	9	2	3				10 (2)	0	0
Bub3$^{+/-}$/Rae1$^{+/-}$	5 mo (4)	200	36 (2)	6	9	9	128	8	16	10	6	5		3	14 (1)	ND	ND
	12 mo (3)	150	39 (3)	4	5	8	92	9	11	11	6	1	1	2	18 (2)	ND	ND
	18 mo (3)	150	45 (2)	5	9	6	83	11	8	17	3	4	2	2	22 (2)	ND	ND
	24 mo (3)	150	47 (1)	8	6	8	80	12	16	7	8	2	1	2	24 (5)	0	0
BubR1$^{H/H}$	5 mo (4)	200	15 (4)		2	12	170	16							35 (4)	ND	ND
	12 mo (5)	250	33 (4)		9	22	168	44	7						24 (4)	ND	ND

Empty spaces mean that there were no karyotypes with the indicated chromosome number.

year of life, Bub3$^{+/-}$/Rae1$^{+/-}$, Bub3$^{+/-}$, and Rae1$^{+/-}$ mice were indistinguishable from wild-type mice and exhibited no overt abnormalities (Fig. 1, A and B; and not depicted). However, in the second year, a substantial proportion of Bub3$^{+/-}$/Rae1$^{+/-}$ mice began to develop an aged appearance (Fig. 1 D). Wild-type mice did not show this appearance (Fig. 1 C), nor did Bub3$^{+/-}$ or Rae1$^{+/-}$ mice. The median overall survival of Bub3$^{+/-}$ and Rae1$^{+/-}$ mice was slightly reduced in comparison with wild-type animals (24 vs. 25 mo, respectively), but these differences were not significant (Fig. 1 E). In contrast, the median survival of Bub3$^{+/-}$/Rae1$^{+/-}$ mice was significantly reduced to 22 mo, which translates into a 12% decrease in lifespan. We note that the reduced lifespan of Bub3$^{+/-}$/Rae1$^{+/-}$ mice may be the result of the sum of the lifespan reductions in Bub3$^{+/-}$ and Rae1$^{+/-}$ mice.

Spontaneous tumorigenesis is not accelerated in Bub3$^{+/-}$/Rae1$^{+/-}$ mice despite high aneuploidy

We performed biopsies on moribund mice from our cohorts to investigate whether chromosome number instability predisposes mice to spontaneous tumorigenesis. The tumor incidences of Bub3$^{+/-}$, Rae1$^{+/-}$, and Bub3$^{+/-}$/Rae1$^{+/-}$ mice were not significantly different from wild-type mice (Fig. 2 A). In addition, the tumor spectra exhibited in these groups were nearly identical. Comparison of the tumor-free survival curves of the various genotypes revealed a slight decrease in tumor latency in Bub3$^{+/-}$/Rae1$^{+/-}$ mice compared with wild-type mice; however, this decrease is not significant (Fig. 2 B). The observed slight reduction in tumor latency most likely relates to the lifespan reduction of ~3 mo in the Bub3$^{+/-}$/Rae1$^{+/-}$ group. This difference is mirrored by the reduction in tumor latency by ~4 mo. Thus, mice in which the mitotic checkpoint genes Bub3 and Rae1 are disrupted individually or in combination are not predisposed to spontaneous tumorigenesis.

Aneuploidy progresses with age in mice with various mitotic checkpoint gene defects

Chromosome counts on splenocytes from 5-mo-old mice have shown that Bub3 and Rae1 single heterozygotes have significant numbers of aneuploid cells and that combined heterozygosity dramatically increases these numbers (Table I; Babu et al., 2003). We sought to determine whether aneuploidy progressed with age in Bub3$^{+/-}$, Rae1$^{+/-}$, and Bub3$^{+/-}$/Rae1$^{+/-}$ mice. Indeed, aneuploidy in single haploinsufficient Bub3 and Rae1 mice increased dramatically over time. Specifically, the aneuploidy in Bub3$^{+/-}$ splenocytes increased from 9% at 5 mo to 29% at 27 mo, whereas in Rae1$^{+/-}$ splenocytes, it increased from 9% at 5 mo to 33% at 24 mo (Table I). In splenocytes of Bub3$^{+/-}$/Rae1$^{+/-}$ mice, aneuploidy was already 37% at 5 mo of age but further increased by 10% over the next 19 mo. Wild-type mice had no aneuploidy at 27 mo, but 3% aneuploidy was detected at 35 mo. Aside from aneuploidy, another feature of defective or weakened spindle assembly checkpoint activity in mice is premature sister chromatid separation (PMSCS; Michel et al., 2001; Baker et al., 2004). Mitotic figures from Bub3 and Rae1 single heterozygotes showed no PMSCS at 5 mo, but 10–11% of metaphases examined at 24–27 mo displayed this feature. As Bub3$^{+/-}$/Rae1$^{+/-}$ mice aged, the percentage of cells exhibiting PMSCS also increased (Table I), going from 14% at 5 mo to 24% at 24 mo. The increases in PMSCS in Bub3$^{+/-}$, Rae1$^{+/-}$, and Bub3$^{+/-}$/Rae1$^{+/-}$ mice suggest that the activity of the spindle assembly checkpoint further declines as these animals age. Splenocytes from wild-type mice displayed no PMSCS at 27 mo, but 4% of splenocytes had PMSCS at 35 mo, suggesting that checkpoint activity declines as normal mice reach an extremely old age. We observed no chromosome breaks or fusions in metaphase spreads from 27-mo-old wild-type and 24-mo-old Bub3$^{+/-}$, Rae1$^{+/-}$, and Bub3$^{+/-}$/Rae1$^{+/-}$ mice (Table I). Thus, aneuploidy and PMSCS progress as mice in which Bub3

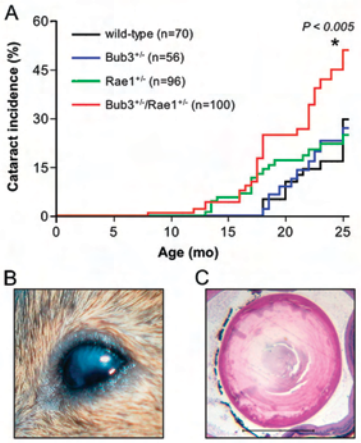

Figure 3. **Combined Bub3 and Rae1 haploinsufficiency accelerates cataract formation.** (A) Cataract incidence of wild-type, Bub3$^{+/-}$, Rae1$^{+/-}$, and Bub3$^{+/-}$/Rae1$^{+/-}$ mice as detected by the use of slit light after dilating the eyes. The asterisk indicates that the curve is statistically different from that of wild-type mice using a log-rank test. (B) Overt cataract detected in a 15-mo-old Bub3$^{+/-}$/Rae1$^{+/-}$ mouse. (C) Cross section of a cataractous lens from a 15-mo-old Bub3$^{+/-}$/Rae1$^{+/-}$ mouse stained with hematoxylin and eosin. Note that the posterior portion of the eye has Morgagnian globules, whereas the inner portion has profound calcification. Bar, 1 mm.

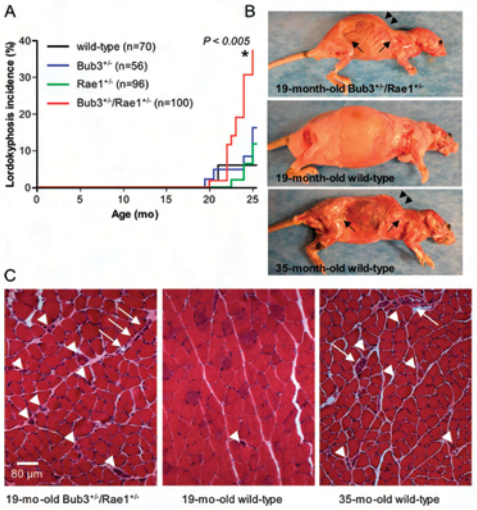

Figure 4. **Lordokyphosis develops early in mice with combined Bub3 and Rae1 haploinsufficiency.** (A) Incidence of lordokyphosis in wild-type, Bub3$^{+/-}$, Rae1$^{+/-}$, and Bub3$^{+/-}$/Rae1$^{+/-}$ mice. The asterisk indicates that the curve is statistically different from that of wild-type mice using a log-rank test. (B) Skinned 19-mo-old Bub3$^{+/-}$/Rae1$^{+/-}$, 19-mo-old wild-type, and 35-mo-old wild-type mice. The Bub3$^{+/-}$/Rae1$^{+/-}$ mouse and the 35-mo-old wild-type mouse exhibit lordokyphosis (arrowheads) and have little subcutaneous fat (arrows). (C) Cross section of gastrocnemius muscles of the animals shown in B. Arrowheads mark degenerated fibers, and arrows mark areas of fibroblast infiltration.

and Rae1 are disrupted individually or in combination age. Furthermore, mild aneuploidy and PMSCS are features of very old wild-type mice.

Bub3$^{+/-}$/Rae1$^{+/-}$ mice display early aging-associated phenotypes

The finding that several Bub3$^{+/-}$/Rae1$^{+/-}$ mice displayed an aged appearance at a relatively young age prompted us to screen for aging-associated phenotypes in a systematic fashion. All mice of our cohort were screened every 2 wk for the development of cataracts and lordokyphosis (abnormal convexity in the curvature of the spine when viewed from the side). This monitoring strategy revealed that the incidence of cataract formation was significantly higher in Bub3$^{+/-}$/Rae1$^{+/-}$ mice than in Bub3$^{+/-}$, Rae1$^{+/-}$, and wild-type mice (Fig. 3 A). Furthermore, the latency of cataract formation was shorter in Bub3$^{+/-}$/Rae1$^{+/-}$ mice than in mice of the other genotypes. Histological examination confirmed that cataractous eyes from Bub3$^{+/-}$/Rae1$^{+/-}$ mice had features reminiscent of human age–related cataracts (Fig. 3, B and C). Bub3$^{+/-}$/Rae1$^{+/-}$ mice developed lordokyphosis at an earlier age and with greater severity than Bub3$^{+/-}$, Rae1$^{+/-}$, and wild-type mice (Fig. 4, A and B). Mutant mice with early lordokyphosis, but not age-matched control animals, showed clear signs of skeletal muscle atrophy and degeneration (Fig. 4 C).

We next screened for additional aging-associated phenotypes by comparative analysis of mice from our Bub3$^{+/-}$/Rae1$^{+/-}$ and wild-type cohorts. A well-established feature of aging is loss of body weight (MacIntosh et al., 2000). Although the weight of Bub3$^{+/-}$/Rae1$^{+/-}$ mice at 5 mo was similar to that of age-matched wild-type mice, Bub3$^{+/-}$/Rae1$^{+/-}$ mice had significantly lower body mass than wild-type mice at 24 mo (Fig. 5 A). Dual energy X-ray absorptiometry was used to determine whether this loss of weight was caused by a reduction in total body fat. At 5 mo of age, Bub3$^{+/-}$/Rae1$^{+/-}$ and wild-type mice had similar percentages of total body adipose tissue; however, at 27 mo, Bub3$^{+/-}$/Rae1$^{+/-}$ showed a dramatic reduction in body fat compared with wild-type mice (Fig. 5 B). Reduced dermal thickness and subdermal adipose are characteristics of aged mice (de Boer et al., 2002; Tyner et al., 2002). Histological examination of the skin revealed significant reductions in subcutaneous adipose thickness in 27-mo-old Bub3$^{+/-}$/Rae1$^{+/-}$ mice but not in age-matched control animals (Fig. 5, C and E). The mean dermal thickness of 27-mo-old Bub3$^{+/-}$/Rae1$^{+/-}$ mice was 21% lower than that of 5-mo-old Bub3$^{+/-}$/Rae1$^{+/-}$ mice (Fig. 5 D), whereas in 27-mo-old wild-type mice, it was only 9% lower than in 5-mo-old wild-type mice (Fig. 5 D).

We then investigated whether the age-related phenotypes present in Bub3$^{+/-}$/Rae1$^{+/-}$ mice could also be observed in very old wild-type mice. We found that wild-type mice of 35 mo had lordokyphosis (Fig. 4 B), muscle atrophy (Fig. 4 C), and osteoporosis (not depicted). These mice also had significantly lower amounts of total body fat and subcutaneous adipose tissue than 5-mo-old wild-type mice (Fig. 5, B and C). As expected, the dermis of 35-mo-old wild-type mice was significantly thinner

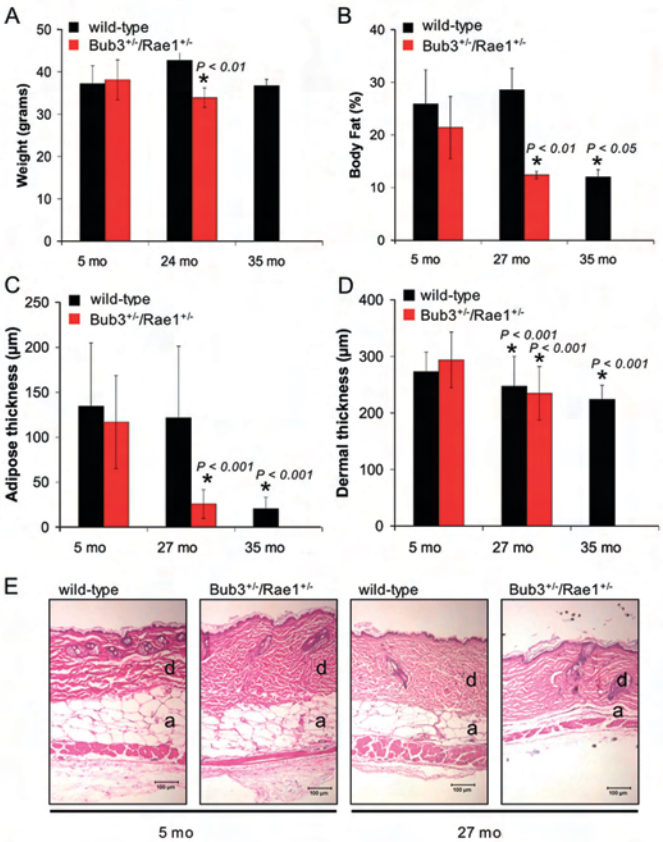

Figure 5. **Early aging–related phenotypes of combined Bub3/Rae1 haploinsufficient mice.** (A) Body weight analysis of wild-type and Bub3$^{+/-}$/Rae1$^{+/-}$ male mice ($n \geq 4$ male mice per genotype). Bub3$^{+/-}$/Rae1$^{+/-}$ mice have normal body weights at 5 mo but significantly reduced body weights at 24 mo. We note that neither Bub3$^{+/-}$ nor Rae1$^{+/-}$ mice show this reduction (not depicted). The decrease in body weight between the 24- and 35-mo-old wild-type mice is not significant but does show a trend of reduction in body weight. (B) Graph showing total body fat content in wild-type and Bub3$^{+/-}$/Rae1$^{+/-}$ mice at 5, 27, and 35 mo ($n = 4$ male mice per genotype at each age). (C) Graph showing subcutaneous adipose layer thickness of wild-type and Bub3$^{+/-}$/Rae1$^{+/-}$ mice at 5 and 27 mo along with 35-mo-old wild-type mice. Note the reduced thickness in 27-mo-old Bub3$^{+/-}$/Rae1$^{+/-}$ mice and 35-mo-old wild-type mice ($n = 4$ males per genotype). (D) Graph showing dermal thickness of wild-type and Bub3$^{+/-}$/Rae1$^{+/-}$ mice at 5 and 27 mo along with 35-mo-old wild-type mice. (A–D) Error bars represent SD. Asterisks mark values that are significantly different from wild-type values using a Mann-Whitney test. (E) Representative hematoxylin and eosin–stained dorsal skin sections of 5- and 27-mo-old wild-type and Bub3$^{+/-}$/Rae1$^{+/-}$ from which the data in C and D were collected. Dermis (d) and adipose layer (a) are indicated. Bars, 100 µm.

than that of 5-mo-old wild-type mice (Fig. 5 D). Together, the aforementioned data show that several aging-associated phenotypes appear early in mice that are double haploinsufficient for the mitotic checkpoint genes Bub3 and Rae1 but not in mice that are single haploinsufficient for these genes. The data also show that most of these phenotypes do occur in wild-type mice of extremely advanced age.

Combined haploinsufficiency of Bub3 and Rae1 results in premature senescence

We next investigated whether combined haploinsufficiency of Bub3 and Rae1 triggers cell death or cellular senescence, which are two processes that have been linked to aging (Campisi, 2005; Lombard et al., 2005). We intercrossed Bub3$^{+/-}$ and Rae1$^{+/-}$ mice to produce Bub3$^{+/-}$/Rae1$^{+/-}$, Bub3$^{+/-}$, Rae1$^{+/-}$, and wild-type MEFs from 13.5-d-old fetuses. At passage 5 (P5), we assayed Bub3$^{+/-}$/Rae1$^{+/-}$ and wild-type MEFs for cell death by TUNEL staining. We observed no difference in amounts of TUNEL-positive cells in Bub3$^{+/-}$/Rae1$^{+/-}$ and wild-type MEFs cultures (Fig. 6 A), indicating that combined haploinsufficiency of Bub3 and Rae1 did not increase the rate of cell death. Combined annexin V–FITC and propidium iodide (PI) staining of P5 Bub3$^{+/-}$/Rae1$^{+/-}$ and wild-type MEFs showed that neither apoptotic nor nonapoptotic cell death was significantly increased in Bub3$^{+/-}$/Rae1$^{+/-}$ MEFs (Fig. 6 B) despite high rates of chromosome missegregation in mitosis. This is remarkable because high rates of cell death have been observed in studies in which the mitotic checkpoint proteins Mad2 and BubR1 were depleted by short inhibitory RNA (Kops et al., 2004; Meraldi et al., 2004; Michel et al., 2004). Thus, it seems that cell death only occurs when mitotic checkpoint proteins drop below a critical threshold level and that aberrant chromosome segregation itself is insufficient to trigger cell death.

Cellular senescence is characterized in vitro by a decline in growth rate (Atadja et al., 1995). At P3, Bub3$^{+/-}$/Rae1$^{+/-}$ growth rates were similar to those of Bub3$^{+/-}$, Rae1$^{+/-}$, and wild-type MEFs (Fig. 6 C). On the other hand, at P7, Bub3$^{+/-}$/Rae1$^{+/-}$ MEFs showed significantly reduced growth rates

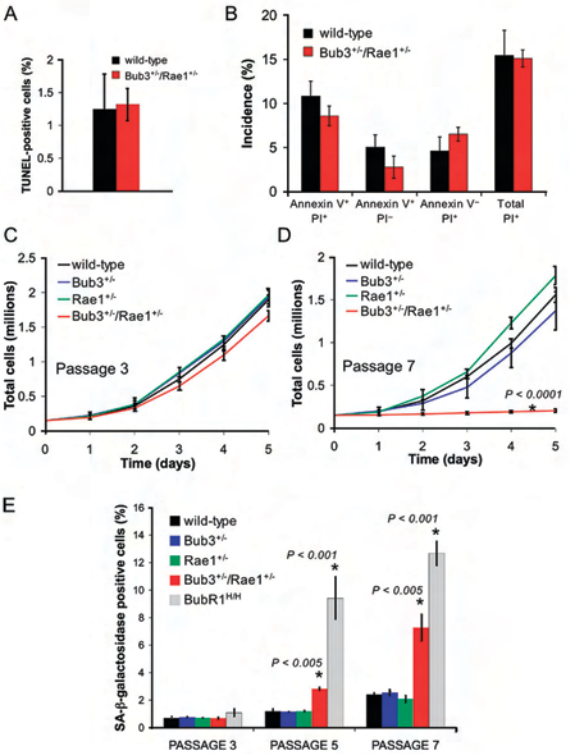

Figure 6. **Early onset of cellular senescence in Bub3/Rae1 double haploinsufficient MEFs.** (A) Analysis of the percentages of cell death in Bub3$^{+/-}$/Rae1$^{+/-}$ and wild-type MEFs cultures by TUNEL assay (n = 3 MEF lines per genotype). (B) Percentages of Bub3$^{+/-}$/Rae1$^{+/-}$ and wild-type MEFs that are in the early stages of apoptosis (annexin V$^+$/PI$^-$ cells), in the late stages of apoptosis, already dead (annexin V$^+$/PI$^+$ cells), that undergo nonapoptotic cell death (annexin V$^-$/PI$^+$ cells), or that are dead (PI$^+$ cells). We used 3 MEF lines per genotype. We note that the differences between Bub3$^{+/-}$/Rae1$^{+/-}$ and wild-type MEFs were not statistically significant using an unpaired t test. (C and D) Growth curves of wild-type, Bub3$^{+/-}$, Rae1$^{+/-}$, and Bub3$^{+/-}$/Rae1$^{+/-}$ MEF cells at P3 (C) and P7 (D). 1.5 × 10^5 cells of indicated passages were seeded in duplicate on day 0 and counted for five consecutive days. Lines represent three independent MEF lines. Note that Bub3$^{+/-}$/Rae1$^{+/-}$ MEF cells have reduced proliferation potential at P7, whereas single heterozygous Bub3$^{+/-}$ and Rae1$^{+/-}$ MEFs do not. (E) Percentages of wild-type, Bub3$^{+/-}$, Rae1$^{+/-}$, BubR1$^{H/H}$, and Bub3$^{+/-}$/Rae1$^{+/-}$ MEF cells that were positive for SA β-galactosidase activity at the indicated passages (n = 3 lines for each genotype at each passage). Asterisks in D and E mark values that are significantly different from those of wild-type mice using an unpaired t test. Error bars represent SD.

compared with MEFs of the other three genotypes (Fig. 6 D). At P3, MEF cultures of all four genotypes had comparable numbers of cells that were positive for senescence-associated (SA) β-galactosidase activity (Fig. 6 E). However, at P5 and P7, Bub3$^{+/-}$/Rae1$^{+/-}$ MEFs showed a profound increase in the number of cells staining positively for SA β-galactosidase in comparison with Bub3$^{+/-}$, Rae1$^{+/-}$, and wild-type MEFs. Consistent with these data, the senescence response genes p53, p21, p19, and p16 were induced earlier in Bub3$^{+/-}$/Rae1$^{+/-}$ MEFs than in Bub3$^{+/-}$, Rae1$^{+/-}$, and wild-type MEFs (Fig. 7 A). Together, these findings indicate that compound heterozygosity of Bub3 and Rae1 causes early onset of cellular senescence.

The induction of p53, p21, and p19 indicates that the lesion triggering cellular senescence in Bub3/Rae1 double haploinsufficient MEFs activates the p53 DNA damage response pathway. To investigate whether activation of the p53 pathway might be caused by defective DNA repair, we analyzed the fidelity of distinct DNA damage repair pathways by measuring cell survival and colony formation ability after exposing Bub3$^{+/-}$/Rae1$^{+/-}$ MEF cultures to various kinds of DNA-damaging agents. As shown in Fig. 7 (C–H), the DNA repair capacities of Bub3$^{+/-}$/Rae1$^{+/-}$ and wild-type MEFs were very similar, suggesting that increased accumulation of DNA damage is an unlikely cause of increased senescence in Bub3$^{+/-}$/Rae1$^{+/-}$ cultures.

The early aging–associated phenotypes that develop in Bub3$^{+/-}$/Rae1$^{+/-}$ mice resemble those detected in mice with low levels of BubR1 (Baker et al., 2004). However, BubR1$^{H/H}$ mice had a much earlier onset of aging phenotypes than Bub3$^{+/-}$/Rae1$^{+/-}$ mice. Consistent with this, BubR1 hypomorphic MEF cultures contained significantly higher numbers of SA β-galactosidase–positive cells than Bub3$^{+/-}$/Rae1$^{+/-}$ MEF cultures (Fig. 6 E). In addition, BubR1$^{H/H}$ MEFs showed a more robust activation of the p53 and p16 pathways than Bub3$^{+/-}$/Rae1$^{+/-}$ MEFs (Fig. 7 B). These data draw a clear correlation between the level of induction of senescence response genes and the rate of premature aging.

To further test this correlation, we prepared MEFs from Mad2 haploinsufficient mice and measured the degree of senescence at P3, P5, and P7. At each passage, the percentage of SA β-galactosidase–positive Mad2$^{+/-}$ MEFs was similar to that of wild-type MEFs (Fig. S1 A, available at http://www.jcb.org/cgi/content/full/jcb.200507081/DC1). Furthermore, at each passage, p53, p21, p19, and p16 levels of Mad2$^{+/-}$ MEFs were comparable with those of wild-type MEFs (Fig. S1 B).

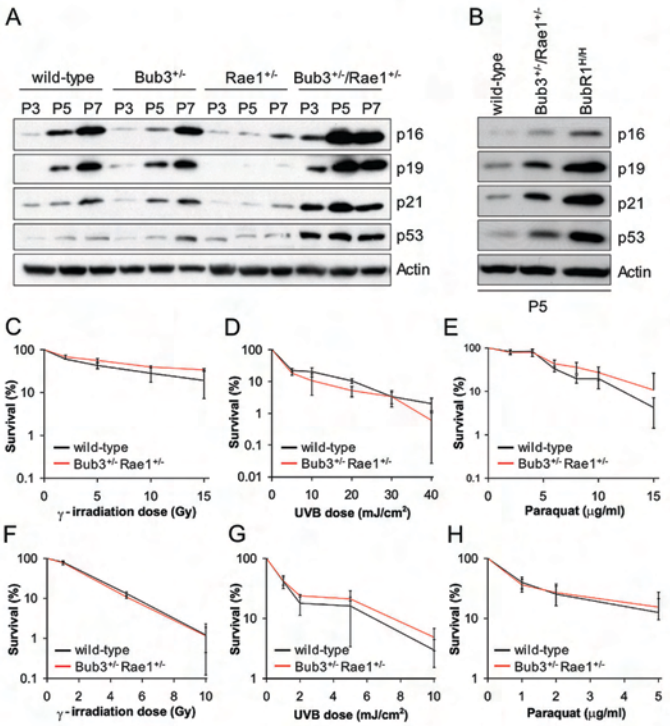

Figure 7. **Bub3$^{+/-}$/Rae1$^{+/-}$ MEFs have higher levels of SA molecular markers.** (A) Western blot analysis of proteins in extracts from wild-type, Bub3$^{+/-}$, Rae1$^{+/-}$, and Bub3$^{+/-}$/Rae1$^{+/-}$ MEFs at P3, P5, and P7. Blots were probed with antibodies against the indicated proteins. Note that the induction of senescence markers is delayed in Rae1$^{+/-}$ MEFs; this delay was consistently seen in three independent Rae1$^{+/-}$ MEF lines. (B) Western blots of protein extracts from P5 wild-type, Bub3$^{+/-}$/Rae1$^{+/-}$, and BubR1$^{H/H}$ MEFs probed with the indicated antibodies. The results shown in A and B are representative for three independently generated MEF lines of each genotype. (C–H) Analysis of the fidelity of distinct DNA damage repair pathways by measuring cell survival and colony formation ability after exposing early passage MEFs to various kinds of DNA-damaging agents. (C–E) Survival curves of wild-type and Bub3$^{+/-}$/Rae1$^{+/-}$ MEFs after DNA damage by γ-irradiation (C), UV type B (D), or paraquat (E). (F–H) Colony-forming assay of wild-type and Bub3$^{+/-}$/Rae1$^{+/-}$ MEFs after DNA damage by γ-irradiation (F), UV type B (G), or paraquat (H). Error bars represent SD.

Consistent with these findings, we observed no early aging–related phenotypes in the small cohort of Mad2$^{+/-}$ mice that we followed for a period of 19–27 mo (Fig. S1 C). Chromosome counts showed that 18% of Mad2$^{+/-}$ splenocytes were aneuploid when mice were 5 mo of age (Fig. S1 D). Thus, Mad2 haploinsufficiency does not promote cellular senescence in MEFs and does not seem to trigger aging-related phenotypes in mice, although aneuploidy is increased.

Spindle assembly checkpoint activity measurements

Our chromosome counts suggested that there is a rather weak link between checkpoint dysfunction and the early onset of senescence and aging. To further investigate this issue, we obtained two additional measures for checkpoint activity by methods involving live cell imaging. The first assay is a nocodazole challenge assay. MEFs carrying various mitotic checkpoint gene defects were first transduced with a retrovirus carrying a YFP-tagged H2B gene to allow visualization of chromosomes by fluorescent microscopy. We then challenged the MEFs with nocodazole and measured the duration of the ensuing checkpoint-dependent mitotic arrest. This duration of arrest in mitosis was defined as the interval between nuclear envelope breakdown (NEBD; onset of mitosis) and chromatin decondensation (exit from mitosis without cytokinesis). We used the time at which 50% of the cells had exited mitosis for comparison. Nocodazole-challenged wild-type MEFs typically remained arrested in prometaphase for 7.2 h (Fig. 8 A). However, single haploinsufficient MEFs of Bub3 and Rae1 showed a profound decrease in their ability to maintain this arrest, with 50% of the cells exiting at 3 h. Bub3$^{+/-}$/Rae1$^{+/-}$ MEFs had an even further reduction in their ability to sustain arrest, with 50% of the cells exiting mitosis at 2.2 h. BubR1$^{+/H}$ and BubR1$^{+/-}$ MEFs, which express ∼60 and 30% of normal BubR1 protein, respectively (Baker et al., 2004), also had significant reductions in their ability to maintain a mitotic arrest, with 50% of the cells exiting at 5.3 and 3.8 h (Fig. 8 B). BubR1$^{H/H}$ MEFs (∼10% BubR1) had the most profound inability to maintain mitotic arrest, with 50% of the cells exiting at 1.1 h. It surprised us that the duration of arrest of BubR1$^{H/H}$ MEFs was substantially shorter than that of Bub3$^{+/-}$/Rae1$^{+/-}$ MEFs, because BubR1$^{H/H}$ MEFs have less severe aneuploidy than Bub3$^{+/-}$/Rae1$^{+/-}$ MEFs (Table II; also see Discussion). As an alternative measure for spindle checkpoint activity, we measured the accuracy of chromosome segregation during mitosis. In essence, we followed YFP-H2B–positive MEFs through an unchallenged mitosis by live cell imaging and determined the fraction of mitotic cells with chromosome segregation defects. We observed little or no misaligned

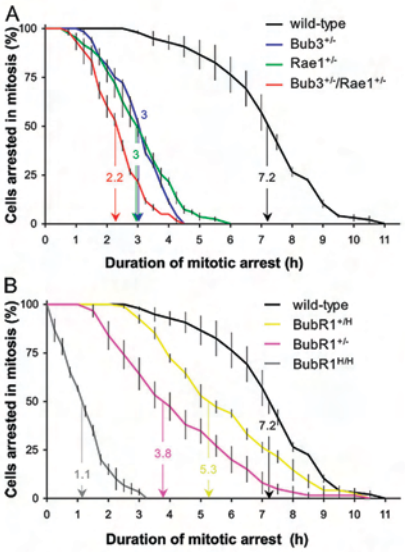

Figure 8. **Spindle assembly checkpoint activity analysis.** (A) Analysis of mitotic checkpoint activity of wild-type, Bub3$^{+/-}$, Rae1$^{+/-}$, and Bub3$^{+/-}$/Rae1$^{+/-}$ MEFs. MEF cultures were challenged with nocodazole, and cells undergoing NEBD were marked. We continued to monitor these cells at 15-min intervals until their chromosomes decondensed. The duration of arrest in mitosis was defined as the interval between NEBD (onset of mitosis) and chromatin decondensation (exit from mitosis without cytokinesis). The time at which 50% of the cells had exited mitosis has been indicated. This time was used as a measure for spindle assembly checkpoint activity. (B) Analysis of mitotic checkpoint activity of wild-type, BubR1$^{+/H}$, BubR1$^{+/-}$, and BubR1$^{H/H}$ MEFs. We note that BubR1$^{+/H}$ and BubR1$^{+/-}$ mice have a normal lifespan and lack early aging–associated phenotypes (Baker et al., 2004). Error bars represent SEM.

chromosomes in wild-type, Bub3$^{+/-}$, Rae1$^{+/-}$, Bub3$^{+/-}$/Rae1$^{+/-}$, and BubR1$^{H/H}$ metaphases (Table III). However, a relatively large proportion of Bub3$^{+/-}$/Rae1$^{+/-}$ and BubR1$^{H/H}$ anaphases had lagging chromosomes (Table III, Videos 1–3, and Fig. S4, available at http://www.jcb.org/cgi/content/full/jcb.200507081/DC1). The incidence of lagging chromosomes was also increased in Bub3$^{+/-}$ and Rae1$^{+/-}$ anaphases, but to a lesser extent. It should be noted that lagging chromosomes are not necessarily a sign of failed mitotic checkpoint signaling because they could result from merotelically attached kinetochores that do not activate the mitotic checkpoint (Cimini et al., 2001). Bub3$^{+/-}$/Rae1$^{+/-}$ MEFs had not only a somewhat higher percentage of anaphases with lagging chromosomes than BubR1$^{H/H}$ MEFs but also a higher percentage of abnormal anaphases with more than one lagging chromosome (Table III and Video 3). This may explain why the spectrum of chromosome losses and gains is wider for Bub3$^{+/-}$/Rae1$^{+/-}$ MEFs than for BubR1$^{H/H}$ MEFs (Table II). Collectively, the aforementioned data confirm that spindle assembly checkpoint dysfunction and chromosome missegregation do not correlate well with cellular senescence and aging.

Discussion

In this study, we used mice in which the mitotic checkpoint proteins Bub3 and Rae1 were disrupted individually or in combination to address whether premature aging is a common consequence of mitotic checkpoint gene defects. We found that Bub3 and Rae1 single haploinsufficient mice exhibit no signs of early aging despite their weakened checkpoint and progressive aneuploidy. Conversely, several aging-related phenotypes appear early in mice that are haploinsufficient for both Bub3 and Rae1. However, BubR1 hypomorphic mice age much faster but have less aneuploidy than Bub3/Rae1 haploinsufficient mice. This suggests that spindle assembly checkpoint dysfunction, which leads to the accumulation of aneuploidy, is unlikely to cause premature aging in BubR1 and Bub3/Rae1 mutant mice. We find that only mitotic checkpoint gene defects that can provoke cellular senescence in MEFs cause the early onset of aging-associated phenotypes in mice, with levels of induction of p19, p53, p21, and p16 highly correlating with the rate of cellular senescence and aging.

In the study of hypomorphic BubR1 mice (Baker et al., 2004), it became apparent that as these mice began to show signs of premature aging, they also started to accumulate aneuploid splenocytes. This led to the hypothesis that aneuploidy might be the primary lesion triggering cellular senescence and the process of aging. The use of Bub3 and Rae1 haploinsufficient mice allowed for rigorous testing of this hypothesis. At 5 mo, BubR1 hypomorphic mice have an aged appearance with detectable aneuploidy in 15% of their splenocytes (Baker et al., 2004). Age-matched single heterozygous Bub3 and Rae1

Table II. **Bub3/Rae1 double haploinsufficient MEFs develop more severe aneuploidy than BubR1 hypomorphic MEFs**

Mitotic MEF genotype (*n*)	Mitotic figures inspected	Percent aneuploid figures (SD)	Karyotypes with indicated chromosome number																	Percent mitotic figures with PMSCS (SD)
			33	34	36	37	38	39	40	41	42	43	44	45	46	47	49	51	53	
Wild type (3)	150	9 (1)						7	136	7										<1
Bub3$^{+/-}$ (3)	150	19 (2)				1	4	9	121	8	2	2	3							0
Rae1$^{+/-}$ (3)	150	19 (2)				5	2	6	121	9	1	2	4							0
Bub3$^{+/-}$/Rae1$^{+/-}$ (3)	150	41 (2)	1	6	5	3	3	15	88	6	2	3	4	4	5	1	2	1	1	19 (3)
BubR1$^{H/H}$ (3)	125	36 (6)					5	13	80	20	6	1								15 (3)

Empty spaces mean that there were no karyotypes with the indicated chromosome number. Karyotyping was performed at passage 5.

Table III. **Chromosome missegregation rates in MEFs with various mitotic checkpoint gene mutations**

Genotype (n)	Mitotic cells inspected	Metaphases with misaligned chromosomes	Anaphases with lagging chromosomes	Anaphases with indicated number of lagging chromosomes							Percent abnormal anaphases with multiple lagging chromosomes
				0	1	2	3	4	5	8	
Wild type (6)	114	0 (0%)	3 (2.6%)	111	3						0
$Bub3^{+/-}$ (5)	152	1 (0.7%)	9 (5.9%)	143	8	1					11
$Rae1^{+/-}$ (5)	100	0 (0%)	7 (7.0%)	93	7						0
$Bub3^{+/-}/Rae1^{+/-}$ (6)	130	0 (0%)	19 (14.6%)	114	10	3	3	1	1	1	47
$BubR1^{H/H}$ (6)	149	0 (0%)	18 (12.1%)	131	15	2	1				17

Empty spaces mean that there were no karyotypes with the indicated chromosome number.

mice each have 9% aneuploid splenocytes but show no signs of early aging. One could argue that this may be the result of having aneuploidy that remains below a critical level. Splenocytes from 5-mo-old compound Bub3/Rae1 mice have 36% aneuploidy and a wide spectrum of chromosome losses and gains (Table I), but these animals show no overt features of aging at this age. If aneuploidy alone was a driving force of aging, these mice should have shown phenotypes of aging earlier than BubR1 hypomorphic mice. It is possible that the degree of aneuploidy in splenocytes is not representative of the degree present in tissues and cell types that develop early aging phenotypes. Although we cannot exclude this possibility with our current methods for measuring aneuploidy in vivo, the view that aneuploidy does not correlate with aging is further underscored by the finding that $Bub3^{+/-}/Rae1^{+/-}$ MEFs are more aneuploid than BubR1 hypomorphic MEFs but exhibit lower levels of cellular senescence. In contrast, in mice with mitotic checkpoint gene defects, the rate of aging strongly correlates with the rate of cellular senescence. The induction of p53, p21, and p19 in both BubR1 hypomorphic and combined Bub3/Rae1 haploinsufficient cells but not Bub3 and Rae1 single haploinsufficient cells suggests that the lesion triggering cellular senescence and aging activates the p53 pathway. Like $BubR1^{H/H}$ MEFs (Baker et al., 2004), $Bub3^{+/-}/Rae1^{+/-}$ MEFs have no detectable defects in DNA repair, suggesting that the lesion that triggers p53 activation is unlikely to be the accumulation of DNA damage or mutations. Various stress signals other than DNA damage are known to activate the p53 pathway (Ben-Porath and Weinberg, 2005; Harris and Levine, 2005), and future experiments will be necessary to determine whether any of these signals might be active in BubR1 hypomorphic and Bub3/Rae1 mutant mice.

Rae1, Bub3, and BubR1 have all been implicated in functions outside of the spindle assembly checkpoint. For example, Rae1 was originally discovered as a nucleocytoplasmic transport factor that regulates the export of mRNA from the nucleus (Brown et al., 1995; Kraemer and Blobel, 1997; Pritchard et al., 1999). How Rae1 regulates nuclear transport and whether Bub3 functions also in the transport machinery has not yet been established. We found that combined Bub3/Rae1 haploinsufficiency does not cause overt defects in global mRNA export or nuclear pore complex biogenesis (Fig. S2, available at http://www.jcb.org/cgi/content/full/jcb.200507081/DC1). However, our experiments by no means represent a comprehensive analysis of the transport machinery, and it is certainly possible that Bub3/Rae1 haploinsufficient cells have subtle trafficking defects. A recent study has suggested that Bub3 can interact with histone deacetylases and that, in this context, Bub3 might act to repress gene transcription in interphase (Yoon et al., 2004). BubR1 can also repress gene transcription in a heterologous DNA-binding context, although not in conjunction with histone deacetylases (Yoon et al., 2004). BubR1 also seems to mediate apoptosis of cells that exit mitosis without chromosome segregation (Shin et al., 2003), and, in yeast, the BubR1 homologue Mad3 and Bub3 have both been linked to the accumulation of gross chromosomal rearrangements (Myung et al., 2004). Thus, it is possible that functions outside of the spindle assembly checkpoint are compromised in BubR1 hypomorphic and Bub3/Rae1 haploinsufficient mice and that early onset of aging-related phenotypes is linked to such defects.

Although BubR1 hypomorphic mice age much faster than Bub3/Rae1 mutant mice, both models have a common spectrum of age-related phenotypes that is distinctive from that of mouse strains in which DNA damage repair or telomere maintenance defects cause premature aging (Hasty et al., 2003; Lombard et al., 2005). For example, mice with mitotic checkpoint gene defects develop cataracts at high incidence, whereas the other models do not. Conversely, mice with defects in DNA damage repair or telomere maintenance show hematopoietic stem cell depletion and glucose intolerance, whereas mice with a weakened mitotic checkpoint do not (unpublished data). This distinction supports the idea that the lesion that triggers aging in BubR1 hypomorphic mice and Bub3/Rae1 mutant mice is distinct from that of other aging models. This suggestion is further supported by the demonstration that DNA damage repair and telomere maintenance functions are seemingly intact in Bub3/Rae1 haploinsufficient mice and BubR1 hypomorphic mice (Baker et al., 2004).

In this study, we have used a modified nocodazole challenge assay to measure the duration of sustained spindle checkpoint activity of MEFs with various mitotic checkpoint gene defects. In essence, we treated MEFs with nocodazole and determined how long individual cells remained in mitosis by live cell imaging and then used this time as a measure for spindle checkpoint activity. We validated our nocodazole challenge assay by using a series of MEFs with a graded reduction of BubR1 protein level. We found that the duration of arrest in mitosis declined as the amount of BubR1 decreased. We found further that this time of arrest correlated well with the rate of aneuploidy

and chromosome missegregation. However, the finding that Bub3/Rae1 double-insufficient MEFs are more aneuploid than BubR1$^{H/H}$ MEFs (the percentage of aneuploid cells is higher and the spectrum of chromosome losses and gains is wider) appears inconsistent, as we find that Bub3/Rae1 haploinsufficient MEFs sustain their mitotic arrest in nocodazole for twice as long as BubR1$^{H/H}$ MEFs. A possible explanation for this discrepancy is that the nocodazole challenge assay may not provide a reliable measure for spindle assembly checkpoint activity; the reasoning is that the checkpoint functions to protect cells against chromosome missegregation rather than against microtubule poisoning. Alternatively, increased aneuploidy in Bub3/Rae1 haploinsufficient cells might be caused by the dysfunction of proteins involved in chromosome segregation but not in the spindle assembly checkpoint. Examples of such proteins are AdAPC (adenomatous polyposis coli; Kaplan et al., 2001), securin (Jallepalli and Lengauer, 2001), and separase (Waizenegger et al., 2002; Chestukhin et al., 2003).

Abnormal numbers of chromosomes, termed aneuploidy, is one of the most common properties of cancer cells (Rajagopalan and Lengauer, 2004). Because aneuploidy occurs with such high frequency, it has been suggested that aneuploidy is an essential step in the process of tumorigenesis (Lengauer et al., 1998). In this study, we have demonstrated that Bub3$^{+/-}$, Rae1$^{+/-}$, and Bub3$^{+/-}$/Rae1$^{+/-}$ mice do not show any differences in both the rate of tumor formation and the type of tumor formed in comparison with wild-type animals. An earlier cancer susceptibility study on Bub3$^{+/-}$ mice yielded similar data (Kalitsis et al., 2005). That study further showed that even on a p53 or Rb1 heterozygous background, Bub3 haploinsufficiency had no significant effect on tumorigenesis. A suggested explanation for these findings was that the degree of impairment of the checkpoint machinery was too low to cause substantial aneuploidy (Kalitsis et al., 2005). However, although the aneuploidy in our double heterozygous Bub3/Rae1 mice is quite severe at 5 mo, we find no increased susceptibility to lifetime spontaneous tumor development. This result is consistent with our earlier observation that BubR1 hypomorphic mice are not tumor prone despite having severe aneuploidy (Baker et al., 2004). So far, only Mad2 haploinsufficiency has been shown to increase the risk for spontaneous tumors in mice (Michel et al., 2001). However, several studies have shown that impaired spindle checkpoint function increases the risk for carcinogen-induced tumors. For instance, we have shown previously that Rae1$^{+/-}$ and Bub3$^{+/-}$/Rae1$^{+/-}$ mice are susceptible to lung adenoma formation after early postnatal treatment with dimethylbenzanthrene (DMBA; Babu et al., 2003). Others have shown that BubR1$^{+/-}$ mice have a susceptibility to azoxymethane-induced intestinal and lung tumor development (Dai et al., 2004), and, consistent with this finding, we observed that DMBA-treated BubR1$^{H/H}$ mice are prone to lung tumors (Fig. S3, available at http://www.jcb.org/cgi/content/full/jcb.200507081/DC1). All of these studies illustrate an important point that challenging these mice with carcinogenic agents introduces cooperating mutations that synergize with mitotic checkpoint failure to cause tumorigenesis and that these mutations may not occur under normal situations. It seems that the identification of gene mutations that cooperate with spindle assembly checkpoint gene alterations in tumorigenesis will be important to provide a better understanding of the role of aneuploidy in cancer. The link between spindle assembly checkpoint impairment and cancer predisposition is further supported by a recent report showing that a high proportion of individuals with mosaic variegated aneuploidy (MVA) syndrome carry bi-allelic mutations in the BubR1 gene (Hanks et al., 2004). MVA is a rare recessive disorder that is characterized by severe aneuploidy and a high risk for neoplasms such as rhabdomyosarcoma, Wilms tumor, and leukemia (Kajii et al., 2001; Plaja et al., 2001). Other characteristics of MVA syndrome include microcephaly, growth retardation, and eye abnormalities such as cataracts. Whether MVA patients with bi-allelic mutations in BubR1 develop progeroid features other than growth retardation and cataracts remains to be established: so far, only four patients with BubR1 mutations have been identified, three of which are <3 yr of age.

In a recent study, Kalitsis et al. (2005) confirmed that MEFs from Bub3 haploinsufficient mice have increased aneuploidy, but the increase was not as profound as the one we previously observed (Babu et al., 2003). The smaller increase most likely results from the fact that chromosome counts were performed at P3 instead of P5. Furthermore, BubR1$^{+/-}$ mice generated by Wang et al. (2004) typically exhibited splenomegaly and extramedullary megakaryopoiesis, but we did not detect these phenotypes in our BubR1$^{+/-}$ and BubR1$^{H/H}$ mice (Baker et al., 2004). It is unclear why that is, but it might be the result of the different methods used to create the models (enhancer trapping vs. homologous recombination), differences in the mouse housing facilities, and/or possible differences in genetic background.

Materials and methods

Generation of knockout mice and DMBA treatments

Bub3 and Rae1 heterozygous knockout mice and BubR1 hypomorphic mice were generated as described previously (Babu et al., 2003; Baker et al., 2004). These mice were derived from 129Sv/E embryonic stem cells and maintained on a mixed 129Sv/E × C57BL/6 genetic background. Mad2$^{+/-}$ mice were gifts from R. Benezra (Weill Medical College of Cornell University, New York, NY; Dobles et al., 2000). All mice were housed in a pathogen-free barrier facility for the duration of the study. Experimental procedures involving laboratory mice were reviewed and approved by the Institutional Animal Care and Use Committee of the Mayo Clinic. Prism software (GraphPad Software, Inc.) was used for the generation of survival curves and for statistical analysis. DMBA treatments were performed as described, except the duration of treatment was 4 mo instead of 5 (Babu et al., 2003).

Karyotype analysis

Metaphase spreads were prepared from splenocytes as described previously (Babu et al., 2003). The aneuploidy data for Bub3$^{+/-}$, Rae1$^{+/-}$, and Bub3$^{+/-}$/Rae1$^{+/-}$ MEFs presented in Table II were first published in Babu et al. (2003); the data for BubR1$^{H/H}$ MEFs and mice were first published in Baker et al. (2004).

Collection and analysis of tumors

Moribund mice were killed, and major organs were screened for overt tumors using a dissection microscope. Collected tumors were processed for histopathology by standard methods. A chi square or Fisher's exact test was used to compare tumor incidence proportions across the genotypes for mice that developed tumors. Board-certified pathologists assisted in tumor analysis.

Cataract and body fat analysis

Biweekly, mice were screened for overt cataracts by examining dilated eyes with a slit light. At biopsy, cataractous eyes were collected and processed by standard methods for histological evaluation. Body fat content was measured using a small animal densitometer (Lunar PIXImus Corp.) as described previously (Nagy and Clair, 2000). A Mann-Whitney test was used for statistics.

Analysis of skin and skeletal muscle

Dorsal skin was dissected, fixed in 10% formalin, processed, and embedded in paraffin. 5-μm cross sections were prepared and stained with hematoxylin and eosin using standard procedures. Sections were stained, and the thickness of the dermal and adipose layers was calculated using a calibrated computer program (Spot Advanced; BioSpot). 40 random measurements were taken for each mouse of each genotype at the indicated age (n = 4 males). Histopathology on gastrocnemius muscle was performed as previously described (Kane et al., 2004; O'Cochlain et al., 2004). A Mann-Whitney test was used for statistics.

Generation and culture of MEFs

MEFs were generated from wild-type Bub3$^{+/-}$, Rae1$^{+/-}$, or Bub3$^{+/-}$/Rae1$^{+/-}$ 13.5-d-old embryos as previously described (Babu et al., 2003). Growth curves of MEFs were generated as previously described (Baker et al., 2004). BubR1$^{H/H}$, BubR1$^{+/-}$, and BubR1$^{+/H}$ MEFs were previously generated (Baker et al., 2004).

Analysis of cell death, apoptosis, and DNA repair

TUNEL/Hoechst stainings were performed on P5 MEFs according to the manufacturer's protocol (Roche), as were annexin V/PI stainings (BD Biosciences). FACS analysis was performed as previously described (Tran et al., 2005). DNA damage survival experiments were performed as described previously (Baker et al., 2004).

SA β-galactosidase staining

MEFs were stained with an SA β-galactosidase kit according to the manufacturer's protocol (Cell Signal Technology). Nuclei were stained with Hoechst for visualization. The percentage of senescent cells is the total number of senescent cells divided by the total number of cells.

Western blot analysis

We performed Western blot analysis as previously described (Kasper et al., 1999). Antibodies for SA proteins were used at a 1:200 dilution (purchased from Santa Cruz Biotechnology, Inc. unless otherwise noted): p16 (M-156), p19 (NB200-106; Novus Biologicals), p21 (M-19), and p53 (FL-393-G). β-actin was used as a loading control (1:50,000 dilution; Sigma-Aldrich).

Time-lapse live microscopy

To allow visualization of chromosomes by fluorescent microscopy on live cells, we used a retrovirus expressing YFP-tagged H2B that was constructed as previously described (Jeganathan et al., 2005). P2 MEFs cells were seeded in T25 flasks at 50% confluence and cultured in DME/10% FBS. The next day, these MEFs were grown for 24 h in medium harvested from EcoPACK cells that produce pMCSV-puro H2B-YFP virus. 24 h after transduction with pMCSV-H2B-YFP retrovirus, MEFs were seeded in 35-mm glass-bottomed culture dishes (MatTek Corporation). The next day, Hepes was added to the culture medium at a final concentration of 20 mM. 4 h later, the dish was placed in a heat-controlled stage of a microscope (Axiovert 200; Carl Zeiss MicroImaging, Inc.). The temperature was maintained at 37°C. CO_2 levels were maintained at 10% using a controller (CTI 3700; Carl Zeiss MicroImaging, Inc.). For nocodazole challenge experiments, nocodazole was added to a final concentration of 100 ng/ml. During the next 30 min, 20–30 cells undergoing NEBD were marked by the use of a mark/find module (AV4 MOD; Carl Zeiss MicroImaging, Inc.). Subsequently, time-lapse sequences were captured by using a plan Apo 63× NA 1.4 differential interference contrast (D = 0.18) oil objective (Carl Zeiss MicroImaging, Inc.) and a camera (AxioCam Hrm; Carl Zeiss MicroImaging, Inc.). The exposure times in nocodazole challenge experiments were always 100 ms at 2 × 2 binning. Interframe intervals were 15 min except for wild-type, BubR1$^{+/H}$, and BubR1$^{+/-}$ MEFs (intervals were 30 min). Imaging WS/20A software (Carl Zeiss MicroImaging, Inc.) was used to determine the time of arrest in mitosis of individual cells. The time of arrest in mitosis was defined as the interval between NEBD (onset of mitosis) and chromatin decondensation (exit from mitosis without cytokinesis). For analysis of mitotic defects, cells entering mitosis were marked, and images were acquired at 2- or 3-min interframe intervals until the completion of mitosis.

Indirect immunofluorescence and staining for poly(A)$^+$ RNA

Indirect immunofluorescence for mAb414 was performed as described previously (Wu et al., 2001), as were stainings for poly(A)$^+$ RNA (Bastos et al., 1996).

Online supplemental material

Fig. S1 shows that Mad2 haploinsufficiency does not accelerate cellular senescence or aging. Fig. S2 shows that Bub3$^{+/-}$/Rae1$^{+/-}$ MEFs have no overt defects in nuclear pore complex architecture and mRNA export. Fig. S3 shows that BubR1$^{H/H}$ mice are highly susceptible to DMBA-induced tumor formation. Fig. S4 shows examples of BubR1$^{H/H}$ anaphases with lagging chromosomes. Video 1 shows a Bub3$^{+/-}$/Rae1$^{+/-}$ cell undergoing normal mitosis. Videos 2 and 3 show mitotic Bub3$^{+/-}$/Rae1$^{+/-}$ cells with one and two lagging chromosomes, respectively. Online supplemental material is available at http://www.jcb.org/cgi/content/full/jcb.200507081/DC1.

We thank Robert Benezra for providing Mad2 heterozygous knockout mice. We are grateful to Rick Bram, Meelad Dawlaty, and Debra Pearson for critical reading of the manuscript and Michael Thompson, Caili Tong, and Jay Hiddinga for assistance. We thank Douglas Cameron, Susan Abraham, and Cynthia Inwards for histopathological evaluations.

This work was supported by grants from the National Institutes of Health to J. van Deursen (CA77262 and CA96985).

Submitted: 18 July 2005
Accepted: 10 January 2006

References

Atadja, P., H. Wong, I. Garkavtsev, C. Veillette, and K. Riabowol. 1995. Increased activity of p53 in senescing fibroblasts. *Proc. Natl. Acad. Sci. USA*. 92:8348–8352.

Babu, J.R., K.B. Jeganathan, D.J. Baker, X. Wu, N. Kang-Decker, and J.M. van Deursen. 2003. Rae1 is an essential mitotic checkpoint regulator that cooperates with Bub3 to prevent chromosome missegregation. *J. Cell Biol.* 160:341–353.

Baker, D.J., K.B. Jeganathan, J.D. Cameron, M. Thompson, S. Juneja, A. Kopecka, R. Kumar, R.B. Jenkins, P.C. de Groen, P. Roche, and J.M. van Deursen. 2004. BubR1 insufficiency causes early onset of aging-associated phenotypes and infertility in mice. *Nat. Genet.* 36:744–749.

Baker, D.J., J. Chen, and J.M. van Deursen. 2005. The mitotic checkpoint in cancer and aging: what have mice taught us? *Curr. Opin. Cell Biol.* 17:583–589.

Bastos, R., A. Lin, M. Enarson, and B. Burke. 1996. Targeting and function in mRNA export of nuclear pore complex protein Nup153. *J. Cell Biol.* 134:1141–1156.

Ben-Porath, I., and R.A. Weinberg. 2005. The signals and pathways activating cellular senescence. *Int. J. Biochem. Cell Biol.* 37:961–976.

Brown, J.A., A. Bharathi, A. Ghosh, W. Whalen, E. Fitzgerald, and R. Dhar. 1995. A mutation in the *Schizosaccharomyces pombe* rae1 gene causes defects in poly(A)+ RNA export and in the cytoskeleton. *J. Biol. Chem.* 270:7411–7419.

Burds, A.A., A.S. Lutum, and P.K. Sorger. 2005. Generating chromosome instability through the simultaneous deletion of Mad2 and p53. *Proc. Natl. Acad. Sci. USA*. 102:11296–11301.

Campisi, J. 2005. Senescent cells, tumor suppression, and organismal aging: good citizens, bad neighbors. *Cell*. 120:513–522.

Chestukhin, A., C. Pfeffer, S. Milligan, J.A. DeCaprio, and D. Pellman. 2003. Processing, localization, and requirement of human separase for normal anaphase progression. *Proc. Natl. Acad. Sci. USA*. 100:4574–4579.

Cimini, D., B. Howell, P. Maddox, A. Khodjakov, F. Degrassi, and E.D. Salmon. 2001. Merotelic kinetochore orientation is a major mechanism of aneuploidy in mitotic mammalian tissue cells. *J. Cell Biol.* 153:517–527.

Dai, W., Q. Wang, T. Liu, M. Swamy, Y. Fang, S. Xie, R. Mahmood, Y.M. Yang, M. Xu, and C.V. Rao. 2004. Slippage of mitotic arrest and enhanced tumor development in mice with BubR1 haploinsufficiency. *Cancer Res.* 64:440–445.

de Boer, J., J.O. Andressoo, J. de Wit, J. Huijmans, R.B. Beems, H. van Steeg, G. Weeda, G.T. van der Horst, W. van Leeuwen, A.P. Themmen, et al. 2002. Premature aging in mice deficient in DNA repair and transcription. *Science*. 296:1276–1279.

Dobles, M., V. Liberal, M.L. Scott, R. Benezra, and P.K. Sorger. 2000. Chromosome missegregation and apoptosis in mice lacking the mitotic checkpoint protein Mad2. *Cell*. 101:635–645.

Draviam, V.M., S. Xie, and P.K. Sorger. 2004. Chromosome segregation and genomic stability. *Curr. Opin. Genet. Dev.* 14:120–125.

Fang, G., H. Yu, and M.W. Kirschner. 1998. The checkpoint protein MAD2 and the mitotic regulator CDC20 form a ternary complex with the anaphase-promoting complex to control anaphase initiation. *Genes Dev.* 12:1871–1883.

Hanks, S., K. Coleman, S. Reid, A. Plaja, H. Firth, D. Fitzpatrick, A. Kidd, K. Mehes, R. Nash, N. Robin, et al. 2004. Constitutional aneuploidy and cancer predisposition caused by biallelic mutations in BUB1B. *Nat. Genet.* 36:1159–1161.

Harris, S.L., and A.J. Levine. 2005. The p53 pathway: positive and negative feedback loops. *Oncogene*. 24:2899–2908.

Hasty, P., J. Campisi, J. Hoeijmakers, H. van Steeg, and J. Vijg. 2003. Aging and genome maintenance: lessons from the mouse? *Science*. 299:1355–1359.

Jallepalli, P.V., and C. Lengauer. 2001. Chromosome segregation and cancer: cutting through the mystery. *Nat. Rev. Cancer*. 1:109–117.

Jeganathan, K.B., L. Malureanu, and J.M. van Deursen. 2005. The Rae1-Nup98 complex prevents aneuploidy by inhibiting securin degradation. *Nature*. 438:1036–1039.

Kajii, T., T. Ikeuchi, Z.Q. Yang, Y. Nakamura, Y. Tsuji, K. Yokomori, M. Kawamura, S. Fukuda, S. Horita, and A. Asamoto. 2001. Cancer-prone syndrome of mosaic variegated aneuploidy and total premature chromatid separation: report of five infants. *Am. J. Med. Genet.* 104:57–64.

Kalitsis, P., E. Earle, K.J. Fowler, and K.H. Choo. 2000. Bub3 gene disruption in mice reveals essential mitotic spindle checkpoint function during early embryogenesis. *Genes Dev.* 14:2277–2282.

Kalitsis, P., K.J. Fowler, B. Griffiths, E. Earle, C.W. Chow, K. Jamsen, and K.H. Choo. 2005. Increased chromosome instability but not cancer predisposition in haploinsufficient Bub3 mice. *Genes Chromosomes Cancer*. 44:29–36.

Kane, G.C., A. Behfar, S. Yamada, C. Perez-Terzic, F. O'Cochlain, S. Reyes, P.P. Dzeja, T. Miki, S. Seino, and A. Terzic. 2004. ATP-sensitive K+ channel knockout compromises the metabolic benefit of exercise training, resulting in cardiac deficits. *Diabetes*. 53:S169–S175.

Kaplan, K.B., A.A. Burds, J.R. Swedlow, S.S. Bekir, P.K. Sorger, and I.S. Nathke. 2001. A role for the Adenomatous Polyposis Coli protein in chromosome segregation. *Nat. Cell Biol.* 3:429–432.

Kasper, L.H., P.K. Brindle, C.A. Schnabel, C.E. Pritchard, M.L. Cleary, and J.M. van Deursen. 1999. CREB binding protein interacts with nucleoporin-specific FG repeats that activate transcription and mediate NUP98-HOXA9 oncogenicity. *Mol. Cell. Biol.* 19:764–776.

Kops, G.J., D.R. Foltz, and D.W. Cleveland. 2004. Lethality to human cancer cells through massive chromosome loss by inhibition of the mitotic checkpoint. *Proc. Natl. Acad. Sci. USA*. 101:8699–8704.

Kops, G.J., B.A. Weaver, and D.W. Cleveland. 2005. On the road to cancer: aneuploidy and the mitotic checkpoint. *Nat. Rev. Cancer*. 5:773–785.

Kraemer, D., and G. Blobel. 1997. mRNA binding protein mrnp 41 localizes to both nucleus and cytoplasm. *Proc. Natl. Acad. Sci. USA*. 94:9119–9124.

Larsen, N.A., and S.C. Harrison. 2004. Crystal structure of the spindle assembly checkpoint protein Bub3. *J. Mol. Biol.* 344:885–892.

Lengauer, C., K.W. Kinzler, and B. Vogelstein. 1998. Genetic instabilities in human cancers. *Nature*. 396:643–649.

Lombard, D.B., K.F. Chua, R. Mostoslavsky, S. Franco, M. Gostissa, and F.W. Alt. 2005. DNA repair, genome stability, and aging. *Cell*. 120:497–512.

MacIntosh, C., J.E. Morley, and I.M. Chapman. 2000. The anorexia of aging. *Nutrition*. 16:983–995.

Meraldi, P., V.M. Draviam, and P.K. Sorger. 2004. Timing and checkpoints in the regulation of mitotic progression. *Dev. Cell*. 7:45–60.

Michel, L.S., V. Liberal, A. Chatterjee, R. Kirchwegger, B. Pasche, W. Gerald, M. Dobles, P.K. Sorger, V.V. Murty, and R. Benezra. 2001. MAD2 haploinsufficiency causes premature anaphase and chromosome instability in mammalian cells. *Nature*. 409:355–359.

Michel, L., E. Diaz-Rodriguez, G. Narayan, E. Hernando, V.V. Murty, and R. Benezra. 2004. Complete loss of the tumor suppressor MAD2 causes premature cyclin B degradation and mitotic failure in human somatic cells. *Proc. Natl. Acad. Sci. USA*. 101:4459–4464.

Myung, K., S. Smith, and R.D. Kolodner. 2004. Mitotic checkpoint function in the formation of gross chromosomal rearrangements in *Saccharomyces cerevisiae*. *Proc. Natl. Acad. Sci. USA*. 101:15980–15985.

Nagy, T.R., and A.L. Clair. 2000. Precision and accuracy of dual-energy X-ray absorptiometry for determining in vivo body composition of mice. *Obes. Res.* 8:392–398.

Nasmyth, K., and C.H. Haering. 2005. The structure and function of SMC and kleisin complexes. *Annu. Rev. Biochem.* 74:595–648.

O'Cochlain, D.F., C. Perez-Terzic, S. Reyes, G.C. Kane, A. Behfar, D.M. Hodgson, J.A. Strommen, X.K. Liu, W. van den Broek, D.G. Wansink, et al. 2004. Transgenic overexpression of human DMPK accumulates into hypertrophic cardiomyopathy, myotonic myopathy and hypotension traits of myotonic dystrophy. *Hum. Mol. Genet.* 13:2505–2518.

Peters, J.M. 2002. The anaphase-promoting complex: proteolysis in mitosis and beyond. *Mol. Cell*. 9:931–943.

Plaja, A., T. Vendrell, D. Smeets, E. Sarret, T. Gili, V. Catala, C. Mediano, and J.M. Scheres. 2001. Variegated aneuploidy related to premature centromere division (PCD) is expressed in vivo and is a cancer-prone disease. *Am. J. Med. Genet.* 98:216–223.

Pritchard, C.E., M. Fornerod, L.H. Kasper, and J.M. van Deursen. 1999. RAE1 is a shuttling mRNA export factor that binds to a GLEBS-like NUP98 motif at the nuclear pore complex through multiple domains. *J. Cell Biol.* 145:237–254.

Rajagopalan, H., and C. Lengauer. 2004. Aneuploidy and cancer. *Nature*. 432:338–341.

Rieder, C.L., and H. Maiato. 2004. Stuck in division or passing through: what happens when cells cannot satisfy the spindle assembly checkpoint. *Dev. Cell*. 7:637–651.

Shah, J.V., and D.W. Cleveland. 2000. Waiting for anaphase: Mad2 and the spindle assembly checkpoint. *Cell*. 103:997–1000.

Shin, H.J., K.H. Baek, A.H. Jeon, M.T. Park, S.J. Lee, C.M. Kang, H.S. Lee, S.H. Yoo, D.H. Chung, Y.C. Sung, et al. 2003. Dual roles of human BubR1, a mitotic checkpoint kinase, in the monitoring of chromosomal instability. *Cancer Cell*. 4:483–497.

Sudakin, V., G.K. Chan, and T.J. Yen. 2001. Checkpoint inhibition of the APC/C in HeLa cells is mediated by a complex of BUBR1, BUB3, CDC20, and MAD2. *J. Cell Biol.* 154:925–936.

Tang, Z., R. Bharadawaj, B. Li, and H. Yu. 2001. Mad2-independent inhibition of APC^{Cdc20} by the mitotic checkpoint protein BUBR1. *Dev. Cell*. 1:227–237.

Tran, D.D., C.E. Edgar, K.L. Heckman, S.L. Sutor, C.J. Huntoon, J. van Deursen, D.L. McKean, and R.J. Bram. 2005. CAML is a p56Lck-interacting protein that is required for thymocyte development. *Immunity*. 23:139–152.

Tyner, S.D., S. Venkatachalam, J. Choi, S. Jones, N. Ghebranious, H. Igelmann, X. Lu, G. Soron, B. Cooper, C. Brayton, et al. 2002. p53 mutant mice that display early ageing-associated phenotypes. *Nature*. 415:45–53.

Waizenegger, I., J.F. Gimenez-Abian, D. Wernic, and J.M. Peters. 2002. Regulation of human separase by securin binding and autocleavage. *Curr. Biol.* 12:1368–1378.

Wang, Q., T. Liu, Y. Fang, S. Xie, X. Huang, R. Mahmood, G. Ramaswamy, K.M. Sakamoto, Z. Darzynkiewicz, M. Xu, and W. Dai. 2004. BUBR1 deficiency results in abnormal megakaryopoiesis. *Blood*. 103:1278–1285.

Weaver, B.A., and D.W. Cleveland. 2005. Decoding the links between mitosis, cancer, and chemotherapy: the mitotic checkpoint, adaptation, and cell death. *Cancer Cell*. 8:7–12.

Wu, X., L.H. Kasper, R.T. Mantcheva, G.T. Mantchev, M.J. Springett, and J.M. van Deursen. 2001. Disruption of the FG nucleoporin NUP98 causes selective changes in nuclear pore complex stoichiometry and function. *Proc. Natl. Acad. Sci. USA*. 98:3191–3196.

Yoon, Y.M., K.H. Baek, S.J. Jeong, H.J. Shin, G.H. Ha, A.H. Jeon, S.G. Hwang, J.S. Chun, and C.W. Lee. 2004. WD repeat-containing mitotic checkpoint proteins act as transcriptional repressors during interphase. *FEBS Lett.* 575:23–29.

Yu, H. 2002. Regulation of APC-Cdc20 by the spindle checkpoint. *Curr. Opin. Cell Biol.* 14:706–714.

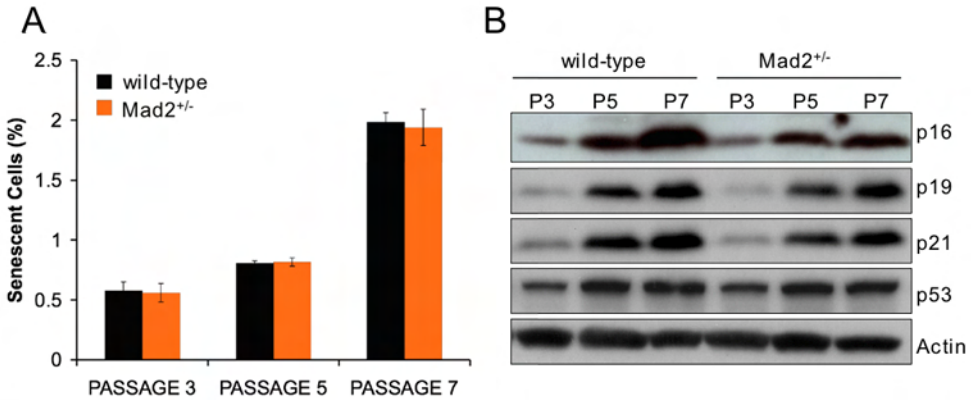

C

Mad2$^{+/-}$ mouse ID	Age at death	Tumors	Tumor Type	Aging*
MT1543	27 months	No		No
MT1403	24 months	Yes	Lymphoma	No
MT1405	23 months	Yes	Lymphoma	No
MT3219	22 months	Yes	Sarcoma	No
MT3322	22 months	No		No
MT1407	20 months	No		No
MT1972	19 months	No		No
MT1408	17 months	Yes	Lymphoma	No

* Mice were monitored for overt aging-related phenotypes (lordokyphosis, cataracts and weight loss)

D

Mad2$^{+/-}$ mouse ID	Age	Mitotic figures inspected	Percent aneuploid figures	Karyotypes with indicated # of chromosomes						Percent mitotic figures with PMSCS
				38	39	40	41	42	43	
MT1538	5 months	50	18	2		41	6	1		17
MT1539	5 months	50	16	2	1	42	4		1	17
MT1540	5 months	50	20	4	2	40	3	1		20

Figure S1

Mad2 haploinsufficiency leads to aneuploidy but does not seem to accelerate cellular senescence or aging. (A) Analysis of Mad2$^{+/-}$ MEFs for premature senescence. MEFs of indicated passages were stained for SA-ß-galactosidase activity. Note that the rate of cellular senescence in wild-type and Mad2$^{+/-}$ MEFs is similar at each passage. (B) Western blot analysis of serial passage MEF cell lysates for the senescence-associated markers p16, p19, p21 and p53. (C) Analysis of a cohort of 8 Mad2$^{+/-}$ mice for development of tumors and overt aging-associated phenotypes. (D) Karyotype analysis of splenocytes from 5-month-old Mad2$^{+/-}$ mice.

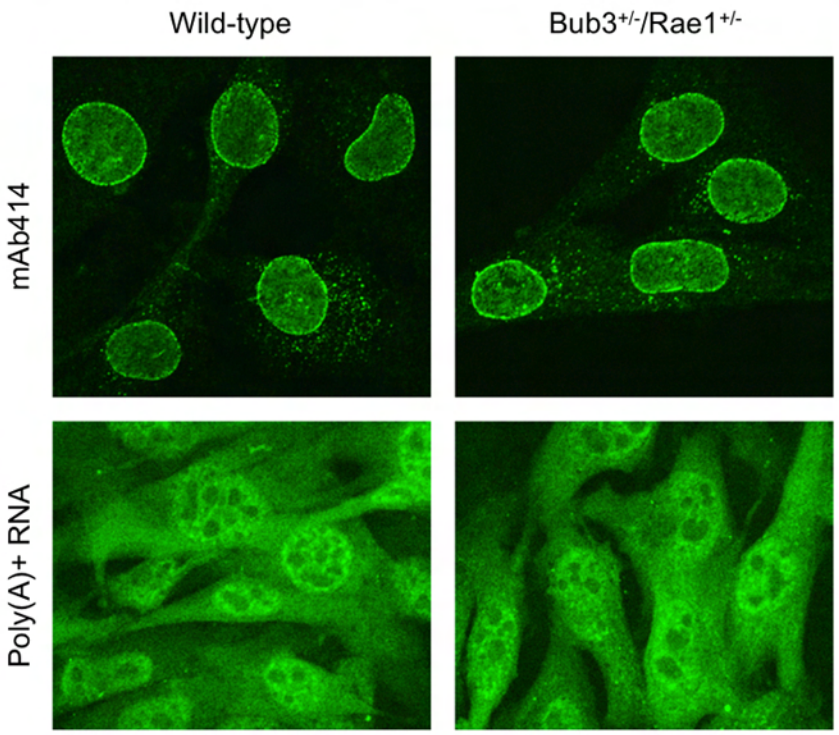

Figure S2

Bub3$^{+/-}$/Rae1$^{+/-}$ MEFs exhibit no overt defects in NPC architecture and mRNA export. (Top panels) Immunostaining with monoclonal antibody mAb414. This antibody recognizes a series of FG repeat-containing nucleoporins, including Nup358, Nup214, Nup153, Nup98 and p62. Note that the intensity of nuclear rim staining is similar in MEFs of both genotypes. In addition, we noticed no difference in nuclear pore density between wild-type and Bub3$^{+/-}$/Rae1$^{+/-}$ (data not shown). (Bottom panels) Localization of polyadenylated RNA. A biotin-labeled oligo(dT)$_{50}$ probe was used for *in situ* hybridization. mRNA-bound probe was then visualized by FITC-conjugated streptavidin. Note that the distribution patterns of polyadenylated RNA are similar in wild-type and Bub3$^{+/-}$/Rae1$^{+/-}$ MEFs.

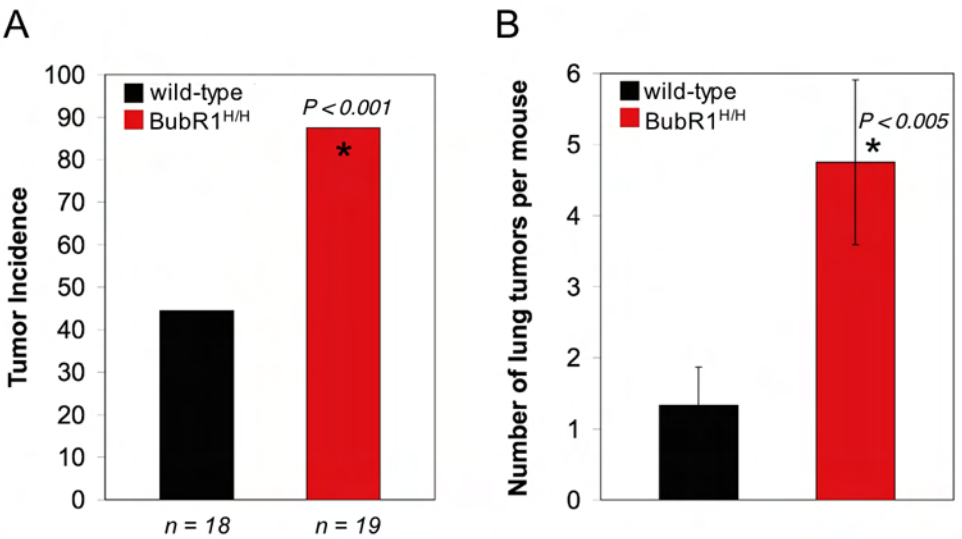

Figure S3

DMBA-induced tumor formation in BubR1$^{H/H}$ mice. (A) The occurrence of lung tumors in 4-month-old mice plotted as percentage incidence. The asterisk mark values that are significantly different from wild-type using a Chi-squared test. (B) The average number of lung adenomas per mouse (±SEM). The asterisk mark values that are significantly different from wild-type using a Wilcoxon rank sum test.

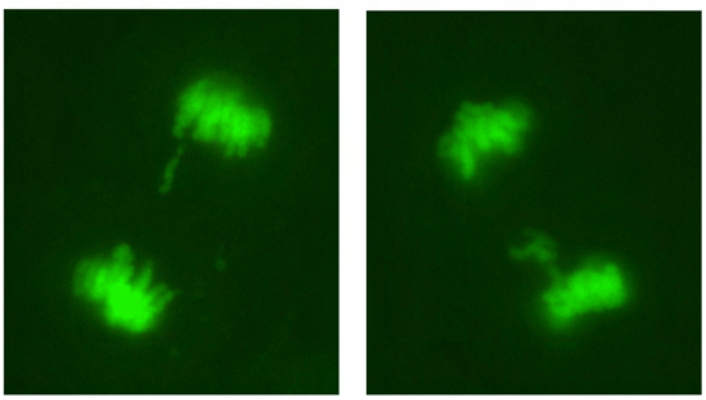

Figure S4

Representative images of BubR1$^{H/H}$ MEFs with lagging chromosomes captured by live-cell imaging. BubR1$^{H/H}$ MEFs were transduced with a retrovirus carrying an YFP-tagged H2B gene for visualization of chromosomes.

Chapter 7

Securin associated with APC^{Cdh1} in prometaphase but its destruction is delayed by Rae1 and Nup98 until the metaphase/anaphase transition

Cell Cycle 5, 366-370
Reprinted with permission

Securin Associates with APC^{Cdh1} in Prometaphase but its Destruction is Delayed by Rae1 and Nup98 until the Metaphase/Anaphase Transition

Karthik B. Jeganathan

Darren J. Baker

Jan M. van Deursen*

Departments of Pediatric and Adolescent Medicine, Biochemistry and Molecular Biology; Mayo College of Medicine; Rochester, Minnesota USA

*Correspondence to: Jan van Deursen; Departments of Pediatric and Adolescent Medicine, Biochemistry and Molecular Biology; Mayo College of Medicine; 200 First Street SW; Rochester, Minnesota 55905 USA; Tel.: 507.284.2524; Fax: 507.284.3383; Email: vandeursen.jan@mayo.edu

Original manuscript submitted: 01/05/06
Revised manuscript submitted: 01/06/06
Manuscript accepted: 01/06/06

Previously published online as a Cell Cycle E-publication:
http://www.landesbioscience.com/journals/cc/abstract.php?id=2483

KEY WORDS

Nup98, Rae1, anaphase promoting complex (APC), Cdh1, securin, tumorigenesis, spindle assembly checkpoint, aneuploidy

ACKNOWLEDGEMENTS

We thank Caili Tong and Michael Thompson for excellent technical assistance, Debbie Pearson and Janine van Ree for helpful comments on the manuscript. This work was supported by NIH grants CA77262 (J.v.D.) and CA96985 (J.v.D).

ABSTRACT

Precisely timed ubiquitin-mediated proteolysis of mitotic regulators by the anaphase-promoting complex (APC) governs the orderly passage of cells through mitosis. The established view is that Cdc20-activated APC (APC^{Cdc20}) mediates the destruction of cyclin B and securin at the metaphase/anaphase transition, and that Cdh1-activated APC (APC^{Cdh1}) has no role in this process. We recently reported that securin, but not cyclin B, is prematurely targeted for destruction by the APC in mutant mice that have low levels of the nuclear transport factors Rae1 and Nup98. We found that Rae1 and Nup98 assemble into a complex with APC^{Cdh1} in prometaphase and act to delay APC^{Cdh1}-mediated ubiquitination of securin until the metaphase/anaphase transition. Here we show that Rae1 and Nup98 not only form a complex with APC^{Cdh1} in prometaphase but also with securin. This finding suggests that the Rae1-Nup98 complex does not inhibit early destruction of securin by preventing APC^{Cdh1} from binding to securin, but by preventing ubiquitination of APC^{Cdh1}-bound securin. We propose that the formation of APC^{Cdh1}-securin complexes in prometaphase primes the cell for rapid securin degradation after release of the inhibitory Rae1-Nup98 complex at the metaphase/anaphase transition. We further report here that mutant mice with low levels of the Rae1-Nup98 complex are not prone to develop spontaneous tumors, despite massive aneuploidy. However, Rae1/Nup98 mutant mice are significantly more susceptible to DMBA-induced lung tumors than wild-type mice, indicating that combined Rae1/ Nup98 haplo-insufficiency does promote tumorigenesis when certain cancer-critical genes are also mutated.

The regulatory networks that direct orderly progression through mitosis are very complex and only partly understood. Important steps in the mitotic process are known to be regulated through the actions of the APC, a large multi-protein E3-ubiquitin ligase that targets key mitotic regulators for degradation by the proteosome.[1-3] These proteins include cyclin A and B, Nek2, securin, Cdc20, aurora A and B, and Plk1. The APC is activated in prometaphase and remains active until late G_1 but its ligase activity is tightly controlled by various mechanisms to ensure proper timing of degradation of each of its substrates.[4] Initial activation of the APC involves phosphorylation of various APC subunits by the mitotic kinases Cdk1/cyclin B and Plk1[5-7] and the subsequent recruitment of the activator protein Cdc20.[8-10] In prometaphase, Cdc20-activated APC mediates proteolysis of cyclin A,[11,12] while at the metaphase-anaphase transition it targets cyclin B and securin for destruction to allow for separase activation, sister chromatid separation and initiation of anaphase.[2,13-16] Following cyclin B destruction, phosphatases remove inhibitory phosphates from the Cdc20-related activator Cdh1, which allows formation of Cdh1-activated APC that targets Cdc20 for destruction.[10,17] Besides activators, several inhibitors control the appropriate timing of APC-mediated substrate degradation. One such inhibitor, Emi1, has been shown to delay APC activation at the beginning of mitosis by binding to Cdc20.[18] Furthermore, mitotic checkpoint protein complexes consisting of BubR1, Bub3 and Mad2 bind to and inhibit APC^{Cdc20} to prevent degradation of cyclin B and securin until all chromosomes are properly attached to the mitotic spindle and aligned in the metaphase plate.[19-21] A recent study using *Xenopus laevis* egg extracts suggests that the ubiquitin ligase Xnf7 functions as an additional inhibitor of APC-mediated degradation of cyclin B and securin.[22]

Our latest work on the nuclear transport factors Nup98 and Rae1 has challenged several aspects of the above model of APC activation and substrate destruction.[23] We found that mutant mice that express low levels of both Nup98 and Rae1 exhibit premature sister chromatid separation and massive aneuploidy. In cells with low levels of Rae1 and Nup98, APC mediates destruction of securin in prometaphase instead of at the metaphase/anaphase

transition. In contrast, cyclin B is not prematurely degraded in these cells. Subsequent biochemical studies demonstrated that, in prometaphase, Rae1 and Nup98 interact with the APC to prevent degradation of securin (Fig. 1). Rae1 and Nup98 specifically bind to APC^{Cdh1} and have no affinity for APC^{Cdc20}. This was unexpected because previous studies suggested that the formation of APC^{Cdh1} in early mitosis is inhibited through phosphorylation of Cdh1. However, we found that this mechanism does not fully prevent formation of APC^{Cdh1} in early mitosis because Cdh1 coimmunoprecipitates with the APC subunit Cdc27 from prometaphase cell extracts. In fact, comparative coimmunoprecipitation experiments suggest that prometaphase cell extracts contain similar amounts of APC^{Cdc20} and APC^{Cdh1} (Fig. 2A). We found that dissociation of Rae1 and Nup98 from APC^{Cdh1} coincides with the release of BubR1 from APC^{Cdc20}. Because the release of BubR1, and its coinhibitors Bub3 and Mad2, is known to occur at the metaphase/anaphase transition to activate APC^{Cdc20} and drive cells into anaphase,[2,24] it is reasonable to assume that the dissociation of Rae1 and Nup98 from APC^{Cdh1} also occurs at this mitotic stage and for the same purpose. If APC^{Cdc20} promotes anaphase by triggering destruction of both cyclin B and securin, one would expect to see premature degradation of both of these proteins in cells with low levels of BubR1. We critically tested this by using BubR1 hypomorphic cells that express only one-tenth of normal BubR1 levels.[25] To our surprise, we found that only cyclin B was prematurely degraded. This finding suggests that Cdc20 is the primary APC activator of cyclin B destruction, but not of securin destruction. On the other hand, APC^{Cdh1} activated by release of Rae1 and Nup98 might have a more important role in the destruction of securin (Fig. 1).

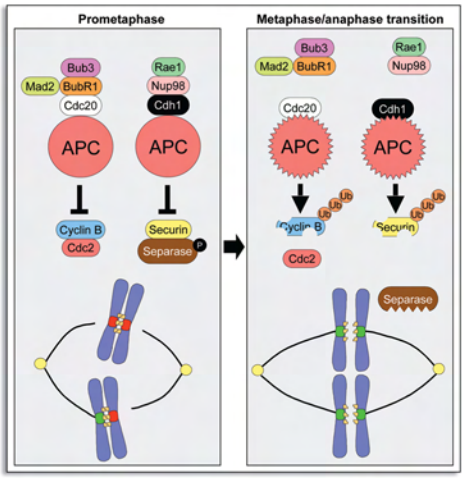

Figure 1. Timing of APC-mediated degradation of securin and cyclin B at the metaphase/anaphase transition. In prometaphase, APC^{Cdc20} is inhibited by complexes of Mad2, Bub3 and BubR1. Low levels of BubR1 result in premature degradation of cyclin B, suggesting that APC^{Cdc20} primarily ubiquitinates this substrate at the metaphase/anaphase transition following release of Mad2, Bub3 and BubR1. APC^{Cdh1} is also present in prometaphase but is inhibited by complexes of Rae1 and Nup98. Low levels of these inhibitors result in premature degradation of securin, suggesting that APC^{Cdh1} primarily ubiquitinates this substrate at the metaphase/anaphase transition after release of Nup98–Rae1 complexes from APC^{Cdh1}. It should be emphasized that it is currently unclear how the Rae1–Nup98 complex interacts with APC^{Cdh1}.

Rae1 AND Nup98 FORM A COMPLEX WITH APC^{CDH1} AND SECURIN IN PROMETAPHASE

There are several possible mechanisms by which Rae1 and Nup98 might stabilize securin in prometaphase and allow for its rapid destruction at the metaphase/anaphase transition. One potential scenario is that the Rae1-Nup98 complex binds to APC^{Cdh1} and prevents recruitment of securin, and that release of Rae1 and Nup98 from APC^{Cdh1} at the metaphase/anaphase transition allows for APC^{Cdh1}-securin binding and ubiquitination. An alternative scenario is that the Rae1-Nup98 complex does not prevent APC^{Cdh1}-securin binding but instead inhibits ubiquitination of APC-bound securin until the metaphase/anaphase transition. To test for these possibilities, we assessed whether Rae1 and Nup98 not only interact with APC^{Cdh1} in prometaphase, but also with securin. We found that securin indeed coimmunoprecipitated with Nup98 and Rae1 from extracts of prometaphase-arrested HeLa cells (Fig. 2B and C). This interaction was specific because cyclin B did not precipitate with either Rae1 or Nup98 (Fig. 2B and C). In addition, securin failed to precipitate with Nup98 from G_1 or G_2 HeLa extracts (Fig. 2B), indicating that complex formation only occurs in M phase. In the reverse experiment, Rae1 and Nup98 coimmunoprecipitated with securin (Fig. 2D). Securin also coprecipitated the APC subunit Cdc27 and Cdh1 (Fig. 2D). By contrast, neither Rae1 nor Nup98 coprecipitated with cyclin B, although Cdc27 did (Fig. 2E). Together, these data suggest that Rae1 and Nup98 exist in a physical complex with securin and APC^{Cdh1} prior to the onset of the metaphase/anaphase transition. These data are consistent with a model in which the Rae1-Nup98 complex functions to inhibit degradation of APC^{Cdh1}-bound securin. Formation of APC^{Cdh1}-securin complexes in prometaphase might prime the cell for swift securin degradation at the metaphase/anaphase transition (Fig. 3). It will be interesting to determine in future experiments whether mitotic cells prime themselves for rapid cyclin B destruction at the metaphase/anaphase transition through a similar mechanism. It is currently unknown how Rae1, Nup98, APC, Cdh1 and securin assemble into a complex. Perhaps the use of photocrosslinking might be helpful in identifying the contacts between these proteins. Recent work involving this method indicates that Cdh1 establishes direct connections with both the Cdc27 subunit of the APC and the D box and KEN boxes of APC substrates.[26,27] Another study, however, suggests that the APC interacts directly with the D box.[28] Release of BubR1 from APC^{Cdc20} is regulated by the spindle assembly checkpoint and it will be interesting to determine whether dissociation of Rae1 and Nup98 from APC^{Cdh1} is also controlled by this checkpoint, and, if so, how. Nup98 is not targeted to kinetochores at the onset of mitosis, but Rae1 is.[29] Rae1 has been shown to form a complex with Bub1 and might target to kinetochores in conjunction with this partner, just like the Rae1-related mitotic checkpoint protein Bub3.[29,30] One possibility is that complexes consisting of Rae1 and Bub1 at kinetochores contribute to the generation of the so-called "anaphase wait" signal that targets inhibitory complexes to the APC.

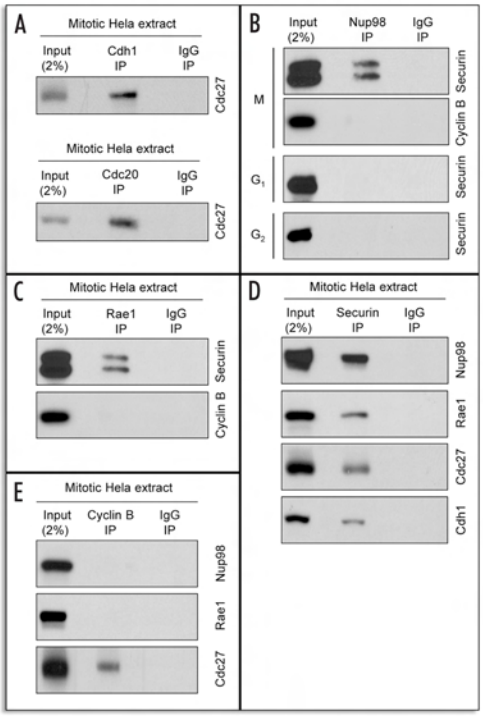

Figure 2. The Rae1–Nup98 complex binds to securin but not cyclin B in early mitosis. (A) Immunoblots of mitotic HeLa extracts subjected to immunoprecipitation with the indicated antibodies and probed with anti-Cdc27 antibody. (B) Immunoblots of mitotic (M), G_1 or G_2 HeLa extracts subjected to immunoprecipitation with Nup98 antibody. Immunoprecipitated proteins were analyzed by immunoblot analysis with the indicated antibodies. (C–E) Immunoblots of mitotic HeLa extracts subjected to immunoprecipitation with the indicated antibodies. Immunoprecipitated proteins were analyzed by immunoblot analysis with the indicated antibodies. In lanes marked "2% input", 5 µl of the 250 µl HeLa extract used per immunoprecipitation was loaded. Methods to conduct the experiments presented in this figure were as previously described.[23]

Rae1$^{+/-}$/Nup98$^{+/-}$ MICE ARE NOT PRONE TO SPONTANEOUS TUMORS DESPITE HIGH ANEUPLOIDY

Chromosome number instability is a trait of most human cancers but how aneuploidy develops and contributes to the malignant phenotype has not been firmly established. Rae1$^{+/-}$/Nup98$^{+/-}$ mice develop severe aneuploidy at an early age[23] and, therefore, provide an excellent model for critical testing of the role of chromosome number instability in tumor development. We monitored a cohort of 91 wild-type and 50 Rae1$^{+/-}$/Nup98$^{+/-}$ mice for about three years and performed biopsies on moribund animals to screen for spontaneous tumors. Comparison of the wild-type and Rae1$^{+/-}$/Nup98$^{+/-}$ tumor-free survival curves revealed no significant difference (Fig. 4A). Futhermore, Rae1$^{+/-}$/Nup98$^{+/-}$ and wild-type mice had a similar spectrum of tumors (Fig. 4B). Thus, despite high rates of chromosome missegregation, spontaneous tumor formation is not affected in Rae1$^{+/-}$/Nup98$^{+/-}$ mice in comparison to wild-type animals.

INCREASED RISK FOR CARCINOGEN-INDUCED TUMORS IN Rae1$^{+/-}$/Nup98$^{+/-}$ MICE

In addition, we performed a tumor bioassay to determine whether mice with chromosome number instability have increased susceptibility to carcinogen-induced tumorigenesis. In essence, we administered a single dose of 0.5% DMBA in acetone to the dorsal skin of 3- to 5-day-old pups generated from Rae1$^{+/-}$ times Nup98$^{+/-}$ intercrosses. After 5 months, we sacrificed the mice and screened them for tumors. Common sites of tumor formation in DMBA-treated animals include the skin, lung and thymus. We found that tumors formed only in the lungs of these mice, regardless of the genotype (Fig. 4C and D). Consistent with our earlier work,[31] Rae1$^{+/-}$ mice had an increased tumor incidence (Fig. 4C) and an increased tumor burden (Fig. 4D). Nup98$^{+/-}$ mice, which show no chromosome number instability at five months, had a similar incidence and tumor number to wild-type mice. Like Rae1$^{+/-}$ mice, Rae1$^{+/-}$/Nup98$^{+/-}$ mice exhibited an increased predisposition to DMBA-induced lung tumor formation (Fig. 4C and D). Although the incidence and number of tumors displayed in these mice were slightly higher than in Rae1$^{+/-}$ mice, the differences were not statistically significant. Thus, although Rae1$^{+/-}$/Nup98$^{+/-}$ mice are much more aneuploid than Rae1$^{+/-}$ mice, the added aneuploidy does not seem to predispose them to additional chemically induced tumors.

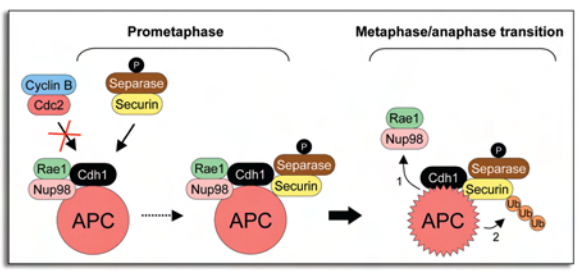

Figure 3. Hypothetical model for selective securin degradation by APC^{Cdh1}. In prometaphase, Rae1 and Nup98 form a complex with Cdh1-bound APC and securin, but not with cyclin B. This complex remains intact until the metaphase/anaphase transition, which commences when all kinetochores are attached to the mitotic spindle and chromosomes are aligned in the metaphase plate. At the onset of the metaphase/anaphase transition, the inhibitory Rae1-Nup98 complex is released from the APC^{Cdh1}-securin complex (1), thereby allowing rapid ubiquitination of securin (2). Subsequent proteolysis of securin releases separase.

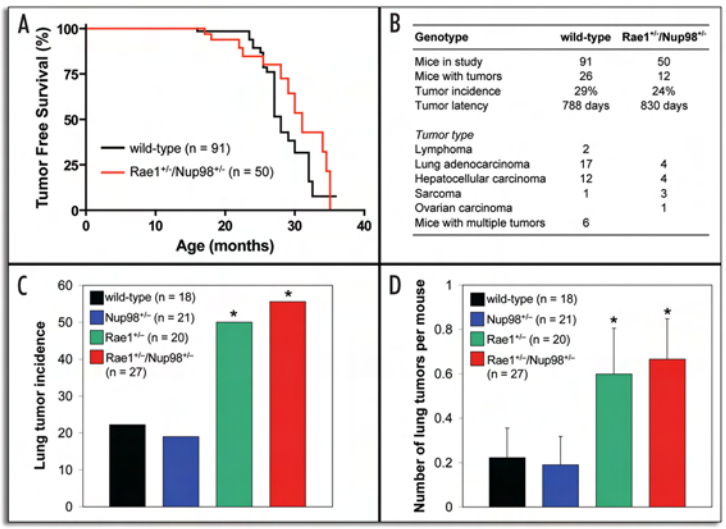

Figure 4. Rae1$^{+/-}$/Nup98$^{+/-}$ mice show increased susceptibility to DMBA-induced tumors but not spontaneous tumors. (A) Tumor-free survival curves of wild-type and Rae1$^{+/-}$/Nup98$^{+/-}$ mice. We note that these curves are not significantly different from each other using a log-rank test.[31] (B) Spontaneous tumor formation spectrum in wild-type and Rae1$^{+/-}$/Nup98$^{+/-}$ mice. (C) Incidence of DMBA-induced lung tumors in 5-month-old mice, plotted as a percentage. The asterisk indicates a p value of < 0.05 compared to wild-type mice by a Fisher's exact test. (D) Average number of DMBA-induced lung adenomas per mouse (SEM). The asterisks indicate a p value of < 0.05 compared to wild-type mice using a Wilcoxon Rank Sum test. DMBA treatments were done as previously described.[31]

HOW DO MITOTIC CHECKPOINT DEFECTS PROMOTE TUMORIGENESIS?

So far, every mouse model for mitotic checkpoint deficiency, with the exception of Mad2 haplo-insufficient mice,[32] has shown a normal rate of spontaneous tumorigenesis.[33] One could argue that the rate of chromosome number instability in Rae1, Bub3 or BubR1 haplo-insufficient mice is too low to be of significance, but that argument does not apply to Rae1/Nup98 double haplo-insufficient mice.[23] On the other hand, mouse models with mitotic checkpoint gene mutations are clearly prone to carcinogen-induced tumors,[31,34] suggesting that mitotic checkpoint gene defects promote tumorigenesis when certain cancer-critical genes are mutated. It will be important to identify these genes in future experiments. A recent study suggests that the tumor suppressor genes p53 and Rb do not cooperate with mitotic checkpoint gene mutations.[35] Even though mice with mitotic checkpoint gene mutations have an increased risk for carcinogen-induced tumors, there appears to be no link between the degree of aneuploidy and tumor incidence/burden. It is therefore possible that functions outside of the spindle assembly checkpoint are compromised in BubR1, Bub3 and Rae1 mutant mice, and that increased susceptibility to carcinogen-induced tumorigenesis is linked to such defects. For example, Rae1 is a nucleocytoplasmic transport factor that regulates export of mRNA from the nucleus in interphase.[36-38] Moreover, Bub3 interacts with histone deacetylases in interphase and might as such act to repress gene transcription.[39] BubR1 could function as a transcriptional regulator as well[39] and appears to play a role in apoptosis.[40]

References

1. Harper JW, Burton JL, Solomon MJ. The anaphase-promoting complex: It's not just for mitosis any more. Genes Dev 2002; 16:2179-206.
2. Peters JM. The anaphase-promoting complex: Proteolysis in mitosis and beyond. Mol Cell 2002; 9:931-43.
3. Yanagida M. Basic mechanism of eukaryotic chromosome segregation. Philos Trans R Soc Lond B Biol Sci 2005; 360:609-21.
4. Murray AW. Recycling the cell cycle: Cyclins revisited. Cell 2004; 116:221-34.
5. Shteinberg M, Protopopov Y, Listovsky T, Brandeis M, Hershko A. Phosphorylation of the cyclosome is required for its stimulation by Fizzy/cdc20. Biochem Biophys Res Commun 1999; 260:193-8.
6. Rudner AD, Murray AW. Phosphorylation by Cdc28 activates the Cdc20-dependent activity of the anaphase-promoting complex. J Cell Biol 2000; 149:1377-90.
7. Golan A, Yudkovsky Y, Hershko A. The cyclin-ubiquitin ligase activity of cyclosome/APC is jointly activated by protein kinases Cdk1-cyclin B and Plk. J Biol Chem 2002; 277:15552-7.
8. Fang G, Yu H, Kirschner MW. Direct binding of CDC20 protein family members activates the anaphase- promoting complex in mitosis and G_1. Mol Cell 1998; 2:163-71.
9. Zachariae W, Schwab M, Nasmyth K, Seufert W. Control of cyclin ubiquitination by CDK-regulated binding of Hct1 to the anaphase promoting complex. Science 1998; 282:1721-4.
10. Kramer ER, Scheuringer N, Podtelejnikov AV, Mann M, Peters JM. Mitotic regulation of the APC activator proteins CDC20 and CDH1. Mol Biol Cell 2000; 11:1555-69.
11. Ohtoshi A, Maeda T, Higashi H, Ashizawa S, Hatakeyama M. Human p55(CDC)/Cdc20 associates with cyclin A and is phosphorylated by the cyclin A-Cdk2 complex. Biochem Biophys Res Commun 2000; 268:530-4.
12. Geley S, Kramer E, Gieffers C, Gannon J, Peters JM, Hunt T. Anaphase-promoting complex/cyclosome-dependent proteolysis of human cyclin A starts at the beginning of mitosis and is not subject to the spindle assembly checkpoint. J Cell Biol 2001; 153:137-48.
13. Kops GJ, Weaver BA, Cleveland DW. On the road to cancer: Aneuploidy and the mitotic checkpoint. Nat Rev Cancer 2005; 5:773-85.
14. Nasmyth K, Haering CH. The structure and function of SMC and kleisin complexes. Annu Rev Biochem 2005; 74:595-648.
15. Gimenez-Abian JF, Diaz-Martinez LA, Wirth KG, De la Torre C, Clarke DJ. Proteasome activity is required for centromere separation independently of securin degradation in human cells. Cell Cycle 2005; 4:1558-60.

16. Stemmann O, Gorr IH, Boos D. Anaphase Topsy-turvy: Cdk1 a securin, separase a CKI. Cell Cycle 2006; 5.
17. Kotani S, Tanaka H, Yasuda H, Todokoro K. Regulation of APC activity by phosphorylation and regulatory factors. J Cell Biol 1999; 146:791-800.
18. Reimann JD, Freed E, Hsu JY, Kramer ER, Peters JM, Jackson PK. Emi1 is a mitotic regulator that interacts with Cdc20 and inhibits the anaphase promoting complex. Cell 2001; 105:645-55.
19. Fang G, Yu H, Kirschner MW. The checkpoint protein MAD2 and the mitotic regulator CDC20 form a ternary complex with the anaphase-promoting complex to control anaphase initiation. Genes Dev 1998; 12:1871-83.
20. Sudakin V, Chan GK, Yen TJ. Checkpoint inhibition of the APC/C in HeLa cells is mediated by a complex of BUBR1, BUB3, CDC20, and MAD2. J Cell Biol 2001; 154:925-36.
21. Tang Z, Bharadawaj R, Li B, Yu H. Mad2-independent inhibition of APC^{Cdc20} by the mitotic checkpoint protein BUBR1. Developmental Cell 2001; 1:227-37.
22. Casaletto JB, Nutt LK, Wu Q, Moore JD, Etkin LD, Jackson PK, Hunt T, Kornbluth S. Inhibition of the anaphase-promoting complex by the Xnf7 ubiquitin ligase. J Cell Biol 2005; 169:61-71.
23. Jeganathan KB, Malureanu L, van Deursen JM. The Rae1-Nup98 complex prevents aneuploidy by inhibiting securin degradation. Nature 2005; 438:1036-9.
24. Kops GJ, Foltz DR, Cleveland DW. Lethality to human cancer cells through massive chromosome loss by inhibition of the mitotic checkpoint. Proc Natl Acad Sci USA 2004; 101:8699-704.
25. Baker DJ, Jeganathan KB, Cameron JD, Thompson M, Juneja S, Kopecka A, Kumar R, Jenkins RB, de Groen PC, Roche P, van Deursen JM. BubR1 insufficiency causes early onset of aging-associated phenotypes and infertility in mice. Nat Genet 2004; 36:744-9.
26. Burton JL, Tsakraklides V, Solomon MJ. Assembly of an APC-Cdh1-substrate complex is stimulated by engagement of a destruction box. Mol Cell 2005; 18:533-42.
27. Kraft C, Vodermaier HC, Maurer-Stroh S, Eisenhaber F, Peters JM. The WD40 propeller domain of Cdh1 functions as a destruction box receptor for APC/C substrates. Mol Cell 2005; 18:543-53.
28. Yamano H, Gannon J, Mahbubani H, Hunt T. Cell cycle-regulated recognition of the destruction box of cyclin B by the APC/C in *Xenopus* egg extracts. Mol Cell 2004; 13:137-47.
29. Wang X, Babu JR, Harden JM, Jablonski SA, Gazi MH, Lingle WL, de Groen PC, Yen TJ, van Deursen JM. The mitotic checkpoint protein hBUB3 and the mRNA export factor hRAE1 interact with GLE2p-binding sequence (GLEBS)-containing proteins. J Biol Chem 2001; 276:26559-67.
30. Taylor SS, Ha E, McKeon F. The human homologue of Bub3 is required for kinetochore localization of Bub1 and a Mad3/Bub1-related protein kinase. J Cell Biol 1998; 142:1-11.
31. Babu JR, Jeganathan KB, Baker DJ, Wu X, Kang-Decker N, van Deursen JM. Rae1 is an essential mitotic checkpoint regulator that cooperates with Bub3 to prevent chromosome missegregation. J Cell Biol 2003; 160:341-53.
32. Michel LS, Liberal V, Chatterjee A, Kirchwegger R, Pasche B, Gerald W, Dobles M, Sorger PK, Murty VV, Benezra R. MAD2 haplo-insufficiency causes premature anaphase and chromosome instability in mammalian cells. Nature 2001; 409:355-9.
33. Baker DJ, Chen J, van Deursen JM. The mitotic checkpoint in cancer and aging: What have mice taught us? Curr Opin Cell Biol 2005; 17:583-9.
34. Dai W, Wang Q, Liu T, Swamy M, Fang Y, Xie S, Mahmood R, Yang YM, Xu M, Rao CV. Slippage of mitotic arrest and enhanced tumor development in mice with *BubR1* haploinsufficiency. Cancer Res 2004; 64:440-5.
35. Kalitsis P, Fowler KJ, Griffiths B, Earle E, Chow CW, Jamsen K, Choo KH. Increased chromosome instability but not cancer predisposition in haploinsufficient *Bub3* mice. Genes Chromosomes Cancer 2005; 44:29-36.
36. Pritchard CE, Fornerod M, Kasper LH, van Deursen JM. RAE1 is a shuttling mRNA export factor that binds to a GLEBS-like NUP98 motif at the nuclear pore complex through multiple domains. J Cell Biol 1999; 145:237-54.
37. Kraemer D, Blobel G. mRNA binding protein mrnp 41 localizes to both nucleus and cytoplasm. Proc Natl Acad Sci USA 1997; 94:9119-24.
38. Brown JA, Bharathi A, Ghosh A, Whalen W, Fitzgerald E, Dhar R. A mutation in the *Schizosaccharomyces pombe rae1* gene causes defects in poly(A)+ RNA export and in the cytoskeleton. J Biol Chem 1995; 270:7411-9.
39. Yoon YM, Baek KH, Jeong SJ, Shin HJ, Ha GH, Jeon AH, Hwang SG, Chun JS, Lee CW. WD repeat-containing mitotic checkpoint proteins act as transcriptional repressors during interphase. FEBS Lett 2004; 575:23-9.
40. Shin HJ, Baek KH, Jeon AH, Park MT, Lee SJ, Kang CM, Lee HS, Yoo SH, Chung DH, Sung YC, McKeon F, Lee CW. Dual roles of human BubR1, a mitotic checkpoint kinase, in the monitoring of chromosomal instability. Cancer Cell 2003; 4:483-97.

Chapter 8

Bub1 mediates cell death in response to chromosome missegregation and acts to suppress spontaneous tumorigenesis

Journal of Cell Biology 179, 255-267
Reprinted with permission

Bub1 mediates cell death in response to chromosome missegregation and acts to suppress spontaneous tumorigenesis

Karthik Jeganathan,[1] Liviu Malureanu,[1] Darren J. Baker,[1] Susan C. Abraham,[3] and Jan M. van Deursen[1,2]

[1]Department of Pediatrics, [2]Department of Molecular Biology and Biochemistry, and [3]Department of Anatomic Pathology, Mayo Clinic College of Medicine, Rochester, MN 55905

The physiological role of the mitotic checkpoint protein Bub1 is unknown. To study this role, we generated a series of mutant mice with a gradient of reduced Bub1 expression using wild-type, hypomorphic, and knockout alleles. Bub1 hypomorphic mice are viable, fertile, and overtly normal despite weakened mitotic checkpoint activity and high percentages of aneuploid cells. Bub1 haploinsufficient mice, which have a milder reduction in Bub1 protein than Bub1 hypomorphic mice, also exhibit reduced checkpoint activity and increased aneuploidy, but to a lesser extent. Although cells from Bub1 hypomorphic and haploinsufficient mice have similar rates of chromosome missegregation, cell death after an aberrant separation decreases dramatically with declining Bub1 levels. Importantly, Bub1 hypomorphic mice are highly susceptible to spontaneous tumors, whereas Bub1 haploinsufficient mice are not. These findings demonstrate that loss of Bub1 below a critical threshold drives spontaneous tumorigenesis and suggest that in addition to ensuring proper chromosome segregation, Bub1 is important for mediating cell death when chromosomes missegregate.

Introduction

Accurate segregation of replicated chromosomes during mitosis is essential for the maintenance of genomic integrity. To ensure faithful chromosome segregation, eukaryotic cells have developed a surveillance network called the mitotic checkpoint that delays anaphase onset until sister kinetochores of duplicated chromosomes are properly attached to microtubules emanating from opposite spindle poles (for reviews see Kops et al., 2004; Musacchio and Salmon, 2007). Early in mitosis, various mitotic checkpoint proteins, including Bub1, Bub3, BubR1, Mad1, Mad2, and Mps1, are recruited to unattached kinetochores. These kinetochore-associated checkpoint proteins promote the formation of diffusible Mad2, BubR1, Bub3, and Cdc20 protein complexes that inhibit the anaphase-promoting complex/cyclosome (APC/C), an E3 ubiquitin ligase that drives cells into anaphase by targeting securin and cyclin B for destruction by the 26S proteasome (for reviews see Kops et al., 2005; Peters, 2006; Musacchio and Salmon, 2007). After all chromosome pairs are properly attached to the spindle and aligned in the metaphase plate, mitotic checkpoint proteins dissociate from the APC/C, thus triggering the ubiquitin-mediated destruction of securin and cyclin B. Separase, a protease that is inhibited by securin binding and cyclin B/Cdk1-mediated phosphorylation, then cleaves the kleisin subunit Scc1 of cohesin, thereby allowing sister chromatid disjunction and anaphase onset (for reviews see Nasmyth and Haering, 2005; Peters, 2006).

The discovery of the mitotic checkpoint led to speculation that mutations in mitotic checkpoint genes might play a role in the development of aneuploidy in human cancers (Jallepalli and Lengauer, 2001; Draviam et al., 2004). Over recent years, mutant mitotic checkpoint genes have indeed been identified in various human cancers, although at relatively low frequency (Weaver and Cleveland, 2006; for reviews see Kops et al., 2005; Yuen et al., 2005). The Bub1 kinase is mutated in several cancer types, including colorectal, lung and thyroid cancer, and T cell leukemia (Cahill et al., 1998; Ohshima et al., 2000; Ru et al., 2002; Shichiri et al., 2002). In addition, Bub1 expression is frequently reduced in several human cancers, including colorectal, gastric, and esophageal cancers (Shigeishi et al., 2001; Shichiri et al., 2002; Doak et al., 2004).

Bub1 is a serine/threonine protein kinase that targets to unattached kinetochores at the onset of mitosis (Roberts et al., 1994;

K. Jeganathan, L. Malureanu, and D.J. Baker contributed equally to this paper.

Correspondence to Jan M. van Deursen: vandeursen.jan@mayo.edu

Abbreviations used in this paper: APC/C, anaphase-promoting complex/cyclosome; CENP, centromere protein; ES, embryonic stem; MEF, mouse embryonic fibroblast; NEBD, nuclear envelope breakdown; PMSCS, premature separation of sister chromatids.

The online version of this article contains supplemental material.

Taylor and McKeon, 1997; Yu and Tang, 2005). There it is thought to phosphorylate Cdc20, thereby preventing Cdc20 from activating the APC/C (Chung and Chen, 2003; Chen, 2004; Tang et al., 2004a). Additionally, Bub1 is required for Mad1–Mad2 localization to unattached kinetochores. These complexes function to prevent premature APC/C activation by changing the conformation of monomeric Mad2 such that it can efficiently bind to and inhibit the APC/C coactivator Cdc20 (Luo et al., 2002, 2004; Sironi et al., 2002). Besides Mad1 and Mad2, Bub1 also recruits BubR1, Bub3, centromere protein E (CENP-E), and CENP-F to unattached kinetochores (Sharp-Baker and Chen, 2001; Johnson et al., 2004). Several of these proteins are important for microtubule-kinetochore attachment, which may explain why Bub1-depleted cells have chromosome congression defects (Meraldi and Sorger, 2005). In addition, Bub1 contributes to the stability and inner centromere localization of Shugoshin (Sgo1), a protein that functions as an adaptor for phosphatase PP2A (Tang et al., 2004b, 2006; Kitajima et al., 2005). At the inner centromere, PP2A counteracts the Plk1-mediated release of cohesin until anaphase onset, thus preventing the premature separation of sister centromeres (Riedel et al., 2006). Bub1 also controls the stability and correct positioning of the chromosomal passenger complex to the inner centromeric region of sister chromosomes, a function that appears to be critical for the recruitment of Sgo1 to centromeres (Boyarchuk et al., 2007).

Although the molecular mechanisms of Bub1 action are beginning to emerge, the physiological role of Bub1 in higher eukaryotes is still unknown. The most definitive way to address this role would be to generate Bub1 knockout mice by homologous recombination in embryonic stem (ES) cells. However, previous gene knockout studies for Mad1, Mad2, BubR1, and Bub3 revealed that these mitotic checkpoint proteins are essential for cell proliferation, causing mice to die during the early

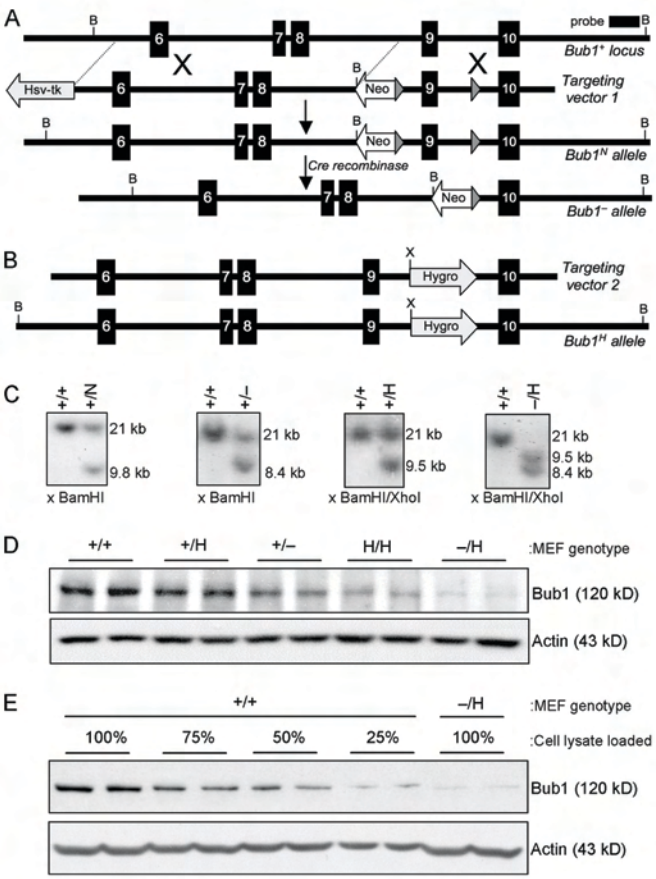

Figure 1. **Generation of mice with graded reduction in Bub1 dosage.** (A) Schematic representation of the primary Bub1 gene–targeting strategy. Part of the Bub1 locus (+), the first targeting vector with *loxP* sites (gray triangles), the Neo hypomorphic allele, the knockout allele generated by the expression of Cre recombinase (–), BamHI (B) restriction sites, and the Southern probe are indicated. (B) Schematic representation of the second Bub1 gene–targeting strategy. The second targeting vector, the Hyg hypomorphic allele, and the BamHI (B) and XhoI (X) restriction sites for Southern blotting are indicated. (C) Southern blot analysis of mice with the indicated Bub1 genotypes. The 21-kb, 9.8-kb, 8.4-kb, and 9.5-kb fragments represent the wild-type, Neo hypomorphic, knockout, and Hyg hypomorphic alleles, respectively. (D) Western blot analysis of MEFs isolated from mice carrying the indicated Bub1 alleles with a Bub1-specific antibody (actin was used as a loading control). The – and H alleles can produce truncated protein products of 267 amino acids and 318 amino acids, respectively. However, we were unable to detect these truncated products with our polyclonal antibody against Bub1(25–165) (Fig. S1, available at http://www.jcb.org/cgi/content/full/jcb.200706015/DC1), sugesting that the products are rapidly degraded and/or that their messengers are unstable. (E) Quantitation of the level of Bub1 reduction in Bub1$^{-/H}$ MEFs as compared with Bub1$^{+/+}$ MEFs.

Table I. **Inverse correlation between Bub1 expression and aneuploidy in mouse splenocytes**

Mouse genotype	Age (*n*)	Mitotic figures inspected	Aneuploid figures (SD)	Karyotypes with indicated chromosome number								Mitotic figures with PMSCS (SD)
				37	38	39	40	41	42	43	44	
	mo		%									%
$Bub1^{+/+}$	5 (3)	150	1 (1)			1	149					0 (0)
$Bub1^{+/H}$	5 (5)	250	6 (1)		2	6	236	4	2			2 (1)
$Bub1^{+/-}$	5 (3)	150	16 (2)	1	4	6	126	7	6			14 (2)
$Bub1^{H/H}$	5 (3)	150	35 (2)	3	8	9	97	16	12	5		4 (1)
$Bub1^{-/H}$	5 (3)	150	39 (2)	1	8	15	91	12	15	7	1	15 (2)

Empty spaces mean that there were no karyotypes with the indicated chromosome number.

stages of embryonic development (Dobles et al., 2000; Kalitsis et al., 2000; Babu et al., 2003; Baker et al., 2004; Wang et al., 2004; Iwanaga et al., 2007). Anticipating that Bub1-null mice would be embryonically lethal as well, we generated a series of mice in which the expression of Bub1 protein is reduced in a graded fashion from normal to zero. We find that Bub1-null mice are indeed embryonically lethal but that mice with very low levels of Bub1 protein are viable. Here, we show that Bub1 deficiency is associated with aneuploidy and spontaneous tumorigenesis in a dose-dependent fashion. Furthermore, we provide evidence for a novel role of Bub1 in eliminating cells that have undergone chromosome missegregation.

Results

Generation of mutant mice with graded reduction in Bub1 levels

By homologous recombination, we inserted a neomycin-resistance (Neo) gene flanked by a *loxP* site into intron 8 and a *loxP* site into intron 9 of the mouse Bub1 gene (Fig. 1 A). This created a hypomorphic allele (called $Bub1^{N}$) because the Neo gene harbors a cryptic exon that is known to reduce the level of normally spliced messenger RNA (Jacks et al., 1994; Meyers et al., 1998; Baker et al., 2004). Correctly targeted ES clones were injected into blastocysts, and $Bub1^{+/N}$ offspring were obtained from the resulting chimeras (Fig. 1 C). $Bub1^{+/-}$ mice were established by crossing $Bub1^{+/N}$ males with transgenic females that express Cre recombinase in the germline (Fig. 1 C). Both $Bub1^{+/N}$ and $Bub1^{+/-}$ mice were healthy and indistinguishable from wild-type littermates. Subsequent intercrosses of $Bub1^{+/-}$ mice produced no $Bub1^{-/-}$ newborn mice. Further analysis revealed that $Bub1^{-/-}$ embryos died between days 4.5 and 6.5 of development (unpublished data), which is in agreement with other mitotic checkpoint gene knockout mice. Also, no $Bub1^{N/N}$ pups were born from intercrosses of $Bub1^{+/N}$ mice, implying that the level of wild-type Bub1 protein produced by these hypomorphic alleles was not sufficient for successful embryonic development.

To bypass this problem, we created a Bub1 hypomorphic allele by the use of an alternative method. This method takes advantage of a hygromycin B phosphotransferase expression (Hyg) cassette that causes a high incidence of premature transcriptional termination when inserted into intronic sequences (van Deursen et al., 1994). We constructed a targeting vector to introduce this Hyg cassette into intron 9 of the endogenous Bub1 gene (Fig. 1 B). Properly targeted ES clones were used to produce $Bub1^{+/H}$ mice. Intercrosses of $Bub1^{+/H}$ mice yielded viable $Bub1^{H/H}$ offspring at the expected Mendelian frequency. Furthermore, interbreeding of $Bub1^{+/H}$ and $Bub1^{+/-}$ mice yielded viable $Bub1^{-/H}$ offspring with normal Mendelian frequency (Fig. 1 C). Like $Bub1^{+/-}$ mice, $Bub1^{H/H}$ and $Bub1^{-/H}$ mice exhibited no changes in development or appearance when compared with wild-type mice. We performed Western blotting to measure the level of wild-type Bub1 protein in mouse embryonic fibroblasts (MEFs) derived from $Bub1^{+/+}$, $Bub1^{+/H}$, $Bub1^{+/-}$, $Bub1^{H/H}$, and $Bub1^{-/H}$ mice (Fig. 1, D and E). We assessed that Bub1 signals from $Bub1^{+/H}$, $Bub1^{+/-}$, $Bub1^{H/H}$, and $Bub1^{-/H}$ MEFs were ~75%, 50%, 30%, and 20% of those from $Bub1^{+/+}$ MEFs,

Table II. **Gradual reduction in Bub1 causes progressively more aneuploidy in MEFs**

Mitotic MEF genotype (*n*)	Mitotic figures inspected	Aneuploid figures (SD)	SD	Karyotypes with indicated chromosome number											Mitotic figures with PMSCS (SD)
				37	38	39	40	41	42	43	44	45	46	80	
		%													%
$Bub1^{+/+}$ (3)	150	7 (1)	1		2	3	132	3	2					8	2 (1)
$Bub1^{+/H}$ (3)	150	11 (1)	1			5	123	6	6					10	2 (1)
$Bub1^{+/-}$ (3)	150	14 (0)	0		3	8	120	10						9	3 (0)
$Bub1^{H/H}$ (3)	150	35 (1)	1		4	10	88	21	10	8				9	2 (1)
$Bub1^{-/H}$ (3)	150	36 (5)	5	3	4	7	83	16	7	9	5	3	2	11	3 (0)

Empty spaces mean that there were no karyotypes with the indicated chromosome number. Karyotyping was performed at passage 5.

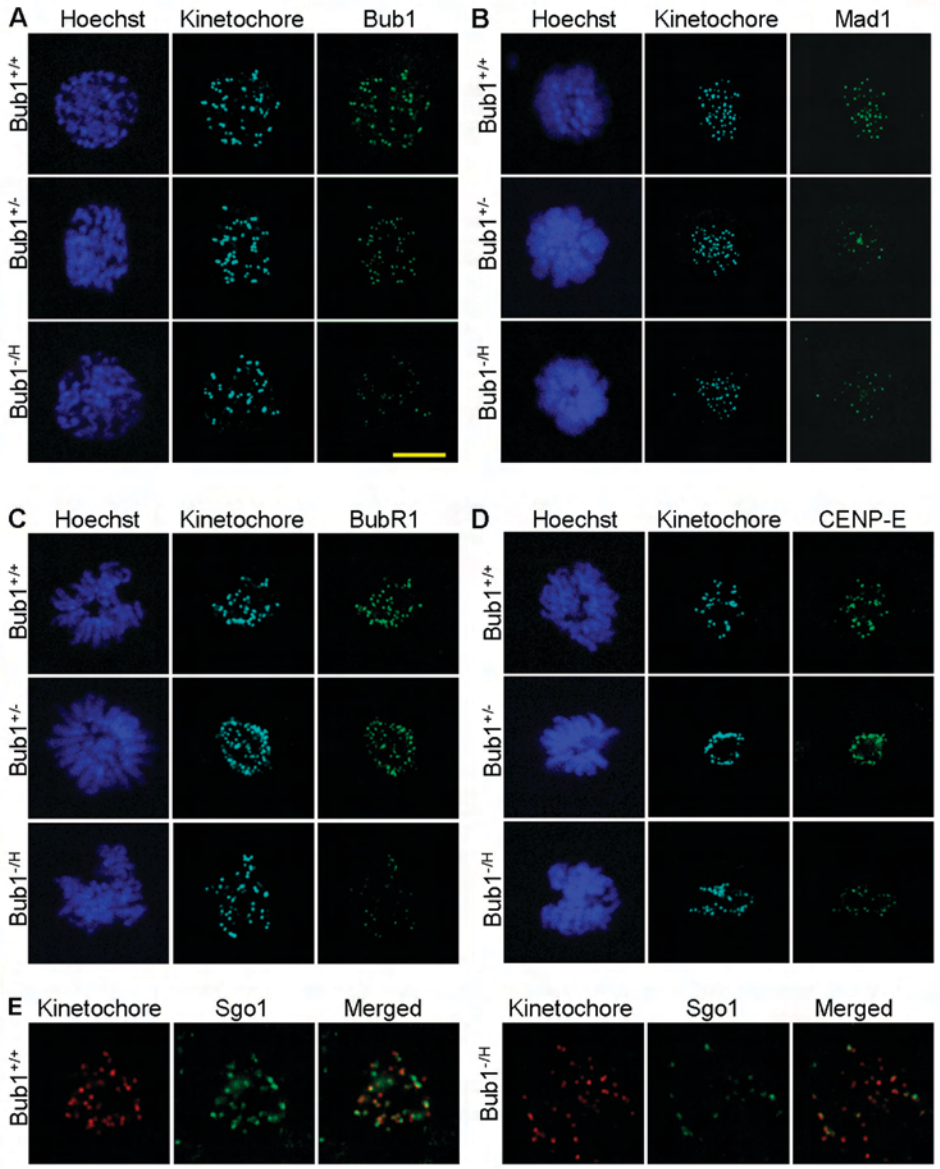

Figure 2. **Proper targeting of Mad1 to kinetochores is highly sensitive to Bub1 down-regulation.** MEFs with various levels of Bub1 expression were analyzed for the proper localization of proteins whose association with kinetochores or centromeres is known to be Bub1 dependent. (A) Fluorescent images of Bub1$^{+/+}$, Bub1$^{+/-}$, and Bub1$^{-/H}$ prophase cells stained for kinetochores, Bub1, and DNA showing that the gradual reduction of cellular Bub1 protein levels corresponds with a gradual decline in kinetochore-associated Bub1 protein. (B) Images of Bub1$^{+/+}$, Bub1$^{+/-}$, and Bub1$^{-/H}$ prometaphase cells stained for kinetochores, Mad1, and DNA demonstrating that kinetochore targeting of Mad1 is highly sensitive to Bub1 down-regulation. (C) Fluorescent images of prometaphase cells of the indicated genotypes stained for kinetochores, BubR1, and DNA showing that BubR1 localization to kinetochores is severely perturbed in Bub1$^{-/H}$ MEFs but not in Bub1$^{+/-}$ MEFs. (D) Fluorescent images of prometaphase cells of the indicated genotypes stained for kinetochores, CENP-E, and DNA demonstrating that CENP-E localization to kinetochores is impaired in Bub1$^{-/H}$ MEFs but not in Bub1$^{+/-}$ MEFs. (E) Fluorescent images of

respectively. Truncated forms of Bub1 encoded by the – and H alleles were undetectable even after overexposure of the Western blots (Fig. S1, available at http://www.jcb.org/cgi/content/full/jcb.200706015/DC1). Together, these results demonstrated that we had produced a series of mice with decreasing Bub1 protein dosage.

Mice with low amounts of Bub1 have a high percentage of aneuploid cells

To determine whether the reduced expression of Bub1 protein affects the accuracy of chromosome segregation, we collected splenocytes from $Bub1^{+/+}$, $Bub1^{+/H}$, $Bub1^{+/-}$, $Bub1^{H/H}$, and $Bub1^{-/H}$ mice at 5 mo of age and prepared metaphase spreads for karyotype analyses. Chromosome counts showed that <1% of wild-type splenocytes were aneuploid (Table I). In contrast, splenocytes from $Bub1^{+/H}$, $Bub1^{+/-}$, $Bub1^{H/H}$, and $Bub1^{-/H}$ mice had a 6%, 16%, 35%, and 39% incidence of aneuploidy, respectively, revealing an inverse correlation between the level of Bub1 protein and the percentage of aneuploidy in this cell type. Moreover, the range of abnormal chromosome numbers broadened with the decreasing expression of Bub1 protein (Table I). We observed the premature separation of sister chromatids (PMSCS) in 14 and 15% of the mitotic figures from $Bub1^{+/-}$ and $Bub1^{-/H}$ splenocytes but only in 4% of the mitotic figures from $Bub1^{H/H}$ splenocytes (Table I). Thus, there seems to be no clear link between PMSCS and Bub1 dosage in splenocytes.

We further investigated the effect of Bub1 insufficiency on chromosome number stability by performing chromosome counts on metaphase spreads from $Bub1^{+/+}$, $Bub1^{+/H}$, $Bub1^{+/-}$, $Bub1^{H/H}$, and $Bub1^{-/H}$ MEFs at passage 5. We found that the percentage of aneuploid metaphases was much higher in $Bub1^{H/H}$ and $Bub1^{-/H}$ MEFs than in $Bub1^{+/-}$ and $Bub1^{+/H}$ MEFs, which, in turn, had a higher percentage than $Bub1^{+/+}$ MEFs (Table II). PMSCS was not increased in $Bub1^{+/H}$, $Bub1^{+/-}$, $Bub1^{H/H}$, and $Bub1^{-/H}$ MEFs compared with $Bub1^{+/+}$ MEFs (Table II). These data confirm that a high percentage of cells with low levels of Bub1 become aneuploid without the apparent requirement of PMSCS.

Kinetochore-associated proteins require distinct Bub1 levels for proper localization

Many of Bub1's critical functions during mitosis occur at the kinetochore. Therefore, we tested whether the graded reduction of Bub1 expression corresponds to a graded reduction in Bub1 levels at kinetochores. Immunostaining of $Bub1^{+/+}$, $Bub1^{+/-}$, and $Bub1^{-/H}$ MEFs with affinity-purified Bub1-specific antibody showed that fluorescence signals at kinetochores progressively declined with decreasing cellular levels of Bub1 expression (Fig. 2 A). To examine how this graded reduction in kinetochore-bound Bub1 affected the localization of mitotic checkpoint proteins whose targeting to kinetochores is Bub1 dependent, we immunostained $Bub1^{+/+}$, $Bub1^{+/-}$, and $Bub1^{-/H}$ MEFs with antibodies against the mitotic checkpoint proteins Mad1, Mad2, BubR1, and CENP-E. In $Bub1^{+/+}$ prometaphase cells, Mad1 staining was concentrated on kinetochores visualized by anti-kinetochore antibody (Fig. 2 B). However, kinetochore-associated Mad1 signals were much less abundant in the corresponding $Bub1^{+/-}$ and $Bub1^{-/H}$ cells. As Mad1 is required for the kinetochore localization of Mad2 (Chen et al., 1998, 1999), we anticipated that Mad2 staining patterns would also be reduced in $Bub1^{+/-}$ and $Bub1^{-/H}$ prometaphase cells. We tested this prediction, but despite numerous attempts, we were unsuccessful in obtaining kinetochore-associated Mad2 signals in $Bub1^{+/+}$ MEFs with antibodies that are known to detect Mad2 at kinetochores of human prometaphase cells (see Materials and methods for details). Unlike Mad1, kinetochore-associated BubR1 and CENP-E signals were unaffected in $Bub1^{+/-}$ cells during prometaphase (Fig. 2, C and D). However, kinetochore signals for both of these proteins were dramatically reduced in prometaphase $Bub1^{-/H}$ cells. Western blot analysis showed that Mad1, BubR1, and CENP-E protein levels were similar in $Bub1^{+/+}$ and $Bub1^{-/H}$ cells (Fig. S2 A, available at http://www.jcb.org/cgi/content/full/jcb.200706015/DC1), excluding the possibility that the reduction in kinetochore localization of these proteins in $Bub1^{-/H}$ cells is caused by reduced protein stability.

Next, we tested how the graded reduction in kinetochore-bound Bub1 levels affected the subcellular localization of Sgo1 and Aurora B, both of which have been reported to require Bub1 for their proper localization to the centromeres (Tang et al., 2004b, 2006; Kitajima et al., 2005; Boyarchuk et al., 2007). Fewer Sgo1-positive centromeres were observed in $Bub1^{-/H}$ prometaphases than in $Bub1^{+/+}$ prometaphases (Fig. 2 E). In contrast, no such decrease was observed in $Bub1^{+/-}$ prometaphase cells (unpublished data). Immunostainings for Aurora B revealed that the localization of this protein was normal in both $Bub1^{+/-}$ and $Bub1^{-/H}$ prometaphase cells (Fig. S2 B). Thus, whereas most proteins that require Bub1 for proper localization to kinetochores/centromeres are mislocalized in $Bub1^{-/H}$ MEFs, only Mad1 is mislocalized in $Bub1^{+/-}$ cells.

Bub1 insufficient cells have a weakened mitotic checkpoint

To analyze the activity of the mitotic checkpoint in MEFs with a graded reduction in Bub1 expression, we performed a nocodazole challenge assay (Jeganathan et al., 2005; Baker et al., 2006). In this assay, MEFs were first transduced with a retrovirus encoding a YFP-tagged H2B fusion protein to allow the visualization of chromosomes by fluorescence microscopy (Fig. 3 A). MEFs were then challenged with nocodazole, and 20–30 cells undergoing nuclear envelope breakdown (NEBD) were marked and monitored at 15-min intervals to determine when their chromatin decondenses. The duration of arrest in mitosis, which is defined as the interval between NEBD (onset of mitosis) and chromatin decondensation (exit from mitosis without cytokinesis), was calculated and plotted. The time at which 50% of the cells have exited mitosis was used for comparison. Nocodazole-challenged $Bub1^{+/+}$ MEFs typically remained arrested in

$Bub1^{+/+}$ and $Bub1^{-/H}$ prometaphase cells stained for kinetochores and Sgo1 showing that considerably fewer Sgo1-positive centromeres are present in $Bub1^{-/H}$ MEFs. Bar, 10 μM.

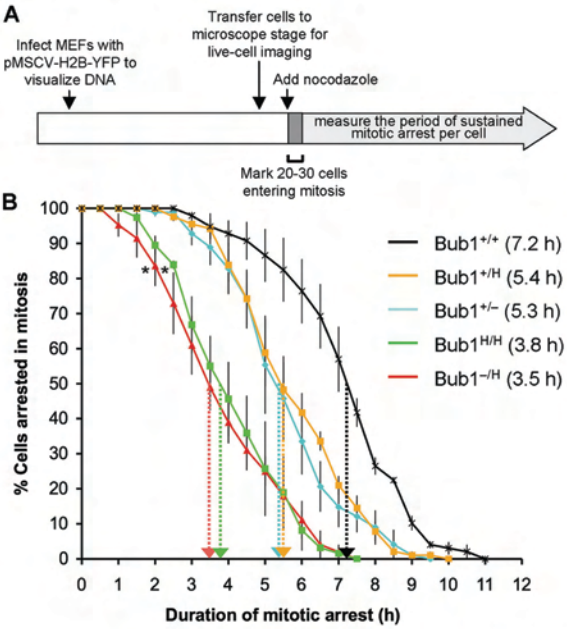

Figure 3. **Mitotic checkpoint activity analysis.** (A) Schematic of the experimental design (for details see the first two paragraphs of Results). (B) Analysis of mitotic checkpoint activity of MEFs of the indicated genotypes ($n = 3$ for each genotype). Error bars represent the SEM. Dotted arrows mark the times at which 50% of cells had exited from mitosis. Asterisks indicate a statistical difference from Bub1$^{+/+}$, Bub1$^{+/H}$, and Bub1$^{+/-}$ MEFs using the logrank test (*, $P < 0.001$).

prometaphase for 7.2 h (Fig. 3 B). Bub1$^{+/H}$ and Bub1$^{+/-}$ MEFs were impaired in their ability to maintain this arrest, with 50% of the cells exiting around 5.4 h. However, Bub1$^{H/H}$ and Bub1$^{-/H}$ MEFs exhibited a more profound defect, with 50% of the cells exiting mitosis at 3.8 h and 3.5 h, respectively. Thus, the mitotic checkpoint appears to be considerably weaker in Bub1$^{H/H}$ and Bub1$^{-/H}$ MEFs than in Bub1$^{+/H}$ and Bub1$^{+/-}$ MEFs.

Bub1 insufficiency causes various chromosome segregation defects

Next, MEFs with graded reductions in Bub1 expression were screened for chromosome segregation defects. In essence, we followed YFP-H2B–positive MEFs through an unchallenged mitosis by live cell imaging and determined the fraction of mitotic cells with chromosome segregation abnormalities. Two known defects underlying chromosome missegregation, congression failure and chromosome lagging (Fig. 4, A and B), were observed at higher rates in Bub1$^{+/H}$, Bub1$^{+/-}$, Bub1$^{H/H}$, and Bub1$^{-/H}$ MEFs than in Bub1$^{+/+}$ MEFs (Table III). The combined incidence of the aforementioned defects was remarkably similar in Bub1$^{+/H}$, Bub1$^{+/-}$, Bub1$^{H/H}$, and Bub1$^{-/H}$ MEFs (Table III). Furthermore, anaphases with centrophilic chromosomes that segregate faster than the other chromosomes (Fig. 4 C) were observed at an approximately two- to fivefold higher frequency in Bub1$^{+/H}$, Bub1$^{+/-}$, Bub1$^{H/H}$, and Bub1$^{-/H}$ MEFs than in Bub1$^{+/+}$ MEFs (Table III). Whether this type of abnormality leads to chromosome missegregation is unclear, but even with the inclusion of this defect, the overall incidence of chromosome segregation abnormalities remains very similar in Bub1$^{+/H}$, Bub1$^{+/-}$, Bub1$^{H/H}$, and Bub1$^{-/H}$ MEFs (Table III). Irrespective of Bub1 genotype, most cells with abnormal chromosome segregation events involved a single chromosome (or a duplicated chromosome). Occasionally, two or three chromosomes were implicated (Table IV and Table S1, available at http://www.jcb.org/cgi/content/full/jcb.200706015/DC1). Thus, the aforementioned analyses suggest that the accuracy of

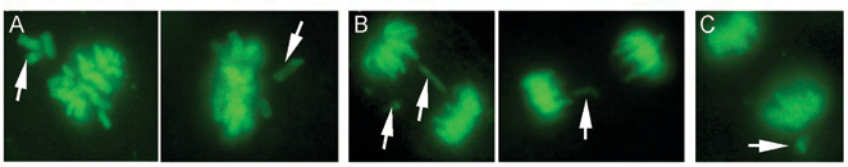

Figure 4. **Bub1 insufficiency causes various chromosome segregation errors.** (A) Examples of metaphases with misaligned chromosomes (arrows). (B) Anaphases with lagging chromosomes (arrows). (C) Anaphase with a centrophilic chromosome (arrow).

Table III. **Analysis of chromosome segregation abnormalities in Bub1-insufficient MEFs**

MEF genotype (*n*)	Mitotic cells inspected	Metaphases with misaligned chromosomes	Anaphases with lagging chromosomes	Anaphases with centrophilic chromosomes	Cells with segregation defects[a]
		%	%	%	%
$Bub1^{+/+}$ (5)	106	0.9	3.8	0.9	4.7 (5.6)
$Bub1^{+/H}$ (4)	91	3.3	6.6	3.3	9.9 (13.2)
$Bub1^{+/-}$ (6)	142	7.7	6.3	2.1	12 (14.1)
$Bub1^{H/H}$ (4)	122	6.5	4.9	4.8	11.6 (16.4)
$Bub1^{-/H}$ (5)	168	7.1	6.6	2.4	13.1 (15.5)

All cells scored as metaphases with misaligned chromosomes displayed congression failure at anaphase onset.
[a]Percentage of cells with misaligned and/or lagging chromosomes. The percentage of cells with chromosome segregation abnormalities is presented in parentheses.

chromosome segregation is highly dependent on a full complement of Bub1 protein and that both small and large reductions in Bub1 cause chromosome missegregation at comparable rates.

Reduced cell death after chromosome missegregation as Bub1 levels decline

Initially, we were surprised that chromosome missegregation rates were similar in $Bub1^{+/H}$, $Bub1^{+/-}$, $Bub1^{H/H}$, and $Bub1^{-/H}$ MEFs because the percentage of aneuploid cells was much higher in $Bub1^{H/H}$ and $Bub1^{-/H}$ cultures than in $Bub1^{+/H}$ and $Bub1^{+/-}$ cultures (Table II). One explanation could be that cell survival after chromosome missegregation increases with decreasing Bub1 levels. To explore this possibility, we infected $Bub1^{+/+}$, $Bub1^{+/H}$, $Bub1^{+/-}$, $Bub1^{H/H}$, and $Bub1^{-/H}$ MEFs with the YFP-H2B virus and monitored the fate of cells undergoing chromosome missegregation for up to 12 h by live cell imaging. Typically, 95% of $Bub1^{+/+}$ MEFs died within several hours after chromosome missegregation (Table V and Videos 5 and 6, available at http://www.jcb.org/cgi/content/full/jcb.200706015/DC1). This percentage declined progressively and sharply as Bub1 expression decreased, with only 32% of $Bub1^{-/H}$ MEFs dying after a missegregation event (Table V, Fig. 5 A, and Videos 1 and 2). Cells dying after chromosome missegregation consistently showed nuclear fragmentation and/or cytoplasmic blebbing (Fig. 5, B and C; and Videos 3, 4, 7, and 8). Cells with accurate segregation rarely died during the 12-h observation period, irrespective of Bub1 genotype (Table V and Videos 9 and 10). From this, we conclude that although the rates of chromosome missegregation are comparable at various levels of Bub1 reduction, aneuploid cells accumulate to higher steady-state levels in cultures with low amounts of the protein because cells in these cultures are more likely to survive after chromosome missegregation. Consistent with this interpretation, we found that micronuclei, which we observed by live cell imaging to result from misaligned, centrophilic, or lagging chromosomes, accumulated steadily with decreasing Bub1 levels (Fig. S3).

To explore whether Bub1 plays a more general role in cell death signaling, we measured cell survival to various kinds of DNA-damaging agents. MEFs with graded reduction in Bub1 protein levels were exposed to increasing concentrations of doxorubicin, mitomycin C, or paraquat for 48 h. Cell survival was then determined by using the MTS assay. Cell survival in these agents was similar for $Bub1^{+/+}$, $Bub1^{+/H}$, $Bub1^{+/-}$, $Bub1^{H/H}$, and $Bub1^{-/H}$ MEFs (Fig. S4, A–C; available at http://www.jcb.org/cgi/content/full/jcb.200706015/DC1). In addition, decreased Bub1 expression also did not increase survival to prolonged exposure to nocodazole, a spindle poison that induces tetraploidization by driving prometaphase cells into G1 without chromosome segregation (Fig. S4 D). These experiments suggest a rather specific role for Bub1 in mediating cell death after the missegregation of one or a few chromosomes.

Spontaneous tumorigenesis is increased in Bub1 hypomorphic mice

To determine the long-term consequences of Bub1 down-regulation, we created and monitored cohorts of $Bub1^{+/+}$ (n = 160), $Bub1^{+/-}$ (n = 142), $Bub1^{H/H}$ (n = 137), and $Bub1^{-/H}$ (n = 238) mice on a mixed 129 × C57BL/6 background. Earlier, we reported that BubR1 hypomorphic mice have a short lifespan, are infertile, and develop various early aging–associated phenotypes (Baker et al., 2004). We note that no such phenotypes were observed in any of our Bub1 mutant mice (unpublished data). However, we found that $Bub1^{-/H}$ and $Bub1^{H/H}$ mice were significantly more prone to spontaneous tumors than $Bub1^{+/+}$

Table IV. **Most chromosome missegregation events involve a single chromosome irrespective of the level of Bub1 expression**

Mitotic figures inspected (*n*)	Number of cells with segregation defects[a]	Number of cells with one abnormally segregated chromosome	Number of cells with two or three abnormally segregated chromosomes[b]
$Bub1^{+/+}$ (106)	6	6 (100%)	0 (0%)
$Bub1^{+/H}$ (91)	12	11 (92%)	1 (8%)
$Bub1^{+/-}$ (142)	20	15 (75%)	5 (25%)
$Bub1^{H/H}$ (122)	20	17 (85%)	3 (15%)
$Bub1^{-/H}$ (168)	26	21 (81%)	5 (19%)

[a]The chromosomes involved were either single chromosomes or duplicated chromosomes.
[b]None of the cells had more than three abnormally segregated chromosomes (see Table S1).

Table V. **Cell death after chromosome missegregation decreases as Bub1 expression declines**

MEF genotype (*n*)	Cells with missegregation monitored*	Apoptosis incidence	Apoptosis (1 cell)	Apoptosis (2 cells)	Cells with normal mitosis monitored	Apoptosis incidence
		%	%	%		%
$Bub1^{+/+}$ (3)	16	94	0	100	38	3
$Bub1^{+/H}$ (3)	28	68	26	74	17	6
$Bub1^{+/-}$ (3)	23	65	9	91	7	0
$Bub1^{H/H}$ (3)	26	42	12	88	16	0
$Bub1^{-/H}$ (3)	31	32	14	86	14	0

*Cells analyzed had either one or a few missegregated chromosomes.

mice (Fig. 6, A and B). $Bub1^{-/H}$ mice had a significantly shorter median tumor-free survival (530 d) than $Bub1^{H/H}$ mice (676 d), which, in turn, had a significantly shorter median tumor-free survival than $Bub1^{+/+}$ mice (772 d; Fig. 6 B). Moreover, $Bub1^{-/H}$ and $Bub1^{H/H}$ mice developed a different spectrum of tumors than did $Bub1^{+/+}$ mice (Fig. 6, C–F′). $Bub1^{-/H}$ mice developed significantly more sarcomas, lymphomas, and lung tumors. $Bub1^{H/H}$ mice were also prone to develop sarcomas but not lymphomas and lung tumors. $Bub1^{H/H}$ mice were highly susceptible to hepatocellular carcinomas, a tumor type that was not significantly increased in $Bub1^{-/H}$ mice. In contrast to $Bub1^{-/H}$ and $Bub1^{H/H}$ mice, $Bub1^{+/-}$ mice showed a trend toward decreased tumor formation, particularly in liver and lung tissue (Fig. 6, B and C). Collectively, these data establish a causal relationship between the down-regulation of Bub1 expression and cancer development and suggest that there is a threshold level of Bub1 below which the incidence of neoplastic transformation progressively increases. Our data further imply that Bub1 reductions above the threshold may slightly inhibit tumor formation in particular tissues.

Increased incidence of DMBA-induced tumors in Bub1 mutant mice

Based on the aforementioned data, we conclude that $Bub1^{+/-}$ mice have enough Bub1 protein to protect themselves against spontaneous tumorigenesis. To determine whether this level is sufficient to guard against carcinogen-induced tumors, we administered a single dose of 0.5% DMBA (9,10-dimethylbenz-A-athracene) in acetone to the dorsal skin of 3–5-d-old pups generated from $Bub1^{+/-} \times Bub1^{+/+}$ intercrosses. 5 mo after

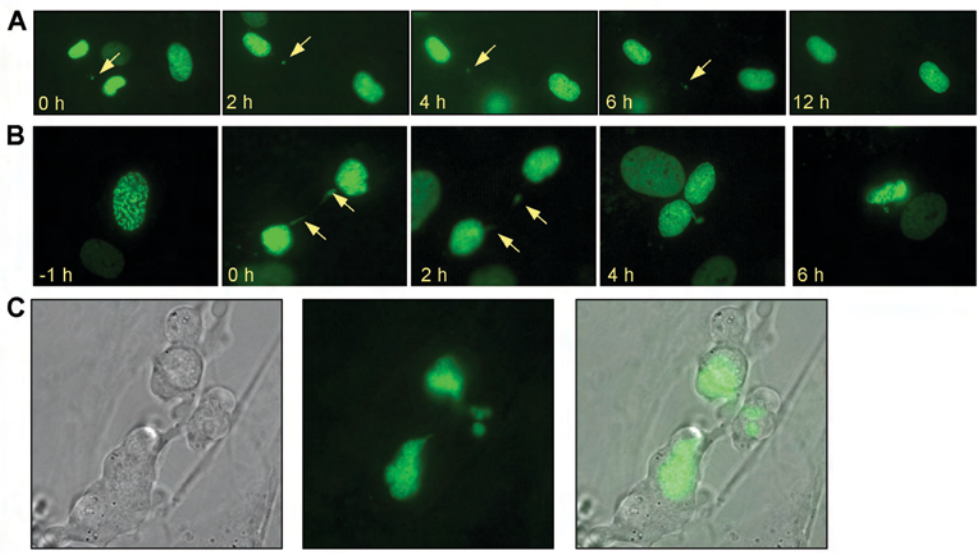

Figure 5. **Analysis of cell fate after chromosome missegregation by live cell imaging.** MEF cultures expressing YFP-tagged H2B were screened for cells entering mitosis by live cell imaging. Cells undergoing chromosome missegregation were monitored for up to 12 h after the missegregation occurred to determine cell fate. (A) Time-lapse sequence of a $Bub1^{-/H}$ cell undergoing chromosome missegregation and whose daughter cells survived for at least 12 h. t = 0 is the time at which missegregation occurred. (B) Time-lapse sequence of a $Bub1^{+/-}$ cell undergoing chromosome missegregation whose daughter cells died ~7 h after the defect occurred. (A and B) Arrows mark the locations of the missegregated chromosomes. (C) High resolution images of two $Bub1^{+/-}$ daughter cells undergoing cell death ~5 h after they underwent chromosome missegregation.

treatment, we killed the mice and screened for tumors. Irrespective of the genotype, tumors were exclusively detectable in the lungs. Bub1$^{+/-}$ mice exhibited a two- to threefold higher incidence of lung tumors than in Bub1$^{+/+}$ mice (Fig. 7 A). Moreover, the tumor burden of Bub1$^{+/-}$ mice was increased approximately threefold (Fig. 7 B). From this experiment, we conclude that Bub1 heterozygous knockout mice are prone to carcinogen-induced tumorigenesis.

Discussion

In this study, we produced a series of mutant mice in which the expression of Bub1 is reduced in a graded fashion from normal to zero by the use of wild-type, hypomorphic, and knockout alleles to determine the physiological role of Bub1. As anticipated, we find that the complete loss of Bub1 leads to embryonic lethality. Strongly reduced Bub1 expression (up to approximately

A

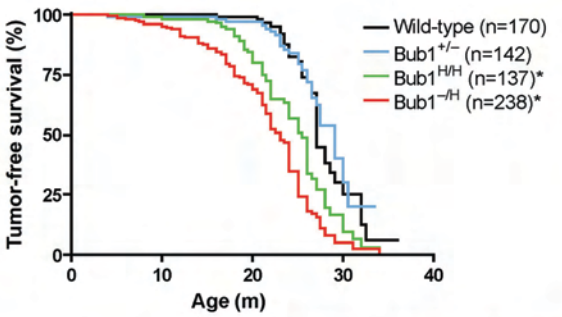

B

Genotype	Wild-type	Bub1$^{+/-}$	Bub1$^{H/H}$	Bub1$^{-/H}$
Mice in study	170	110	120	226
Mice with tumors	55	28	57	126
Tumor incidence	32%	25%	48%	56%
Tumor latency	768 days	741 days	687 days	591 days

C

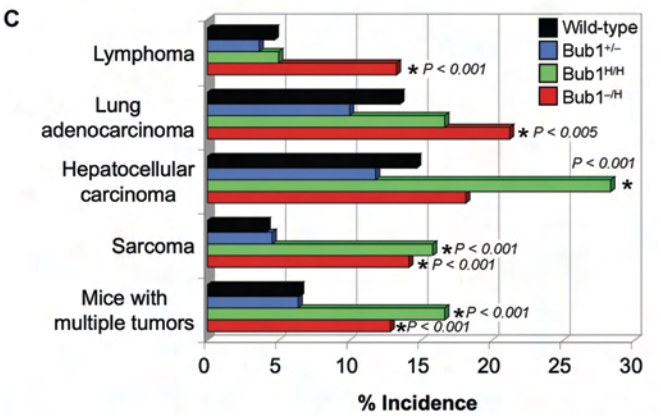

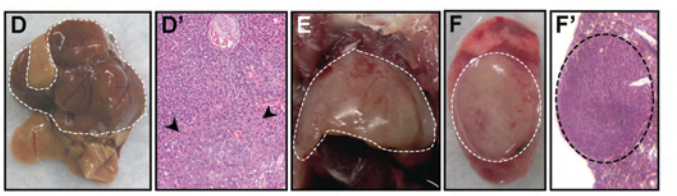

Figure 6. **Bub1$^{-/H}$ and Bub1$^{H/H}$ mice are prone to spontaneous tumors.** (A) Tumor-free survival curves of Bub1$^{+/+}$, Bub1$^{+/-}$, Bub1$^{H/H}$, and Bub1$^{-/H}$ mice. The asterisks mark curves that are significantly different from wild-type using a logrank test ($P < 0.0001$). We note that the tumor-free survival of a small cohort of Bub1$^{+/H}$ mice ($n = 10$) was similar to that of Bub1$^{+/+}$ mice (not depicted). Furthermore, the median tumor-free survival of Bub1$^{-/H}$ mice was significantly shorter than that of Bub1$^{H/H}$ mice ($P < 0.01$). (B) Spontaneous tumor incidence and tumor latency of Bub1$^{+/+}$, Bub1$^{+/-}$, Bub1$^{H/H}$, and Bub1$^{-/H}$ mice. (C) Tumor spectrum of Bub1$^{+/+}$, Bub1$^{+/-}$, Bub1$^{H/H}$, and Bub1$^{-/H}$ mice. Asterisks mark values that are significantly different from wild type using a Fisher exact Chi-square test. (D) An overt hepatocellular carcinoma is indicated by the dashed line. (D') Hematoxylin and eosin stained well-differentiated hepatocellular carcinoma, showing a proliferation of mildly atypical hepatocytes with abundant vascular channels, a lack of normal portal tracts, and a nodular focus (arrowheads) with mildly thickened trabeculae. (E) Thymic lymphoma (dashed line). (F) Overt lung adenocarcinoma (dashed circle). (F') Hematoxylin and eosin–stained low-power magnification of a typical lung adenocarcinoma (dashed circle).

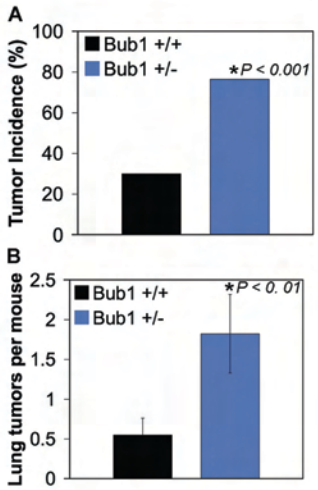

Figure 7. **DMBA-induced tumor formation in Bub1 haploinsufficient mice.** (A) The occurrence of lung tumors in 5-mo-old mice plotted as the percentage of incidence. (B) The mean number of lung adenomas per mouse ± SEM (error bars). (A and B) The asterisk marks a value that is significantly different from wild type using a chi-squared test (A) and a Wilcoxon rank sum test (B).

fivefold reduction) does not interfere with embryogenesis and allows for the development of adult mice that are overtly indistinguishable from their wild-type littermates. However, the reduction of Bub1 levels does have adverse consequences on genomic stability in these cells. Karyotyping of splenocytes and MEFs from our series of mutant mice established an inverse correlation between Bub1 expression level and aneuploidy. Failure of chromosome congression during metaphase is the main chromosome segregation defect resulting from Bub1 insufficiency. Although small and large reductions in Bub1 levels cause similar rates of chromosome missegregation, rates of cell survival after aberrant chromosome segregation increase considerably with declining Bub1 levels, providing a plausible explanation for why large reductions cause more aneuploidy than small ones. Furthermore, the reduction of Bub1 protein affected the strength of the mitotic checkpoint and loading of certain proteins onto centromeres or kinetochores. Bub1 haploinsufficiency in mice does not cause spontaneous tumors, but, as Bub1 levels drop further, animals become highly susceptible to a variety of spontaneous tumors, with the highest rate of tumorigenesis seen at the lowest level of Bub1 expression.

Bub1 is known to be required for the binding of several other mitotic checkpoint proteins to kinetochores (Sharp-Baker and Chen, 2001; Johnson et al., 2004; Meraldi et al., 2004). Our analysis of MEFs with graded reduction in Bub1 expression now reveals that these proteins require different levels of Bub1 protein for their normal recruitment to kinetochores. In particular, the recruitment of Mad1 to kinetochores is dramatically reduced when Bub1 is down-regulated. We speculate that Mad2, which forms a complex with Mad1 at kinetochores (Yu, 2006), is similarly sensitive to Bub1 down-regulation, although we were unable to confirm this because of the lack of an antibody that detects mouse Mad2 at kinetochores. Besides Mad1, the recruitment of BubR1 and CENP-E to kinetochores is also sensitive to Bub1 down-regulation, but not as sensitive as Mad1, as their localization is normal in Bub1 heterozygous MEFs. Recent studies have presented evidence that Bub1 functions to recruit Sgo1 to centromeres to prevent the precocious separation of sister kinetochores (Tang et al., 2004b; Kitajima et al., 2005). Consistent with these studies, we find that centromeric Sgo1 levels are reduced in Bub1 mutant MEFs, but only when Bub1 expression is strongly down-regulated. However, this did not result in premature sister kinetochore separation, implying that an even further drop in centromeric Sgo1 is required to trigger the cleavage of cohesin molecules that link sister centromeres. A recent study has implicated Bub1 in the targeting of chromosomal passenger complexes to centromeres in early mitosis (Boyarchuk et al., 2007). Our finding that very low amounts of Bub1 are sufficient for directing these complexes to centromeres suggests that near complete Bub1 depletion is required to dislocate the passenger complex from mitotic centromeres.

One of our more surprising findings is the observation that a relatively small reduction in Bub1 expression has a major impact on the accuracy of chromosome congression. What could be the explanation for this observation? Although the precise role of Bub1 in chromosome congression is currently not known, it is believed that this role involves kinetochore assembly (Meraldi and Sorger, 2005). Of the mitotic checkpoint proteins whose recruitment is Bub1 dependent, only CENP-E has so far been implicated in chromosome congression. Thus, one explanation for the congression failure in Bub1 mutant MEFs might be a CENP-E recruitment defect. Consistent with this, we find that the targeting of CENP-E to kinetochores is perturbed in Bub1 hypomorphic MEFs. On the other hand, Bub1 haploinsufficient MEFs, which display similar rates of congression failure as Bub1 hypomorphic MEFs, exhibit normal CENP-E recruitment to kinetochores, implying that the mechanism of congression failure is CENP-E independent. This conclusion is further supported by data of Meraldi and Sorger (2005) demonstrating that the depletion of Bub1 in HeLa cells by RNA interference causes chromosome congression defects in the absence of CENP-E mislocalization. Therefore, it remains unclear how Bub1 promotes proper chromosome congression. Nonetheless, we suspect that it involves a known or novel kinetochore-associated protein that functions in microtubule capture and whose recruitment to kinetochores is highly dependent on a full complement of Bub1.

Our analysis of MEFs with graded reduction in Bub1 expression indicates that relatively small shortages in Bub1, such as those seen in $Bub1^{+/H}$ and $Bub1^{+/-}$ MEFs, weaken the mitotic checkpoint considerably. It is plausible that the impaired recruitment of Mad1 (and presumably Mad2) to kinetochores undermines the mitotic checkpoint in these cells, as kinetochore-associated Mad1–Mad2 complexes generate soluble Mad2–Cdc20 complexes that bind to and inactivate APC/C. Larger reductions in Bub1, as present in $Bub1^{H/H}$ and $Bub1^{-/H}$ MEFs, had an even

more profound impact on mitotic checkpoint activity. We propose that this is caused, at least in part, by the added loss of CENP-E and BubR1 from kinetochores, as kinetochore-bound CENP-E and BubR1 molecules have been implicated in the assembly of various inhibitory protein complexes that target APC/C (Mao et al., 2003, 2005). The Bub1 kinase also can inhibit APC/C directly through the phosphorylation of Cdc20 (Chung and Chen, 2003; Chen, 2004; Tang et al., 2004a). We have not addressed whether the phosphorylation of Cdc20 is affected in our mutant series of MEFs as a result of the current lack of antibodies that recognize phosphorylated mouse Cdc20.

Although it has been well established that gross abnormalities of chromosome segregation (frequently referred to as mitotic catastrophe) often cause cell death (Castedo et al., 2004), the fate of cells undergoing the random missegregation of only one or a few chromosomes has been unknown. Here, we show by the use of live cell imaging that wild-type primary MEFs die at very high rates after minor abnormalities in chromosome segregation. The implication of this finding is that aneuploidy rates in cultured wild-type MEFs are substantially higher than metaphase spread karyotypes reveal. Our discovery that cell death rates after chromosome missegregation dramatically decline with decreasing levels of Bub1 creates a molecular entry point for studying the underlying cell death mechanism. Whether Bub1 plays a unique role in this mechanism or whether there is a broader connection between mitotic checkpoint damage and decreased cell death after chromosome missegregation is an important question for future analysis. Bub1's dual function as a guardian of high fidelity chromosome segregation and as a mediator of cell death after aberrant segregation is reminiscent of proteins such as ATM (ataxia telangiectasia mutated) and p53 that function in both DNA repair and apoptosis in response to DNA damage (Sancar et al., 2004). A recent study showed that Bub1-depleted cancer cell lines display increased mitotic cell death when they are exposed to agents that perturb kinetochore-microtubule attachment, such as nocodazole (Niikura et al., 2007). We observed no such effect in nocodazole-treated MEFs with graded reduction in Bub1 expression (Fig. S4 D), suggesting that the impact of the Bub1 level of expression on mitotic cell death induced by spindle poisons is cell type and/or transformation status dependent.

Bub1 expression is reduced in several human cancers, including colorectal, gastric, and esophageal tumors (Shigeishi et al., 2001; Shichiri et al., 2002; Doak et al., 2004); however, it was unknown whether the reduced expression of this mitotic checkpoint protein is causally implicated in tumorigenesis. Analysis of our series of Bub1 mutant mice firmly establishes that the reduced expression of Bub1 leads to the development of spontaneous tumors in mice, but only when Bub1 levels fall below a threshold level. Those with the most drastic reductions of Bub1 expression have the shortest tumor latency and the highest incidence of tumors. The level of Bub1 required to prevent spontaneous tumorigenesis appears to vary per tissue, as illustrated by the fact that only mice with the most profound reduction in Bub1 are predisposed to lymphomas and lung tumors. In the liver, the optimal level of Bub1 down-regulation is not the lowest level, as $Bub1^{H/H}$ mice but not $Bub1^{-/H}$ mice are prone to hepatocellular carcinomas. Adding even more complexity is the discovery that Bub1 haploinsufficiency exerts a slight tumor-suppressive effect in both liver and lung tissue. This finding is consistent with the recent discovery that CENP-E haploinsufficiency inhibits tumorigenesis in certain mouse tissues (Weaver et al., 2007). However, unlike CENP-E insufficiency, Bub1 haploinsufficiency does not inhibit DMBA-induced tumorigenesis. In fact, Bub1 haploinsufficient mice are highly susceptible to lung tumors when challenged with this carcinogen. This observation implies that the loss of one Bub1 gene copy acts to accelerate the development of tumors initiated by particular cancer gene mutations.

Because Bub1 hypomorphic mice have a high percentage of aneuploid cells and are predisposed to spontaneous tumors, whereas Bub1 haploinsufficient mice have a relatively low percentage of aneuploid cells and are not tumor prone, it is tempting to speculate that it is the increase in aneuploidy that drives tumorigenesis in Bub1 hypomorphic mice. However, the fact that both Rae1/Bub3 and Rae1/Nup98 double-haploinsufficient mice develop aneuploidy at rates very similar to that of Bub1 hypomorphic mice but are not prone to spontaneous tumors argues against this idea (Babu et al., 2003; Baker et al., 2006; Jeganathan et al., 2005, 2006). One possible explanation for this discrepancy could be that as a result of the decreased cell death in response to chromosome missegregation, Bub1 hypomorphic mice may develop a wider variety of abnormal karyotypes than Rae1/Bub3 and Rae1/Nup98 double-haploinsufficient mice, thereby perhaps increasing the incidence of karyotypes that have the ability to drive tumorigenesis. However, the role of aneuploidy in tumorigenesis is clearly highly complex, and it will be necessary to carefully examine each individual regulator of chromosome segregation for its involvement in tumorigenesis through the use of animal models. We expect these efforts to allow the identification of a subset of mitotic regulators that are particularly important for tumor prevention. Among them may be mitotic regulators that serve as molecular hubs within the mitotic checkpoint or other networks that regulate proper chromosome segregation or mitotic regulators with connectivity to other pathways that guard against neoplastic transformation.

In this study, we have used a series of mutant mice to demonstrate that only after reducing Bub1 levels beyond a threshold level do mice start to develop spontaneous tumors. Had we used only Bub1 haploinsufficient mice rather than a series of mice with graded reduction in Bub1 expression, our conclusions would have been dramatically different in that we would conclude that Bub1 does not act as a tumor suppressor itself. Heterozygous knockout models for several other mitotic checkpoint genes are also not predisposed to spontaneous tumorigenesis. For a more definitive understanding of the roles these genes have in tumor prevention, it will be useful to use hypomorphic alleles to further reduce their level of expression in mice.

Materials and methods

Generation of Bub1 mutant mice and analyses of tumorigenesis

An 8.5-kb Bub1 129Sv/J genomic DNA fragment was used to generate both targeting vectors used. Gene-targeting procedures were performed as previously described (van Deursen et al., 1996). We identified targeted ES

cell clones by Southern blot analysis using a 3′ probe on BamHI-cut genomic DNA (Fig. 1 A). Mutant mice were derived from targeted ES cell clones through standard procedures. These mice were maintained on a mixed 129Sv/E × C57BL/6 genetic background. Mice in tumor susceptibility experiments were observed daily for the development of overt tumors or signs of ill health. Moribund mice were killed, and all major organs were screened for overt tumors using a dissection microscope (SZX12; Olympus). Tumors that were collected were processed by standard procedures for histopathology. Prism software (GraphPad Software, Inc.) was used for the generation of tumor-free survival curves and for statistical analyses. DMBA treatment was performed as previously described (Serrano et al., 1996; Babu et al., 2003). All major organs were screened for overt tumors using a dissection microscope (SZX12; Olympus). Harvested tumors were routinely processed for histopathological confirmation. We note that all mice were housed in a pathogen-free barrier environment.

Western blot analysis and indirect immunofluorescence

Western blot analyses and indirect immunofluorescence were performed as previously described (Kasper et al., 1999). A laser-scanning microscope (LSM 510 v3.2SP2; Carl Zeiss MicroImaging, Inc.) as well as a microscope (Axiovert 100M; Carl Zeiss MicroImaging, Inc.) with a c-Apochromat 100× oil immersion objective (Carl Zeiss MicroImaging, Inc.) was used to analyze immunostained cells and to capture representative images. Primary antibodies were visualized with appropriate secondary antibodies conjugated to AlexaFluor594, -488. or -647 (Invitrogen). Primary antibodies used for Western blotting and indirect immunofluorescence were as follows: rabbit anti–human Bub1(25–165), rabbit anti–human BubR1(382–420) (Baker et al., 2004), rabbit anti–human Mad1 (provided by T. Yen, Fox Chase Cancer Center, Philadelphia, PA), rabbit anti–human Sgo1([1–262][177–351]) (provided by H. Yu, University of Texas Southwestern, Houston, TX; Tang et al., 2004b), mouse anti–Aurora B (BD Biosciences), human anticentromeric antibody (Antibodies, Inc.), and rabbit anti–CENP-E (provided by D. Cleveland, Ludwig Institute for Cancer Research, La Jolla, CA). Mad2 antibodies tested were as follows: rabbit anti–human Mad2(FL-205) (Santa Cruz Biotechnology, Inc.), mouse anti–human Mad2 (BD Biosciences), and rabbit anti–human Mad2 (Covance). None of these Mad2 antibodies detects Mad2 at kinetochores of mitotic MEFs.

Karyotyping of MEFs and splenocytes

Chromosome counts on metaphase spreads were performed as previously described (Babu et al., 2003). We note that cells were scored as diploid (n = 40 chromosomes), tetraploid (n = 80 chromosomes), or aneuploid (Weaver et al., 2007).

Live cell imaging experiments

To allow the visualization of chromosomes by fluorescent microscopy on living cells, we used a retrovirus expressing YFP-tagged H2B (Jeganathan et al., 2005). Passage 2 MEFs were seeded in T25 flasks at 75% confluence and cultured in DME/10% FBS at 3% oxygen. 12 h after seeding and again every 12 h for at least three times, the medium was replaced with medium harvested from EcoPACK pMSCV-puro-H2B-YFP viral producer cell lines. Cells were then seeded onto 35-mm glass-bottomed culture dishes (MatTek Corp.) and cultured in DME/10% FBS. Approximately 24 h later, experiments were performed using a microscope system (Axio Observer; Carl Zeiss MicroImaging, Inc.) with CO_2 Module S, TempModule S, Heating Unit XL S, a plan Apo 63× NA 1.4 oil differential interference contrast III objective (Carl Zeiss MicroImaging, Inc.), camera (AxioCam MRm; Carl Zeiss MicroImaging, Inc.), and AxioVision 4.6 software (Carl Zeiss MicroImaging, Inc.). The imaging medium was DME/10% FBS. The temperature of the imaging medium was kept at 37°C. The exposure times in nocodazole challenge experiments were 100 ms at 2 × 2 binning. Time of arrest in mitosis was defined as the interval between NEBD (onset of mitosis) and chromatin decondensation (exit from mitosis without cytokinesis). Interframe intervals were 15 min for nocodazole challenge. Analysis of mitotic defects was performed as previously described (Baker et al., 2006). For analysis of the incidence of cell death after chromosome missegregation, MEFs undergoing abnormal chromosome segregation were marked and followed with an interframe interval of 30 min for up to 12 h. Cell death was preceded by severe nuclear blebbing and cytoplasmic fragmentation. For each of the aforementioned experiments, we examined at least three independent clones per genotype unless otherwise noted. Prism software (GraphPad Software, Inc.) was used for statistical analyses. To evaluate the incidence of micronuclei formation, at least 600 YFP-H2B–expressing interphase MEFs were screened for the presence of micronuclei by live cell microscopy.

Cell survival assays

Analyses of cell survival in response to doxorubicin, mitomycin C, and paraquat were performed as described previously (Baker et al., 2004) with the exception that passage 3 MEFs were used instead of passage 2 MEFs. For analysis of cell death in response to nocodazole treatment, 10^5 passage 3 MEFs were seeded in duplicate for three independent cell lines of each genotype. After ∼12 h, normal medium was replaced with medium containing 100 ng/ml nocodazole, and cells were cultured for an additional 72 h. All cells were collected after this time, and tryptan blue exclusion was used to count living cells.

Online supplemental material

Fig. S1 shows that truncated proteins encoded by the Bub1 knockout and hypomorphic alleles are undetectable by immunoblotting. Fig. S2 shows that Mad1, BubR1, and CENP-E protein levels were similar in $Bub1^{+/+}$ and $Bub1^{-/H}$ cells and that Aurora B is not mislocalized in $Bub1^{-/H}$ cells. Fig. S3 shows that the incidence of micronuclei increases with declining levels of Bub1. Fig. S4 shows that the Bub1 level of expression has no impact on MEF cell survival to DNA-damaging agents and prolonged nocodazole exposure. Videos 1 and 2 show videos of the $Bub1^{-/H}$ MEF presented in Fig. 5 A. Videos 3 and 4 show videos of the $Bub1^{+/-}$ MEF presented in Fig. 5 B. Videos 5 and 6 show a $Bub1^{+/+}$ MEF undergoing chromosome missegregation in mitosis. Both daughter cells die after exit from mitosis. Videos 7 and 8 show a $Bub1^{+/H}$ MEF undergoing chromosome missegregation. One of the two daughter cells undergoes cell death. Videos 9 and 10 show a $Bub1^{H/H}$ MEF undergoing normal chromosome segregation. Both daughter cells survive. Table S1 presents data about the number of chromosomes that are abnormally segregated in cells with mutliple segregation defects. Online supplemental material is available at http://www.jcb.org/cgi/content/full/jcb.200706015/DC1.

We thank Paul Galardy, Rick Bram, Robin Ricke, and Debbie Pearson for critical reading of the manuscript and helpful discussions. We are grateful to Hongtao Yu, Tim Yen, and Don Cleveland for providing Sgo1, Mad1, and CENP-E antibodies, respectively.

This work was supported by a National Institutes of Health grant to J.M. van Deursen.

Submitted: 4 June 2007
Accepted: 19 September 2007

References

Babu, J.R., K.B. Jeganathan, D.J. Baker, X. Wu, N. Kang-Decker, and J.M. van Deursen. 2003. Rae1 is an essential mitotic checkpoint regulator that cooperates with Bub3 to prevent chromosome missegregation. *J. Cell Biol.* 160:341–353.

Baker, D.J., K.B. Jeganathan, J.D. Cameron, M. Thompson, S. Juneja, A. Kopecka, R. Kumar, R.B. Jenkins, P.C. de Groen, P. Roche, and J.M. van Deursen. 2004. BubR1 insufficiency causes early onset of aging-associated phenotypes and infertility in mice. *Nat. Genet.* 36:744–749.

Baker, D.J., K.B. Jeganathan, L. Malureanu, C. Perez-Terzic, A. Terzic, and J.M. van Deursen. 2006. Early aging-associated phenotypes in Bub3/Rae1 haploinsufficient mice. *J. Cell Biol.* 172:529–540.

Boyarchuk, Y., A. Salic, M. Dasso, and A. Arnaoutov. 2007. Bub1 is essential for assembly of the functional inner centromere. *J. Cell Biol.* 176:919–928.

Cahill, D.P., C. Lengauer, J. Yu, G.J. Riggins, J.K. Willson, S.D. Markowitz, K.W. Kinzler, and B. Vogelstein. 1998. Mutations of mitotic checkpoint genes in human cancers. *Nature.* 392:300–303.

Castedo, M., J.L. Perfettini, T. Roumier, K. Andreau, R. Medema, and G. Kroemer. 2004. Cell death by mitotic catastrophe: a molecular definition. *Oncogene.* 23:2825–2837.

Chen, R.H. 2004. Phosphorylation and activation of Bub1 on unattached chromosomes facilitate the spindle checkpoint. *EMBO J.* 23:3113–3121.

Chen, R.H., A. Shevchenko, M. Mann, and A.W. Murray. 1998. Spindle checkpoint protein Xmad1 recruits Xmad2 to unattached kinetochores. *J. Cell Biol.* 143:283–295.

Chen, R.H., D.M. Brady, D. Smith, A.W. Murray, and K.G. Hardwick. 1999. The spindle checkpoint of budding yeast depends on a tight complex between the Mad1 and Mad2 proteins. *Mol. Biol. Cell.* 10:2607–2618.

Chung, E., and R.H. Chen. 2003. Phosphorylation of Cdc20 is required for its inhibition by the spindle checkpoint. *Nat. Cell Biol.* 5:748–753.

Doak, S.H., G.J. Jenkins, E.M. Parry, A.P. Griffiths, J.N. Baxter, and J.M. Parry. 2004. Differential expression of the MAD2, BUB1 and HSP27 genes in Barrett's oesophagus-their association with aneuploidy and neoplastic progression. *Mutat. Res.* 547:133–144.

Dobles, M., V. Liberal, M.L. Scott, R. Benezra, and P.K. Sorger. 2000. Chromosome missegregation and apoptosis in mice lacking the mitotic checkpoint protein Mad2. *Cell*. 101:635–645.

Draviam, V.M., S. Xie, and P.K. Sorger. 2004. Chromosome segregation and genomic stability. *Curr. Opin. Genet. Dev.* 14:120–125.

Iwanaga, Y., Y.H. Chi, A. Miyazato, S. Sheleg, K. Haller, J.M. Peloponese Jr., Y. Li, J.M. Ward, R. Benezra, and K.T. Jeang. 2007. Heterozygous deletion of mitotic arrest-deficient protein 1 (MAD1) increases the incidence of tumors in mice. *Cancer Res.* 67:160–166.

Jacks, T., T.S. Shih, E.M. Schmitt, R.T. Bronson, A. Bernards, and R.A. Weinberg. 1994. Tumour predisposition in mice heterozygous for a targeted mutation in Nf1. *Nat. Genet.* 7:353–361.

Jallepalli, P.V., and C. Lengauer. 2001. Chromosome segregation and cancer: cutting through the mystery. *Nat. Rev. Cancer*. 1:109–117.

Jeganathan, K.B., L. Malureanu, and J.M. van Deursen. 2005. The Rae1-Nup98 complex prevents aneuploidy by inhibiting securin degradation. *Nature*. 438:1036–1039.

Jeganathan, K.B., D.J. Baker, and J.M. van Deursen. 2006. Securin associates with APCCdh1 in prometaphase but its destruction is delayed by Rae1 and Nup98 until the metaphase/anaphase transition. *Cell Cycle*. 5:366–370.

Johnson, V.L., M.I. Scott, S.V. Holt, D. Hussein, and S.S. Taylor. 2004. Bub1 is required for kinetochore localization of BubR1, Cenp-E, Cenp-F and Mad2, and chromosome congression. *J. Cell Sci.* 117:1577–1589.

Kalitsis, P., E. Earle, K.J. Fowler, and K.H. Choo. 2000. Bub3 gene disruption in mice reveals essential mitotic spindle checkpoint function during early embryogenesis. *Genes Dev.* 14:2277–2282.

Kasper, L.H., P.K. Brindle, C.A. Schnabel, C.E. Pritchard, M.L. Cleary, and J.M. van Deursen. 1999. CREB binding protein interacts with nucleoporin-specific FG repeats that activate transcription and mediate NUP98-HOXA9 oncogenicity. *Mol. Cell. Biol.* 19:764–776.

Kitajima, T.S., S. Hauf, M. Ohsugi, T. Yamamoto, and Y. Watanabe. 2005. Human Bub1 defines the persistent cohesion site along the mitotic chromosome by affecting Shugoshin localization. *Curr. Biol.* 15:353–359.

Kops, G.J., D.R. Foltz, and D.W. Cleveland. 2004. Lethality to human cancer cells through massive chromosome loss by inhibition of the mitotic checkpoint. *Proc. Natl. Acad. Sci. USA*. 101:8699–8704.

Kops, G.J., B.A. Weaver, and D.W. Cleveland. 2005. On the road to cancer: aneuploidy and the mitotic checkpoint. *Nat. Rev. Cancer*. 5:773–785.

Luo, X., Z. Tang, J. Rizo, and H. Yu. 2002. The Mad2 spindle checkpoint protein undergoes similar major conformational changes upon binding to either Mad1 or Cdc20. *Mol. Cell*. 9:59–71.

Luo, X., Z. Tang, G. Xia, K. Wassmann, T. Matsumoto, J. Rizo, and H. Yu. 2004. The Mad2 spindle checkpoint protein has two distinct natively folded states. *Nat. Struct. Mol. Biol.* 11:338–345.

Mao, Y., A. Abrieu, and D.W. Cleveland. 2003. Activating and silencing the mitotic checkpoint through CENP-E-dependent activation/inactivation of BubR1. *Cell*. 114:87–98.

Mao, Y., A. Desai, and D.W. Cleveland. 2005. Microtubule capture by CENP-E silences BubR1-dependent mitotic checkpoint signaling. *J. Cell Biol.* 170:873–880.

Meraldi, P., and P.K. Sorger. 2005. A dual role for Bub1 in the spindle checkpoint and chromosome congression. *EMBO J.* 24:1621–1633.

Meraldi, P., V.M. Draviam, and P.K. Sorger. 2004. Timing and checkpoints in the regulation of mitotic progression. *Dev. Cell*. 7:45–60.

Meyers, E.N., M. Lewandoski, and G.R. Martin. 1998. An Fgf8 mutant allelic series generated by Cre- and Flp-mediated recombination. *Nat. Genet.* 18:136–141.

Musacchio, A., and E.D. Salmon. 2007. The spindle-assembly checkpoint in space and time. *Nat. Rev. Mol. Cell Biol.* 8:379–393.

Nasmyth, K., and C.H. Haering. 2005. The structure and function of SMC and kleisin complexes. *Annu. Rev. Biochem.* 74:595–648.

Niikura, Y., A. Dixit, R. Scott, G. Perkins, and K. Kitagawa. 2007. BUB1 mediation of caspase-independent mitotic death determines cell fate. *J. Cell Biol.* 178:283–296.

Ohshima, K., S. Haraoka, S. Yoshioka, M. Hamasaki, T. Fujiki, J. Suzumiya, C. Kawasaki, M. Kanda, and M. Kikuchi. 2000. Mutation analysis of mitotic checkpoint genes (hBUB1 and hBUBR1) and microsatellite instability in adult T-cell leukemia/lymphoma. *Cancer Lett.* 158:141–150.

Peters, J.M. 2006. The anaphase promoting complex/cyclosome: a machine designed to destroy. *Nat. Rev. Mol. Cell Biol.* 7:644–656.

Riedel, C.G., V.L. Katis, Y. Katou, S. Mori, T. Itoh, W. Helmhart, M. Galova, M. Petronczki, J. Gregan, B. Cetin, et al. 2006. Protein phosphatase 2A protects centromeric sister chromatid cohesion during meiosis I. *Nature*. 441:53–61.

Roberts, B.T., K.A. Farr, and M.A. Hoyt. 1994. The *Saccharomyces cerevisiae* checkpoint gene BUB1 encodes a novel protein kinase. *Mol. Cell. Biol.* 14:8282–8291.

Ru, H.Y., R.L. Chen, W.C. Lu, and J.H. Chen. 2002. hBUB1 defects in leukemia and lymphoma cells. *Oncogene*. 21:4673–4679.

Sancar, A., L.A. Lindsey-Boltz, K. Unsal-Kacmaz, and S. Linn. 2004. Molecular mechanisms of mammalian DNA repair and the DNA damage checkpoints. *Annu. Rev. Biochem.* 73:39–85.

Serrano, M., H. Lee, L. Chin, C. Cordon-Cardo, D. Beach, and R.A. DePinho. 1996. Role of the INK4a locus in tumor suppression and cell mortality. *Cell*. 85:27–37.

Sharp-Baker, H., and R.H. Chen. 2001. Spindle checkpoint protein Bub1 is required for kinetochore localization of Mad1, Mad2, Bub3, and CENP-E, independently of its kinase activity. *J. Cell Biol.* 153:1239–1250.

Shichiri, M., K. Yoshinaga, H. Hisatomi, K. Sugihara, and Y. Hirata. 2002. Genetic and epigenetic inactivation of mitotic checkpoint genes hBUB1 and hBUBR1 and their relationship to survival. *Cancer Res.* 62:13–17.

Shigeishi, H., N. Oue, H. Kuniyasu, A. Wakikawa, H. Yokozaki, T. Ishikawa, and W. Yasui. 2001. Expression of Bub1 gene correlates with tumor proliferating activity in human gastric carcinomas. *Pathobiology*. 69:24–29.

Sironi, L., M. Mapelli, S. Knapp, A. De Antoni, K.T. Jeang, and A. Musacchio. 2002. Crystal structure of the tetrameric Mad1-Mad2 core complex: implications of a 'safety belt' binding mechanism for the spindle checkpoint. *EMBO J.* 21:2496–2506.

Tang, Z., H. Shu, D. Oncel, S. Chen, and H. Yu. 2004a. Phosphorylation of Cdc20 by Bub1 provides a catalytic mechanism for APC/C inhibition by the spindle checkpoint. *Mol. Cell*. 16:387–397.

Tang, Z., Y. Sun, S.E. Harley, H. Zou, and H. Yu. 2004b. Human Bub1 protects centromeric sister-chromatid cohesion through Shugoshin during mitosis. *Proc. Natl. Acad. Sci. USA*. 101:18012–18017.

Tang, Z., H. Shu, W. Qi, N. Mahmood, M.C. Mumby, and H. Yu. 2006. PP2A is required for centromeric localization of Sgo1 and proper chromosome segregation. *Dev. Cell*. 10:575–585.

Taylor, S.S., and F. McKeon. 1997. Kinetochore localization of murine Bub1 is required for normal mitotic timing and checkpoint response to spindle damage. *Cell*. 89:727–735.

van Deursen, J., W. Ruitenbeek, A. Heerschap, P. Jap, H. ter Laak, and B. Wieringa. 1994. Creatine kinase (CK) in skeletal muscle energy metabolism: a study of mouse mutants with graded reduction in muscle CK expression. *Proc. Natl. Acad. Sci. USA*. 91:9091–9095.

van Deursen, J., J. Boer, L. Kasper, and G. Grosveld. 1996. G2 arrest and impaired nucleocytoplasmic transport in mouse embryos lacking the proto-oncogene CAN/Nup214. *EMBO J.* 15:5574–5583.

Wang, Q., T. Liu, Y. Fang, S. Xie, X. Huang, R. Mahmood, G. Ramaswamy, K.M. Sakamoto, Z. Darzynkiewicz, M. Xu, and W. Dai. 2004. BUBR1 deficiency results in abnormal megakaryopoiesis. *Blood*. 103:1278–1285.

Weaver, B.A., and D.W. Cleveland. 2006. Does aneuploidy cause cancer? *Curr. Opin. Cell Biol.* 18:658–667.

Weaver, B.A., A.D. Silk, C. Montagna, P. Verdier-Pinard, and D.W. Cleveland. 2007. Aneuploidy acts both oncogenically and as a tumor suppressor. *Cancer Cell*. 11:25–36.

Yu, H., and Z. Tang. 2005. Bub1 multitasking in mitosis. *Cell Cycle*. 4:262–265.

Yu, H. 2006. Structural activation of Mad2 in the mitotic spindle checkpoint: the two-state Mad2 model versus the Mad2 template model. *J. Cell Biol.* 173:153–157.

Yuen, K.W., B. Montpetit, and P. Hieter. 2005. The kinetochore and cancer: what's the connection? *Curr. Opin. Cell Biol.* 17:576–582.

Supplementary Table 1

Number of chromosomes abnormally segregated in cells with multiple segregation defects

Mitotic figures inspected (n)	Figures with two lagging chromosomes	Figures with two centrophilic chromosomes	Figures with three centrophilic chromosomes	Figures with one lagging and one centrophilic chromosome
$Bub1^{+/+}$ (106)	0	0	0	0
$Bub1^{+/H}$ (91)	0	1	0	0
$Bub1^{+/-}$ (142)	2	0	0	3
$Bub1^{H/H}$ (122)	2	1	0	0
$Bub1^{-/H}$ (168)	2	1	1	1

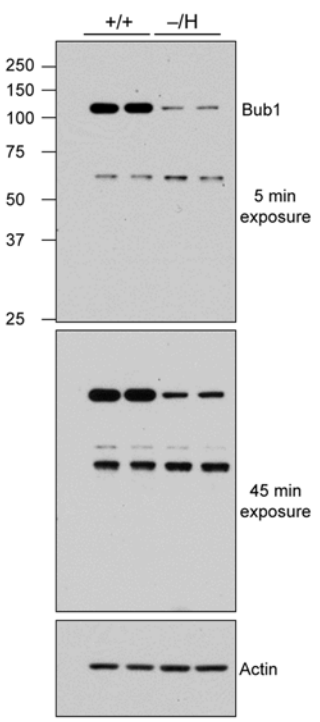

Supplementary Figure 1

Screening for truncated protein products encoded by the Bub1 knockout and hypomorphic alleles. Immunoblots of mitotic extracts from $Bub1^{+/+}$ and $Bub1^{-/H}$ MEFs probed with rabbit anti-Bub1(25-165) antibodies. Besides Bub1, this antibody detects non-specific bands of about 65 and 70 kDa. The – and H alleles were expected to produce truncated protein products of about 32 and 37 kDa, respectively. However, there is no evidence for the presence of these proteins in $Bub1^{-/H}$ mitotic extracts.

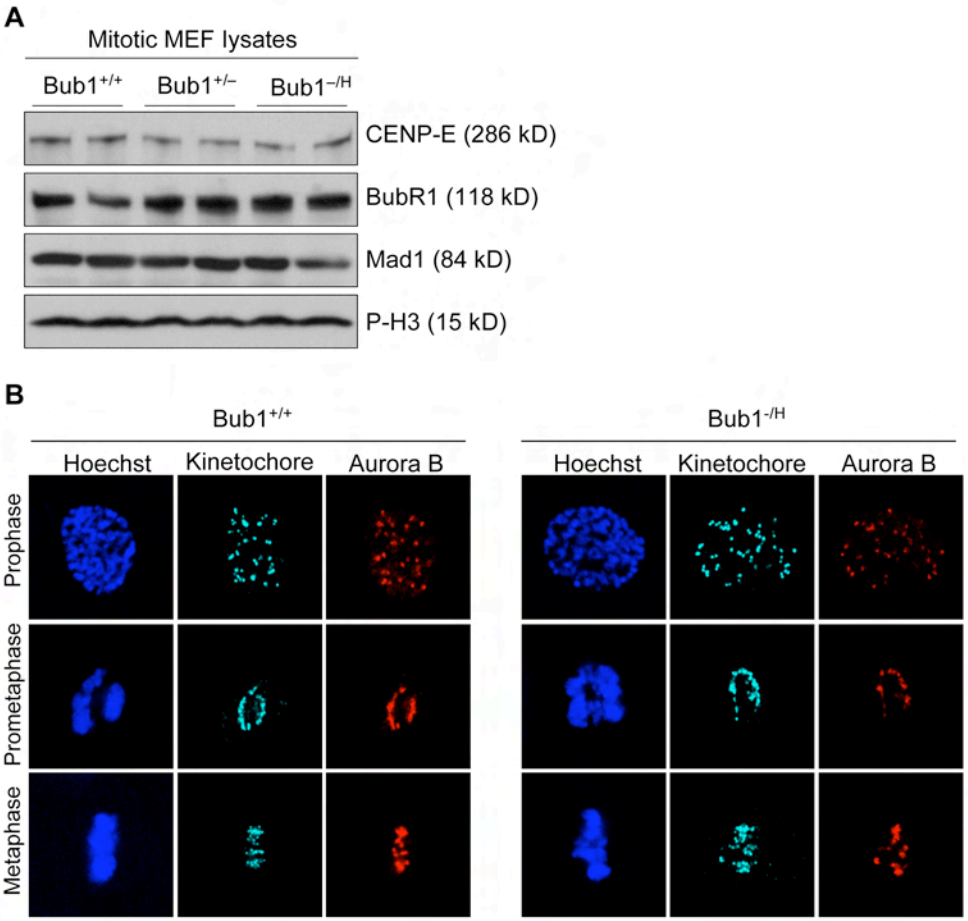

Supplementary Figure 2

Normal Aurora B localization to centromeres in Bub1$^{-/H}$ MEFs. (A) Immunoblots of Bub1$^{+/+}$, Bub1$^{+/-}$ and Bub1$^{-/H}$ cells probed with the indicated antibodies. MEFs were synchronized in G_0 by serum starvation and then released for 28 h in serum-containing medium. Nocodazole (100 ng per ml) was added 23 h after cells were released. Blots were probed with the indicated antibodies. **(B)** Fluorescent images of Bub1$^{+/+}$ and Bub1$^{-/H}$ prophase, prometaphase and metaphase cells costained for kinetochores and Aurora B. DNA was visualized by Hoechst counterstaining. Note that Aurora B targeting to centromeres is normal when Bub1 levels are very low.

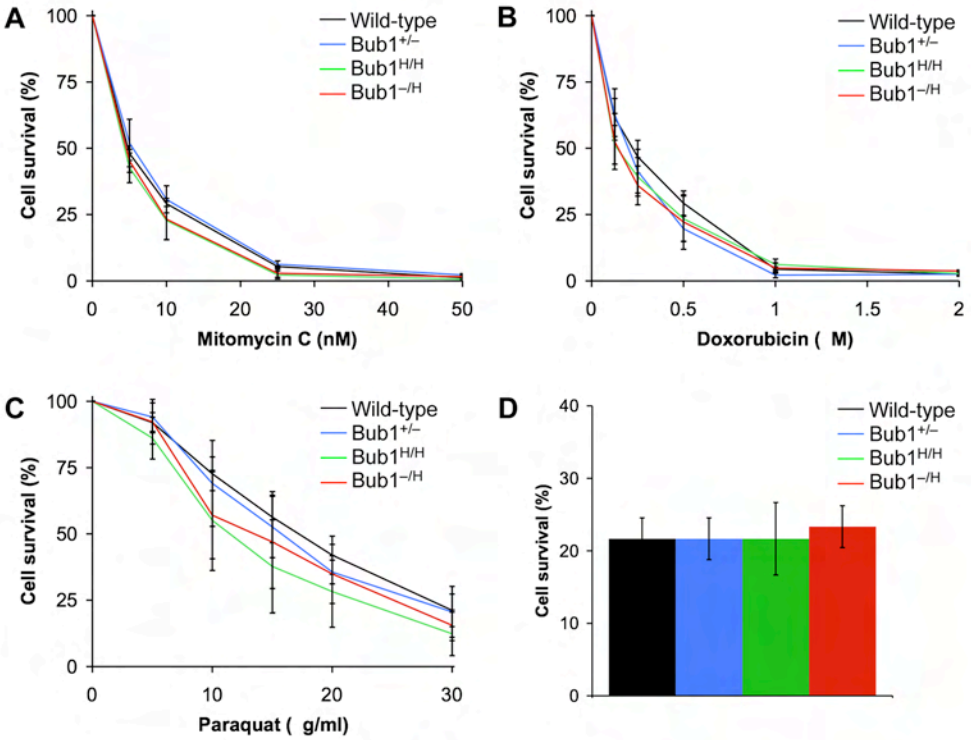

Supplementary Figure 4

Bub1 level of expression has no impact on MEF cell survival to DNA damaging agents and prolonged nocodazole exposure. (A-C) Survival of Bub1$^{+/+}$, Bub1$^{+/-}$, Bub1$^{H/H}$ and Bub1$^{-/H}$ MEFs after exposure to various concentrations of (A) mitomycin C, (B) doxorubicin or (C) paraquat. **(D)** Percent survival of Bub1$^{+/+}$, Bub1$^{+/-}$, Bub1$^{H/H}$ and Bub1$^{-/H}$ MEFs after 72 h nocodazole treatment. Note that cell survival to all these treatments was independent of Bub1 status.

A

MEF genotype (n)	Interphase cells inspected	% Cells with micronuclei
Bub1$^{+/+}$ (5)	1248	2.5
Bub1$^{+/H}$ (3)	600	4.2
Bub1$^{+/-}$ (5)	1653	4.8
Bub1$^{H/H}$ (3)	600	11.5
Bub1$^{-/H}$ (3)	600	16.7

B

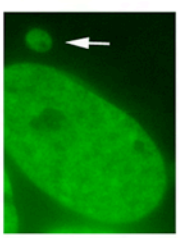

Supplementary Figure 3

Micronuclei formation increases with decreasing Bub1 expression. (A) The percentage of H2B-YFP-positive MEFs with micronuclei per genotype analyzed by live-cell microscopy. **(B)** Example of an H2B-YFP-positive cell with a micronucleus (arrow).

Chapter 9

Summary, Discussion and Future Outlook

Summary

BubR1 is a mitotic checkpoint protein that is mutated or expressed at reduced levels in a variety of human cancers. In our initial studies we sought to answer two main questions: First, does BubR1 insufficiency in mice cause chromosome missegregation and accumulation of aneuploid cells? What is the biologically critical role of BubR1? Data from experiments designed to answer these initial questions led us to pose several new questions: Is BubR1's role in suppression of cancer and aging unique or shared by other mitotic checkpoint proteins? Do BubR1 and other mitotic checkpoint proteins have functions outside of their roles in mediating the metaphase to anaphase transition during mitosis?

To clarify the physiological relevance of BubR1, we generated a series of mice in which protein levels gradually decreased from normal to zero by using BubR1 hypomorphic and knockout alleles (Chapter 3). BubR1-null mice were not obtained, demonstrating that BubR1 is required for normal development. However, hypomorphic BubR1 mice, which express approximately 10% of normal BubR1 protein, were liveborn and able to develop to adulthood. Cells from these mice are unable to segregate their chromosomes with high fidelity and accumulate more and more aneuploid cells as they mature. Despite vast amounts of aneuploidy, these mice rarely develop spontaneous tumors. However, challenging these animals with carcinogens resulted in nearly 3-fold more tumors, indicating that BubR1 acts to reduce the risk of neoplastic transformation. Additionally, these mice develop a wide array of early aging-associated phenotypes, including reduced lifespan, cachetic dwarfism, lordokyphosis, muscle atrophy, cataracts, loss of subcutaneous adipose tissue, and impaired wound healing. Follow-up studies revealed that BubR1 hypomorphic animals had arterial walls that were thin and contained only small amounts of vascular smooth muscle cells, causing arterial stiffening and fibrosis, a hallmark of aging in humans (Chapter 4). This, combined with the observation that BubR1 levels decline in several tissues with age in normal mice, led us to propose that BubR1 is a regulator of natural aging.

Because we propose that BubR1 regulates natural aging, we investigated the relationship between BubR1 and other genes thought to contribute to aging. $p16^{Ink4a}$ or $p19^{Arf}$ are two proteins whose expression goes up with age in many tissues of normal wild-type mice [1]. We also observed that these two proteins are expressed at increased levels in certain tissues of BubR1 hypomorphic mice (Chapter 5). We then tested if $p16^{Ink4a}$ or $p19^{Arf}$ mediated the age-related pathology of BubR1 hypomorphic mice by ablating them. We found that disruption of $p16^{Ink4a}$ in hypomorphic BubR1 mice results in a delayed onset of age-related pathology in tissues that express $p16^{Ink4a}$ at higher than normal levels, including skeletal

muscle, (subdermal) fat and eye. The observed delay in muscle and adipose tissue aging was coupled with a reduction in cellular senescence in these tissues. Interestingly, when we ablate $p19^{Arf}$ in hypomorphic BubR1 animals, all tissues that have this protein elevated exhibit an earlier onset of age-related disease, including increased rates of cellular senescence. Together, these data demonstrate that in hypomorphic BubR1 mice, $p16^{Ink4a}$ acts to promote age-related disease changes and cellular senescence, whereas $p19^{Arf}$ functions to suppress these alterations.

After finding that BubR1 was integral in preventing premature age-related phenotypes, we were curious if other mitotic checkpoint deficient mouse models that exhibited similar rates of chromosome missegregation were also susceptible to these diseases. Although we found that Bub3/Rae1 compound haplo-insufficient animals do have a slight predisposition to development of premature aging, the time to onset is substantially delayed compared to BubR1 hypomorphic mice (Chapter 6). Bub3/Rae1 haplo-insufficient animals engage the Rb-$p16^{Ink4a}$ and p53-$p19^{Arf}$ pathway as well, but to a significantly lesser degree than hypomorphic BubR1 mice, suggesting that premature aging in mitotic checkpoint defective mouse models results from cellular senescence and hyperactivation of the pathways responsible for establishing this removal of cells from the cell cycle rather than from aneuploidy.

Finally, we investigated the physiological role of the BubR1-related protein Bub1. Again we used knockout and hypomorphic mice to create a series of mice with graded reductions in Bub1 (Chapter 8). We find that while Bub1 is required for normal embryogenesis, low levels of this checkpoint protein do not result in premature age-related diseases. Consistent with our earlier work, these animals do not display cellular senescence or engagement of the Rb-$p16^{Ink4a}$ and p53-$p19^{Arf}$ pathways. However, unlike our previous models, Bub1 insufficient mice are especially predisposed to spontaneous tumor formation. Cells that have low levels of Bub1 display high rates of chromosome missegregation, and unlike cells with a full complement of Bub1, increased rates of cellular survival following these segregation aberrancies. These results suggest that Bub1 functions as a tumor suppressor by both protecting cells from having missegregation events during mitosis and by promoting apoptosis in cells that happen to have undergone a defect in separation of chromosomes.

Discussion and Future Outlook

Defective mitotic checkpoint activity promotes the development of aneuploidy. Since nearly all human cancers exhibit this trait, many efforts looking for mutations in mitotic checkpoint genes in human cancer have been undertaken. However, the majority of these studies reveal no consistent mutations in the critical members of the mitotic checkpoint. More interestingly is the finding that certain members of this surveillance machinery are either overexpressed or downregulated in human cancer. Our results demonstrate that utilizing the mouse for testing the physiological relevance of mitotic checkpoint genes can result in some expected, but many more unexpected, functions of these genes. We have used hypomorphic mice in both our Bub1 and BubR1 studies, where we are able to bring the absolute level of expression of these genes below that which is seen in heterozygous null mice. Importantly, the phenotypes of spontaneous cancer predisposition in Bub1 mice and premature aging in BubR1 mice absolutely require these low levels. Many checkpoint models have strictly used a classical gene knockout approach, and have not come to the same findings. It may be interesting to go back to the established models and attempt to reduce the absolute level of each individual checkpoint protein to see if other members of the mitotic checkpoint machinery are able to recapitulate the results that we have obtained. Additionally, compound mutant mice lacking more than one checkpoint protein may yield unforeseen results, such as the earlier onset to age-related diseases in double haplo-insufficient Bub3/Rae1 mice that we have reported.

Many mitotic checkpoint defective models display a predisposition to tumor development when challenged with carcinogens. However, the actual mutations resulting from these treatments that are able to synergize in these animals have been elusive. Additionally, attempts to promote tumor formation in checkpoint defective mice by removing the tumor suppressors p53 or Rb have been ineffective [2]. Therefore, it will be of extreme interest and importance to determine what genes are able to cooperate with mitotic checkpoint deficiency to promote tumors and help provide a better understanding of the role of aneuploidy in cancer. Furthermore, these experiments may allow for identification of similar alterations that occur during the multi-step process of tumorigenesis in humans. Adding further complexity to the role that aneuploidy may have in tumorigenesis, it appears that under certain circumstances aneuploidy actually prevents the formation of cancer. CENP-E haploinsufficient mice, which develop high rates of aneuploidy both *in vitro* and *in vivo*, have higher rates of spontaneous tumors, while challenging these animals with a carcinogen decreases the number and size of tumors [3]. We have found that Bub1 haploinsufficiency does synergize with carcinogen exposure to yield high rates of tumor formation (Chapter 8). However, these mice appear to be slightly protected from spontaneous tumors, implying that loss of one Bub1 gene can act to accelerate the

development of tumors initiated by particular gene mutations that may or may not require aneuploidy. Analysis of our series of Bub1 mutant mice establishes that reduced expression of Bub1 promotes spontaneous tumor formation, but only once the level has breached a critical threshold. Mice with the most dramatic reduction have the highest incidence of tumors, as well as the highest percentage of aneuploid cells. However, we find that animals that have similar rates of aneuploidy (i.e. Nup98/Rae1 double haploinsufficient and Bub3/Rae1 double haploinsufficient) do not have this same predisposition. What could be a potential reason for this discrepancy? Perhaps Bub1 hypomorphic mice are more prone to development of wide varieties of abnormal karyotypes because of decreased apoptosis following missegregation events. However, the role of aneuploidy in tumorigenesis, despite the fact that it is a nearly 100-year-old observation, remains highly complex. It will be necessary to examine each regulator of chromosome separation in order to clarify its role in tumorigenesis through the use of mouse models. These efforts may identify a smaller group of mitotic checkpoint proteins that are especially important for preventing cancer formation. Among these, there may be mitotic regulators that serve as hubs within the checkpoint or are connected to other molecular networks that are essential for protection against neoplastic transformation.

The link between mitotic checkpoint impairment and cancer predisposition is supported by the finding that a high proportion of individuals with mosaic variegated aneuploidy (MVA) syndrome exhibit biallelic mutations in BubR1 [4]. These patients are especially susceptible to neoplasms such as rhabdomyosarcoma, Wilms tumor, and leukemia [5, 6]. Interestingly, these patients also develop a variety of other phenotypes, including microcephaly, growth retardation, and cataracts. Whether these patients develop other progeroid features remains to be established, as only four patients with BubR1 mutations have been identified, three of which are <3 yr of age. Because MVA is such a rare human syndrome, it may be necessary to use the mouse to model these biallelic mutations to learn more about the pathology of this syndrome and its possible link to premature aging. Almost all MVA patients carry one missense mutation in the kinase domain and a truncating mutation upstream of the kinase domain [4]. Therefore, a mouse model where the activity of the kinase domain of BubR1 is investigated would be extremely interesting.

The expression of BubR1 declines with age in a variety of tissues in the mouse and mice with low levels of this gene develop a variety of early aging-related phenotypes. This suggests that BubR1 may be a determinant of natural aging. To test this idea, mice that carry transgenes of BubR1 to offset the natural decline in BubR1 could be used to see if forced overexpression can extend lifespan and prevent or delay aging-related disorders. These experiments may be complicated by an increased tumor formation, as it has been recently reported that mice which overexpress the mitotic checkpoint gene Mad2 are

susceptible to spontaneous tumor formation [7]. Additionally, if BubR1 transgenic mice are able to rescue the age-related pathology of BubR1 hypomorphic mice, additional transgenes lacking certain key domains of BubR1, including the kinase domain, could be utilized to determine what domains are critical for prevention of cancer and premature aging in hypomorphic BubR1 mice. The amount of BubR1 declines with age apparently due to decreased transcription, but the reason for this has not been determined. Therefore several key questions remain. What causes the silencing of the BubR1 gene? Is this process important for preventing the development of adverse conditions later in life? Are there active mechanisms in place to halt the transcription of BubR1 with age or is it simply the by-product of the aging process? These are obvious venues to explore in establishment of the critical functions that BubR1 has during normal organismal aging.

By using BubR1 hypomorphic mice, we have been able to clearly define alternative age-related pathologies in mice lacking the tumor suppressors $p16^{Ink4a}$ or $p19^{Arf}$. Mice that have combined $p16^{Ink4a}$ deficiency along with low levels of BubR1 have substantial delays to age-related disease onset, suggesting that engagement of this tumor suppressor results in increased *in vivo* senescence and aging. Consistent with this, recent work has indicated that increased $p16^{Ink4a}$ expression contributes to age-related depletion of stem cell populations in the brain, pancreas and bone marrow [8-10]. Remarkably, disruption of the alternative reading frame product $p19^{Arf}$ in hypomorphic BubR1 mice accelerates the onset of aging, suggesting that $p19^{Arf}$ functions as an attenuator of *in vivo* senescence and aging. Recent work further supports this hypothesis, as mice which have increased, but normally regulated, levels of $p19^{Arf}$ and p53 have a strong resistance to cancer and have decreased levels of aging-associated damage [11]. Therefore, it will also be imperative to define the role of p53 itself in relation to aging in the context of BubR1 hypomorphic animals. So clearly, the role of BubR1, and other mitotic checkpoint genes, in aging and cancer are only beginning to be elucidated.

One central question remains about aging in BubR1 hypomorphic mice: What is the primary nature of the stress causing the activation of senescence and aging? Initially, we thought that it may be aneuploidy, but have since ruled that out as the sole cause of aging by using many other mitotic checkpoint defective mouse models that also develop severe aneuploidy. We now believe that in certain tissues, the rates of aging correlate very closely with the induction of cellular senescence and engagement of these pathways. However, why do low amounts of BubR1 promote this response? DNA damage is believed to activate these same pathways, but we currently have no evidence for increased DNA damage or a defective ability to repair lesions in BubR1 hypomorphic cells. Single cell gel electrophoresis assays, also known as Comet assays, on hypomorphic BubR1 tissues reveals no increased single-strand or double strand breaks, apurinic or apyrimidinic sites, or

DNA adducts. Preliminary studies indicate BubR1 tissues that age prematurely have increased oxidative stress. If BubR1 hypomorphism indeed promotes the generation of reactive oxygen species (ROS), the next question would be, how would it do so? Also, the role that ROS has during organismal aging remains a topic of intense debate [12]. We are also exploring the possibility that there is oncogene induced senescence in BubR1 hypomorphic mice. Perrhaps key oncogenes that are normally kept inactive when BubR1 is present at normal amounts are aberrantly signaling in conditions where BubR1 drops below a critical threshold level. The use of mass spectrometry may be useful to identify these unknown binding partners of BubR1 that may themselves be influential or essential in promotion of age-related disease. Obviously BubR1 has a pivotal role outside of its function during the mitotic checkpoint, but remains elusive. Hopefully, with good design, this pathway of aging stemming from deficiencies in BubR1 can be completed.

References

1. Krishnamurthy, J., Torrice, C., Ramsey, M.R., Kovalev, G.I., Al-Regaiey, K., Su, L., and Sharpless, N.E. (2004). Ink4a/Arf expression is a biomarker of aging. J Clin Invest *114*, 1299-1307.
2. Kalitsis, P., Fowler, K.J., Griffiths, B., Earle, E., Chow, C.W., Jamsen, K., and Choo, K.H. (2005). Increased chromosome instability but not cancer predisposition in haploinsufficient Bub3 mice. Genes Chromosomes Cancer.
3. Weaver, B.A., Silk, A.D., Montagna, C., Verdier-Pinard, P., and Cleveland, D.W. (2007). Aneuploidy acts both oncogenically and as a tumor suppressor. Cancer Cell *11*, 25-36.
4. Hanks, S., Coleman, K., Reid, S., Plaja, A., Firth, H., Fitzpatrick, D., Kidd, A., Mehes, K., Nash, R., Robin, N., Shannon, N., Tolmie, J., Swansbury, J., Irrthum, A., Douglas, J., and Rahman, N. (2004). Constitutional aneuploidy and cancer predisposition caused by biallelic mutations in BUB1B. Nat Genet *36*, 1159-1161.
5. Kajii, T., Ikeuchi, T., Yang, Z.Q., Nakamura, Y., Tsuji, Y., Yokomori, K., Kawamura, M., Fukuda, S., Horita, S., and Asamoto, A. (2001). Cancer-prone syndrome of mosaic variegated aneuploidy and total premature chromatid separation: report of five infants. Am J Med Genet *104*, 57-64.
6. Plaja, A., Vendrell, T., Smeets, D., Sarret, E., Gili, T., Catala, V., Mediano, C., and Scheres, J.M. (2001). Variegated aneuploidy related to premature centromere division (PCD) is expressed in vivo and is a cancer-prone disease. Am J Med Genet *98*, 216-223.
7. Sotillo, R., Hernando, E., Diaz-Rodriguez, E., Teruya-Feldstein, J., Cordon-Cardo, C., Lowe, S.W., and Benezra, R. (2007). Mad2 overexpression promotes aneuploidy and tumorigenesis in mice. Cancer Cell *11*, 9-23.

8. Molofsky, A.V., Slutsky, S.G., Joseph, N.M., He, S., Pardal, R., Krishnamurthy, J., Sharpless, N.E., and Morrison, S.J. (2006). Increasing p16INK4a expression decreases forebrain progenitors and neurogenesis during ageing. Nature *443*, 448-452.
9. Janzen, V., Forkert, R., Fleming, H.E., Saito, Y., Waring, M.T., Dombkowski, D.M., Cheng, T., DePinho, R.A., Sharpless, N.E., and Scadden, D.T. (2006). Stem-cell ageing modified by the cyclin-dependent kinase inhibitor p16INK4a. Nature *443*, 421-426.
10. Krishnamurthy, J., Ramsey, M.R., Ligon, K.L., Torrice, C., Koh, A., Bonner-Weir, S., and Sharpless, N.E. (2006). p16INK4a induces an age-dependent decline in islet regenerative potential. Nature *443*, 453-457.
11. Matheu, A., Maraver, A., Klatt, P., Flores, I., Garcia-Cao, I., Borras, C., Flores, J.M., Vina, J., Blasco, M.A., and Serrano, M. (2007). Delayed ageing through damage protection by the Arf/p53 pathway. Nature *448*, 375-379.
12. Valko, M., Leibfritz, D., Moncol, J., Cronin, M.T., Mazur, M., and Telser, J. (2007). Free radicals and antioxidants in normal physiological functions and human disease. Int J Biochem Cell Biol *39*, 44-84.

Acknowledgements

I have many people to acknowledge for helping me in my doctoral work. First and foremost, I would especially like to thank Prof. dr. Jan van Deursen for his generous time and commitment. I thank him for giving me my first position out of college and believing in me to steer me towards pursuing a life-long career in science. His abilities as an educator and scientific investigator have been wonderful and I appreciate his sharing these talents with me. He has and will continue to be a great mentor. I am very grateful to Prof. dr. Be Wieringa for serving as my thesis advisor and providing me the opportunity to graduate from Radboud University in Nijmegen. Also, I would like to thank my thesis committee members, Prof. dr. A. Geurts van Kessel, Dr. G. Kops and Prof. dr. M. van Lohuizen for critically reviewing and supporting this thesis.

To all my co-workers, past and present, thank you for your assistance, patience, and knowledge. I would like to thank David Norris, Kevin Pitel, Michael Zimmer and Michael Thompson, who have been instrumental in establishing and maintaining the mice used in many of my studies. My special thanks go to my colleagues in the van Deursen lab: Karthik Jeganathan, Dr. Liviu Malureanu, Dr. Janine van Ree, Dr. Fang Jin and Meelad Dawlaty. You have all been truly terrific collaborators and friends. I thank Dr. Paul Galardy and Dr. Robin Ricke for critically reading many of my manuscripts. It has been a pleasure working with all my past and present colleagues at Mayo Clinic. I especially need to acknowledge Dr. Carmen Perez-Terzic and Prof. dr. Andre Terzic and all the members of his laboratory for being wonderful collaborators. Their input and assistance has been vital for the advancement of many of my studies. I also would like to thank Zvonimir Katusic and his lab, Piet de Groen and Doug Cameron for providing expert advice and guidance when called upon.

Finally, I'd like to thank all the members of my family, for they have all been a constant source of support and for understanding that research doesn't stop for holidays or weekends. I'm especially grateful to my wife and best friend, Betsy, for being so supportive and for understanding during this doctoral endeavor. I also have to thank both Andrew and Caleb, the two sons that keep everything in perspective.

Hopefully I have not forgotten to thank anyone whose help I could not have done without. If I have, my most humble thanks and apologies.

Darren James Baker

Publications

Baker DJ, Perez-Terzic C, Jin F, Pitel KS, Niederlander NJ, Jeganathan KB, Yamada S, Reyes S, Rowe L, Hiddinga, JH, Eberhardt NL, Terzic A & van Deursen JM. **Opposing roles for $p16^{Ink4a}$ and $p19^{Arf}$ in senescence and aging caused by BubR1 insufficiency**. Nature Cell Biology (In press).

Jeganathan KB*, Malureanu L*, **Baker DJ***, Abraham SC, van Deursen JM. **Bub1 mediates cell death in response to chromosome missegregation and acts to suppress spontaneous tumorigenesis.** Journal of Cell Biology *179*, 255-267 (2007).
* shared first authorship

Baker DJ, Dawlaty MM, Galardy P, and van Deursen JM. **Mitotic regulation of the anaphase-promoting complex.** Cellular and Molecular Life Sciences *64*, 589-600 (2007).

Matsumoto T, **Baker DJ**, d'Uscio LV, Gazi MH, Katusic ZS, and van Deursen JM. **Aging associated vascular phenotype in mutant mice with low levels of BubR1.** Stroke *38*, 1050-1056 (2007).

Jeganathan KB, **Baker DJ**, and van Deursen JM. **Securin associates with APC^{Cdh1} in prometaphase but its destruction is delayed by Rae1 and Nup98 until the metaphase to anaphase transition.** Cell Cycle *5*, 366-370 (2006).

Baker DJ, Jeganathan KB, Malureanu L, Perez-Terzic C, Terzic A, and van Deursen JM. **Early aging associated phenotypes in Bub3/Rae1 haplo-insufficient mice.** Journal of Cell Biology *172*, 529-540 (2006).

Niessen P, Rensen S, van Deursen JM, De Man J, De Laet A, Vanderwinden JM, Wedel T, **Baker DJ**, Doevendans P, Hofker M, Gijbels M, and van Eys G. **Smoothelin-a is essential for functional intestinal smooth muscle contractility in mice.** Gastroenterology *129*, 1592-1601 (2005).

Baker DJ, Chen J, and van Deursen JM. **The mitotic checkpoint in cancer and aging: what have mice taught us?** Current Opinions in Cell Biology *17*, 583-589 (2005).

Baker DJ, Jeganathan KB, Cameron JD, Thompson M, Juneja S, Kopecka A, Kumar R, de Groen PC, Roche P, and van Deursen JM. **BubR1 insufficiency causes early onset of aging-associated phenotypes and infertility in mice.** Nature Genetics *36*, 744-749 (2004).

Kang-Decker NL, Tong CL, Boussouar F, **Baker DJ**, Wu X, Leontovich AA, Taylor WR, Brindle PK, and van Deursen JM. **Loss of CBP causes T cell lymphomagenesis in synergy with p27Kip1 insufficiency.** Cancer Cell *2*, 177-189 (2004).

Babu JR, Jeganathan KB, **Baker DJ**, Wu X, Kang-Decker NL, and van Deursen JM. **Rae1 is an essential mitotic checkpoint regulator that cooperates with Bub3 to prevent chromosome missegregation.** Journal of Cell Biology *160*, 341-353 (2003).

Curriculum Vitae

Darren James Baker was born in Willmar, Minnesota, USA on February 24, 1979. He attended public high school in Willmar, Minnesota, USA and graduated with highest honors in May 1997. From September 1997 through May 2001 he studied at the University of Minnesota in Minneapolis, Minnesota, USA and graduated Summa cum laude with a Bachelor of Science degree in Biology with a minor in Chemistry. From September 1999 through May 2001, he worked as an Animal Diversity Laboratory Teaching Assistant, responsible for conducting classes to widespread animal systems and administering exams. In addition, during his last year, he took part in undergraduate research for the honors program. This laboratory experience, under the guidance of Dr. Robert McKinnell, was unpaid and self-directed, but ultimately resulted in a further desire to stay within the research community. Beginning in May 2001, he joined the laboratory of Prof. Dr. Jan van Deursen in the Department of Pediatric and Adolescent medicine located at the Mayo Clinic in Rochester, Minnesota, USA as a research technologist. While employed, he undertook a program of study to earn an employee master's degree in Biomedical Sciences- Tumor Biology from the Mayo Clinic School of Medicine- Mayo Graduate School from July 2003 until June 2005. In 2003, he was promoted to senior research technologist and in 2007 was given the additional title of senior research technologist manager, functioning as the manager of the van Deursen laboratory. His research through 2007 focused on the physiological functions of mitotic checkpoint proteins, most specifically BubR1 and age-related diseases. He continues to work in the van Deursen laboratory on the role of mitotic checkpoint proteins in cancer and aging.